Relativistic runaway electrons in tokamak plasmas

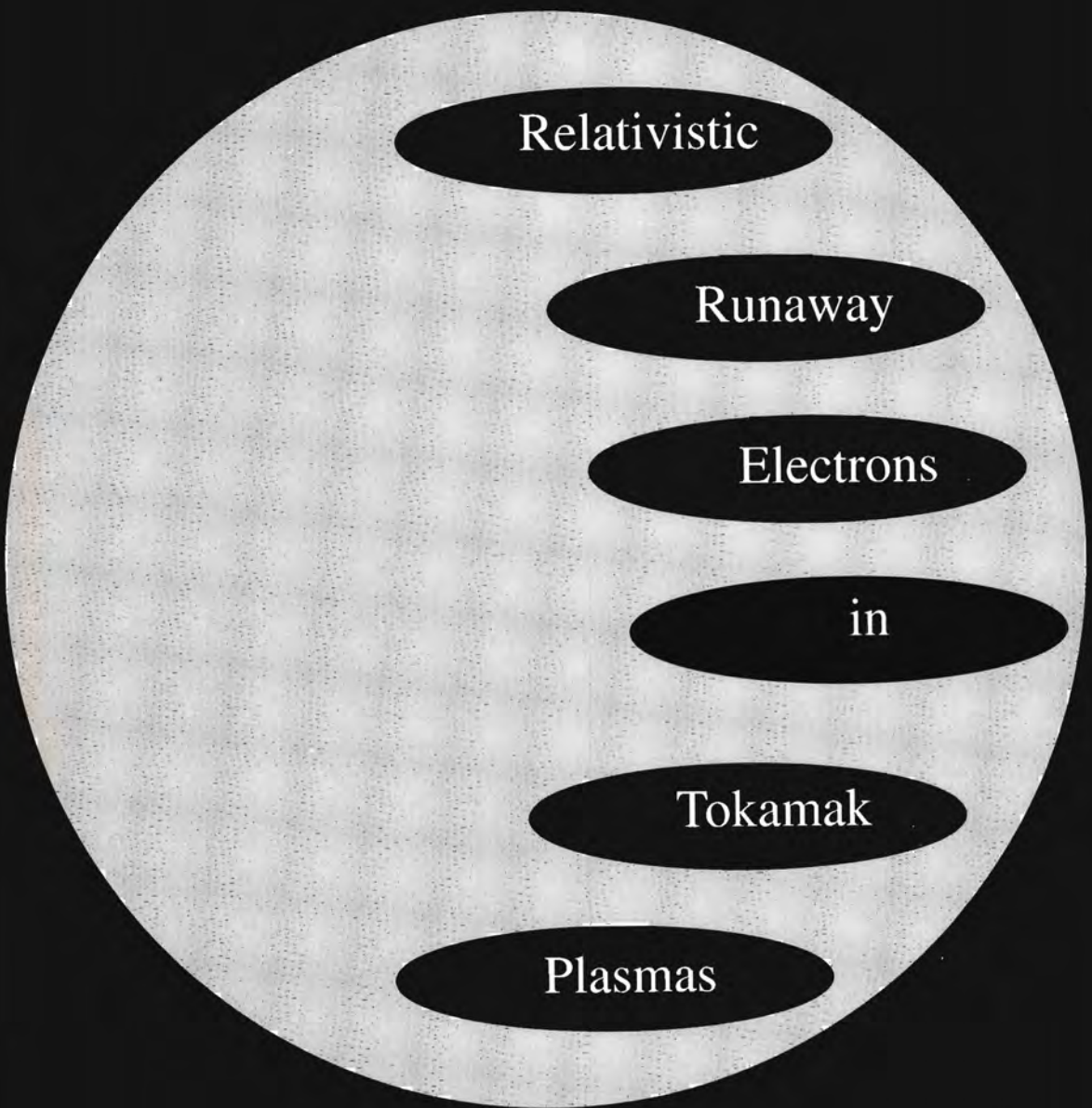

Roger Jaspers

RELATIVISTIC RUNAWAY ELECTRONS IN TOKAMAK PLASMAS

Met een samenvatting in het Nederlands

Proefschrift

ter verkrijging van de graad van doctor aan de Technische Universiteit Eindhoven, op gezag van de Rector Magnificus, prof.dr. J.H. van Lint, voor een commissie aangewezen door het College van Dekanen in het openbaar te verdedigen op

vrijdag 3 februari 1995 om 16.00 uur

door

Roger Jozef Elisabeth Jaspers

geboren op 20 april 1968 te Wittem

Dit proefschrift is goedgekeurd door de promotoren:

Prof.dr. N.J. Lopes Cardozo

en

Prof.dr. F.C. Schüller

en de co-promotor: dr. K.H. Finken

CIP-DATA Koninklijke Bibliotheek, Den Haag

Jaspers, Roger Jozef Elisabeth

Relativistic runaway electrons in tokamak plasmas / Roger Jozef Elisabeth Jaspers
Proefschrift Technische Universiteit Eindhoven - Met een samenvatting in het Nederlands.
ISBN 90-386-0474-2

The work described in this thesis was performed as part of a research programme of the 'Stichting voor Fundamenteel Onderzoek der Materie' (FOM) and 'Institut für Plasmaphysik, Forschungszentrum Jülich GmbH' with financial support from the 'Nederlandse Organisatie voor Wetenschappelijk Onderzoek' (NWO), EURATOM and Forschungszentrum Jülich, and was carried out at the TEXTOR tokamak, Institut für Plasmaphysik, Forschungszentrum Jülich GmbH, Germany.

" If we knew what it was we were doing,
it would not be called research, would it?"

A. Einstein

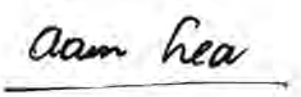

TABLE OF CONTENTS

CHAPTER 1A

GENERAL INTRODUCTION

For an outsider, the title of this work '*relativistic runaway electrons in tokamak plasmas*' perhaps does not contain a single familiar word. For an insider it is obvious that here is meant research into one of the *most* interesting phenomena in the *most* common state of matter in the universe, in the *most* successful experimental device for the *most* promising solution of the *most* pressing problem of the next century. This chapter is meant as a bridge between insider and outsider.

Apart from the three familiar states of matter (solid, liquid and gas), a fourth exists, which is less known, although it is the most common one in universe. This is the plasma, which can be defined as an ionized gas. The best known examples of a plasma are the sun and on earth, lightning. Plasma physics has become an important branch of physics because of the rich variety of phenomena that occur in this system of ions, electrons and neutrals in interaction with electromagnetic fields. The effect of 'electron runaway' is one of these phenomena. The runaway electrons constitute a small fraction of the plasma electrons, that are continuously accelerated to high energy. They are of fundamental interest for the description of plasmas, but have also, as will be shown in this thesis, important consequences for plasma physics applications.

The sun is a gigantic plasma in which energy is produced by fusion reactions of light nuclei. A major effort is put into research to imitate this process under laboratory conditions. Succeeding in this would lead to an inexhaustable energy source. In this field of research, thermonuclear plasma physics, the experiments descibed in this thesis are performed. A short introduction about nuclear fusion, the runaway electrons, the experimental device, called the tokamak, and the motivation for the present work will be presented in the next sections.

1.1 Nuclear Fusion

The world's continuously growing energy demand will lead to an energy crisis, unless new energy sources are developed. In view of the shrinking reserves of coal, oil and gas, the fossil fuels of which most of the energy is produced, a shortage of these conventional energy sources is expected half-way the next century. Even earlier the pollution of the environment as a result of the energy production becomes a problem. The increased carbon dioxide concentration in the atmosphere as a result of the burning of fossil fuel can possibly result in the greenhouse effect, with a disastrous influence on the earth's climate.

Nuclear fusion is one of the most promising solutions to this problem, as it is potentially an almost inexhaustible, comparatively clean and safe energy source. Fusion is the process based on the fact that if two light nuclei fuse into one heavier nucleus, mass is converted into energy. The

reaction which is easiest to access, is the one between the nuclei of the hydrogen isotopes Deuterium and Tritium. A huge amount of energy is set free in this reaction: 1 kg of a D-T mixture produces as much energy as 10 million liters of oil! The raw materials are abundant: D is present in natural water and Li, from which T is bred, can be mined. Fusion energy can therefore supply the world's energy demand for thousands of years. The ash of the reaction, He, is a harmless inert gas. The neutron, the other reaction product, has the disadvantage to make the fusion reactor itself radioactive. Nevertheless, thanks to the relatively short half-life of the materials used (<100 years) this problem is much less severe than the radioactive waste of fission reactors. Another advantage of a fusion reactor compared to a fission reactor is the inherent safety. In the latter the risk of meltdown or other technical failures can cause a worldwide catastrophe, due to the enormous amount of energy stored in the reactor. Since the fuel is continuously flowed into a fusion reactor, only a very limited amount of energy is present in every phase of operation. A technical failure will always result in a direct termination of the burning, excluding the possibility of any calamity.

By far the most promising results in the field of controlled nuclear fusion are achieved in the so-called tokamak. In this torus-shaped device the plasma is heated to temperatures of 100 million degrees. Such a high temperature is required to have a large enough probability that the colliding nuclei can overcome the repulsive Coulomb force and are able to fuse. The plasma is confined by a magnetic field to avoid contact with the material wall.

Notwithstanding the worldwide effort and the impressable progress in thermonuclear research over the past 30 years, a fusion energy reactor is still a dream of the future. Although present tokamak experiments have produced up to 10 MW of fusion power no self sustained burning plasma is accomplished yet. The main problems to be addressed comprise: i) the confinement of energy and particles in a magnetic confinement device is more than one order of magnitude worse than predicted; ii) removal of the exhaust (helium) from the center of the reactor as too high concentrations of the ash will choke the fusion process; iii) extraction of the fusion power from the reactor. High power fluxes to material in contact with the plasma are not tolerable as this will evaporate surface material, thereby reduce the reactor lifetime and polluting the plasma; iv) the avoidance of so called major plasma disruptions, i.e instabilities in which the magnetic confinement of the plasma is suddenly lost. Such disruptions terminate the operation and can cause considerable damage to the device.

1.2 Runaway Electrons

In the tokamak concept the confinement of the plasma is achieved by running a current through the plasma column. This plasma current is generated by an inductive electric field in the toroidal direction. The presence of this electric field leads to the phenomenon of electron 'runaway' [Kno-79]. This is an interesting physical aspect of the kinetic theory of plasmas. Collisions between charged particles in the plasma are governed by the long-range, small-angle scattering Coulomb

interaction. The characteristic feature of this interaction is the rapid decrease of momentum transfer with increasing particle energy. For electrons of sufficiently high energy the friction force due to collisions with plasma particles does not compensate the externally induced electric force. These electrons are continuously accelerated and 'run away' in phase space.

Electron runaway has been an intriguing theme for plasma physicists of both the theoretical and experimental persuasion, since the first publication in 1949 by Giovannelli [Gio-49]. Theories are able to describe the runaway phenomenon and resulting non-linear effects quite successfully. The runaway electrons are collisionally decoupled from the bulk plasma, due to the high relative velocities and the associated small collision cross-section. In spite of this small collisional interaction there is still an interplay between the runaways and the bulk. The mutual influence between collective plasma effects and the runaway electrons can give rise to several instabilities [Mik-74].

From an experimental viewpoint runaway electron studies are motivated by several arguments involving the diagnostic capabilities and the effect of the runaway electrons on the plasma behaviour: - runaway electrons can be regarded as effectively collisionless which makes them a suitable probe for investigating the non-collisional transport in a tokamak; - runaway electrons can affect the plasma behaviour since they can carry a substantial part of the plasma current, they possibly can improve the confinement of the plasma and their interaction with waves can transfer energy to the plasma. Furthermore, since the loss of high energetic runaway electrons can cause considerable damage to fusion machines, investigations into production, acceleration and loss processes of the runaway electrons is required. The damage is particularly alarming during plasma disruptions where a large number of runaway electrons is accelerated to energies high enough to penetrate the solid structure of the reactor.

1.3 This Thesis

Relativistic electrons moving on a curved orbit emit synchrotron radiation. Exploitation of this radiation for the tokamak case provides the possibility to diagnose *confined* runaway electrons inside the plasma. The first pioneering measurements of this kind were performed at the TEXTOR tokamak by Finken et al. [Fin-90]. Following these investigations, more systematic studies were undertaken at TEXTOR. Their results are reported in this thesis.

The unique opportunity of a direct runaway observation gave new insights into the runaway electron behaviour in the plasma. Without this technique runaway electron information is principally obtained from the x-rays emitted when the electrons are lost from the plasma and hit a solid surface. An illustration of the new information of runaway electrons gained from the synchrotron radiation and not directly observable by other diagnostics:

* The process of runaway generation, which takes mainly place in the plasma center, is only indirectly accessible by other techniques. From analysis of the synchrotron radiation a direct

comparison with theories could be made. It was found that the runaway production depends on the number of runaway electrons present in the discharge. This was the first experimentally evidence found for a secondary generation mechanism (Chapter 4).

* The capability of runaway electrons to probe magnetic turbulence has limited application if the runaway electrons are only observed when they are lost. With the synchrotron radiation technique stochastic transport in the plasma core is studied and a new phenomenon, regions of perfect confinement of runaway electrons, is observed (Chapter 5).
* An instability of the runaway electrons, occuring at low densities is only noticed on the synchrotron radiation. This can possibly be used to decrease the maximum attainable runaway energy and thereby reduce the potential danger when high energetic runaway electrons are lost from the plasma (Chapter 6).
* The generation of a runaway electron beam during a plasma disruption can have severe consequences for fusion reactor. It is demonstrated that the synchrotron radiation can directly monitor such a beam (Chapter 7).

To illustrate the power of the synchrotron method, Fig. 1.1 is served up as an appetizer. When viewing the plasma tangentially with a thermographic camera only the wall structures are observed. At low densities, when an appreciable number of runaway electrons are produced a large spot of synchrotron radiation appears in front of this background. After injection of a pellet in such a discharge nearly all runaway electrons are lost from the plasma. Only those situated in a specific, helical tube stay perfectly confined and they are recognized as the small spots of intense emission in Fig. 1.1. From such synchrotron pictures alone runaway energy, current, position of the beam and diffusion coefficients during and after pellet penetration can be derived. The magnetic mode structure in the plasma interior is directly reflected in this runaway behaviour. Such information cannot be obtained by any other runaway diagnostic. A detailed explanation of this experiment is presented in chapter 5.

In the first part of the thesis a detailed treatment of the theory concerning relativistic electrons in tokamaks and synchrotron radiation is presented, together with an extensive description of the experimental technique. Although no new plasma physical problems are tackled here, this lengthy introduction is justified by the fact that no reference work on this subject is available yet. One of the goals of the present work is to eliminate this hiatus. More specific experiments, revealing information about runaway generation, runaway transport, runaway instabilities and runaways during disruption, are described in the subsequent chapters.

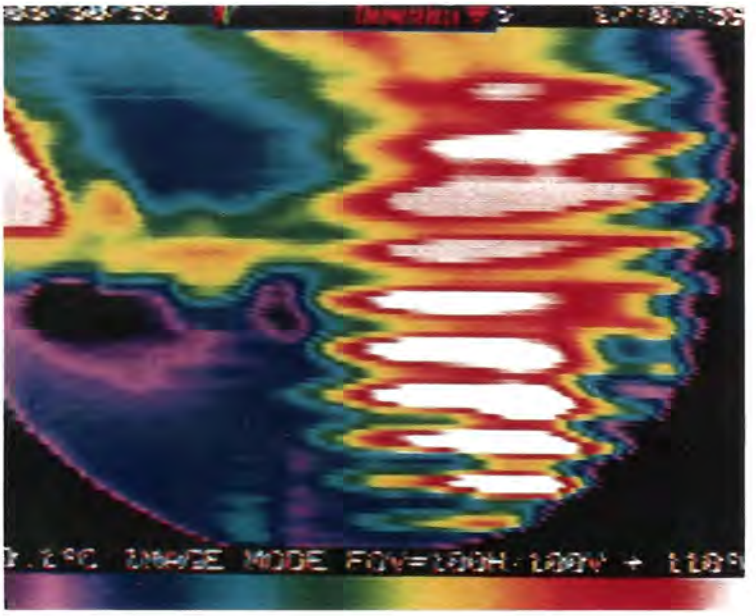

Figure 1.1: *Example of synchrotron emission in the TEXTOR tokamak. This particular example occurs after injection of a pellet into a low density discharge and is explained in chapter 5. Here it is shown to demonstrate the capability of the method: - fast events are recognized as time is increasing from top to bottom, - position measurements of the runaway beam are accomplished by the known reference frame provided by the liner. The runaway energy can be obtained from this, -the intensity is measured absolutely by calibrating with the known background temperature of the limiter, -the dynamic behaviour of the runaway electrons in the core of the plasma is directly recorded, -the shape of the synchrotron spots reflects magnetic modes structures.*

1.4 Publications Related to this Thesis

Journals

- R. Jaspers, K.H. Finken, G. Mank et al., *Experimental Investigation of Runaway Electron Generation in TEXTOR*, Nucl. Fusion **33** (1993) 1775
  Reprinted in Section 4.4.

- R. Jaspers, N.J. Lopes Cardozo, K.H. Finken, B.C.Schokker, G.Mank, G.Fuchs and F.C. Schüller, *Islands of Runaway Electrons in the TEXTOR Tokamak and Relation to Transport in a Stochastic Field*, Phys. Rev. Lett. **72** (1994) 4093
  Reprinted in Section 5.4

- R. Jaspers, T. Grewe, K.H. Finken et al., *Observations of Infrared Radiation during Disruptions in TEXTOR: Heat Pulses and Runaway Electrons*, to be published in J. Nucl. Mater. (1994)
  Reprinted in modified form in Chapter 7.

- R. Jaspers and K.H. Finken, *Experiments on Runaway Discharges in TEXTOR*, Published in: Contributions to High Temperature Plasma Physics, Ed. K.H. Spatschek and J. Uhlenbusch, Akademie Verlag, Berlin (1994)

- F. Hoenen, E. Graffmann, K.H. Finken, H.J. Barrenscheen, H. Klein, R. Jaspers, *Liquid Scintillation Detectors for Gamma and Neutron Diagnostic at TEXTOR and Results of Runaway and Sawtooth Oscillations*, Rev. Sci. Instrum. **65** (1994)

Conference proceedings

- R. Jaspers, N.J. Lopes Cardozo and K. H. Finken, *Confinement of relativistic electrons in TEXTOR*, Proc. Local Transport Studies in Fusion Plasmas, Varenna, Italy (1993) 193.

- R. Jaspers, K. H. Finken, G. Mank, F. Hoenen, J. Boedo, N.J. Lopes Cardozo, F.C. Schüller, *Investigations of Relativistic Runaway Electrons*, Proc. EPS Conf. on Contr. Fus. and Plasma Physics, Lisbon, Portugal (1993) I-123.

- R. Jaspers, K. H. Finken, G. Mank, D. Rusbüldt, N.J. Lopes Cardozo, F.C. Schüller, J.Boedo, F. Hoenen, *Observation of Relativistic Runaway Electrons by Synchrotron Radiation in TEXTOR*, Proc. Int. Conf. on Plasma Physics, Innsbruck, Austria (1992) I-155.

- R. Jaspers, *Diagnostic to measure the infrared synchrotron radiation from relativistic runaway electrons*, Proc. Workshop: Diagnostics for Contemporary Fusion Experiments, Varenna, Italy (1991) 819.

- 6 contributions to international conferences as co-author

CHAPTER 1B

THE TOKAMAK

Before going ahead with the runaway electron measurements a short summary of the tokamak concept, the definition of some related quantities, the TEXTOR machine and its standard discharge parameters is given here for reference.

Basic Lay Out

A schematic of the tokamak is sketched in Fig. 1.2. It consists of a toroidal vacuum vessel in which a gas is injected which is ionized to form a plasma. The plasma is confined by a magnetic field, since charged particles gyrate around the field lines. The main component of the magnetc field, B_ϕ is produced by external coils surrounding the vessel. For stability a poloidal magnetic field (B_θ) is required. In a tokamak B_θ is produced by a toroidal current I_p in the plasma itself. This current is induced by using the plasma as the secondary winding of a transformer. External coils generate additional fields for plasma shaping and position control, such as the vertical field (B_z) which provides the $J \times B$ force (J being the current density) necessary to oppose the hoop force of the plasma and which provides control of the horizontal position of the plasma column.

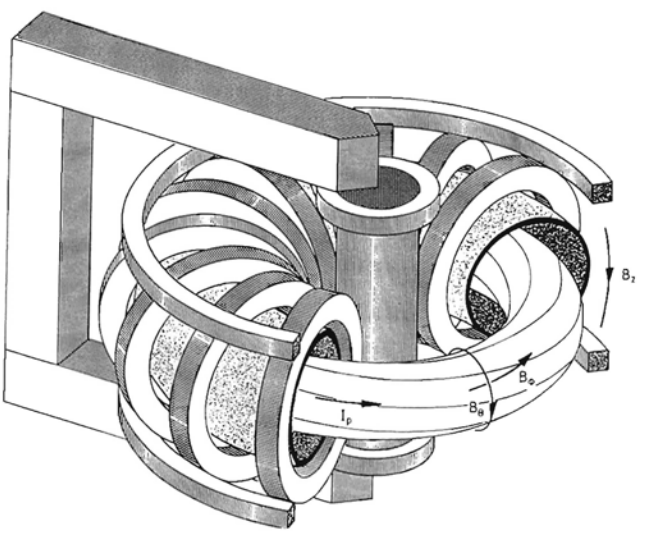

Figure 1.2: *Schematic representation of a tokamak device. The current I_p is induced by the transformer and generates a poloidal magnetic field. A stronger toroidal field is produced by external coils surrounding the vacuum vessel. By adding to this a vertical magnetic field a stable configuration is established. Plasma heating is achieved by the plasma current through ohmic dissipation and by auxiliary methods such as Neutral Beam Injection (NBI) and Ion Cyclotron Resonance Heating (ICRH).*

Apart from the generation of B_θ, the current I_p heats the plasma by ohmic dissipation. Although temperatures of several keV can be reached in this way (1 keV $\triangleq$ 11.6×10^6 K), for a burning fusion reactor temperatures one order of magnitude higher are required. Since the resistivity η of the plasma decreases rapidly with electron temperature T_e: $\eta \propto T_e^{-3/2}$, this process becomes less efficient at high T_e and auxiliary heating becomes necessary. Examples of such methods are: i) Neutral Beam heating (NBI): injection of high energy atoms of hydrogen or deuterium, accelerated to typically 50 keV, into the plasma or ii) launching electro-magnetic waves into the plasma, which are absorbed by a certain class of particles, depending on the frequency of the waves. If the waves are resonantly absorbed by the ion cyclotron motion this heating method is called ICRH.

Related Quantities

-Safety Factor (q)

The combination of the toroidal and poloidal fields results in helical magnetic field lines. The helicity of the field lines is measured by the safety factor, defined as the number of toroidal turns a field line must make to complete a full poloidal turn:

$$q = \frac{1}{2\pi} \int \frac{1}{R} \frac{B_\phi}{B_\theta} = \frac{r}{R} \frac{B_\phi}{B_\theta} \qquad (1.1)$$

The integral is taken over a closed poloidal contour on the flux surface (see below). The last equality is only valid for a large aspect ratio, i.e. $r/R \ll 1$, where r is the distance to the plasma centre and R is the distance to the vertical torus axis.

-Flux Surface

Field lines with the same helicity lie on closed nested surfaces, called magnetic or flux surfaces. It follows from ideal magneto-hydrodynamics (MHD) that on these surfaces the plasma pressure is constant. Moreover, because of the good conduction along field lines, also the temperature is normally assumed to be constant.

-Shafranov Shift (s)

Due to the toroidal geometry the flux surfaces are shifted outward. The shift of the centre, the magnetic axis, is known as the Shafranov shift. This shift, the nested surfaces and the coordinate systems of the geometry as used in this thesis are indicated in Fig. 1.3.

- Gyration Motion

Parallel to the magnetic field line the charged particles can move freely. In the perpendicular direction the movement is restricted to a gyration motion with frequency ω_c and Larmor radius ρ_L:

$$\omega_c = \frac{ZeB}{m}; \qquad \rho_L = \frac{mv_\perp}{ZeB} \tag{1.2}$$

where e is the electron charge, Z is the charge number of the particle, m its mass and $v_\perp$ the velocity perpendicular to the magnetic field B. In this way particles are confined by the magnetic field and transport is only one dimensional: from surface to surface.

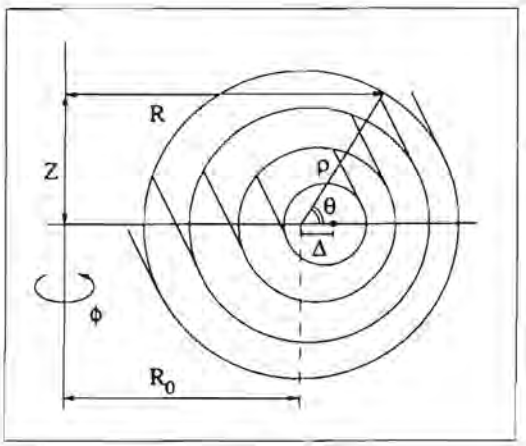

Figure 1.3:
The set of nested flux surfaces in tokamak geometry. The magnetic axis is shifted by an amount Δ with respect to the plasma boundary. The cylindrical coordinate system (R,z,ϕ) as well as the polar coordinate system (ρ,θ,ϕ) are indicated.

TEXTOR

TEXTOR is a medium sized limiter-tokamak with a circular cross-section, dedicated primarily to the study of plasma-wall interaction. To minimize energy losses through radiation from the core the plasma should not be polluted with impurities released from the vessel wall, the liner. Limiters are a way to define the plasma boundary to prevent contact with the liner and reduce the plasma wall interaction. At TEXTOR a toroidal pump limiter, named ALT-II, is installed. Apart from this purpose other aims of the ALT-II limiter are the particle and helium removal as well as the removal of the heat flux from the plasma. Fig. 1.4 shows a view inside TEXTOR where part of the ALT-II limiter attracts the attention. As a consequence of the high heat fluxes deposited on the ALT-II limiter during a discharge the temperature of the blades is such that thermal radiation is emitted in the same wavelength range as the synchrotron radiation of runaway electrons and will be 'visible' on all infrared pictures.

Another procedure to reduce the impurity influx developed at TEXTOR consists of the deposition of a protective amorphous film on the vessel wall. This carbonization, boronization or siliconization (depending on the kind of film) results in values of the effective ion charge Z_{eff} as low as 1.1. For nearly all discharges reported about in this thesis the wall was boronized.

Table I.- TEXTOR machine parameters

major radius	R_0	1.75	m
minor radius	a	0.46	m
magnetic field	B_ϕ	< 2.6	T
plasma current	I_p	< 620 (<800*)	kA
plasma volume	V	7.5	m^3
flux swing	Φ	4.4 (8.8*)	Vs
auxiliary heating power	P_{NBI}	2 × 1.7	MW
	P_{ICRH}	2 × 2.2	MW

* = values for TEXTOR-94

In table I the machine parameters of TEXTOR are listed. Table II gives the parameters for a typical low density runaway discharge, representative of the analyzed discharges in this thesis. Included in that table also are typical results concerning the runaway population as deduced in the course of this thesis from the synchrotron radiation.

Table II. - Typical parameters for ohmic runaway discharges in TEXTOR

central electron temperature	$T_e(0)$	1-1.5	keV
central ion temperature	$T_i(0)$	0.5	keV
central electron density	$n_e(0)$	1×10^{19}	m^{-3}
effective ion charge	Z_{eff}	1.5-2.0	
loop voltage	V_{loop}	0.9	V
electric field	E	0.08	V/m
plasma current	I_p	350	kA
flat top	$\tau_{f.t.}$	2	s
magnetic field	B_ϕ	2.25	T
edge safety factor	q_a	3.9	
Shafranov shift	s	0.03	m
runaway parameter (eq 2.3)	ε	0.02-0.04	
critical electric field (eq 2.4)	E_{crit}	2.0-2.7	V/m
critical energy (eq 2.3)	W_{cril}	100	keV
runaway current	I_r	1-10	kA
maximum runaway energy	W_{max}	25-30	MeV
pitch angle (eq 2.17)	Θ	0.12	rad

TEXTOR is equipped with two tangentially neutral beam injectors, two pairs of ICRH antennas, one 9 shot pellet injector and an extensive diagnostic parc. This includes:

- A 9 channel HCN interferometer for electron density measurements;
- An 11 channel electron cyclotron emission (ECE) diagnostic for electron temperature measurements;
- An 8 channel soft X ray (SXR) system for electron temperature and Z_{eff} measurements;
- A 40 channel SXR tomography system for measurements of MHD oscillations;
- A Rutherford scattering diagnostic for ion temperature measurements;
- A neutral particle analyzer (NPA) for ion temperature measurements;
- A 26 channel bolometer system for measurements of the radiated power;
- Several scintillators and ionisation chambers for hard X- ray (HXR) and neutron measurements;
- A Charge Exchange Recombination Spectroscopy (CXRS) system for ion temperature and impurity concentration measurements, and measurement of plasma rotation;
- Several spectroscopic systems from VUV to NIR for diagnosing line radiation of impurities;
- A large arsenal of edge diagnostics, mainly spectroscopic diagnostics for edge temperature and density measurements and determination of impurity concentrations;
- Probes for fluctuation measurements in the scrape off layer of the plasma;
- A set of magnetics for measurements of plasma current, plasma position, shape, loop voltage etc.;
- 12 Mirnov coils in one poloidal plane and 8 in the toroidal plane which allows to determine the m/n number of MHD oscillations;
- Finally, TEXTOR is equipped with two infrared cameras for thermographic measurements of the liner and limiter temperatures. These cameras are also suitable for measuring the synchrotron radiation of relativistic runaway electrons. This is demonstrated in chapter 3.

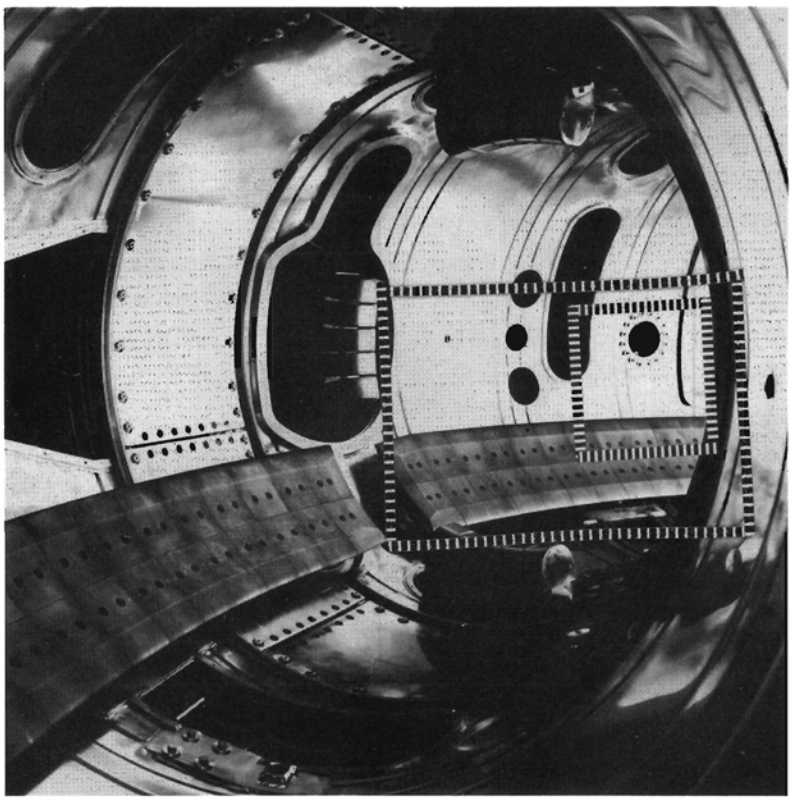

Figure 1.4: *View inside the vacuum vessel of TEXTOR. At 45° below the equatorial midplane, several blades of the ALT-II pump limiter are visible. The areas observed with the infrared camera used for synchrotron radiation measurements are indicated by the boxes.*

CHAPTER 2

RUNAWAY ELECTRONS

In this thesis the behaviour of relativistic runaway electrons in a tokamak is investigated. The basic properties and associated phenomena of these electrons, are briefly summarized and the necessary formularium is introduced in this chapter. The review papers [Kno-79, Par-86] are particularly suited as an introduction into runaway electron physics. The fundamentals of runaway transport and interaction of runaway electrons with plasma waves are given here. New results on these subjects are analyzed and discussed in detail in Chapters 5 and 6 respectively.

2.1 The Phenomenon of Electron Runaway

The presence of a toroidal electric field (**E**) in a tokamak gives rise to the phenomenon of electron runaway. An electron in the plasma experiences a force equal to $\mathbf{F}_e = -e\mathbf{E}$ and a drag force resulting from Coulomb interactions with plasma ions and electrons. The drag force ($\mathbf{F}_d$) is conveniently written in the form:

$$\mathbf{F}_d = m_e \mathbf{v}\, \nu_{coll}(v) \tag{2.1}$$

where m_e is the electron rest mass, v the electron velocity and $\nu_{coll}(v)$ is the collision frequency. For a (non-relativistic) test electron moving much faster than thermal electrons, $\nu_{coll}(v)$ has a v^{-3} dependence and is for a Maxwellian distribution approximated by:

$$\nu_{coll}(v) = \frac{e^4 n_e \ln\Lambda}{4\pi\varepsilon_0^2 m_e^2 v^3}(2+Z_{eff}) \tag{2.2}$$

Here e is the electron charge, n_e the electron density, $\ln\Lambda$ the Coulomb logarithm, ε_0 the vacuum permittivity and Z_{eff} the effective charge number of the ions. Note that several publications give the factor (Z_{eff}) instead of ($2+Z_{eff}$), neglecting electron-electron collisions. The expression obtained in that case is only valid for thermal electrons ($v \approx v_{th}$), for which the electron-ion collisions dominate the drag. A derivation of the drag force for the above case of $v \gg v_{th}$ is given in appendix A.

Electrons with velocities exceeding the critical velocity:

$$v_{crit} = \sqrt{\frac{e^3 n_e \ln\Lambda (2+Z_{eff})}{4\pi\varepsilon_0^2 m_e E}} \tag{2.3a}$$

at which $\mathbf{F}_d$ balances $\mathbf{F}_e$ are continuously accelerated and are called 'runaway electrons'. Runaway electrons have therefore a kinetic energy of at least W_{crit}:

$$W_{crit} = \frac{1}{2} m_e v_{crit}^2 \approx 2.2\,(2+Z_{eff})\,\frac{n_e[10^{19}\,m^{-3}]}{E[V/m]}\ keV \qquad (2.3b)$$

eq. (2.3) gives the correct expression only if $W_{crit} >> T_e$, the situation valid in most tokamak experiments. The electric field for which a thermal electron will run away is called the critical field E_{crit} (about twice the Dreicer field [Dre-59] often encountered in literature) given by:

$$E_{crit} = \frac{e^3 n_e Z_{eff} \ln\Lambda}{4\pi\varepsilon_0^2 m v_{th}^2} \approx \frac{4\,Z_{eff}\,n_e[10^{19}]}{T_e[keV]} \qquad (2.4)$$

As long as the electric field E applied to the plasma is much smaller than this critical field ($\varepsilon \equiv E/E_{crit}(Z_{eff}=1) << 1$) the distribution function of the electrons stays close to a Maxwellian and only an exponentially small fraction of the electrons will run away. This is the case for all the experiments reported about in this thesis. For the discharges investigated typical values are: $E/E_{crit} = 0.02\text{-}0.03$ and $W_{crit} \approx 100$ keV.

The above derived quantities apply for a test electron in the plasma. For an exact kinetic treatment of the total electron population the Fokker Planck equation must be solved to determine the velocity distribution function. The Fokker Planck equation takes into account the change of the distribution function as a result of Coulomb collisions. The runaway production rate, i.e the number of runaways acquiring velocities higher than v_{crit} can be obtained from this calculations, as shown in Chapter 4. Runaway electrons of more than 20 MeV, the ones studied in this thesis, are decoupled from the bulk electrons and their dynamics are the same as for test particles. The use of the Fokker Planck equation does not contribute to a more accurate description of their velocity distribution.

The runaway electrons in a plasma have some special properties that will be considered in the subsequent sections and chapters. These include the displacement of the runaway drift orbit with respect to the magnetic flux surfaces (Section 2.2), the maximum attainable energy (Section 2.3), runaway transport due to magnetic turbulence (Section 2.4), interaction of runaways with waves (Section 2.5) and methods to diagnose these runaways (Section 2.6 and Chapter 3).

2.2 Runaway Orbits

The orbit of a runaway electron in a tokamak is shifted from the magnetic surfaces as a result of the curvature and gradient B drift. This shift is a function of the energy of the electron and of the radial profile of the current density. A basic expression will be derived in this section.

The orbit of a runaway electron in a tokamak consist of three components:
i) a fast gyration about the magnetic field lines with frequency ω_{ce}, Larmor radius ρ_L^e and velocity $v_\perp$:

$$\omega_{ce} = \frac{eB}{\gamma m_e}; \qquad \rho_L^e = \frac{\gamma m_e v_\perp}{eB}; \tag{2.5}$$

where $\gamma = 1/\sqrt{1-v^2/c^2}$ is the relativistic factor and c the velocity of light.
ii) the helical motion of the guiding center, which is the center of mass of the electron averaged over the gyration motion, along the field lines:

$$\mathbf{v}_{//} = v_\phi \hat{\mathbf{e}}_\phi + \frac{v_\phi B_\theta}{B_\phi}\hat{\mathbf{e}}_\theta - \frac{v_\phi B_z}{B_\phi}\hat{\mathbf{e}}_z \tag{2.6}$$

where $\hat{\mathbf{e}}_\phi$, $\hat{\mathbf{e}}_\theta$ and $\hat{\mathbf{e}}_z$ are the unit vectors in the toroidal, poloidal and vertical direction respectively.
iii) the drift of the guiding center as a result of the curvature and gradient of the magnetic field (the $\mathbf{E} \times \mathbf{B}$ drift is neglected, because it is generally much smaller than the other terms):

$$\mathbf{v_d} = \frac{1}{R\omega_{ce}}\left(v_{//}^2 + \frac{1}{2}v_\perp^2\right)\hat{\mathbf{e}}_z \tag{2.7}$$

The effect of the drift velocity is the displacement (δ) of the runaway orbit away from the magnetic flux surface. This is recognized from the conservation of toroidal angular momentum:

$$J_\phi = \gamma m_e R v_\phi - e\psi \tag{2.8}$$

where ψ is the poloidal magnetic flux:

$$\psi(r) = \int_0^r B_\theta R\, dr = \frac{\mu_0 R_0}{2}\int_0^r \frac{dr''}{r''}\int_0^{r''} dr'\, r'\, j(r') \tag{2.9}$$

In which μ_0 is the vacuum permeability and j the current density. Conservation of J_ϕ yields:

$$\Delta\left(\frac{\gamma m_e R v_\phi}{e}\right) = R B_\theta \Delta r \qquad (2.10)$$

Δr can be regarded as the displacement from the flux surface: $\Delta r = \delta$. The kinetic energy $W = p^2/2\gamma m_e$ and the magnetic moment $\mu = p_\perp^2/2\gamma m_e B$ are to a good approximation constants of the motion on one poloidal turn. Therefore the toroidal momentum can be defined as $p_\phi = \gamma m_e v_\phi \equiv \sqrt{W - \mu B}$ and with $\Delta B = \Delta R\, B/R$ the above expression becomes:

$$\delta = \frac{p_\phi}{eRB_\theta}\left(1 + \frac{p_\perp^2}{2p_\phi^2}\right)\Delta R \qquad (2.11)$$

For runaway electrons $p_\phi >> p_\perp$ so that the second term in brackets can be neglected. The change of the coordinate R, averaged over one poloidal turn, is given by $\Delta R = r$. The displacement δ of the runaway orbit from the magnetic surface is given by:

$$\delta \approx \frac{\bar{q} p_\phi}{e B_\phi} \approx \frac{\bar{q} W}{ecB_\phi} \qquad (2.12)$$

where $\bar{q} = \langle r/B_\theta \rangle B_\phi/R$ is the average safety factor along the runaway orbit. Note that for large shifts $\bar{q}$ becomes a function of δ itself. The easiest calculation of δ is then obtained by equating P_ϕ for the left and right intersections of the runaway orbit with the equatorial plane.

The same result as in eq. (2.12) is obtained for electrons displaced from the magnetic axis by the condition that the Lorentz force on the electron as provided by the poloidal magnetic field can balance the centrifugal force:

$$\frac{\gamma m_e v_\phi^2}{R} = e\, v_\phi B_\theta \qquad (2.13)$$

The poloidal projection of the orbit can be approximated by a circle. This is illustrated by describing the poloidal orbit by a velocity $v_\theta = v_\phi B_\theta/B_\phi$ and the drift velocity v_d. From the equations of this orbit (see Fig.2.1 for the appropriate geometry and meaning of x) $dx/dt = -v_\theta \sin\theta$ and $dr/dt = v_d \sin\theta$ it follows that the characteristic orbit is described by the following equation, representing circles centred at $x = \delta$:

$$\frac{dr}{dx} = -\frac{v_d}{v_\theta} \approx \frac{v_\phi B_\phi}{R\, \omega_{ce} B_\theta} \approx \frac{\delta}{r} \qquad (2.14)$$

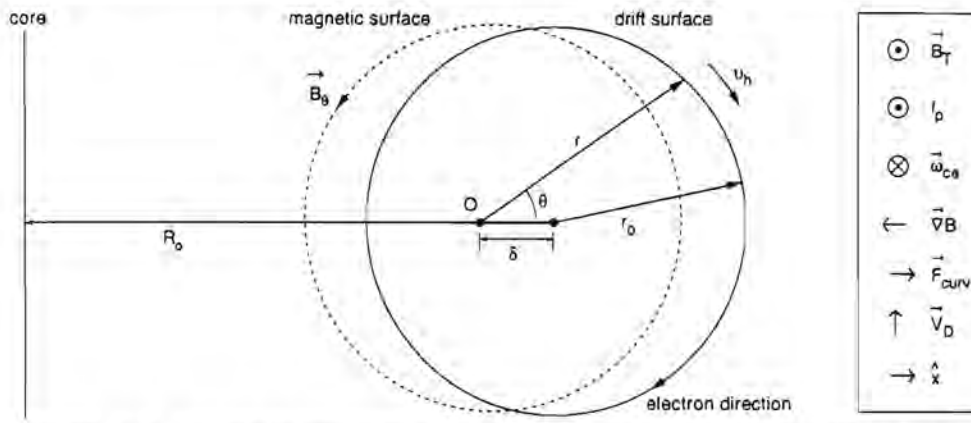

Figure 2.1: *The poloidal projection of the runaway electron orbit. The magnetic surface and the orbit displacement δ are indicated.*

A more exact treatment of the runaway drift orbits and the displacements for different current distribution is given by Zehrfeld et al. [Zeh-81]. They consider the effect of the electric field and hence the increasing runaway energy on the runaway motion. Doing so J_ϕ is not exactly conserved, but the cross-sectional area of the drift orbit is identified as an adiabatic invariant. This causes, in addition to the displacement of the orbits, the occurrence of a separatrix on the drift orbits. For high enough energy of the runaway electrons drift orbits are no longer closed and the runaways on these orbits get lost from the plasma before the drift surface touches the limiter. The condition on the runaway energy for this is approximately given by:

$$W_{max}\,(\mathrm{MeV}) \approx \frac{R_0}{a}\,\frac{I_p}{I_A}\,\frac{c}{v_{//}}\,\frac{B_\theta(r^*)}{[1+s'(a)]B_\theta(a)} \qquad (2.15)$$

where $I_A = 4\pi m_e c/\mu_0 e \approx 17$ kA is the Alfvén current. The outermost point of the runaway orbit is given by $r^*=r - s(r)$, $s(r)$ being the Shafranov shift, i.e the shift between the geometrical centre and the centre of the magnetic flux surface. $s'(a)$ is the derivative of this shift at the plasma boundary and depends on the pressure and current profiles. The above condition is plotted in Fig. 2.2 for different current profiles as a function of minor radius. It is observed that for peaked current profiles the separatrix appears near the maximum of the poloidal magnetic field: higher energies can not be confined by a shift of the orbit to higher minor radius. For a flat current density profiles there is no separatrix.

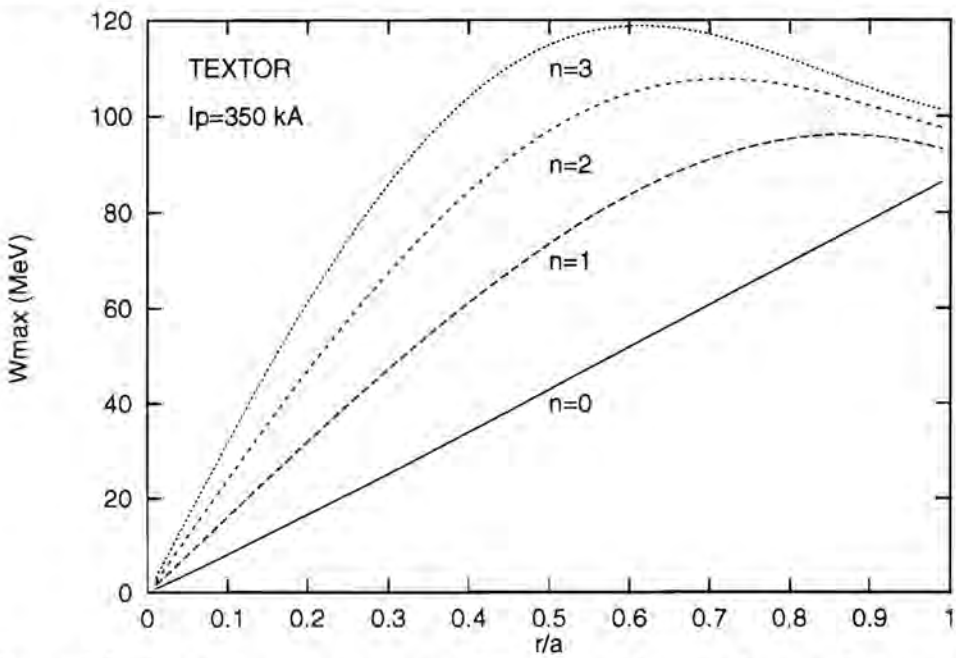

Figure 2.2: *The maximum runaway energy that can be confined as a function of minor radius for different current density profiles. A separatrix of the runaway drift orbit appears for peaked profiles where W_{max} is maximal. For flat profiles no separatrix appears. All profiles are parametrized by $(1-(r/a)^2)^n$.*

2.3 Energy Limit of Runaway Electrons

Once an electron exceeds the critical velocity (eq. 2.3) it is continuously accelerated and can reach energies of several tens of MeV. The energy can be limited by several effects :

1) synchrotron radiation limit
2) orbit shift limit
3) time limit
4) 'magnetic field ripple' limit
5) instabilities

Ad 1) For a relativistic electron moving on a curved path of radius R_{curv} the total power P^e radiated by synchrotron emission by the electron is given by (see Section 3.2 for a detailed treatment):

$$P^e = \frac{2}{3} \frac{r_e m_e c^3}{R^2_{curv}} \gamma^4 \qquad (2.16)$$

where r_e is the classical electron radius and R_{curv} for a helical orbit is approximated by [Rus-91]:

$$\frac{1}{R_{curv}} \approx \frac{1-\Theta^2}{R_0} + \frac{eB\Theta}{m_e c\gamma} \qquad (2.17)$$

Here we introduce the pitch angle of the runaway electron:

$$\Theta = \frac{v_\perp}{v_{//}}$$

Equating this power loss to the power absorbed from the electric field, $P_{gain}=ecV_{loop}/2\pi R_0$ the maximum attainable γ is limited to:

$$\gamma_{max} = \frac{-R_0 eB}{2m_e c}\left(\frac{\Theta}{1-\Theta^2}\right) + \frac{R_0}{2(1-\Theta^2)}\sqrt{\left(\frac{eB\Theta}{m_e c}\right)^2 + 4(1-\Theta^2)\left(\frac{3\varepsilon_0 V_{loop}}{eR_0{}^3}\right)}^{1/2} \qquad (2.18)$$

For the typical TEXTOR values (V_{loop}=1 V, R_0=1.75 m, B=2.25 T and Θ=0.12) the synchrotron radiation limits the maximum energy to W_{max}^{syn} = 25 MeV. Considerably higher values can be obtained during a disruption when the loop voltage is much larger. Changes in Z_{eff} will also affect this limit by the change in loop voltage and pitch-angle Θ (see Section 3.3).

Ad 2) In the previous section the dependence of the orbit shift on the energy was deduced. To keep a runaway confined the orbit shift must be smaller than the minor radius a. Using equation 2.12 this limits the maximum energy for TEXTOR to (q_a=3.8 for I_p=350 kA):

$$W_{max}^{shift} = \frac{a\ e\ c\ B_\phi}{q_a} \approx 80 \text{ MeV} \qquad (2.19)$$

Although this limit is much higher than the synchrotron radiation limit, it can be the limiting factor for runaway electrons whose original orbits do not coincide with the magnetic axis. Runaways moving on an orbit of radius r_{re} are marginally confined if δ=a-r_{re}. For more peaked current density profiles higher energy runaway electrons can be confined, as follows from Fig. 2.2.

Drift separatrices will not occur under standard TEXTOR conditions, since this requires electron energies in excess of 100 MeV, much higher than W_{max}^{syn} . However, for lower plasma currents (for instance during disruptions, or in the current decay phase) condition (2.15) can be satisfied at considerably lower energies.

Ad 3) The total time available for acceleration poses a trivial limit to the attainable electron energy. Neglecting radiation losses, the maximum energy a runaway can reach as a function of time is determined by :

$$W_{max}(t) = \frac{ec}{2\pi R_0}\int V_{loop}dt = \frac{ec}{2\pi R_0}\Phi(t) = 27\,\Phi(t)\ \text{MeV} \qquad (2.20)$$

where $\Phi(t)$ is the flux swing applied to the plasma. Comparing Eqs. (2.18) and (2.20) it follows that as long as $\Phi(t) < 0.8$ this determines the maximum runaway energy. For standard TEXTOR runaway discharges $\Phi(t) = 0.8$ at about t=0.6 s, while the total discharge duration is 4 s.

Ad 4) Due to the finite number of coils N to generate the toroidal magnetic field, this field is slightly modulated as a function of the toroidal angle ϕ. Runaway electron experience this modulation at frequencies:

$$\omega = \frac{nNc}{R_0} \qquad (2.21)$$

n being the harmonic number. Laurent and Rax [Lau-90] have shown that if the electron cyclotron motion is in resonance with this frequency the electrons are scattered in pitch angle Θ. This is not a direct energy loss, but the increase in Θ is accompanied by an enhancement of P^e, and therefore a lower synchrotron radiation limit. Depending on the harmonic resonance and the amplitude of the field ripple an energy blocking of the runaways would occur at energies (for TEXTOR, N=16):

$$W_{max}^{ripple} = \frac{eBR_0E_0}{nNm_ec} \approx \frac{70}{n}\ \text{MeV} \qquad (2.22)$$

Whereas the first harmonic resonance energy is much larger than the radiation limit, the second and lower harmonics can under certain conditions be reached. However, according to ref. [Lau-90], the strength of the resonance decreases with increasing harmonic number and for the ripple at TEXTOR only the second harmonic resonance is expected to be a candidate to block a further increase of the energy, see Section 6.5.

Ad 5) The free energy present in the plasma due to the non Maxwellian component in the electron velocity distribution function can be exchanged between resonant electrons and the plasma oscillations. When a certain threshold is exceeded instabilities can be excited. These instabilities have been investigated experimentally [Ali-75,Bro-78] and theoretically [Par-78]. They either limit the runaway energy or the runaway confinement. However, the runaway energies for which these instabilities are excited are in the range 100 keV- 1 MeV. The observation of synchrotron radiation

at TEXTOR, the subject of this thesis, requires the presence of 20 MeV runaway electrons. This instability determined energy limit is therefore not considered here. Experimentally, a runaway instability was observed at considerably higher energies. These observations are presented and discussed in Chapter 6.

2.4 Runaway Transport

The processes of energy and particle transport in thermonuclear plasmas are poorly understood and form a major research area. The measured diffusivity for electrons are up to two orders of magnitude larger than expected from neo-classical theory. Anomalous transport is thought to be due to micro turbulence, of either electrostatic or magnetic origin. Runaway electrons are mainly sensitive to magnetic turbulence so that they can be used to distinguish between the two possible classes of anomalous transport. Several attempts in this direction have already been carried out [Myn-81, Kwo-88, Myr-92, Rod-94]. In these experiments the runaway confinement time is estimated from the flux of runaway electrons to the limiter or other solid structure. From a comparison with the thermal electron diffusivity and including the fact that runaway orbit are shifted away from magnetic surfaces, a magnetic turbulence level of $(\tilde{B}_r/B)=10^{-5}$ - 10^{-2} was deduced.

Cross field transport in tokamaks is in general governed by several processes:

<u>-collisional transport,</u> denoted classical transport in a cylindrical system and neo-classical in a toroidal geometry. The effect of Coulomb collisions can be treated as a random walk process. The associated diffusion coefficient D is determined by a step-length ΔL and step-time τ, being the Larmor radius ρ^e_L and the electron collision time τ_{col} respectively:

$$D = \frac{<\Delta L>^2}{\tau} = \frac{\rho^e{}_L{}^2}{\tau_{col}} \qquad (2.23)$$

If the magnetic field is curved, the neo-classical case, the step lengths are increased because the particles can traverse a distance larger than the electron Larmor radius across the magnetic field before undergoing a collision. This distance depends on the collisionality. Since runaway electrons have a low collisionality the main effect arises from the banana-effect: trapped particles can complete a banana orbit (see for instance [Wes-84]) in less than a collision time. The step length is in that case determined by the banana width. However, in view of the extremely low collisionality and the fact that the high energetic runaway electrons as considered in this thesis will not be trapped, the neo-classical runaway diffusion coefficient is expected to be vanishingly small.

<u>-transport induced by electrostatic fluctuations</u>. Turbulent electrostatic fields give rise to ExB transport if the density oscillations are in phase with the electric fluctuations: the particle flux Γ is

written as: $\Gamma = \langle \tilde{n}\tilde{v}_r \rangle$, where $\tilde{v}_r = \tilde{E}/B$ is the $\tilde{E}$xB drift velocity and < > denotes averaging over many fluctuation periods. A radial diffusion coefficient can heuristically be attributed to this process by the random walk estimate:

$$D_r = \frac{(\Delta L)^2}{\tau} = \langle \sigma_r^2 \tau \rangle \approx \pi R q \frac{1}{v_{//}} \left(\frac{\tilde{E}}{B} \right)^2 \qquad (2.24)$$

where for the correlation time τ the characteristic transit time $\tau = \pi qR/v_{//}$ is substituted. It is noted that, due to the inverse dependence on the velocity, this transport process can become negligibly small for runaway electrons.

-transport induced by magnetic fluctuations. In the absence of collisions electrons will follow the magnetic field lines without being knocked out of the orbit. However, the electrons exhibit always a certain drift, which can be large for highly relativistic electrons as was shown previously (Section 2.2). Neglecting this effect in the first approximation and therefore assuming that the electrons follow the field lines, they can be used to probe magnetic stochasticity. The concept is that runaway electrons diffuse because they travel along the fluctuating field lines, which diffuse themselves. To describe this process quantitatively correctly has not been accomplished yet by the physical community. An upper estimate for the transport is given by Rechester and Rosenbluth [Res-78]. In the case of a fully stochastic, static B field an estimate of the diffusion of the field lines yields:

$$D_r \sim v_{//} D_{st} \sim \pi q R \, v_{//} \left(\frac{\tilde{B}_r}{B} \right)^2 \qquad (2.25)$$

Where $D_{st} \sim L_{//} (\tilde{B}_r/B)^2$ is the diffusion coefficient of the field lines and $L_{//}$ is the parallel correlation length along the field lines, approximated by $L_{//} = \pi qR$. Note that this diffusion process scales with the particle velocity, and is therefore expected to be dominant for runaway electrons. However, the conditions under which eq. (2.25) is valid (fully stochastic and static B-field) are highly debatable under tokamak operation conditions [Lop-93].

Furthermore, the effect of the drifts must still be taken into account. Since the runaway orbits and magnetic surfaces are shifted by δ, they make excursions of this amount away from the magnetic surface. If the perpendicular correlation length of the turbulence (l_{turb}) is smaller than δ, the effect of the fluctuations is averaged out. Mynick and Strachan [Myn-81] calculated the reduction of the transport as a function of $f = \delta/l_{turb}$ and found that for f=3 this reduction can already be as large as a factor 10^3. The presence of regions with low turbulence can also reduce the runaway transport [Heg-93]. Experimental results and a discussion of relativistic runaway

transport in a stochastic field, orbit shift effects and regions of good magnetic surfaces are presented in Chapter 5.

2.5 Wave Interaction

Relativistic runaway electrons are decoupled from the plasma with respect to Coulomb collisions. However, they can still interact with collective plasma oscillations. For oblique waves with frequency ω_k the phase velocity in the electron direction can be indefinitely high allowing a resonant interaction. The resonance condition is:

$$\omega_k - n\,\omega_{ce} = k_{//}\,v_{//} \qquad (2.26)$$

where the index // represents the direction along the magnetic field, ω_{ce} is the electron cyclotron frequency, n is the harmonic number, v the electron velocity and k the wave number. (Only the component along the field line contributes as a result of the averaging over the gyration motion). For n=0 the interaction is called Cerenkov resonance. The wave will grow unstable if the electron distribution has a positive slope: $df(v)/dv > 0$. Energy is exchanged between the resonant electrons and the wave. For negative slopes of the distribution function the wave will be Landau damped.

For negative n, the anomalous Doppler resonance, longitudinal energy of the electron is converted into transverse energy. This is conveniently illustrated by a quantum mechanical consideration. Let the electron emit a quantum of energy $\hbar\,\omega_k$ and parallel momentum $\hbar\,k_{//}$. Then the electron energy change is equal to: $\delta W = \delta W_{//} + \delta W_{\perp} = -\hbar\,\omega_k$. Due to momentum conservation the longitudinal energy change is equal to $\delta W_{//} = -v_{//}\,\hbar\,k_{//}$, from which it follows that $\delta W_{\perp} = -\hbar\,(\omega_k - v_{//}k_{//})$, which is positive in the case of anomalous Doppler resonance. Furthermore this shows that with a small energy exchange with the wave ($\hbar\,\omega_k$) the perpendicular energy of the electron can grow appreciably ($\hbar\,\omega_{ce}$), since $\omega_{ce} >> \omega_k$.

The excited oscillations may grow unstable for an electron velocity distribution function even without positive slope. This is experimentally observed in the so-called slide-away regime [Sch-94, Par-86, Oom-76].

For positive n the resonance is called the normal Doppler resonance. These high frequency waves ($\omega_k > \omega_{ce}$) convert transverse energy of the electron into longitudinal energy. Runaway electrons are not expected to excite unstable oscillations by this resonance as a result of the comparatively small perpendicular energy of the runaway electrons.

2.6 Runaway Diagnostics

Several techniques can be employed to diagnose runaway electrons. They are based on runaway induced reactions which result in the emission of X-rays or neutrons, or on the emission of

synchrotron radiation. Detection of the latter is the main diagnostic method used in this thesis, which is treated in detail in a separate chapter, Chapter 3. In this section we will focus on the X-ray and neutron emission events, that are used as complimentary information on the behaviour of the runaway electrons in TEXTOR.

Processes that lead to x-ray (γ) and neutron (N) production are classified as follows:

- *plasma bremstrahlung (γ)*: Although the collision frequency becomes very low for runaway electrons, they continue to have Coulomb interaction with plasma ions, resulting in the emission of photons. This emission has a continuous energy spectrum up to the kinetic energy of the electron.
- *limiter bremstrahlung (γ)*: When a runaway electron strikes a solid state structure, it is slowed down as a result of collisions. This slowing down is accompanied by the emission of a continuous spectrum of photons.
- *photo-nuclear processes (γ,N) and subsequent radioactive decay:* The photons emitted by electrons interacting with the limiter may, instead of leaving the limiter, interact with nuclei and cause photo-nuclear processes. The energy of the photon can be high enough to break up the normally stable nucleus and cause photon and neutron emission. For this process, however, a threshold energy of the photon is required to overcome the binding energy of the emitted particle. For neutron emission of carbon this threshold energy is about 10 MeV. The residual nuclei may become radio-active and analysis of the limiter material can give information on the energy of the impinging electrons [Bar-81]. For TEXTOR, however, this analysis is not performed.
- *electro-desintegration (N)*: High energy electrons in the plasma can interact with the plasma ions and disintegrate them, resulting in neutron emission in the case of a deuterium plasma. The energy threshold of this process is lower than in the previous case and amounts to a few MeV.
- *electron-positron pair production (γ)*: Energetic collisions of runaway electrons with nuclei can produce electron-positron pairs. The natural threshold for this process is 1.02 MeV. For typical tokamak densities and electron energies the cross-section of this process is too low to be detectable.

From this list it may become clear that simultaneous detection of neutrons, x-rays and their energies is a necessary condition to establish the origin of the radiation. This measurement is provided by the liquid scintillator detector of the type NE-213 used on TEXTOR. An incident neutron generates recoil protons by means of (n,p) elastic scattering, while an incident photon produces Compton scattered electrons. These charged particles excite the organic molecules and produce fluorescence, measured by photo-multipliers. The excited states have different decay times, and the fraction of states with the longest life time depends on the stopping power which is larger for the recoil protons than for the Compton scattered electrons. This provides the opportunity to discriminate between neutron and photon induced events on the basis of pulse shape analysis. The system operational at TEXTOR [Hoe-94] can process count rates of up to 3×10^5 s^{-1}.

The detector can be aligned either tangentially or radially to the plasma current. Almost complete N/γ discrimination is obtained for electron energies ≥ 0.1 MeV and corresponding proton energies ≥ 0.8 MeV. The pulse height (energy) resolution is about 8 % for 2.5 MeV protons.

APPENDIX A

THE DRAG FORCE

The runaway phenomenon is based on the fact that the drag force electrons experience in a plasma as a result of Coulomb interactions with plasma electrons and ions decreases with increasing velocity. A short derivation of this drag force is therefore justified.
If an electron undergoes a Coulomb interaction in the plasma its momentum is changed. The drag force is defined as the change of the parallel momentum due to collisions:

$$F_d = \left(\frac{\Delta p_{//}}{\Delta t} \right)_{coll} \quad (A.1)$$

This can be cast in the form:

$$F_d = \left(\frac{dW}{dx} - \frac{m_e v^2 \gamma}{2} \frac{d\Theta^2}{dx} \right)_{coll} \quad (A.2)$$

where $W=\sqrt{(c^2p^2+m_e^2c^4)}$, $\Delta x=v\Delta t$, and γ the relativistic factor. It has further been assumed that the pitch angle $\Theta = v_\perp/v_{//} \approx p_\perp/p \ll 1$. The first term on the right hand side is the stopping power and describes the energy loss and the second term describes the pitch angle scattering of the electron. For electron-ion collisions the cross-section for the scattering process is given by (assume $m_i = \infty$):

$$\left(\frac{d\sigma}{d\Theta} \right)_{e\text{-}i} = \frac{e^4 Z^2}{2\pi\varepsilon_0{}^2 m_e{}^2 v^4 \gamma \Theta^3} \quad (A.3)$$

and the energy transfer

$$(dW)_{e\text{-}i} = 0 \quad (A.4)$$

For electron-electron collisions this becomes:

$$\left(\frac{d\sigma}{d\Theta} \right)_{e\text{-}e} = \frac{e^4}{2\pi\varepsilon_0{}^2 m_e{}^2 v^4 \gamma \Theta^3} \quad (A.5)$$

$$(dW)_{e\text{-}e} = -\frac{1}{2} m_e v^2 \gamma^2 d\Theta^2 \quad (A.6)$$

Now the drag force is calculated by averaging the two contributions over the collisions as follows:

$$\left(\frac{d\Theta^2}{dx}\right)_{coll} = n \int_{\Theta_{min}}^{\Theta_{max}} \Theta^2 \frac{d\sigma}{d\Theta} d\Theta \qquad (A.7)$$

where n is either the electron or ion density. The contributions of each species can be summed up with the following result:

$$F_d = - \frac{e^4 n_e \ln\Lambda}{4\pi\varepsilon_0^2 m_e v^2} \left(1 + \frac{Z_{eff} + 1}{\gamma}\right) \qquad (A.8)$$

Here $\ln\Lambda = \ln(\Theta_{max}/\Theta_{min})$ is the Coulomb logarithm and $Z_{eff}=\sum_i n_i Z_i^2/n_e$. The second term in this expression accounts for the pitch angle scattering and disappears for the higher energies. Nevertheless, the drag force remains finite owing to the energy exchange in electron-electron collisions.

CHAPTER 3

SYNCHROTRON RADIATION IN A TOKAMAK

Theory, Measurements and Analysis

3.1 Introduction

The measurements described in this thesis on runaway electrons in the TEXTOR tokamak are mainly performed by diagnosing the synchrotron radiation emitted by relativistic electrons. As these investigations are the first of their kind employing this radiation a brief summary of the theory behind the radiation and the application to the tokamak situation is justified.

It is well known that accelerated charged particles emit electro-magnetic radiation, as follows from Maxwell theory. For relativistic electrons in a magnetic field this is called synchrotron radiation. In several branches of physics this radiation is encountered: astrophysicists use synchrotron radiation to obtain information about galaxies and pulsars; in electron accelerators synchrotron radiation limits the attainable energy; in atomic and molecular physics this radiation is used as a light source for spectroscopic investigations; there are many more applications, taking advantage of the continuous and tunable spectrum [Cat-90].

Special devices are built to generate synchrotron radiation. Apart from the circular electron accelerator (the so-called synchrotrons that gave the electron radiation its name) where the radiation is in fact a by-product, other examples are the free electron lasers. Here a beam of relativistic electrons is forced to oscillate in a periodic magnetic field. Laser working is obtained by putting mirrors at each end of this undulator. Bunched electrons travel through the undulator, amplifying the radiation produced by previous bunches. By varying the electron energy or the frequency of the undulator the wavelength of the laser can rapidly be tuned. A good example is the Rijnhuizen FEL, FELIX [Bak-93], todays most versatile free electron laser facility, which is tunable in the infrared wavelength range from 6-110 μm. Also at FOM Rijnhuizen, a free electron maser is under construction. This apparatus, the FOM Fusion FEM [Urb-93], is designed for plasma heating and profile control in tokamaks and will produce 1 MW of radiation in the frequency range 150-250 GHz.

A similar kind of radiation is encountered in thermonuclear research, emitted by electrons gyrating in the magnetic field. For the bulk electrons (not relativistic) this radiation is called cyclotron radiation, emitted at the gyration frequency. The radiation at the second harmonic is employed in most present day tokamaks to measure the electron temperature. Higher harmonics of the cyclotron radiation, generated predominantly by slightly relativistic electrons (W_{kin} <

$W_0=m_ec^2$, the electron rest energy), are also called synchrotron radiation in nuclear fusion literature.
In the context of this thesis by synchrotron radiation is meant the infrared radiation emitted by relativistic electrons in the energy range of roughly 10-40 MeV as a result of their helical orbit. Whereas for slightly relativistic electrons only the lower harmonic cyclotron frequencies contribute to the emitted power, for higher energies the highest harmonics contribute most to the radiation, resulting in a continuous spectrum. For relativistic electrons the parallel motion determines the main characteristics of the spectrum. Another difference with the lower energetic electrons is the fact that due to the higher toroidal revolution frequency and the lower cyclotron frequency the effective radius of curvature of the electron orbit is predominantly determined by the major radius of the guiding center orbit, rather than by the Larmor radius of the electron. Nevertheless, as will be shown in Sec. 3.3 the Larmor motion cannot be neglected.

This chapter is devoted to the various aspects of this synchrotron radiation: a brief summary of the theory (Sec. 3.2), synchrotron radiation in tokamaks (Sec. 3.3), a description of the measurement setup used at TEXTOR (Sec. 3.4), a discussion of a typical example of synchroton radiation measurements (Sec. 3.5) and an overview of the methods used to deduce the runaways parameters like energy and perpendicular momentum from these observations (Sec.3.6).

3.2 Theory of Synchrotron Radiation

A brief summary of the synchrotron radiation is given in a classical treatment, following the work of Schwinger [Sch-49] and Sokolov [Sok-68]. This classical description is valid as long as quantum effects do not come into play. In ref. [Sok-68] it is shown that this does not occur for energies lower than :

$$W = m_0c^2\left(\frac{m_0cR}{\hbar}\right)^{1/5} = O(250\ \text{MeV}).$$

Electrons with energies higher than 80 MeV cannot be confined in TEXTOR, because for these energies the runaway orbits are shifted an amount larger than the minor radius away from the magnetic surface, see Sec. 2.3. The classical theory is thus sufficient for the work described in this thesis.

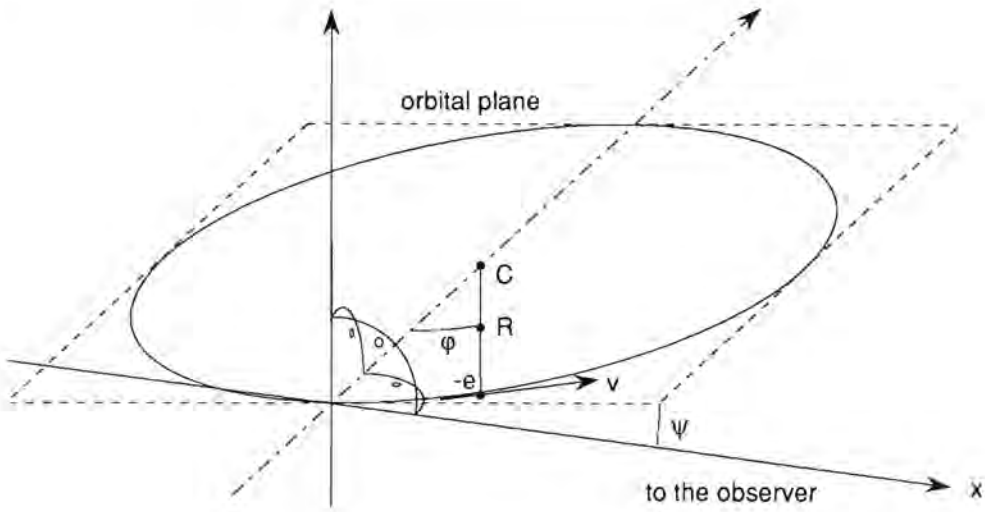

Figure 3.1: *Electron orbit in Carthesian coordinate system as used in the calculation.*

Starting point of the derivation of the spectral and angular properties of the synchrotron radiation is the general expression of the retarded vector potential **A** of a moving electron with charge e:

$$\mathbf{A}(\mathbf{r},t) = \frac{e}{4\pi} \int_{-\infty}^{+\infty} \frac{\mathbf{v}(\tau)}{l(\tau)} \delta(\tau - t + l(\tau)/c)\, d\tau \qquad (3.1)$$

Here, $l(t) = |\mathbf{r} - \mathbf{r}_e|$ is the distance from the observer at position $\mathbf{r}$ to the electron at $\mathbf{r}_e$, $\mathbf{v}$ the electron velocity the and the delta function δ accounts for the required retardation. To derive the spectral distribution of the radiation, the Fourier transform of eq. (3.1) is taken:

$$\mathbf{a}(\mathbf{r},\omega) = \frac{e}{4\pi} \int_{-\infty}^{+\infty} \frac{\mathbf{v}(\tau)}{l(\tau)} \exp[-i\omega(\tau - l(\tau)/c)]\, d\tau \qquad (3.2)$$

To proceed further use is made of the Carthesian coordinate system as shown in Fig. 3.1. The electron motion is assumed circular with $\omega_0 = v/R$, and is described by:

$$\mathbf{r}_e(t) = (r_x, r_y, r_x) = R\,(\cos\psi\sin\omega_0 t,\ 1-\cos\omega_0 t,\ \sin\psi\sin\omega_0 t) \qquad (3.3)$$

For an observer at $\mathbf{r}_0=(x_0,0,0)$ with $x_0 \gg R$, $l(t)$ is approximated by $l(t) \approx x_0 - R\cos\psi\sin\omega_0 t \approx x_0 - v\cos\psi(t - \omega_0^2 t^3/6)$. For relativistic electrons ($W \gg m_e c^2$) the radiation is concentrated in a narrow cone around $\mathbf{v}$ (as will be deduced from the angular distribution, later on). We therefore substitute: $\sin\psi \approx \psi$, $\cos\psi \approx 1$, $\beta = v/c \approx 1$, $1-\beta\cos\psi \approx 1/2\,(1-\beta^2+\psi^2)$. This results in:

$$\mathbf{a}(\mathbf{r}_0,\omega) \approx \frac{e\exp(i\omega x_0/c)}{4\pi x_0}\int_{-\infty}^{+\infty}(1,\omega_0\tau,\psi)\times\exp\{-i\omega\tau[\tfrac{1}{2}(1-\beta^2+\psi^2)+\tfrac{1}{6}\omega_0^2\tau^2]\}d\tau \qquad (3.4)$$

This integral is calculated with the help of the Airy integral and its derivative [Wat-66]:

$$\int_0^{+\infty}\cos(3zu+u^3)du = \sqrt{\frac{z}{3}}\,K_{1/3}(2z^{3/2})\,; \qquad \int_0^{+\infty}u\sin(3zu+u^3)du = \frac{z}{3}\sqrt{3}\,K_{2/3}(2z^{3/2})$$

This yields:

$$a_x(\mathbf{r}_0,\omega) = \frac{2e}{4\pi\sqrt{3}\omega_0 x_0}\exp(i\omega x_0/c)\,(1-\beta^2+\psi^2)^{1/2}K_{1/3}(\xi) \qquad (3.5.a)$$

$$a_y(\mathbf{r}_0,\omega) = \frac{-2e}{4\pi\sqrt{3}\omega_0 x_0}\exp(i\omega x_0/c)\,i\,(1-\beta^2+\psi^2)K_{2/3}(\xi) \qquad (3.5.b)$$

$$a_z(\mathbf{r}_0,\omega) = \frac{2e}{4\pi\sqrt{3}\omega_0 x_0}\exp(i\omega x_0/c)\,\psi\,(1-\beta^2+\psi^2)^{1/2}K_{1/3}(\xi) \qquad (3.5.c)$$

where $\xi = \dfrac{\omega}{\omega_0}\,(1-\beta^2+\psi^2)^{3/2}$

The radiated power through a unit area is given by the Poynting vector $\mathbf{S}$:

$$\mathbf{S} = \frac{[\mathbf{E}\times\mathbf{B}]}{\mu_0} = \frac{c}{\mu_0}[[\mathbf{B}\times\hat{\mathbf{x}}]\times\mathbf{B}] = \frac{cB^2\hat{\mathbf{x}}}{\mu_0} \qquad (3.6)$$

The magnetic field $\mathbf{B}$ is calculated from the vector potential $\mathbf{B}(\mathbf{r},t) = \mu_0[\nabla\times\mathbf{A}(\mathbf{r},t)]$. The Fourier transformation of this vector: $\mathbf{b}(\mathbf{r},\omega) = \mu_0[\nabla\times\mathbf{a}(\mathbf{r},\omega)] = (i\omega\mu_0/c)\,[\hat{\mathbf{x}}\times\mathbf{a}(\mathbf{r},\omega)]$ yields the radiated energy:

$$\int_{-\infty}^{+\infty} |S|\, dt = \frac{c}{\pi\, \mu_0} \int_0^{+\infty} |\mathbf{b}(\omega)|^2\, d\omega = \frac{\omega^2 \mu_0}{\pi\, c} \int_0^{+\infty} |\mathbf{a}_y(\omega)|^2 + |\mathbf{a}_z(\omega)|^2\, d\omega$$

$$= \frac{1}{x_0^2} \int_0^{+\infty} W_{\psi\,\phi\,\omega}\, d\omega \qquad (3.7)$$

$W_{\psi\,\phi\,\omega}$ is the energy emitted by a relativistic electron moving on a circular orbit per unit angular frequency interval $d\omega$ and per unit solid angle $d\Omega = d\psi d\phi$. The power P^e detected at x_0 is found by multiplying $W_{\psi\,\phi\,\omega}$ by the repetition frequency $c/2\pi R$. This results in the following equation, obtained by Schwinger [Sch-49]:

$$\frac{d^2P^e}{d\Omega d\omega} = \frac{c}{2\pi R} W_{\psi\,\phi\,\omega}$$

$$= \frac{e^2\omega^2}{24\pi^4 \varepsilon_0 \omega_0^2 R} (1-\beta^2+\psi^2)^2 \left[K_{1/3}^2(\xi) + \frac{\psi^2}{(1-\beta^2+\psi^2)} K_{2/3}^2(\xi) \right] \qquad (3.8)$$

Integrating this equation over the solid angle yield the spectrum of the radiation. This can be done analytically with the use of some relations of the modified Bessel functions (see [Sch-49]), with the result:

$$\frac{dP^e}{d\omega} = \frac{e^2}{4\pi\varepsilon_0 c} \frac{1}{\pi\sqrt{3}} \frac{\omega}{\gamma^2} \int_a^{+\infty} K_{5/3}(\xi)\, d\xi \qquad (3.9)$$

Here $a = 2\omega(1-\beta^2)^{3/2}/3\omega_0$ and $\gamma^2 = (1-\beta^2)^{-1}$.

To obtain the angular distribution of the synchrotron radiation or the total emitted power by the electron Eq. (3.8) can be integrated. It is easier to calculate the Poynting vector in Eq. 3.6 directly without making use of the Fourier transform.

$$P^e = \int |S| \frac{dt}{d\tau} r^2\, d\Omega = \int S\, (1-\beta\cos\theta)\, r^2\, d\Omega \qquad (3.10)$$

From $\mathbf{B} = \mu_0 [\nabla \times \mathbf{A}]$ and the Liénard Wiechert potential $\mathbf{A} = \frac{-e\, c\, \beta}{4\, \pi\, (1-\hat{\mathbf{x}}\cdot\beta)}$ [Oha-88] the magnetic field is given by:

$$\mathbf{B} = \frac{-e}{4\pi\varepsilon_0 c r^2 (1-\hat{\mathbf{x}}\cdot\beta)^3} \left([\hat{\mathbf{x}}\times(\hat{\mathbf{x}}-\beta)]\, (1-\beta^2) + \frac{r}{c} [\hat{\mathbf{x}}\times[\hat{\mathbf{x}}\times[(\hat{\mathbf{x}}-\beta)\times\dot{\beta}]]] \right) \qquad (3.11)$$

Substituting this expression in eq. (3.6) and (3.10) we obtain the instantaneous angular distribution:

$$\frac{dP^e}{d\Omega} = \frac{c\, e^2\, \beta^4}{4\pi\varepsilon_0\, 4\pi R^2} \left(\frac{(1-\beta\cos\theta)^2 - (1-\beta^2)\sin^2\theta\sin^2\phi}{(1-\beta\cos\theta)^5} \right) \tag{3.12}$$

This function is plotted in Fig.3.3 in the orbital plane (ϕ=0) as a function of $\zeta=\gamma\cos\theta$. The width of the aperture is approximately $\delta\approx 1/\gamma$.
Finally, the total power radiated by an electron is given by:

$$P^e = \frac{2}{3}\frac{r_e m_e c^3}{R^2}\,\beta^4\gamma^4 \tag{3.13}$$

where $r_e = e^2/(4\pi\varepsilon_0 m_e c^2) = 2.82\times10^{-15}$ m is the classical electron radius.

3.3 Synchrotron Radiation in Tokamaks

To apply the above derived theory of synchrotron radiation to the tokamak case, the main problem encountered arises from the orbit of the electrons not being perfectly circular. The orbit of collisionless particles in a tokamak is composed of two parts: the guiding center motion along the helical field lines and the gyration around the field lines with frequency $\omega_{ce}=eB/\gamma m_0$ and radius $\rho_L=\gamma m_0 v_\perp/eB$. Therefore the radius of curvature R_{curv} of the electron orbit does not equal the major radius R_0 of the tokamak but depends strongly on the perpendicular velocity $v_\perp$ of the electron. This radius of curvature is plotted in Fig.3.2a as a function of the phase of the gyration motion for different perpendicular velocities, according to the vector equation for the radius of curvature of a bent helix [Bro-88]:

$$R_{curv}^2 = \frac{\dot{\mathbf{r}}^6}{(\dot{\mathbf{r}} \times \ddot{\mathbf{r}})^2} \tag{3.14}$$

where $\mathbf{r}$ is the vector describing the electron's path. From the figure it is observed that on the average radius $\langle 1/R_{curv}^2\rangle$ is larger than $1/R_0^2$. As the perpendicular velocity becomes larger the deviation $\langle 1/R_{curv}^2\rangle - 1/R_0^2$ increases, implying that more power is radiated. The poloidal motion of the electron can be neglected because the change in the radius of curvature as a result of the Larmor motion is the dominant effect, as follows from Fig.3.2. For a purely toroidal motion in combination with the Larmor motion, the average radius of curvature is approximated by Eq.

(2.17). This equation shows the dependencies of R_{curv} on the main runaway parameters Θ and γ, i.e. pitch angle and energy. Nevertheless, because of the strong dependence of the radius of curvature on the phase of the Larmor motion, in the analysis of the radiated power performed in this thesis eq. (3.14) is used instead of the approximation (2.17). The average R_{curv} as a function of $v_\perp/c$ for different energies is plotted in Fig. 3.2b.

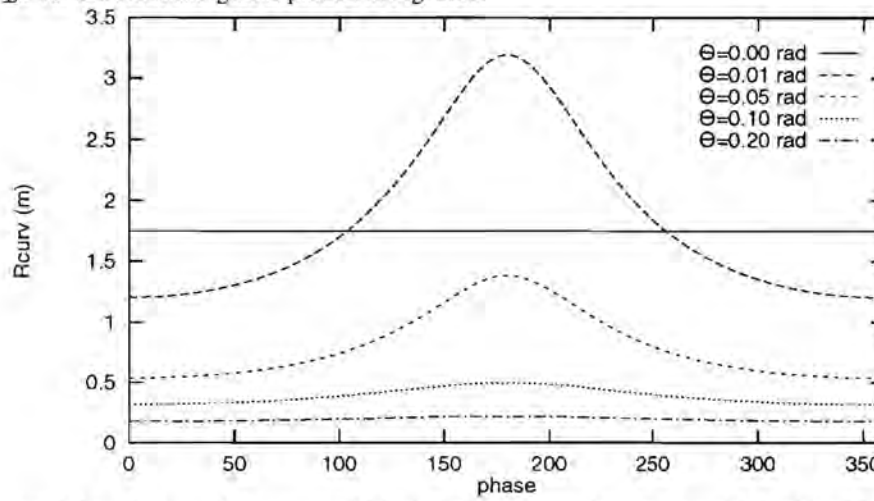

Figure 3.2a: *Radius of curvature of 25 MeV electron, moving on a toroidal orbit of R=1.75 m and a poloidal orbit given by the cyclotron motion. R_{curv} is plotted as a function of the phase of the cyclotron motion for different perpendicular velocities $\Theta = v_\perp/c$.*

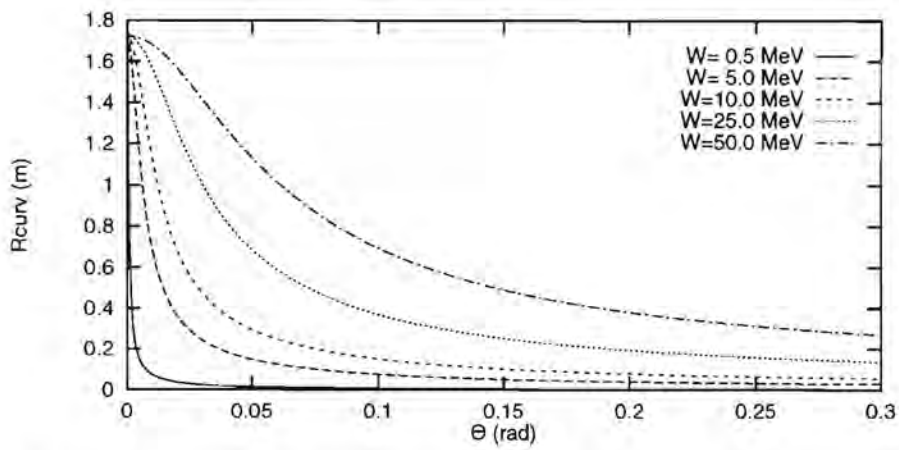

Figure 3.2b: *Average R_{curv} for electron orbit consisting of a toroidal orbit with R=1.75 m and the cyclotron motion perpendicular to this. R_{curv} is plotted as a function of Θ for different runaway energies.*

In the previous section it was shown that the radiation is emitted in a cone with aperture $\delta \approx 1/\gamma$. For the runaway electrons energies of the order of 25-30 MeV this cone is very narrow. However, due to the Larmor motion, the velocity vector of the electron makes an angle $\Theta = v_{\perp}/v_{//}$ with the magnetic field line and rotates about this line. The radiation emitted from the plasma thus forms a cone with an additional aperture angle of Θ.

Spectra of the synchrotron radiation, as given by eq. (3.9), are plotted in Fig.3.3. In Fig. 3.3a, the normalized spectra are shown for different energies and pitch angle. The spectral power per electron is plotted as a function of the wavelength λ, so that eq. (3.9) turns into:

$$\frac{dP^e}{d\lambda} = \frac{4\pi}{\sqrt{3}} \frac{m_e c^3 r_e}{\gamma^2 \lambda^3} \int_{\frac{4\pi R_{curv}}{3\lambda\gamma^3}}^{\infty} K_{(5/3)}(x)\, dx \qquad (3.15)$$

On the next page, the effect of changes in the energy (Fig3.3b), pitch angle (Fig3.3c), energy distribution (Fig3.3d) and pitch angle distribution (representing the effect of the Larmor motion, parameterized by Θ, Fig3.3e) are plotted. Note the extremely strong decrease of the spectrum with decreasing λ and the strong energy and pitch angle dependence, indicating that the highest energy and largest pitch angle dominates the spectrum. In Fig.3.3d the effect of the electron energy distribution function on the spectrum is shown, for 3 limiting cases: a mono-energetic distribution of 25 MeV, a flat distribution up to an energy of 25 MeV, and an exponentially decaying distribution $\exp(-W/W_0)$, with W_0=5 MeV. In these plots the radiated spectral power is normalized by dividing by the number of electrons in the distribution. Finally in Fig. 3.3e the spectra for three pitch angle distributions are plotted: a constant value of the pitch angle of 0.1 rad, a flat distribution of Θ up to 0.1 rad and a Gaussian distribution of Θ with $\Delta\Theta$ =0.1 rad. Here W=25 MeV has been assumed.

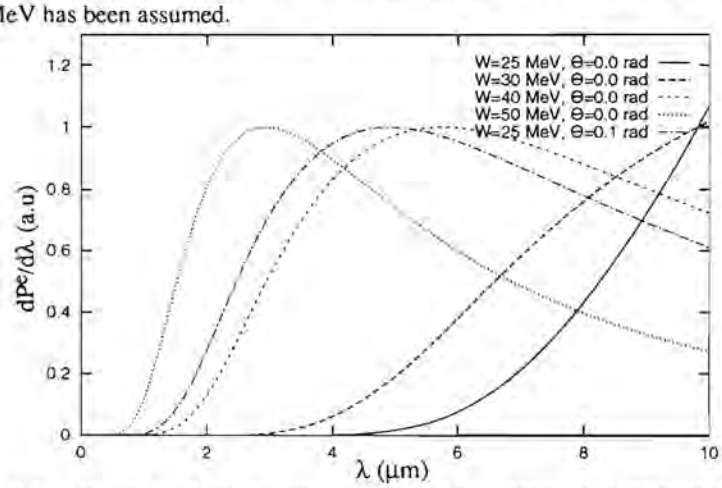

Figure 3.3a: *Normalized synchrotron spectrum of one electron for different W_r and Θ*

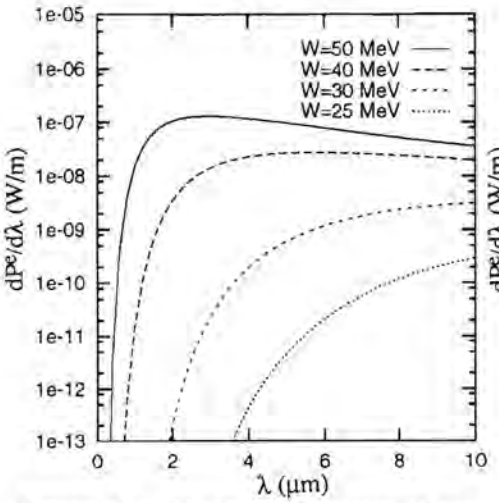

Figure 3.3b: *Synchrotron spectra of one electrons for different values of W_r .Here, R_{curv}=1.75 m and Θ = 0 rad has been assumed.*

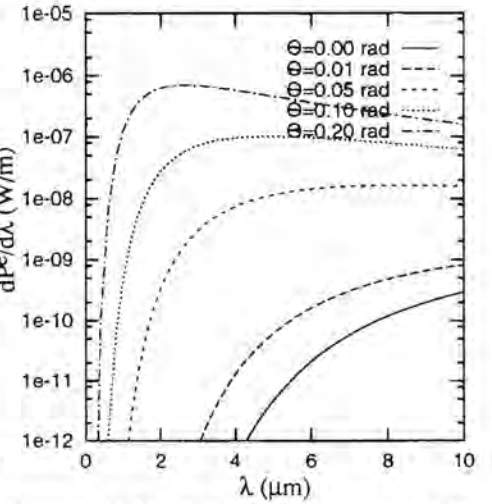

Figure 3.3c: *Synchrotron spectra for different values of the pitch angle Θ. The electron energy is W_r=25 MeV.*

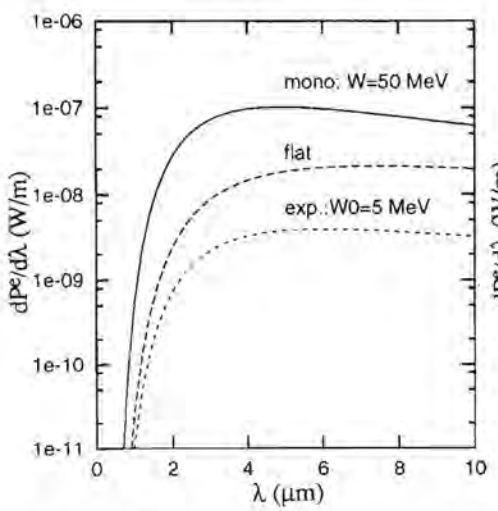

Figure 3.3d: *Synchrotron spectra for three different energy distribution functions: a mono-energetic distribution at W_r=25 MeV, a flat distribution up to W_{max} = 25 MeV, and an exponentially decaying distribution with W_{max}=25 MeV and W_0=5 MeV. For all calculations Θ=0 rad has been used.*

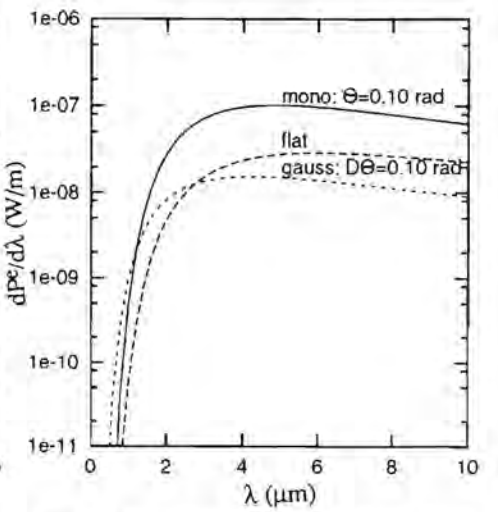

Figure 3.3e: *Synchrotron spectra for three different distributions in pitch angle: a mono pitch angle distribution at Θ = 0.10 rad, a flat distribution up to Θ = 0.10 rad and a Gaussian distribution with $\Delta\Theta$=0.10 rad. Here W_r =25 MeV has been used.*

3.4 Detection of Synchrotron Radiation at TEXTOR

As the synchrotron emission is in the middle IR spectral range, a thermographic camera is used to record this radiation. This camera views the plasma tangentially in the direction of electron approach. The experimental setup is drawn schematically in Fig. 3.4. A lens images the object to the field lens which projects the light into the camera objective. The camera, Inframetrics model 600, consists of a single, liquid nitrogen cooled, HgCdTe diode (area 25×25 μm), a focussing lens and two scanning mirrors. The detector is sensitive in the wavelength range of 3-14 μm. However, the CaF_2 used for the lenses and the vacuum window, limits the long wavelength range of the camera to about 8 μm. By rapidly scanning the two mirrors, one horizontally and one vertically, a TV picture is generated according to the NTSC standard. The individual points of the picture are consecutive in time. One TV line is scanned in 65 μs, a 2 dimensional TV frame, consisting of 256 lines, is recorded in 16.6 ms. Each point of the observed area is thus probed once every 16.6 ms. The camera provides the possibility to sweep only the horizontally scanning mirror, resulting in a 1 dimensional measurement each 65 μs.

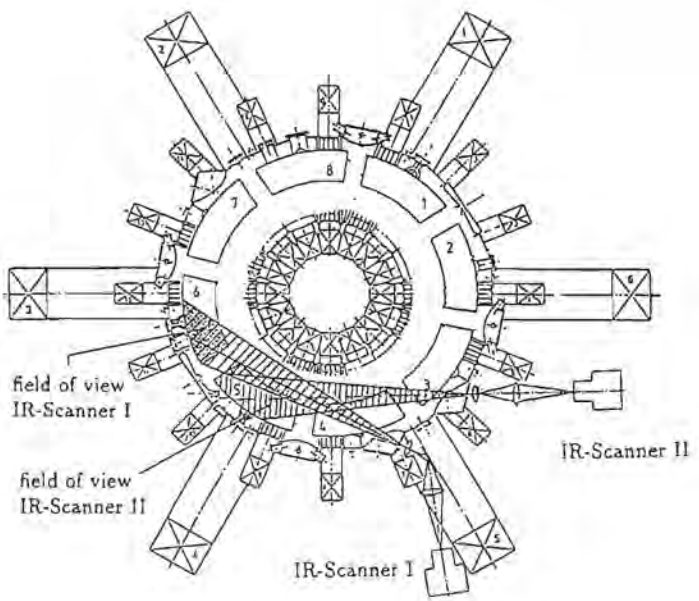

Figure 3.4: *Experimental set up of the infrared camera at TEXTOR.*

Thermal radiation from the limiter, liner or RF antennas in TEXTOR has the maximum emission in the wavelength range where the camera is sensitive. This radiation is also present in the camera picture as it is not absorbed by the plasma. This limits to a certain extent the sensitivity of the synchrotron radiation measurements, because at low runaway intensity the radiation is lost in the thermal background. Aside from this undesired influence on the measurements, the thermal radiation is a helpful tool for aligning the diagnostic and it provides a suitable reference frame for the position measurements. Moreover, the thermal radiation from the limiter, of which the temperature is measured independently, provides an accurate in-situ calibration source allowing absolute measurements of the synchrotron radiation intensity.
Spectral measurements of the synchrotron radiation are performed by putting filters with different long wavelength cut-offs in front of the camera. The major drawback of this method is that only one spectral point is measured each discharge. To obtain spectral information reproducible discharges are necessary.

3.5 Typical Example of a Measurement of Synchrotron Radiation in TEXTOR

A typical example of a measurement of synchrotron radiation during a low density ($n_e<1\times10^{19}m^{-3}$) ohmic discharge at TEXTOR is presented in Fig.3.5a. The first frame is recorded at t = 0.5 s after the start of the discharge and shows the thermal radiation from the background. The view of the camera corresponds to the box drawn in Fig. 1.4. Part of the ALT-II limiter, extending toroidally around the torus, is clearly observable. This is the only part that is expected to heat up during the discharge and therefore emit more infrared radiation. The second picture is taken at t = 1.5 s. The spot in the centre of the picture is the synchrotron radiation. Subtracting with image processing techniques the thermal background radiation, the shape of the spot is more pronounced, as shown in Fig. 3.5b. The intensity of the spot increases further up to the end of the discharge at t ≈ 3 s. Then it disappears from one frame to the next, i.e. within 16.6 ms.
The arguments leading to the conclusion that this must be synchrotron radiation are:

- The radiation disappears simultaneously with the plasma. This shows that it cannot be thermal radiation of a wall component, in which case the decay time would be of the order of minutes. Hence the radiation must originate from the plasma.
- The radiation is only detected in the direction of electron approach. When the plasma current is reversed the radiation does not show up.
- At the end of the discharge, when the current is decaying, the spot of radiation moves to the low field side of the plasma in agreement with the predicted orbit shift of runaway electrons (see section 2.2)
- The radiation is only detected at low electron densities, showing the relation with runaway electrons.

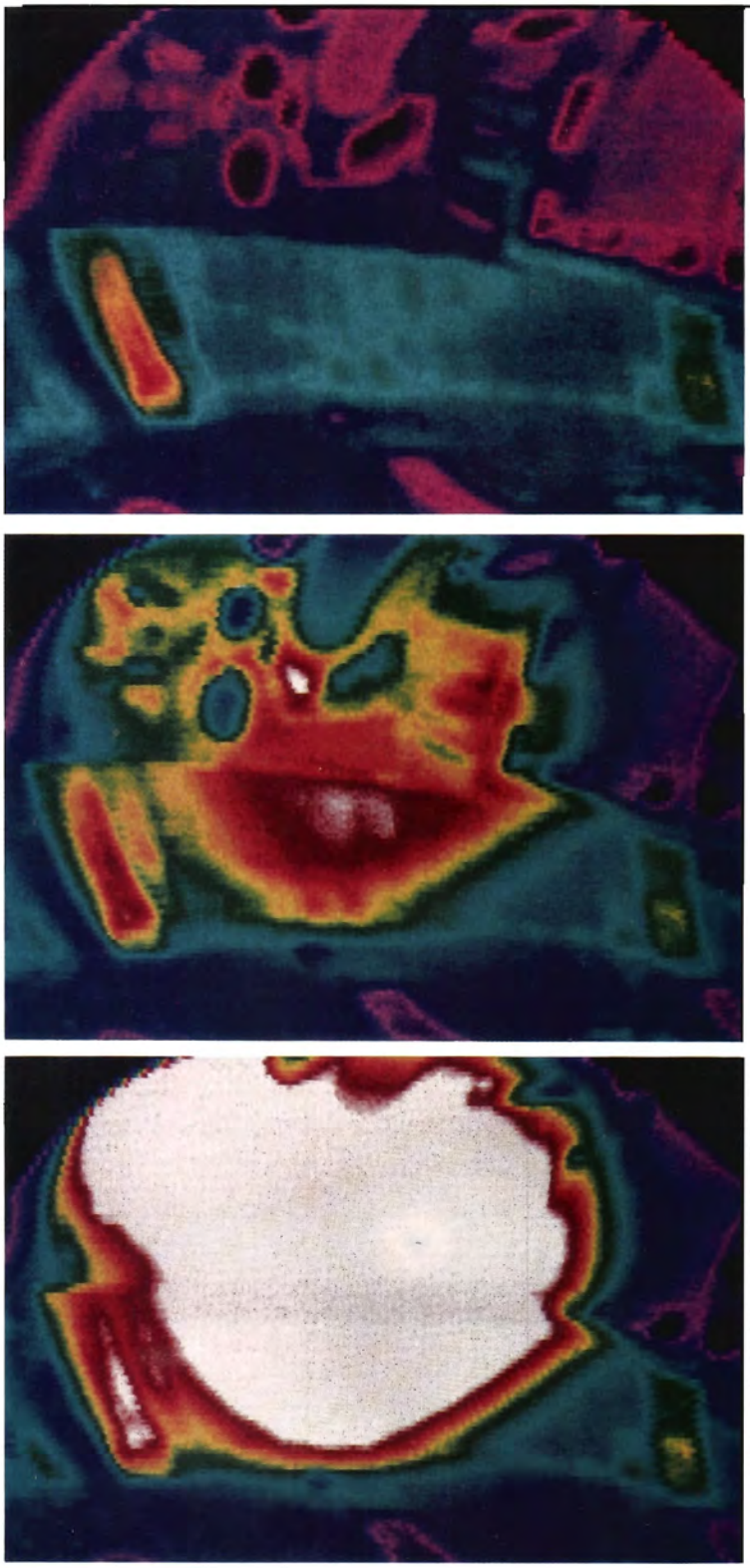

Figure 3.5a: *Typical example of measurement of synchrotron radiation in TEXTOR. In the top picture, taken at t=0.5 s, only thermal radiation from the limiter and liner is observed. On the picture in the middle the synchrotron radiation becomes apparent. This picture is recorded at t=1.5 s. From the bottom picture, recorded at t=3 s, the extent of the spot can be determined directly.*

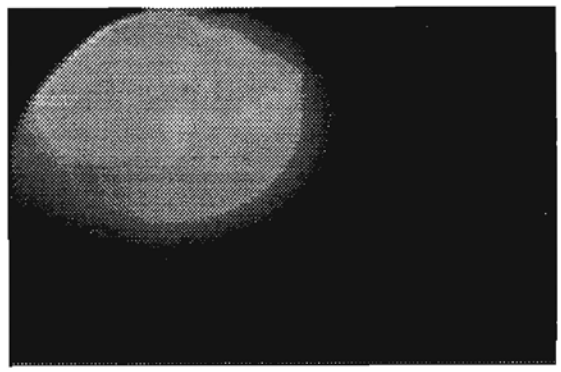

Figure 3.5b:
Typical picture of the synchrotron radiation after subtracting the thermal background.

- The radiation does not become apparent earlier than about 1 second after the start of the discharge. This is the time needed for the runaway electrons to gain the energy necessary to radiate in the spectral region of the camera.
- Finally, it is noted that on another CCD camera, which is sensitive up to a wavelength of 1.2 μm, no special features were observed coinciding with the appearence of the infrared spot. Although this is no direct confirmation of the hypothesis that we observe synchrotron radiation, we can deduce an absolute upper limit of the runaway energy of 50 MeV from it.

3.6 Deduction of Runaway Parameters

As was shown in section 3.2 the synchrotron spectrum depends on only two quantities: the energy of the electron (γ) and its pitch angle (Θ). By analysing the spectrum, the divergence and the intensity of the synchrotron radiation, γ, Θ and the absolute number of the runaway electrons can in principle be obtained. The methods used in the course of this thesis are briefly introduced in this section.

- Determination of the Pitch Angle Θ

The pitch angle can be deduced directly from the divergence of the radiation, which in turn can be deduced from the 2D image measured with the IR camera. This has already been pointed out in [Fin-90]. Effectively, the emission of one electron is radiated into a cone with full opening angle of $(2\Theta+\delta)\approx 2\Theta$, where $\delta\approx 1/\gamma$ and will be neglected as it is nearly an order of magnitude smaller than the experimentally deduced value of Θ.

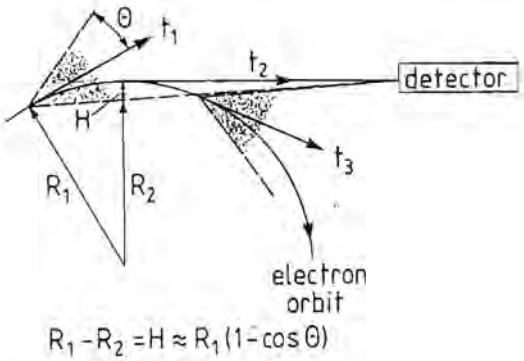

Figure 3.6: *The extension of the synchrotron spot in the horizontal direction as a result of the finite opening angle Θ of the cone of radiation.*

Let us assume that the synchrotron radiation is emitted by a toroidal runaway beam with radius r_{beam}, whose center is horizontally displaced by δ from the magnetic axis, as a result of the curvature B drift (see section 2.2). For such a situation radiation can be detected by the camera if the line of sight of the camera is tangent to the electron orbit or, as a result of the finite opening angle of the radiation cone, makes an angle $\leq \Theta$ with the runaway orbit. Hence in a horizontal plane light can be detected over the full beam diameter. For every orbit such a tangent can be drawn if the camera is looking tangentially into the torus covering the full cross-section. On the high field side the horizontal divergence is even enlarged by an amount $H = R_1 (1-\cos \Theta) \approx R_1 \Theta^2$, as a result of the toroidal curvature. This effect is depicted in Fig. 3.6.

In the vertical direction the picture is somewhat more complicated. Neglecting for a moment the poloidal inclination of the runaway orbits, there are three cases possible. These are sketched in Fig. 3.7. If the radiation were only emitted in forward direction, i.e. if $\Theta \approx 0$ (case a), only a narrow band of radiation falls on the entrance lens determined by the natural opening angle δ of the radiation. For a large value of Θ ($D\sin\Theta > r_{beam}$, D=distance from detector to runaway beam, case c) the vertical extent is limited by the beam radius. For the intermediate case, i.e. ($D\sin\Theta < r_{beam}$, case b), the pitch angle Θ determines the vertical extent. However, one cannot distinguish beforehand between cases b and c, as in both cases an elliptical spot is visible. A distinction between these two cases is provided if the detector is not positioned in the midplane, but at some distance Z_{det} away from the equatorial plane. The three possible shapes are drawn in Fig. 3.9d,e and f respectively. Here a cut through the plane spanned by the line of sight and the vertical direction is also given. For a spot vertically symmetric around Z_{det} the vertical height is given by: $L = L_{max} - L_{min} = 2D\sin\Theta$. In the case of a spot vertically symmetric around the equator $L = 2\, r_{beam}$. Finally for an intermediate case the spot can be extended in one direction up to the beam radius, whereas in the other direction the finite opening angle is limiting the size of the spot.

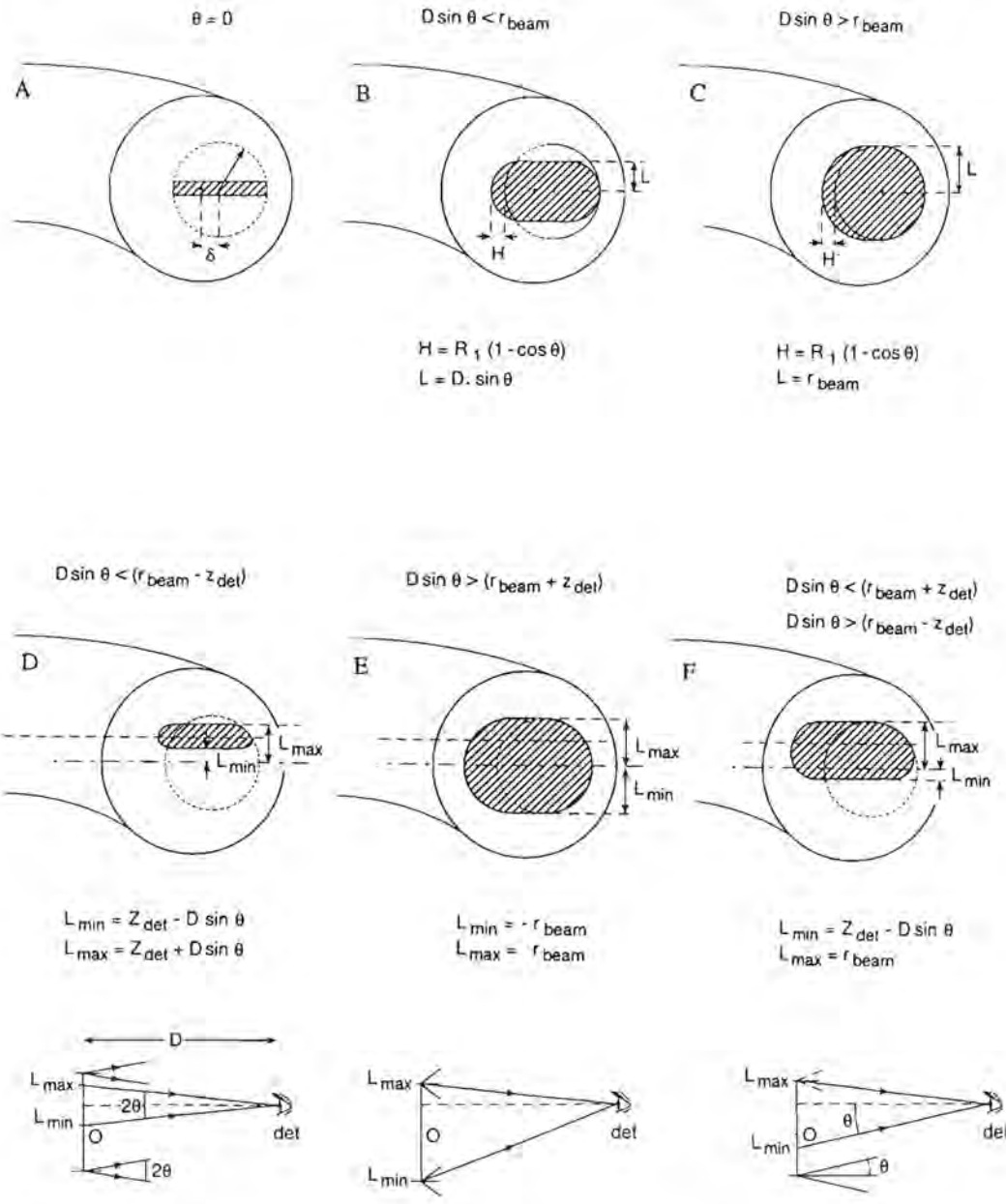

Figure 3.7: *Shape of the synchrotron spot for 6 different cases. The dashed circle represents the runaway beam. For the cases a, b and c the detector is positioned in the midplane, whereas for d,e and f it is positioned above the midplane. In case a, b and d the vertical extent of the spot is limited by Θ. In case c and e the size of the runaway beam limits the vertical spot size. Case f is an intermediate case.*

At TEXTOR two positions for the IR camera are used, one in the equatorial plane, and one position above this plane with Z_{det}=0.20 m. In both situations D=2.25 m. In the latter situation a limited field of view masked part of the spot of synchrotron radiation. By tilting the camera it was shown that the situation of Fig 3.9f holds. As typical parameters were deduced: $\Theta = 0.12 \pm 0.02$ and r_{beam} = 0.20-0.25 m. These values are consistent with the ones obtained from the camera in the equatorial plane, but that measurement alone does not allow a distinction between r_{beam} and Θ. Not discussed yet is the effect of the poloidal motion of the guiding center, due to the pitch q of the field lines as given by the safety factor (eq.1.1). This motion has opposite direction on the low and high field side and would therefore result in a tilt of the elongated radiation pattern. This inclination angle α between the major axis of the ellips and the equatorial plane can be estimated by:

$$\tan \alpha = \frac{r_{beam}}{R_0 \, q(r_{beam})} \qquad (3.16)$$

which for the typical case (r_{beam} = 20 cm, q(20 cm)≈1.5) would yield $\alpha \approx 0.08$ rad. Because the spot is only slightly elliptical, an inclination of this magnitude is difficult to observe.
Note that this inclination does not influence the determination of the pitch angle as this is measured from the vertical extent, i.e. on top and bottom, where the direction of the velocity is not inclined with respect to the purely toroidal direction.

- *Determination of the Runaway Energy*

Having determined the pitch angle from the spot size, the energy of the runaways can be deduced from the radiated spectrum. Spectral information is obtained by putting different filters in front of the IR camera. Different quarz filters, which had a long wavelength cutoff in the range λ_c=[3-4.5μm] (depending on the thickness) as well as sapphire filters (λ_c≈5μm) were used. Since for electrons of 10-40 MeV the spectrum drops exponentially at these short wavelengths, the ratio of intensities measured with different filters is a function of the runaway energy.
For this method to be accurate enough at least three conditions must be fullfilled: 1) the discharges must be reproducible, i.e contain the same amount of runaways electrons, to compare the intensities; 2) the pitch angle Θ, or the Θ–distribution must be known, with sufficient accuracy; 3) the distribution function of the runaway electron energy should be available.
The first condition is normally met since ohmic discharges at TEXTOR showed to be very reproducible, giving the same amount of synchrotron radiation within 10 %. Moreover, the small differences could be corrected by comparing the intensities of the HXR signal. The other two requirements are inherent in every spectral method to determine the runaway energy. In all calculations Θ is assumed a constant, no distribution in Θ is considered. The justification of this is given in Chapter 6. The distribution function of the energy, however, is unknown. Two extreme

case will be considered: a mono-energetic and a flat distribution, corresponding to either a limited time of runaway generation (for instance during start-up) or a continuous generation, respectively. The results of measurements with three different filters in front of the infrared camera are presented in Fig.3.8. The detector response is included in the calculations. For the pitch angle Θ=0.12 is used, as deduced from the shape of the spot (see above). For both distribution functions a similar curve is found, differing not more than 4 MeV in energy. This shows that the determination of the energy is not very sensitive to the exact shape of the distribution function. It is observed that the runaway energy saturates after about 2-2.5 s as expected from integrating the loopvoltage, if the deceleration by the synchrotron radiation is taken into account, as illustrated by the solid line. For the interpretation of other measurements described in this thesis, where no spectral measurements were performed, the energy was calculated according to this simple model. On the basis of these measurements, however, no final judgement on the energy distribution of the runaway electrons can be made.

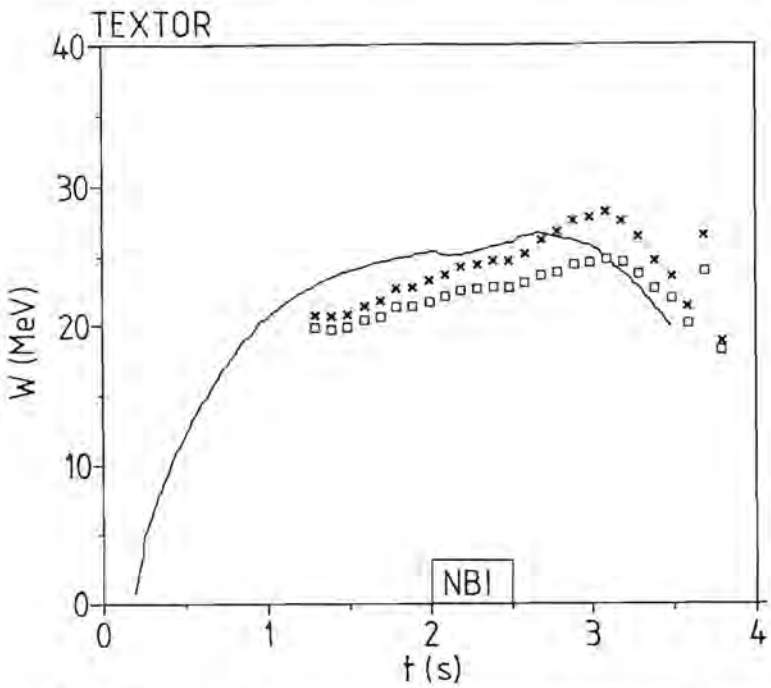

Figure 3.8: *The maximum energy of the runaway electron, as derived from the filter measurements. The squares are the results if a flat energy distribution is assumed and the crosses assume a mono-energetic distribution. The curve results from free fall calculation with synchrotron radiation losses taken into account. In this particular case 500 kW of neural beam power was injected.*

- Determination of the absolute Number of Runaways

The number of runaways N_r, deduced from the observed synchrotron radiation is calculated from [Fin-90]:

$$N_r \int \frac{dP}{d\lambda} T(\lambda) d\lambda = \int L_\lambda^S T(\lambda)\, d\lambda\, A\, \Omega\,, \qquad (3.17)$$

where A is the cross-sectional area of the ring filled with runaways, $\Omega=4\pi\Theta$ is the solid angle into which the synchrotron radiation is emitted, L_λ^S is the measured spectral radiance, $T(\lambda)$ is the transmission function of the optical system, and $(dP/d\lambda)$ is the average of eq. (3.15) over the energy distribution function. The absolute value of the radiance $\int L_\lambda^S T(\lambda)\, d\lambda$ is obtained by comparing the synchrotron radiation with the thermal radiation from the toroidal limiter of which the temperature is measured independently (about 425 K in normal discharges) and emissivity is known (limiter surface: graphite, emission coefficient ≈ 0.8). While the absolute intensity can be determined rather accurately, the absolute number of runaways in the discharge can only be determined within an order of magnitude due to the uncertainty about the energy distribution function.

CHAPTER 4

GENERATION OF RUNAWAY ELECTRONS

4.1 Introduction

The generation of runaway electrons in a plasma under the action of an electric field has been examined in numerous papers from the early days [Dre-59,Har-60,Gur-61,Kru-64,Kul-73,Con-75]]. Several processes are studied in which electrons can overcome the critical velocity v_{crit}: i) the primary generation (often called the Dreicer process) in which a steady state solution of the electron distribution function from the Fokker Planck function is calculated [Kno-79,Par-86]. The diffusion of electrons around $v=v_{crit}$ gives rise to runaway production; ii) the secondary generation, the process in which new runaways are created through collisions of already existing runaway electrons with bulk electrons [Bes-86,Jay-92]; iii) instabilities [Par-78], giving rise to sudden increases in electric fields and isotropisation of the electron velocity distribution which can alter the rate at which electrons overcome the runaway threshold energy; iv) The application of external electromagnetic waves to the plasma, such as lower hybrid waves or electron cyclotron waves; v) the untrapping of trapped electrons after a disruption [Fle-93]. Trapped electrons have a certain chance to survive the thermal quench during a disruption, as they do no follow the magnetic field lines. In the post-quench plasma, the electron temperature has dropped to a few eV, and if these electrons are untrapped they will probably run away as a result of their relatively high energy.

The comparison of the runaway generation rate of these processes with experiment is always difficult, due to the strong exponential dependencies on the plasma parameters E, T_e, Z_{eff} and n_e, and the limited accuracy of runaway electron measurements. The synchrotron radiation diagnostic provides a new tool for investigating the runaway generation. The experimental results described in this chapter are compared with the first two mechanisms listed above, these being the basic generation processes in stable tokamak discharges. This work has been published in Nucl. Fusion **33** (1993) 1775 and is reprinted here in Section 4.4. Although a short description of the primary and secondary generation is already given in the paper, a separate treatment in Sec. 4.2 and 4.3 is believed to be useful to illustrate some features of these processes that were only sligthly addressed in the paper, such as the relativistic correction to the birthrate, the region of runaway production, the trapping effect and the change of the energy distribution as a result of the secondary generation. This introduces some overlap which is unavoidable. Based on the experimental results some implications for runaway production in TEXTOR-94 (having a discharge length two times longer than TEXTOR) and ITER (a

tokamak currently being designed to demonstrate the technical feasibility of a fusion reactor) are discussed in section 4.5.

4.2 Primary Generation

The production rate for the primary generation process is calculated from a solution of the electron distribution function using the Fokker Planck equation. In this kinetic treatment the diffusion of electrons around $v=v_{crit}$ gives the production rate. A general description of this process is far out of reach but for tokamak conditions several approximations can be made: i) the case of a weak electric field, i.e. $E/E_{crit} << 1$, implying that only an exponentially small fraction of the electrons will run away, ii) the bulk distribution is taken Maxwellian, iii) only suprathermal electrons will run away: $v_{crit} >> v_{therm}$, iv) the plasma is fully ionized, v) the electric field E is constant in time and space and vi) the neglection of collective effects. A relativistic treatment is given by Connor and Hastie [Con-75], the influence of impurity ions ($Z_{eff}>1$) is treated by Cohen [Coh-76]. Collisions of fast (runaway) electrons with thermal ones are not taken into account, since the collision frequency is very low. However, if the lifetime of runaway electrons is sufficiently long, these collisions give rise to the secondary generation process, which can alter the production rate appreciable as is demonstrated in the next section.

Starting point in these calculations is the Fokker Planck equation for a fully ionized, infinite plasma in a homogeneous and constant electric field E:

$$\frac{\partial f}{\partial t} + \frac{eE}{m_e}\left(\cos\Theta \frac{\partial f}{\partial v} - \frac{\sin\Theta}{v}\frac{\partial f}{\partial \Theta}\right) = \frac{1}{v^2}\frac{\partial}{\partial v}\left\{v^2 \nu_e(v)\left[\frac{T_e}{m_e}\frac{\partial f}{\partial v} + v f\right]\right\} + \frac{\nu(v)}{2\sin\Theta}\frac{\partial}{\partial \Theta}\sin\Theta\frac{\partial f}{\partial \Theta} \qquad (4.1)$$

In this equation f represents the electron velocity distribution function and $\nu(v)$ is the collision frequency of electrons with plasma ions and electrons. This equation states how the distribution function changes as a result of the acceleration due to the electric field E (second term on the left hand side) and as a result of collisions (right hand side). The first term describes the change of energy of a fast electron due to collisions with other electrons (change of energy due to collisions with ions can be neglected). The second term describes the change of the direction of the momentum in collisions with electrons and ions.
In dimensionless variables $\mu=\cos\Theta$, $u=v/\sqrt{T_e/m_e}$, $\tau = t\,\nu_e\left(\sqrt{T_e/m_e}\right)$ this equation assumes the form:

$$\frac{\partial f}{\partial \tau} + \frac{E}{E_c}\left(\mu\frac{\partial f}{\partial u} - \frac{1-\mu^2}{u}\frac{\partial f}{\partial \mu}\right) = \frac{1}{u^2}\frac{\partial}{\partial u}\left\{\frac{1}{u}\frac{\partial f}{\partial u} + f\right\} + \frac{(1+Z_{eff})/2 - 1/(4u^2)}{u^3}\frac{\partial}{\partial \mu}(1-\mu^2)\frac{\partial f}{\partial \mu} \qquad (4.2)$$

To solve this equation analytically for the stationary case ($\partial f/\partial \tau = 0$) it is noted that for higher velocities the distribution function will become directional, concentrated near $\mu=1$. Therefore the solution is expanded in powers of $(1-\mu)$:

$$f = C \exp\{\varphi_0(u) + (\mu - 1)\varphi_1(u) + (\mu-1)^2 \varphi_2(u) + \ldots\} \qquad (4.3)$$

By substituting this expansion into eq. 4.1 a chain of equations for the functions φ_i is obtained, which can be solved by matching the solution for small v to a Maxwellian, as was first carried out by Gurevich [Gur-61]. A more self-consistent and sophisticated treatment is given by Kruskal and Bernstein [Kru-64], who divide the velocity space into five different regions. Appropriate matching of the solutions for each region yielded the functions φ_i. Once this distribution function is found the runaway generation rate can be obtained. The growth of the distribution for $v>v_{crit}$ in time, i.e the flow of electrons into the runaway region, determines the production rate λ, which has the following form:

$$\frac{dn_r}{dt} = n_e \nu_{col}(v_{th})\,\lambda \qquad (4.4a)$$

with

$$\lambda = K(Z_{eff})\ \varepsilon^{-3(Z_{eff}+1)/16}\ \exp\left\{\frac{-1}{4\varepsilon} - \sqrt{(Z_{eff}+1)/\varepsilon}\right\} \qquad (4.4b)$$

Here $\varepsilon = E/E_{crit}(Z_{eff}=1)$ and is independent of Z_{eff}, E_{crit} the critical electric field (see Sec. 2.1), v_{th} is the thermal electron velocity and n_r is the density of the runaway population. $K(Z_{eff})$ is a weak function of Z_{eff} ($K(1)=0.32, K(2)=0.43$, [Coh-76]), $\nu_{col}(v_{th})$ is the collision frequency of the electrons at the thermal velocity, given by:

$$\nu_{col}(v_{th}) = \frac{Z_{eff}\, n_e \ln\Lambda\, e^4}{4\pi\varepsilon_0^2\, m_e^{1/2} T_e^{3/2}} \qquad (4.5)$$

The analytic result for the birth rate is corroborated by a numerical solution to the Fokker Planck equation [Kul-73], which study also allowed the evaluation of $K(Z_{eff})$.

The relativistic correction made by Connor and Hastie [Con-75] can modify this result significantly for present day tokamak parameters. Relativistic effects become important if ε is of the same order as T_e/m_ec^2. An important result is that for $E/E_{crit} \leq T_e/m_ec^2$ the runaway phenomenon ceases to exist altogether. This follows from the relativistic drag force (App. A):

$$F_{drag} = \frac{e^4 n_e \ln\Lambda}{4\pi\varepsilon_0^2 m_e v^2}\left(1 + \frac{Z_{eff}+1}{\gamma}\right) \tag{4.6}$$

which is nearly constant for relativistic particles ($v \approx c$, $(Z_{eff}+1)/\gamma << 1$). Therefore no runaway production will occur for electric fields smaller than a limiting value:

$$E_{lim} = \frac{e^3 n_e \ln\Lambda}{4\pi\varepsilon_0^2 m_e c^2} = \frac{T_e}{m_e c^2}\frac{E_{crit}}{Z_{eff}} \tag{4.7}$$

For TEXTOR ($E = 0.1$ V/m) this will occur for densities $n_e > 4\pi\varepsilon_0^2 m_e c^2 E/(e^3 \ln\Lambda) = 1.1 \times 10^{20} m^{-3}$, which is higher than the ohmic density limit. Hence the relativistic effect does not stop the runaway electron production. Still, the effect is noticable also at low densities as a reduction of the production rate. The dominant relativistic correction on the birth rate for $\varepsilon >> T_e/m_ec^2$ is given by:

$$\lambda_{rel} = \lambda_{nonrel} \exp\left\{-\frac{T_e}{m_e c^2}\left[\frac{\varepsilon^2}{8} + \frac{2\varepsilon^{3/2}}{3}(1 + Z_{eff})^{1/2}\right]\right\} \tag{4.8}$$

For the discharges described in this thesis ($n_e \approx 0.6\text{-}1\times10^{19} m^{-3}$, $T_e \approx 1\text{-}1.5$ keV, $Z_{eff} \approx 1.5\text{-}2$) the runaway production in the nonrelativistic treatment (Eq. 4.4) overestimates the runaway birth rate by a factor varying between 1.4 and 3.5.

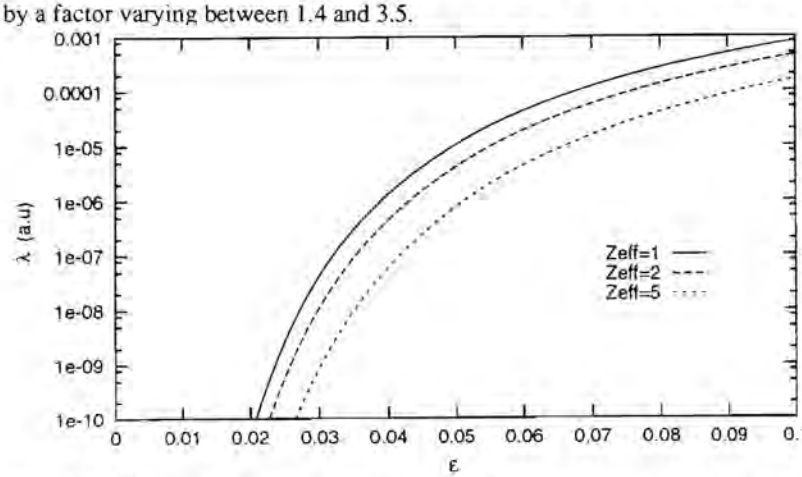

Figure 4.1: *The runaway production parameter λ_{rel} as a function of ε for 3 different values of Z_{eff}*

A plot of the relativistic runaway production rate λ_{rel} as a function of ε for Z_{eff} =1,2 and 5 is given in Fig. 4.1. The strong exponential decay of the production rate with decreasing ε (i.e increasing n_e, decreasing T_e or E) makes that a comparison of the experimental and theoretical production rates is only feasible on a logarithmic scale.

It is generally expected that the runaway production is strongly concentrated in the center, because the T_e profile is more peaked than the n_e profile. To illustrate this the production rate is calculated for two parametric forms of the T_e and n_e profiles:

$$T_e(r/a) = T_e(0)\,(1-(r/a)^2)^{\alpha} \tag{4.9a}$$

$$n_e(r/a) = n_e(0)\,(1-(r/a)^2)^{\beta} \tag{4.9b}$$

with α=2,3 and β=1; and for n_e and T_e profiles as follow from the profile consistency principle [Sch-91] that have been shown to describe the experimental tokamak n_e and T_e profiles well:

$$T_e(r/a) = T_e(0)\,(1+q_a(r/a)^2)^{-4/3} \tag{4.9c}$$

$$n_e(r/a) = n_e(0)\,(1+q_a(r/a)^2)^{-2/3} \tag{4.9d}$$

The runaway production rate as a function of minor radius, normalized to the central value, is shown in Fig. 4.2 for typical TEXTOR parameters: Z_{eff} =2, $T_e(0)$=1 keV, $n_e(0)=1\times10^{19}m^{-3}$ and q_a=4. It is found that the runaway creation zone has a width (HWHM) of approximately 7 cm. For lower absolute values of the runaway production, the region of runaway production decreases even further as shown by curve 4 (with $n_e(0)=2.5\times10^{19}m^{-3}$ and $T_e(0)$=0.7 keV, and with the profiles of eqs. 4.9c,d).

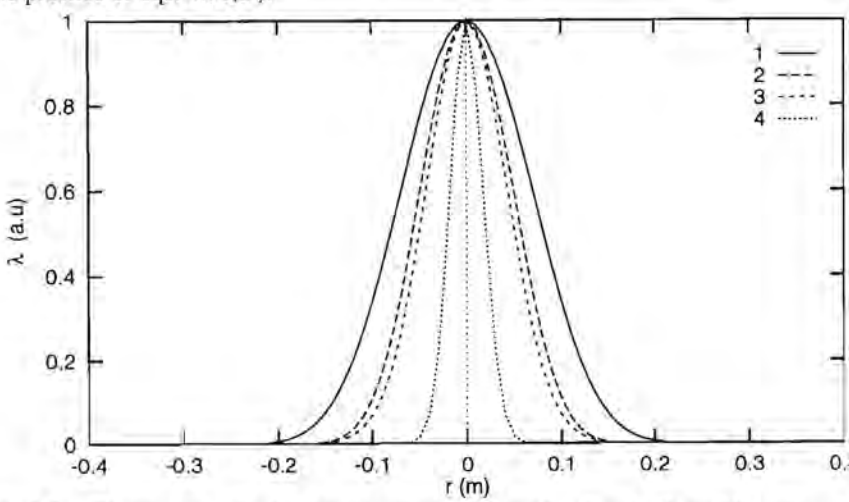

Figure 4.2: *The runaway production rate as a function of radius for four different cases: 1) α=2, 2) α=3, 3) α=-4/3, 4) α=-4/3, but lower production rate.*

4.3 Secondary Generation

In the previous section close Coulomb collisions were neglected, as in the Fokker Planck equation 4.1 the Landau collision integral is used, which takes into account only distant collisions, resulting in slight variations in momenta. However, several authors [Sok-81, Bes-86, Jay-92, Fle-93] have pointed out that in the presence of runaway electrons of about 10-20 MeV close collisions can greatly enhance the runaway production rate. As a result of such a collision the velocity of a plasma electron can overcome the critical value v_{crit}, i.e the runaway threshold. This mechanism will be discussed in this section.

The cross-section of a single Coulomb interaction of a relativistic electron and a cold electron with an energy transfer larger than ΔW is equal to [Sok-81]:

$$\sigma(\Delta W) = 2\pi r_e^2 \frac{m_e c^2}{\Delta W} \tag{4.10}$$

A simple estimate of the number of new runaway electrons created per unit time by one relativistic electron (ν_s) is obtained by the frequency of collisions in which $\Delta W > W_{crit}$:

$$\nu_s = \sigma(W_{crit})\, n_e\, c \tag{4.11}$$

Hence, each relativistic runaway creates a new runaway electron in a time t_0:

$$t_0 = \frac{1}{\nu_s} = \frac{(2+Z_{eff})\, m_e c \ln\Lambda}{eE} \tag{4.12}$$

Note that the secondary generation is nearly independent of electron density and temperature (only through $\ln\Lambda$). The net effect of the secondary generation is obtained if the runaway confinement time is known. This is parametrized by the runaway confinement time τ. The runaway production can now be described as:

$$\frac{dn_r}{dt} = S_{prim} + \frac{n_r}{t_0} - \frac{n_r}{\tau} = \left(S_{prim} + \frac{n_r(0)}{t_{eff}}\right) e^{t/t_{eff}} \tag{4.13}$$

where $t_{eff}^{-1} = t_0^{-1} - \tau^{-1}$; S_{prim} denotes the primary runaway generation and N_r represents the number of runaway electrons. The last term accounts for start-up generated runaways. The factor $\exp(t/t_{eff})$ is the net effect of the secondary generation process. Note that for $t_0 < \tau$ the secondary generation causes an avalanche-like runaway production. For normal TEXTOR operation conditions this $t_0 \sim 1$ s. Runaway electrons that have been confined for such a long

time have acquired an energy of at 20 MeV and thereby fulfil the requirement (W≥10 MeV) for the secondary generation.

As a result of the secondary generation the energy spectrum of the runaway electrons will become exponential, since the most recently born runaways have gained the least energy. We expect the energy spectrum to be like:

$$f(W) \sim e^{-W/W_0} \tag{4.14}$$

Here $W_0 = eEct_0$ is the energy gained by the electrons in one avalanche time t_0. For TEXTOR we calculate $W_0 \approx 30$ MeV. Since W_0 is as large as the maximum observed energy at TEXTOR this energy distribution will tend to a flat distribution if particle and radiation loss is taken into account. Particle loss will increase W_0 or, put differently, reduce the relative number of low energetic electrons. Radiation losses will apart from decreasing W, result in an accumulation of runaway electrons at the highest energies, partly counteracting the effect of the exponential decreasing energy spectrum.

A more detailed analysis of the secondary generation proces must take into account the energy distribution of the primary runaway electrons as well as the angular distribution of the electron momentum of the secondary electron. This will gain a considerable perpendicular momentum as a result of a close collision. Therefore, some of the electrons will become trapped and do not immediately contribute to the runaway population. This problem is treated by Besedin and Pankratov [Bes-86]. The momentum distribution of the secondary electrons is calculated from the expression:

$$I(\mathbf{p},t) = \int d\sigma \; d\mathbf{p}_1 \; v_{rel} \; f(\mathbf{p}_1') \; f(\mathbf{p}') \tag{4.15}$$

which describes the entry of the electrons into the runaway region as a result of collisions between runaways with momentum $\mathbf{p}_1'$ and thermal particles with momentum $\mathbf{p}'$, where the prime identifies the parameters before the collision and the index 1 is used for the fast electron. Using the relativistic differential scattering cross-section ($d\sigma$) they found for the rate of the secondary generation [Bes-86]:

$$I(p_{//},p_{\perp},t) = 4\, n_e\, c\, r_e^2 \left[\frac{p_{//}+p_{//1}}{\sqrt{(p_{//}+p_{//1})^2+m_e^2c^2}} - \frac{p_{//1}}{\sqrt{p_1^2+m_e^2c^2}}\right]^{-1}$$

$$\times \; \frac{p_{//1}^4}{p_{\perp}^4} \; \frac{m_e^2c^2}{(p_{//}+p_{//1})^4} \; \bar{f}(p_{//}+p_{//1},t) \tag{4.16}$$

where p_1 is the momentum of the runaway electron after the collision and $\bar{f}$ is the one-dimensional runaway distribution function. From momentum and energy conservation it follows that:

$$p_{//1} = p_{//} \frac{p_\perp^2}{p_{//}^2 - (\sqrt{p^2 + m_e^2 c^2} - m_e c)^2}; \qquad p_\perp^2 < 2 m_e c p_{//} \tag{4.17}$$

To become runaway, secondary electrons must have sufficient momentum to exceed the collisional drag, which imposes a lower limit on their momentum:

$$(p_\perp^2 + p_{//}^2)^{3/2} > p_{cr}^2 p_{//} \tag{4.18}$$

where $p_{cr}^2 = e^3 n_e \ln\Lambda \, m_e \, (2+Z_{eff}) / (4\pi\varepsilon_0^2 E)$. Since the integral of I over $p_{//}$ and $p_\perp$, under condition (4.18), yield the total number of runaway electrons created per unit time, we can define an avalanche time t_a for the secondary process analog to our previous definition of t_0:

$$t_a = n_r \left(\frac{dn_r}{dt}\right)^{-1} = \frac{\int \bar{f} dp_{//}}{\int\int I(p_{//}, p_\perp, t) \, 2\pi p_\perp \, dp_{//} dp_\perp} \tag{4.19}$$

Depending on the energy distribution of the runaway electrons t_a may differ from t_0. For a flat energy distribution we find for TEXTOR $t_a = 0.44$ s (using E=0.1 V/m and Z_{eff}=2), significantly smaller than t_0.

With the treatment of Besedin and Pankratov the effect of trapping can be addressed. Using eqs. (4.16-4.18) $p_\perp/p_{//}$ is calculated, which is larger for smaller momenta. In Fig. 4.3 this ratio is plotted for TEXTOR parameters. It follows that for secondary runaway electrons, i.e those obeying eq. (4.18), the ratio $\Theta_c = p_\perp/p_{//} < 3$. This shows that these electrons will not be trapped for $r < R_0/(2\Theta_c^2) \approx 10$ cm. As this coincides with the region where the main runaway production occurs, trapping effects are considered negligible.

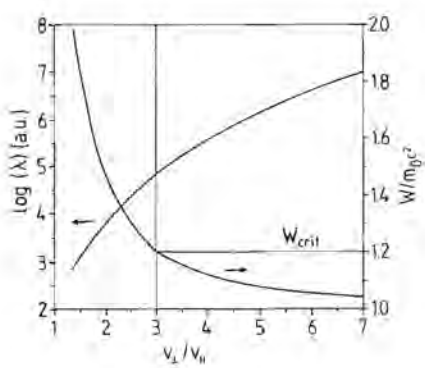

Figure 4.3:
The pitch angle of the secondary generated electrons. For $W>W_{crit}$, $\Theta<3$. Indicated also is the production rate I as a function of Θ.

4.4 Experimental Investigation of Runaway Electron Generation in TEXTOR

R. Jaspers[1], K.H. Finken[2], G.Mank[2], F. Hoenen[2], J. Boedo[3], N.J. Lopes Cardozo[1], F.C. Schüller[1].

[1]FOM Instituut voor Plasmafysica Rijnhuizen, Ass. Euratom-FOM, P.O. Box 1207, Nieuwegein, The Netherlands

[2]Institut für Plasmaphysik, Ass.Euratom-KFA, Forschungszentrum Jülich, D-52425 Jülich, Germany

[3]Institute for Plasma and Fusion Research, University of California at Los Angeles, USA

Abstract

An experimental study of the generation of runaway electrons in TEXTOR has been performed. From the infrared synchrotron radiation emitted by relativistic electrons, the number of runaway electrons can be obtained as a function of time. In low density discharges ($\overline{n_e} < 1\times10^{19}$ m^{-3}) runaways are created throughout the discharge and not predominantly in the start-up phase. From the exponential increase in the runaway population and the ongoing runaway production after increasing the density, it is concluded that the secondary generation, i.e. the creation of runaways through close collisions of already existing runaways with thermal electrons, provides an essential contribution to the runaway production. The effective avalanche time of this secondary process is determined to be $t_{eff} = 0.9 \pm 0.2$ s.

1. Introduction

As is well-known, the fact that the mean free path of an electron in a plasma is a strongly increasing function of its energy gives rise to the phenomenon of electron runaway. In an applied electric field, electrons that exceed the critical velocity (for which the collisional drag balances the acceleration by the field) are freely accelerated and can reach very high energies. In low density tokamak discharges a considerable amount of runaway electrons can be created, with energies up to tens of MeV. These can cause severe damage to the vacuum vessel and are a potentially dangerous source of hard X-rays. On the other hand, runaway electrons can carry a substantial amount of the plasma current and may have beneficial effects on plasma confinement (such as in the slide-away regime).

The creation of runaways in current-carrying plasmas has been studied extensively in the literature in the 60's and early 70's. In these theoretical studies [1-5] the creation rate of runaways is calculated from a kinetic treatment of the electron energy distribution around the critical velocity. The experimental check of these models is hampered by considerable uncertainties, due to the strong exponential dependencies on parameters such as electrical field, plasma density, impurity level and electron temperature, which can only be measured with limited accuracy. Attempts have been made to measure the production rate, using bremstrahlung in tokamaks [2,6] and Thomson scattering in a reversed field pinch experiment

where the subscripts r and s denote runaway and secondary respectively. $P_r(W_s)$ is the probability that an electron that has energy W_s after the collision becomes a runaway. In [10] the simple model $P_r(W_s)=0$ for $W_s<W_{crit}$ and $P_r(W_s)=1$ for $W_s>W_{crit}$ is used. A more detailed analysis brings into account the angular distribution of the velocity (see below). The number of secondary runaways generated by total runaway population is found as:

$$\frac{dn_{sr}}{dt} = \frac{n_r\ e\ E\ c}{2m_0c^2 \ln\Lambda a(Z_{eff})} = \frac{n_r}{t_0} \qquad (5)$$

where $a(1)=1$. Following the derivations in [10] it can be shown that $a(Z_{eff}) =(2+Z_{eff})/3$. Note that the secondary generation is independent of n_e.

Assuming a finite number of runaways $n_r(0)$ at $t=0$ as the result of the breakdown, a constant rate of primary generation, and describing runaway losses by a confinement time τ, the evolution of the runaway population is given by:

$$\frac{dn_r}{dt} = \lambda \nu_e(v_{th})\, n_e + \frac{n_r}{t_0} - \frac{n_r}{\tau} = F\lambda \nu_e(v_{th})\, n_e + \frac{Fn_r(0)}{t_{eff}} \qquad (6)$$

where $t_0=2m_0c\ \ln\Lambda a(Z_{eff})/eE$, $t_{eff}^{-1}= t_0^{-1} - \tau^{-1}$, and the multiplication factor $F=\exp(t/t_{eff})$ is the net effect of the secondary generation process. Integrating eq.(6) yields the runaway population as a function of time:

$$n_r(t) = \lambda\ \nu_e(v_{th})\, n_e\, t_{eff}\, \left(e^{t/t_{eff}} -1\right) + n_r(o)e^{t/t_{eff}} \qquad (7)$$

If t_0 goes to infinity, i.e. if it takes an infinitely long time for an existing runaway to create a new one, the classical result (eq.2) is obtained. If, however, $t_0<\tau$, i.e. if a runaway creates a secondary runaway within a runaway confinement time, then the secondary generation becomes apparent by the exponential growth of the runaway population.

It should be noted that as a result of close collisions the electrons gain a considerable transverse momentum. Therefore part of them are trapped and do not immediately contribute to the runaway population. This problem is treated by Besedin and Pankratov [8]. Using the relativistic Rutherford cross-section they found for the creation rate of the secondary generation:

$$\frac{dn_{sr}(p_{//},p_{\perp},t)}{dt} = 4\, n_e\, c\, r_0^2 \left[\frac{p_{//}+p_{//1}}{\sqrt{(p_{//}+p_{//1})^2+m_e^2c^2}} - \frac{p_{//1}}{\sqrt{p_1^2+m_e^2c^2}}\right]^{-1}$$

$$\times\ \frac{p_{//1}^4}{p_{\perp}^4}\ \frac{m_e^2c^2}{(p_{//}+p_{//1})^4}\ n_r(p_{//}+p_{//1},t) \qquad (8)$$

where r_0 is the classical electron radius and p_1 is the momentum of the primary electron after the collision. From momentum and energy conservation it follows that:

$$p_{//1} = p_{//} \frac{p_\perp^2}{p_{//}^2 - (\sqrt{p^2 + m_e^2 c^2} - m_e c)^2} \quad ; \quad p_\perp^2 < 2 m_e c p_{//} \tag{9}$$

Noting that the secondary runaways must have sufficient momentum to exceed the collisional drag imposes a lower limit on the momentum for the secondaries to become runaways:

$$(p_\perp^2 + p_{//}^2)^{3/2} > p_{cr}^2 p_{//} \tag{10}$$

where $p_{cr}^2 = e^3 n_e \ln\Lambda \, m_e (2+Z_{eff}) / (4\pi\varepsilon_0^2 E)$.
Using eqs. 8-10 the ratio of perpendicular to parallel momentum can be calculated. This ratio determines whether the electrons will be trapped.

2.3 Generation mechanisms under different conditions

In several publications the creation of runaways during the start up phase of the discharge is considered to be the most important generation process [13,14]. The basis for this assumption is the high value of E and the low value of n_e in the initial phase of the discharge. However, there are several effects that complicate the issue. Firstly, shortly after breakdown the plasma is only partially ionized whereas the theory treats only fully ionized plasmas. Secondly, in that phase of the discharge the distribution function of the bulk electrons may deviate strongly from Maxwellian, and thirdly, because of the relatively slow penetration of the applied electric field, it is most likely that in the start up phase the runaways are generated predominantly in the outer regions of the plasma [12].

Moreover, there are experimental indications of runaway loss during the start-up phase. These may be related to the concentration of the generation in the outer part of the plasma, to enhanced magnetic turbulence, especially when the edge safety factor q_a passes through a rational number (see e.g.[13,15]), and to too low plasma current for runaway confinement. As to the latter, assuming a linear current increase with a uniform current distribution and the approximation that runaways are born at $r > 0.5a$ the criterion for confining runaways is [12]:

$$dI_{pl}/dt > 1\times10^4 \frac{E\,a}{R_0} \quad \text{kA/s} . \tag{11}$$

In conclusion, while in the start-up phase of the discharge E/E_c may have a high value, it is likely that the generation of runaways at this stage is restricted to the outer part of the plasma, and that a considerable part of the runaways is quickly lost.

During the steady state phase of a tokamak discharge, the classical models predict a continuous generation of runaways according to eq. 2, which is significant only when E and T_e are high and/or n_e low enough. Normally, in high density discharges no measurable runaway production can be expected in the current plateau phase.

As a result, there are two options to experimentally investigate whether the secondary generation process contributes to the runaway population in a tokamak. First, by comparing discharges with different densities during the start-up phase but the same density in the current plateau, it can be checked whether there is significant runaway production during the current plateau. Secondly, if conditions can be found in which the secondary generation prevails, e.g. by raising the density after establishing a runaway population, the number of runaways should show an exponential growth. This approach is followed in the experiments described below.

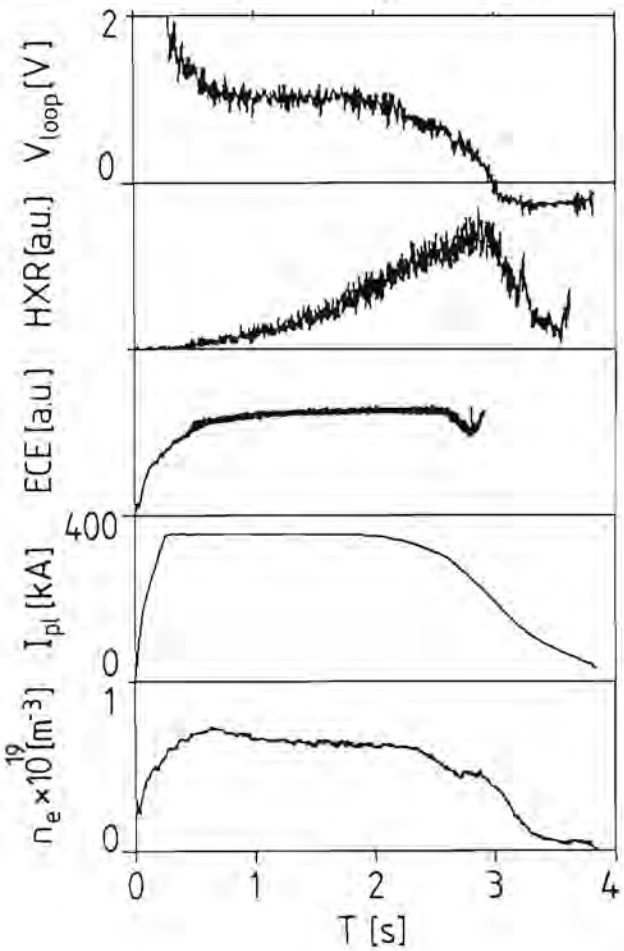

Figure 1:
Plasma parameters for a typical low density ohmic discharge. From top to bottom: the loop voltage, the HXR signal (measured tangentially), the ECE signal, the plasma current and the line averaged electron density.

3. Experimental Set-up

Experiments were performed in the TEXTOR tokamak (major radius R_0=1.75 m, minor radius a=0.46 m). Typical plasma parameters used for this set of experiments are: I_{pl}=350 kA, B_t=2.25 T, flat top time ≈ 2 s, V_{loop} ≈ 1.0 V during flat top, deuterium discharges. To obtain typical runaway discharges the line averaged electron density was kept below $1\times10^{19}m^{-3}$. Plasma parameters of these discharges are plotted in Fig. 1. The discharges analyzed in this paper are not low enough in density to reach the slide away regime [6,16]. The hard X-ray - (HXR) and neutron (N) spectra in the range 100 keV to 5 MeV are measured with a NE-213 type scintillator. This detector is shielded with 25 cm of lead in front and 10 cm elsewhere. A collimator with an opening angle of 5° is used. The detector is aligned tangentially to one of the ALT-II limiter blades under an angle of 3° (given by the q-value at the plasma edge), i.e. directed to the hard X-rays from the runaways hitting the limiter. Because of the relativistic energies of the runaways, the X-rays are emitted in the direction of the incident electrons.

In the low density ohmic discharges almost all detected neutrons are (γ, n) neutrons, created when a runaway electron hits the carbon limiter or when highly energetic X-rays hit the lead collimator of the detector. For both processes the incident energy of the photon must be >10 MeV. Hence both the N-signal and the synchrotron signal are sensitive to the most energetic runaways, the difference being that the synchrotron signal diagnoses the runaways in the interior of the plasma, whereas the neutron signal measures the loss rate of energetic runaways.

The synchrotron radiation, originating from the movement of highly relativistic electrons in the toroidal direction, is measured with an Inframetrics thermographic camera. This is sensitive in the wavelength range of 3-14 μm, but as CaF_2 optics is used the working range is limited to 8 μm. The camera is aligned tangentially to the plasma in the direction of electron approach. The synchrotron radiation is compared with the thermal radiation of the limiter (limiter surface: graphite, emission coefficient ≈ 0.8) of which the temperature is known, giving an in situ absolute calibration of the camera.

The number of runaways N_r, deduced from the observed synchrotron radiation is calculated from [11]:

$$N_r \int P_\lambda\, T(\lambda) d\lambda = \int L_\lambda^s\, T(\lambda)\, d\lambda A\ \Omega\,, \qquad (12)$$

where A is the cross-sectional area of the ring filled with runaways , $\Omega=2\pi\,.\,2\Theta$ is the solid angle into which the synchrotron radiation is emitted, Θ is the pitch angle of the runaways, L_λ^s is the measured spectral radiance, and $T(\lambda)$ is the transmission function of the optical system. $P_\lambda = N_r^{-1} \int P^e_\lambda f(E) dE$, where P^e_λ is the synchrotron radiation emitted by one electron, and f(E)

the energy distribution function. The emitted synchrotron power P^e_λ depends on the energy of the runaway electron and on the radius of curvature of the electron orbit. This curvature is calculated from the pitch angle $\Theta = v_\perp / v_{//}$ of the runaways [11], which can be deduced directly from the vertical extent of the radiation. Information about the energy distribution of the runaway population is contained in the spectrum of the synchrotron radiation. Because the contribution to the radiation is strongly weighed with the energy of the runaway, from a spectral analysis mainly the maximum energy of the runaway population can be determined.

4. Results and Interpretation

4.1 Determination of pitch angle, energy and number of runaways.

The pitch angle Θ is determined directly from the vertical extent of the synchrotron radiation:

$$\Theta = 0.12 \pm 0.02 \text{ rad.}$$

This value is in agreement with a 'diffusive' increase of Θ during the acceleration process under the influence of electron-ion collisions [17].

The spectrum of the synchrotron radiation is crudely measured by putting filters with different transmission curves in front of the IR camera, in a series of reproducible discharges. To interpret the result, an assumption about the shape of the energy distribution must be made. Two different energy distributions were compared: a flat distribution out to E_{max}, and a mono energetic distribution at E_{max}. From the spectral measurements E_{max} was determined for both distributions (Fig.2). For a given energy distribution, the experimental uncertainty in the determination of E_{max} is ≈ 2 MeV. Fig.2 also shows a theoretical curve calculated taking into account the acceleration in the electric field and the energy loss due to synchrotron radiation. It is noted that

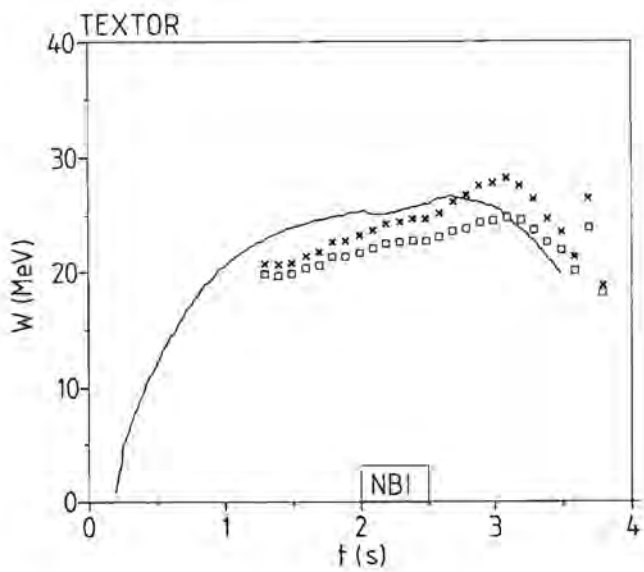

Figure 2:
The maximum energy W_{max} of runaways, as derived from the spectrum of the synchrotron radiation assuming either a flat distribution function (squares) or a mono-energetic distribution (crosses). The curve results from a free fall calculation with synchrotron radiation losses included. A pitch angle of 0.1 rad was measured and used in the calculations. In this case 500 kW NBI power was applied.

• the resulting value of E_{max} is fairly independent of the shape of the energy distribution function. This reflects the fact that the radiation is dominated by the contribution of the electrons with the highest energy, and means that we may interpret E_{max} as a measure of the highest energy present in the runaway population.

• the measured evolution of E_{max} agrees well with the theoretical prediction.

• saturation of the runaway energy due to radiative energy loss occurs already early in the discharge.

In the remainder of this paper, a flat energy distribution function up to a maximum energy E_{max} is assumed. This model is plausible if runaways are generated and accelerated at a constant rate during the discharge. According to [8] for the secondary generation mechanism eventually also a flat energy distribution is expected. If losses are important the distribution function can decrease towards higher energies. If that is the case, the values given for the N_r given in this paper are overestimates (see also section 5). On the other hand, the saturation of the runaway energy due to radiation may partly counteract this effect.

Having checked the consistency of the experimental E_{max} with the theoretical model for a number of discharges, the theoretical value will be used in those discharges where no measurement of $E_{max}(t)$ is available. (For the spectral analysis a series of repeated discharges is required).

With the experimental values of Θ and E_{max} and the assumed shape of the energy distribution function, the total number of runaways can be computed using eq. 12. The statistic error introduced by the experimental error on Θ and E_{max} is of the order of 30 %. The systematic error introduced by the choice of the distribution function is several times larger than this. For instance, the two distributions used in Fig.2 yield a runaway population which is a factor of 6 apart.

Hence, while the experimental determination of N_r has necessarily a rather large experimental error, an order of magnitude comparison with theory is certainly possible. Relative changes of N_r can be measured with reasonable accuracy, provided that the energy distribution does not undergo drastic changes.

4.2 The Production Phase of Runaways

To address the question in which phase of the discharge the runaways are created, discharges with different initial conditions but equal flat top parameters were compared. In the top trace of Fig. 3a $n_e(t)$ is plotted for the 'normal' runaway condition, while for the discharge in fig. 3b n_e is about two times higher in the first 0.5 s. Fig. 3 further shows the HXR, neutron (N) and synchrotron radiation (IR) signals.

The HXR signal in Fig 3a is already clearly seen after 100 ms and reaches its maximum at t=1 s, at which time the detector saturates. At the end of the discharge the detector is working in the linear range again. (Saturation occurred because the detector was set sensitive to measure

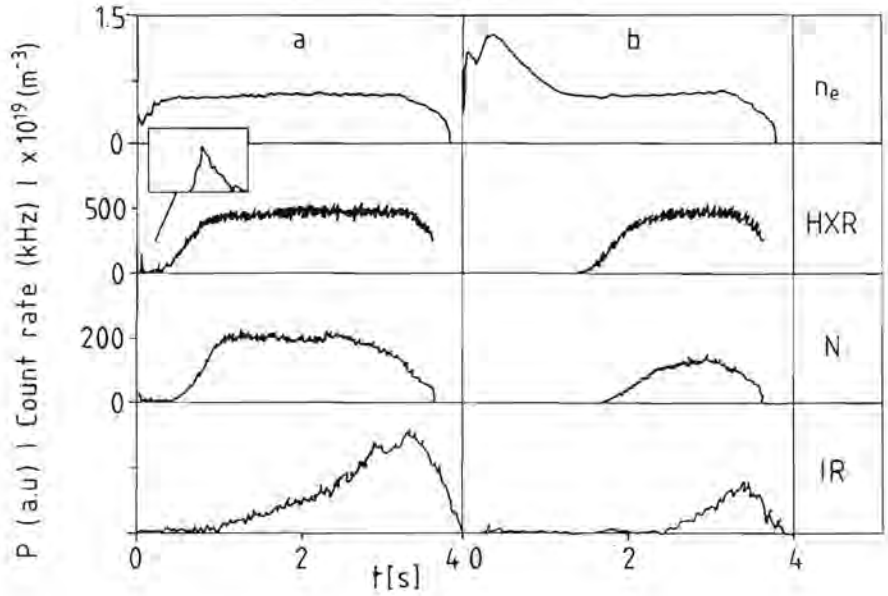

Figure 3: *Comparison of two discharges with different initial densities. Plotted is from top to bottom: the electron line averaged density, the HXR signal (saturated after about 1 s), the neutron signal (also saturated) and the infrared synchrotron signal. It is clearly observed that also during the discharge runaway production takes place. In Fig 3a the burst of HXR during the first 50 ms is magnified, which signals the loss of runaways due to the bad confinement early in the discharge. It should be mentioned that the IR signal in Fig 3b is measured with a different optical filter in front of the IR camera. For this reason are the units in the IR signals not exactly the same.*

the starting phase. For comparison, an unsaturated signal for a similar discharge is shown in Fig. 1.) The N-signal starts about 400 ms after the HXR-signal, which is consistent with the assumption that the neutrons are created by high energy X-rays. This signal also saturates at t≈1 s for the same reason as before. The synchrotron radiation is detectable from t=1 s on and increases until the plasma current has nearly decayed.

In the discharge with the high density in the start up phase, the times at which the HXR, N and IR signals start to rise (Fig. 3b) are delayed by more than one second relative to the low density case (Fig. 3a). Apart from the delay, the rise of the signals is very similar in both discharges.

Clearly, these observations do not support the hypothesis that the runaway electrons are predominantly generated in the start-up phase of the discharge. On the contrary, the fact that in

the high density case the signals start to grow during the flat top clearly indicates that there is a significant production at that time.

A closer look at Fig. 3a. shows that at the very beginning of the discharge, at about 30 ms, a burst of hard x-rays is produced. This indicates that runaways are generated in the start-up phase and partly lost. This loss can possibly be attributed to the bad confinement of runaways early in the discharge or the integer values of the edge safety factor, as discussed in section 2.3. Using eq. (11), it is found that the current ramp rate in these discharges is only marginally large enough to confine the runaways that are created in the first 40 ms.

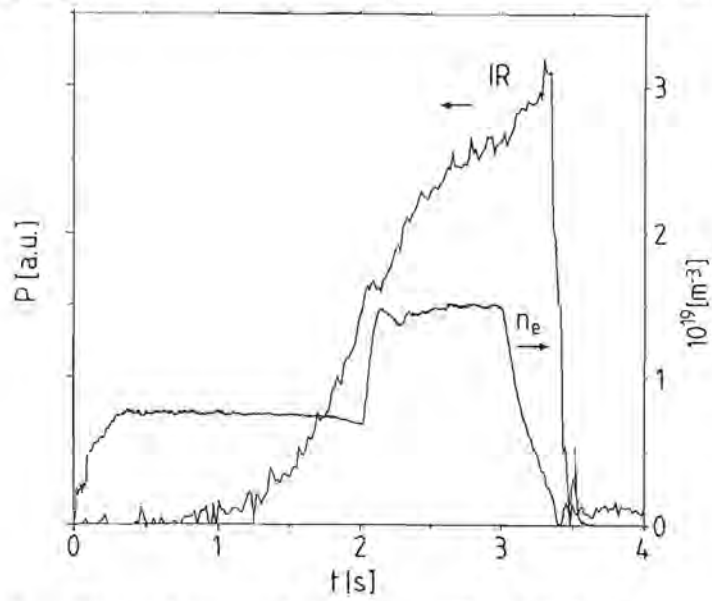

Figure 4: *The synchrotron radiation intensity (IR) and the line averaged electron density as a function of time. The IR signal keeps on increasing when the electron density is doubled,which shows the ongoing runaway production at higher densities.*

4.3 Increasing n_e during the flat top

In a second experiment to discriminate between primary and secondary generation, the electron density was doubled during the discharge, when an appreciable amount of runaways was already present. The density increase, accompanied by a decrease in temperature, should reduce the primary generation to a negligible level. In the experiment it is observed that the synchrotron intensity keeps on increasing for more than 1.5 s after the increase of the density (see Fig.4). The total increase of the IR signal during the period of high density is a factor of 2.

The increase of the IR-signal can be attributed to a combination of causes: increase of Θ, increase of E_{max}, and finally an increase of N_r. Θ is measured independently and no significant increase of Θ is observed, and neither is this to be expected. The decrease of T_e

induces an increase of the E-field, leading to a further acceleration and consequent increase of E_{max}. Taking $E \propto T^{-1.5}$ and using the model for acceleration in the field and energy loss through radiation, an upper estimate for the increase of E_{max} can be given: $\Delta E_{max} \approx 1.8$ MeV. This could result in an increase of the IR-intensity of at most 25 %, which is far insufficient to explain the observed increase of a factor of 2. As a consequence, the increase of the IR-signal is attributed mainly to an increase of N_r, which presents evidence for the occurrence of secondary generation (which is practically independent of density).

To further check the usefulness of the HXR and IR signals as a measure of N_r, a series of discharges were performed with a slight variation in the density. Fig.5 shows the IR intensity and the HXR signal at t= 2.0 s, as a function of the line averaged density. The theoretical predictions (using eq.2, neglecting the possible variation of Z_{eff} over the small range of n_e) are also plotted, showing fair agreement. The comparison is relative, all values are normalized at $n_e = 0.85 \times 10^{19} m^{-3}$. For the measurements shown the HXR detector did not go into saturation. Note that this experiment does not distinguish between primary and secondary generation: the multiplication factor F due to the secondary generation process does not depend on n_e.

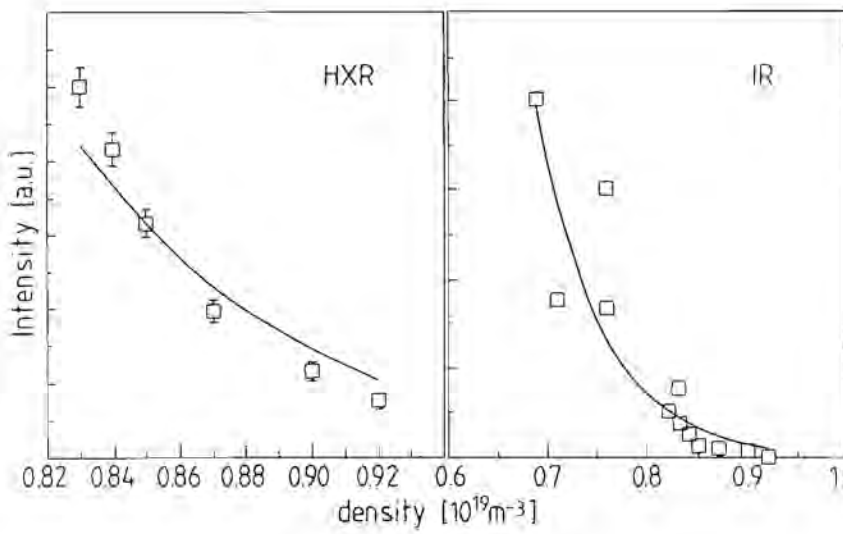

Figure 5: *Density scan of the HXR signal and the infrared synchrotron radiation signal. The curve represents the relative dependence of the creation rate on the density for the primary (or secondary) generation mechanism (according to eq. 2).*

4.4 Analysis of the evolution of N_r

In Fig. 6 N_r is shown as a function of time, as derived from the IR signal, taking into account the increasing E_{max}. The absolute value of N_r has a rather large uncertainty, due to errors in E_{max} and the choice of the energy distribution function, as discussed in section 4.1. However, for this plot only the relative evolution is important and the error in this is small, as seen by the variation of the datapoints. Also shown are the theoretical predictions based on primary and secondary generation, using the effective avalanche time t_{eff} as a free parameter. Clearly in the limit $t_{eff} = \infty$ (primary generation only, no loss of runaways) the theoretical curve does not fit the data, and an even larger discrepancy is found if a finite runaway confinement time is assumed (τ = 2 s for the example in the figure). Good agreement between prediction and measurement is obtained for

$$t_{eff} = 0.9 \pm 0.2 \text{ s} \qquad \text{(experimental value)}$$

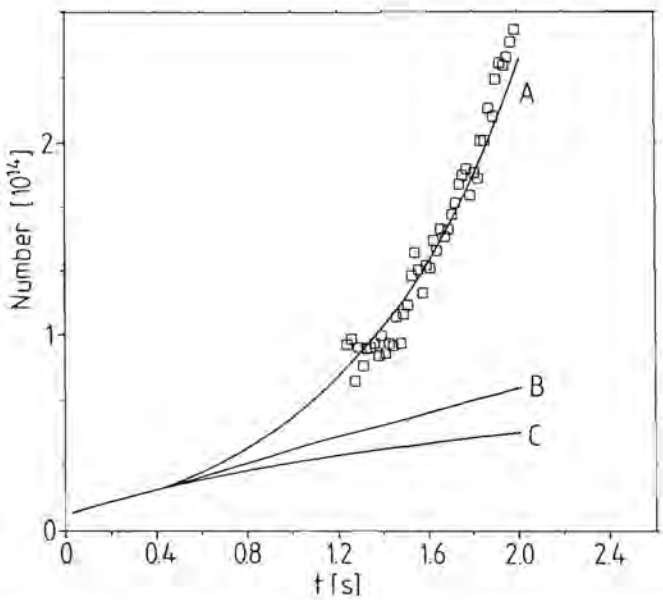

Figure 6: *Time dependence of the number of runaways in the plasma. The absolute number of runaways is given for the experimentally deduced data-points, represented by the squares in the figure. The exponential increase is a clear indication for secondary generation, as seen by the close agreement with curve A, for which t_{eff} =0.9 s. This is obtained by fitting the time dependence of eq. 7 to the data-points. Curve B represents a constant creation rate of runaways without losses for the primary generation model. The same value of λ is used as in curve A. If losses are taken into account in the primary generation model curve C is obtained (for a confinement time of τ = 2.0 s).*

This value should be compared to the theoretical value for $t_0=t_{eff}\,(1+t_{eff}/\tau)^{-1}$, obtained by inserting the relevant TEXTOR parameters into the definition of t_0 ($Z_{eff}\approx 1.5$-2 for boronized TEXTOR):

$$t_0 = 0.75 \pm 0.05 \text{ s} \qquad \text{(theoretical value)}$$

Corrections for trapped particle effects or a higher value of Z_{eff} lead to a somewhat higher value of t_o. From the theory of Besedin and Pankratov [8], the momentum distribution of the secondaries can be calculated using eq. 9. For TEXTOR parameters it follows that secondaries with energies larger than the critical energy have $p_\perp/p_{//}<3$. These secondaries will not be trapped in the central 10 cm, and corrections for trapped secondaries will therefore be small. Moreover, a finite runaway confinement time τ also leads to $t_{eff} > t_o$. The exponential behaviour of the theoretical curves clearly brings out that at t=2 s the multiplication factor F resulting from the secondary generation process is of order 10, so that at that time the secondary generation fully dominates the birth rate.

It should be mentioned that the absolute value for the number of runaways is factor of 50 smaller than the value derived in [11] for a flat energy distribution. This discrepancy arises from an incorrect normalization of the synchrotron power in Fig. 8 of [11].

In conclusion, the evolution in time of the experimentally determined number of runaways is consistent with the occurrence of secondary generation. The effective avalanche time determined from the exponential growth of N_r agrees well with the theoretical value. The runaway confinement time must be very long, $\tau > 2$ s, which in itself is consistent with the fact that an appreciable number reach $E_{max}\approx 20$ MeV, for which they must be accelerated for more than 1 s.

4.5 Absolute Runaway Generation Rate Measurements.

In the literature absolute comparisons of experimental values of the runaway birth rate with theory are sparse and have shown discrepancies of many orders of magnitude [2]. It is interesting to make such a comparison using the present measurements, even if it is unavoidable that the uncertainties in the theoretical prediction are large due to the exponential dependence on $\varepsilon=E/E_c$, and that the experimental value has a systematic error associated with the assumption about the energy distribution function. Fig.7 shows the theoretical values of λ as given by eq.2 (using also the relativistic corrections, about 20 % in the parameter range of these experiments, as given by [3]) as a function of ε, for three different values of Z_{eff}. Results from other low density discharges in the boronized TEXTOR give $1.5 \le Z_{eff} \le 2$ [18].

From the IR-signal $N_r(t)$ is obtained. To compute $F\lambda$ the values of $n_r(t)$, n_e and T_e must be known. For the data shown in Fig.6 $N_r(t=2.0s) = 2.5\times10^{14}$, $dN_r/dt = 2.0\times10^{14}$ s^{-1}, $n_e(r=0)= 1.1\times10^{19}$m^{-3}, and $T_e(0)=1.5$ keV. We will assume that the main production of runaways takes place in the central 10 cm of the discharge, on the ground that the value of λ

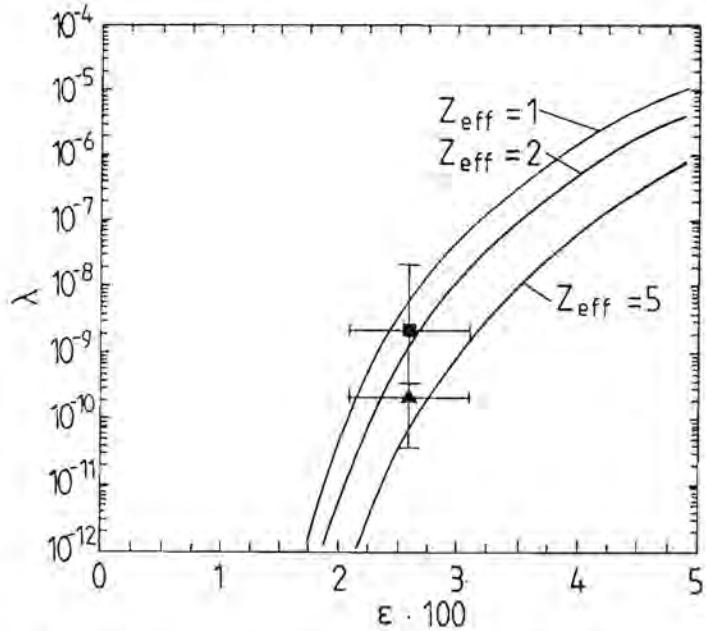

Figure 7: *Theoretical curves for the creation rate λ according to eq. 2b for three different values of Z_{eff}. From the experimentally deduced value Fλ, the birth-rate λ is calculated for the cases F=1 (square) and F=10 (triangle). Within the large errors, agreement is found for both cases. The accuracy is insufficient to judge the effect of secondary generation.*

from eq. 2b will have already decreased strongly at r=10 cm with the given density and temperature profiles. Thus we find for the experimental birth rate:

$$F\lambda = 2\times10^{-9}$$

In the absence of secondary generation F=1, while the results presented in the previous sections show that it is likely that secondary generation does occur, in which case F≈10 for the case under study. The experimental value of ε is computed from the loop voltage, central temperature and density, leading to

$$\varepsilon = E/E_c = (2.6\pm0.5)\times 10^{-2}.$$

Both cases are indicated in Fig. 7, and the large experimental uncertainties are indicated. Clearly, within the large errors that are unavoidable in such a comparison, agreement is found. It may also be noted that the accuracy of this absolute measurement is insufficient to judge the effect of secondary generation.

A note on the estimation of the errors on the experimental value is in place. In the computation of N_r from the IR-signal, an assumption about the energy distribution must be made. The present values were found using a flat energy distribution. To give an impression of

the possible systematic error: assuming a monoenergetic distribution at E_{max} leads to a 6 times lower value of $F\lambda$, while if an exponentially decreasing distribution function $f(E) \sim \exp(E / 5\ MeV)$ is assumed, a more than 10 times higher value for $F\lambda$ would follow. The errorbars given in Fig. 7 correspond to these extreme cases. It is noted that, a monoenergetic distribution is expected neither in the primary nor in the secondary model, and the assumption of a flat distribution is a lower estimate. Other contributions to the experimental error, such as the uncertainty in the determination of E_{max} (leading to a 30% error on λ) and the assumption that the majority of the runaways are confined to a region with $r = 0.1$ m , are relatively unimportant on this scale.

The error in ε results from the Abel inversion of the interferometer data, the extrapolation of the electron temperature and the calculation of the electric field in the center from the loop voltage and is estimated to be 20 %. It should be noted that due to the steep dependence of the birthrate on ε, in the comparison of theory and experiment the error in ε is more significant than the order of magnitude uncertainty in the determination of N_r.

5. Discussion and Conclusions

In conclusion, the observations of the synchrotron radiation, supplemented by the HXR and neutron signals, are fully consistent with the theory for runaway production. In particular, the birth of runaways through secondary generation is found to be the dominant creation mechanism in the low density TEXTOR discharges. This is evidenced: i) by the exponential increase of the number of runaways during the current flat top, and ii) by the further increase of the synchrotron signal if the density is increased when runaways are already present in the discharge. For the effective avalanche time of this mechanism a value of $t_{eff} = 0.9 \pm 0.2$ s is found, which is close to the value that follows from the theory of Jayakumar et al. [10]. The difference can be attributed to the effect of particle trapping and the finite confinement time of runaways.

An absolute birth rate coefficient has been deduced and, within the large experimental error bars, the value agrees with the theoretical predictions. To our knowledge, this is the first experiment in which the absolute measurement of the birth rate is in agreement with the theory. The large error bar on N_r is mainly due to the unknown shape of the energy distribution function. Improvement can be obtained by better spectral resolution of the IR-signal, or by the use of other diagnostics to obtain information on f(E). However, comparison with theory will still be limited by the experimental error in the determination of ε.

The confinement of the runaway electrons appears to be very good in TEXTOR. This is deduced from two independent arguments. First, to reach 20 MeV, the runaways must be confined for more than 1 second. Secondly, the observed exponential increase of N_r requires $\tau > t_0 = 0.75$ s. The good confinement is consistent with the fact that the deduced primary birth

rate agrees with the theoretical prediction. In ref. [2] large discrepancies were found between the experimental and theoretical values of the creation rate, and these were attributed to runaway losses. Limited confinement may also explain why in [13] no secondary generation is observed: there a runaway confinement time of τ=400 ms is given, whereas $t_0 \approx$ 700 ms for their experimental conditions.

At densities even lower than those reported in this paper, i.e. in the slide away regime [16] the secondary mechanism is not expected to make a large contribution to the runaway generation, because of the lack of MeV runaways, which make, according to eq. 8, the dominant effect. In fact, there may be only a small window in the operational parameter space where the secondary generation process is clearly observable.

Acknowledgements
The authors would like to thank their colleagues H.F. Tammen, B.C. Schokker and E.Graffmann for stimulating discussions and A. Hiller for technical assistance. Part of this work was performed under the Euratom-FOM association agreement with financial support from NWO and Euratom.

References

[1] H. Dreicer, Phys. Rev. 115, 238 (1959); and Phys. Rev. 117, 329 (1960);
[2] R.M. Kulsrud, Y.C. Sun, N.K. Winsor, H.A. Fallon, Phys. Rev. Lett. 31, 690 (1973);
[3] J.W. Conner and R.J. Hastie, Nucl. Fusion 15, 415 (1975);
[4] A.V. Gurevich, Sov.Phys.-JETP 12, 904 (1961);
[5] R.H. Cohen, Phys. Fluids,19,239 (1976);
[6] G.Fussmann, G.Becker, K. Behringer et al., Proc. 9th IAEA conference, Vol. III, 295, Baltimore, (1982);
[7] Y.Yagi, Y. Hirano, T. Shimada, K. Hattori, Y. Maejima and I. Hirota, Plasma Phys. Controlled Fusion 33, 1391, (1991);
[8] N.T. Besedin and I.M.Pankratov, Nucl.Fusion 26, 807, (1986).
[9] V.V. Parail and O.P. Pogutse, *Reviews of Plasma Physics*, Vol. 11, Consultants Bureaus, New York, (1986);
[10] R. Jayakumar, H.H. Fleischmann, S.J. Zweben , *Collisional Avalanche Exponentiation of Run-Away Electrons in Electrified Plasmas* , PPPL-2849 (1992);
[11] K.H.Finken, J.G. Watkins, D. Rusbüldt, W.J. Corbett, K.H. Dippel, D.M. Goebel, R.A. Moyer, Nucl. Fusion 30, 859, (1990);
[12] H. Knoepfel and D.A. Spong, Nucl. Fusion 19, 785 (1979);
[13] O.J. Kwon, P.H. Diamond, F. Wagner, G. Fussmann, ASDEX and NI teams, Nucl.Fusion 28, 1931, (1988).
[14] P.J. Catto, J.R. Myra, P.W. Wang, A.J. Wootton, R.D. Bengtson, Phys.Fluids B 3, 2038 (1991).
[15] A.D. Cheetham, J.A. How, G.R. Hogg, H.Kuwahara, A.H. Morton, Nucl. Fusion 23, 1694, (1983);
[16] G. Fussmann, D. Campbell, A. Eberhagen et al., Phys. Rev. Lett. 47, 1004, (1981);
[17] L.Spitzer, *Physics of fully ionized gases*, Intersience Publishers, New York, (1956);
[18] E. Graffmann, Z.S. Fang, H. Soltwisch, K.Wang, Proc. 18th Eur. Conf. on Controlled Fus. and Plasma Phys., 15C, II-13, Berlin (1991);

4.5 Secondary Generation in ITER and TEXTOR

In Sec. 4.4 the occurrence and the importance of the secondary generation was demonstrated. This can have two consequences for tokamak operation. First there is the danger that even at relatively high densities and low electric fields a small initial runaway population can lead to a large, high energy runaway population in normal operation if the discharge duration is long enough. This could be a potential danger to a tokamak reactor because when the confinement of these runaways is lost the machine will be damaged. On the other hand one could deliberately use this mechanism to drive an appreciable fraction of the plasma current by runaway electrons in tokamaks. This would allow for a longer pulse operation or possibly a quasi steady state reactor, even at higher electron densities than in runaway discharges. In both cases the necessary conditions to be fullfilled for the avalanching process to occur is that the runaway confinement time exceeds the time t_0. The effect of such a cascade for ITER and TEXTOR will be investigated in this section.

Three phases of operation for ITER are considered in which the runaway production is drastically different: the start-up phase, the stationary phase and the disruption phase.

-Stationary phase. The projected parameters for ITER in this phase are: I_p= 20 MA, V_{loop} =1 V and $n_e = 1\times10^{20}m^{-3}$. Under such circumstances no runaway generation will occur at all, because the drag experienced by runaway electrons as a result of electron-electron collisions is larger than the electric force eE, see Eq (4.7): $E<E_{lim}$. For runaway generation in ITER to occur the condition to be fullfilled is:

$$\frac{V_{loop}}{n_e} > 4\times10^{-20}\,Vm^3 \qquad (4.20)$$

-Start-up. The start-up phase is characterized by a lower density and a higher electric field compared to the stationary phase and condition (4.20) is likely to be met. Although the primary generation is expected to be low even in this phase, an appreciable runaway current may still be produced through the secondary generation mechanism. Even for very low runaway currents generated by the primary mechanism (I_{pr}), in less than a minute the total plasma current will be carried by runaway electrons. This time (t_r) needed to have a runaway dominated plasma current is estimated from:

$$t_r = t_0 \ln\left(\frac{I_p}{I_{pr}}\right) = \frac{(2+Z_{eff})m_e c \ln\Lambda}{eE} \ln\left(\frac{I_p}{I_{pr}}\right) \qquad (4.21)$$

For values I_{pr} = 1mA and V_{loop}=3 V one finds $t_r < 30$ s, provided τ is sufficiently long. The effect for ITER of this runaway current will be to save a few tens of voltseconds in this phase

due to the low resistance of this current. In the stationary phase where the density is increased and the electric field drops, the runaways will be decelerated and the runaway current decays.
-Disruption. As will be discussed in more detail in chapter 7, the runaway production in a disruption is strongly altered by the occurence of the secondary generation. In this phase E is high enough to meet the criterion of eq. (4.20). The avalanche time t_0, inversely proportional to E, will decrease and the secondary production will increase the runaway generation. Although this will increase the total number of runaway electrons, it will decrease the maximum energy the runaway electrons can reach. A larger runaway production decreases the time in which the electric field is high, and hence suppresses the runaway acceleration. Since the high energy of runaway electrons causes more technical problems than the number of runaway electrons in a disruption, the secondary generation is beneficial in this case.

Summarizing we can state that the occurrence of secondary generation for ITER cannot be used to drive in the stationary phase a runaway current, but on the other hand the danger of runaway electrons in for instance disruptions is reduced as a result of this production mechanism and several tens of voltseconds can be saved in the start up phase.

For TEXTOR-94 in the stationary phase thesituation is different compared to ITER, since already in normal operation, with $n_e=3\times10^{19}m^{-3}$, $E>E_{lim}$ and secondary runaway generation occurs. To illustrate the effect of this mechanism, the time evolution of the runaway current I_r and the consumed flux has been calculated in a simple model: $I_r(t)$ and the electric field E(t) are given by the solution of the set of equations, provided $E>E_{lim}$:

$$\frac{dI_r(t)}{dt} = \frac{I_r(0)\exp(t/t_{eff})}{t_{eff}} \qquad (4.22a)$$

$$t_{eff}(t) = \left(\frac{1}{t_0} - \frac{1}{\tau}\right)^{-1} \qquad (4.22b)$$

$$t_0(t) = \frac{(2+Z_{eff})\, m_e\, c\, \ln\Lambda}{e\, E(t)} \qquad (4.22c)$$

$$E(t) = \frac{V_{loop}\,(1-I_r(t)/I_p)}{2\pi R_0} \qquad (4.22d)$$

The discharge parameters taken for TEXTOR-94 are: $Z_{eff}=1.5$, $V_{loop}=1$ V, $I_p=0.5$ MA, $R_0=1.75$ m. Free parameters are the runaway confinement time τ and the initial runaway current $I_r(0)$ as a result of primary generation early in the discharge. As to the former, it is known that for TEXTOR this confinement time is the order of 1 second or more. This is deduced from the high energies of about 25 MeV the runaways could reach in TEXTOR, the

effect of the secondary generation requires a confinement time longer than t_0, and the small diffusion as observed in the runaway snake (chapter 5). For the initial runaway current, a value of about 1 kA was already achieved in the experiments of section 4.4. By lowering the initial density even more, higher values seem possible. The runaway current as a function of time for different τ and $I_r(0)$ is plotted in fig. 4.4a. In Fig. 4.4b the pulse length (obtained by integrating the consumed volt-seconds) as a function of τ is plotted for different $I_r(0)$. A sizeable extension of the pulselength is expected.

Runaway current drive for ITER is not fully excluded as a possibility to prolong the discharge duration. It has been demonstrated in slide-away discharges that the energy confinement of the plasma is improved if a large runaway current is present [Fus-81]. This would allow to operate ITER at lower densities to reach ignition. This scenario however is highly speculative and we will first aim at demonstrating the secondary generation for TEXTOR-94. Succeeding in this the effect of a large runaway current on normal plasma operation can be investigated.

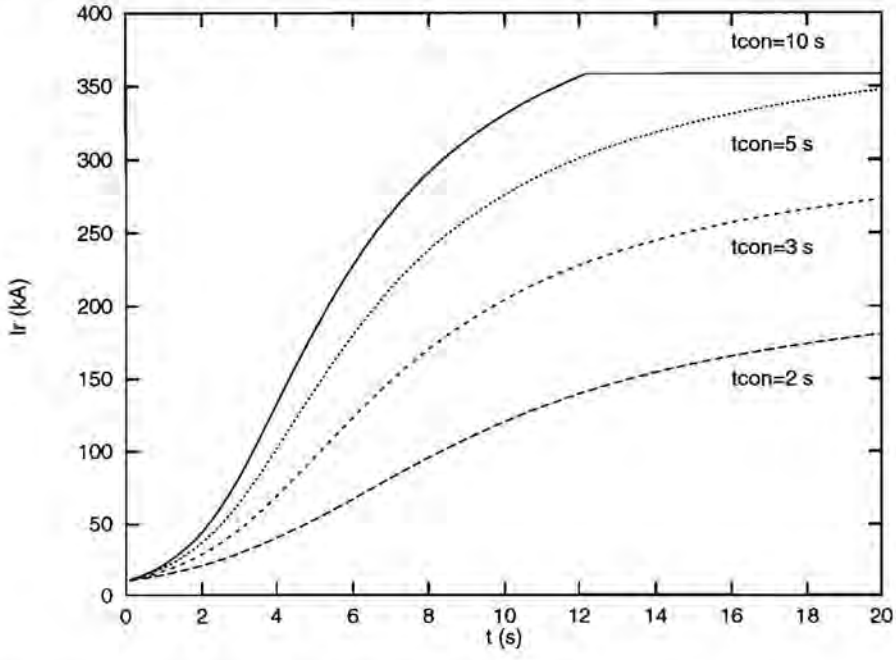

Figure 4.4a: *The runaway current according to the secondary generation for TEXTOR as a function of time for different runaway confinement times. The primary runaway current is assumed to be 10 kA, whereas the plasma current is 350 kA.*

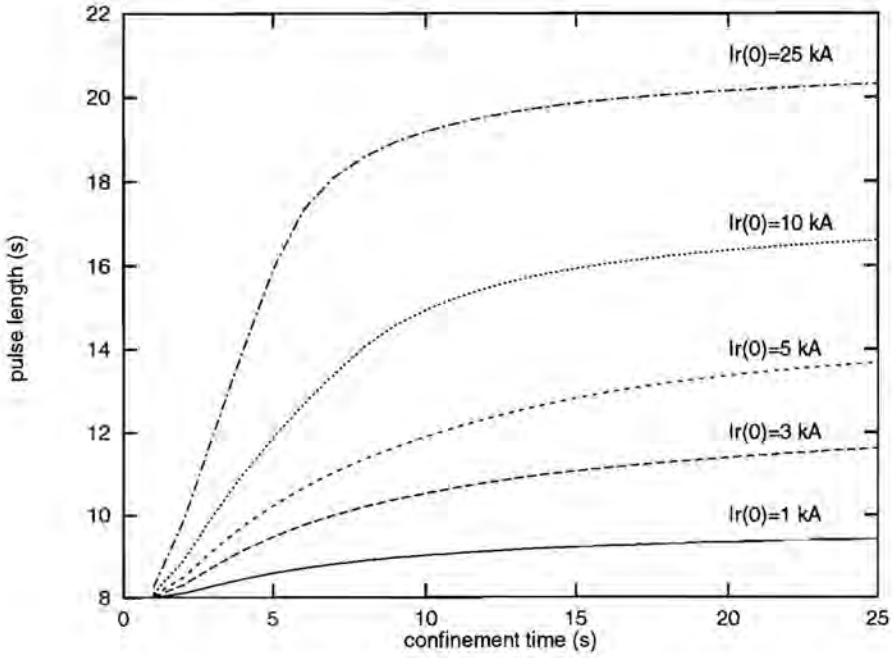

Figure 4.4b: *Extension of the TEXTOR-94 pulslength as a result of secondary generation as a function of the runaway confinement time for different values of the initial runaway current.*

CHAPTER 5

EXPERIMENTS ON RUNAWAY TRANSPORT

5.1 Introduction

One motivation for runaway transport studies is that such investigations can provide a possibility to probe the magnetic turbulence in the core of the plasma. On theoretical grounds it is expected that the diffusion rate of a test particle scales linearly with its velocity for fully stochastic magnetic turbulence, while for electrostatic turbulence the diffusion rate scales inversely with the test particle velocity. Thus, the fast runaway electrons provide a sensitive test for the presence of magnetic turbulence. Moreover, since the runaway population is a very small fraction of the electrons (for TEXTOR $n_r/n_e=O(10^{-6})$), a runaway electron can be regarded as a true test particle. As such it is much less constrained by ambipolar diffusion than thermal particles, so that runaway transport is a measure of energy rather than particle transport.

However, the analysis is complicated by the dependency of the transport rates on the energy of the runaway electron. First, for low energy runaway electrons transport by electrostatic turbulence cannot be neglected in the transport analysis [Rob-93]. On the other hand, high energy electrons, which are insensitive to electrostatic turbulence, are also less sensitive to magnetic turbulence. The reduction of magnetic turbulence induced transport is already briefly addressed in Sec. 2.4, where it was attributed to two effects:

i) the large displacements of the runaway orbits from the magnetic flux surfaces as a consequence of the curvature-B drift. If the radial correlation length of the turbulence is smaller than the orbit shift transport is strongly reduced [Myn-81, Myr-92]. Depending on the characteristics of the turbulence, the reduction can be 3 orders of magnitude for $\delta=2l_{tur}$, l_{tur} being the radial correlation length of the turbulence. For low mode number coherent turbulence, however, a theoretical treatment by Catto et al. [Cat-92] reached a different conclusion: runaway orbits become more stochastic as a result of the orbit shift and an increase in runaway transport is predicted if orbit shift effect are included;
ii) the existence of regions with low levels of magnetic turbulence. Hegna and Callen [Heg-93] treated runaway transport in a mixture of stochastic fields and good magnetic surfaces. They found that runaway diffusion is already smaller than thermal transport if a very small region of good magnetic surfaces embedded in a highly turbulent plasma exists.

Experimentally, the runaway diffusion is generally not observed to scale with the electron velocity. In the previous chapters it has already been shown that for TEXTOR the relativistic runaways are extremely well confined. A confinement time of several seconds must be invoked to explain the high energies reached and the exponential growth of the runaway population due to the secondary generation. Runaway transport much lower than predicted from the magnetic fluctuation level has been reported in more experiments [Myn-81, Bar-81, Kwo-88, Cat-91].

In this chapter experiments on the transport of relativistic runaway electrons in TEXTOR are reported. In Sec. 5.2 measurements of the orbit shift of runaway electron are presented. The synchrotron radiation diagnostic allows a direct measurement of this shift. The effect of the orbit shift on runaway confinement mentioned above can explain the excellent confinement. In Sec. 5.3 the confinement of relativistic runaway electrons is analyzed under different plasma conditions. These include ohmic heating, Ion Cyclotron Resonance Heating (ICRH), and Neutral Beam Injection (NBI) at various power levels. Both co and counter (with respect to I_p) injection was applied. Finally, injection of a pellet into the plasma has a dramatic effect on the runaway electrons. Part of the population is rapidly lost, while a narrow, helical beam remains confined. These observations and their consequences for magnetic turbulence have been published in Phys. Rev. Lett. **72** (1994) 4093, which is reproduced in Sec 5.4.

5.2 The orbit shift, and confinement of new born low energy runaway electrons.

The thermal emission of the limiter and liner provides an accurate reference frame to calibrate the position and intensity of the synchrotron emission. Knowing the camera position and the apparent emitting region, which is a projection on the liner, the real position of the runaway beam can be deduced. In this way the orbit shift of the runaway beam can be measured.

At the end of the current flat top in a standard low density discharge with I_p =350 kA, the shift of the centre of the synchrotron spot is measured to be δ=6.5 cm. In Fig. 5.1a this shift is indicated. With the Shafranov shift Δ=3 cm (measured independently), and taking a standard parabolic q-profile with q_0=1, the runaway energy follows from eq. (2.12): W_r = 25 MeV. This value is in agreement with the independent determination using the filter method to obtain spectral information. During the current flat top phase hardly any shift of the runaway beam is observed. This indicates that the energy of the diagnosed runaway electrons is approximately constant, in agreement with Fig. 3.10. In contrast, in the current decay phase an increasing shift is observed as shown in Fig. 5.1. According to eq. (2.12) the orbit shift δ is proportional to the safety factor q and the energy W_r of the runaway electrons. W_r does not change significantly in the period of interest, as evidenced by the emitted power. The increase in δ is therefore attributed to the change of q. The measurement of δ can thus be used to reveal the change of q in the plasma core during the current decay. In Fig 5.2. δ is plotted as a

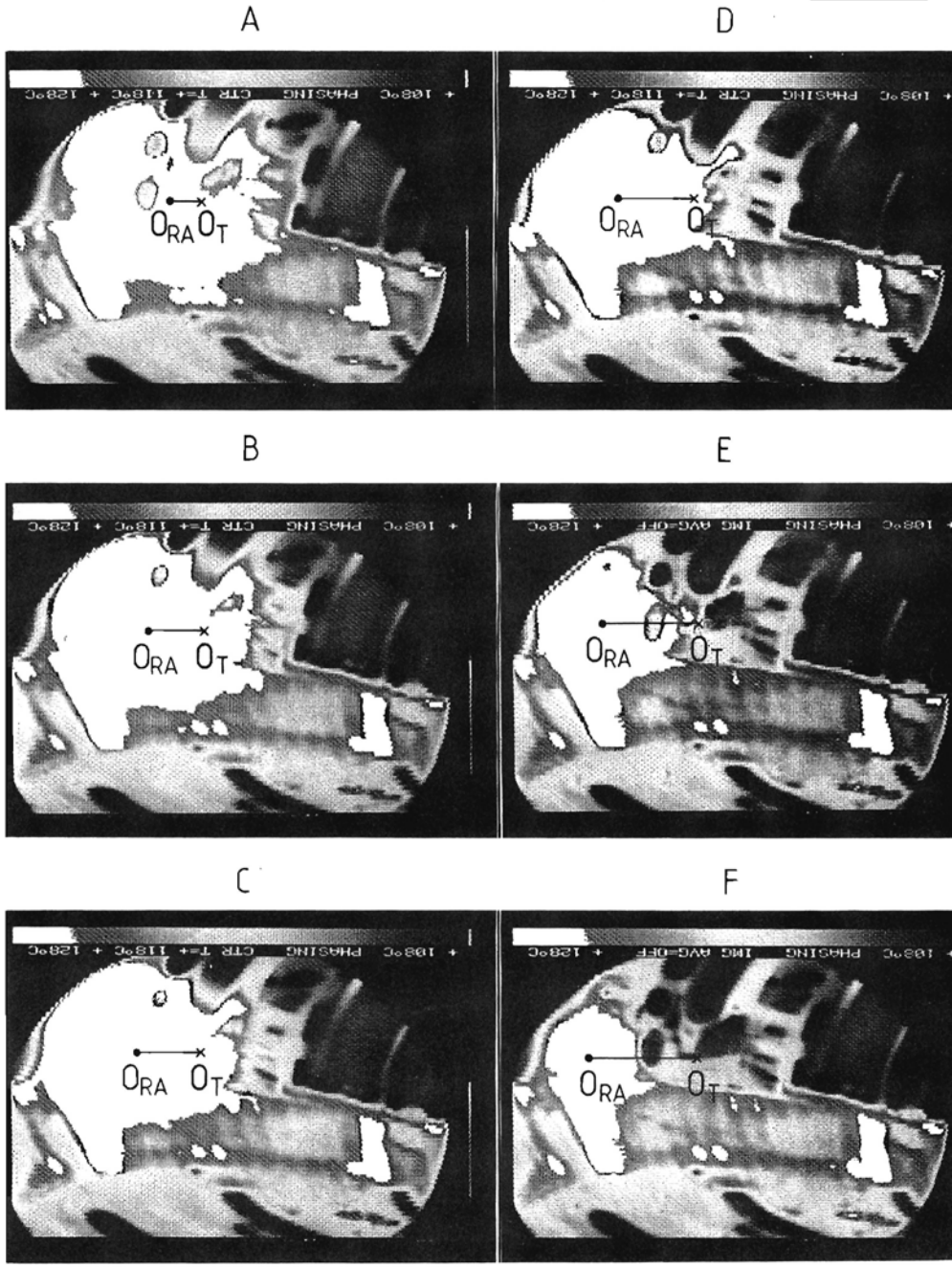

Figure 5.1: *Pictures of the IR camera, showing the synchrotron radiation at different times. Frame A is recorded at t=2.7 s, Frame B at t=3.1 s, Frame C at t=3.3 s, Frame D at t=3.5 s, Frame E at t=3.7 s and Frame F at t=3.8 s. The geometrical centre of the tokamak is indicated by O_T and the centre of the runaway beam by O_{RA}. The increasing orbit shift of the runaway beam is observed.*

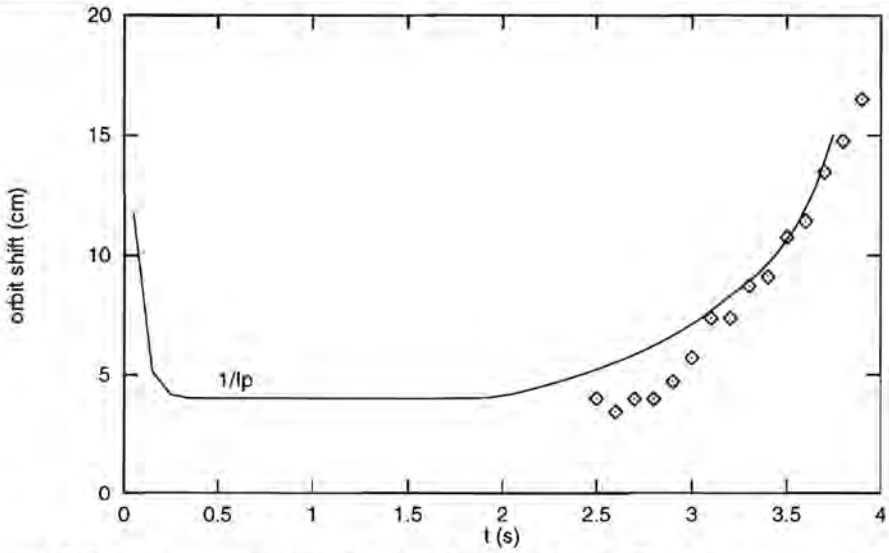

Figure 5.2: *The measured orbit shift as a function of time. The points correspond to the measurements of δ from the IR frames. The curve is proportional to $1/I_p$. It is observed that δ increases about 0.5 s later than the $1/I_p$.*

function of time. The solid line in Fig. 5.2 shows the inverse dependence of δ on I_p. A delay of $\tau_{delay} \approx 0.5$ s is observed between the current decay and the response of δ. This delay demonstrates that the current starts to decay at the edge of the plasma: the negative current perturbation penetrates the conductive plasma column only slowly. The observed value of τ_{delay} is in fair agreement with the skin time τ_s:

$$\tau_s = \frac{\mu_0 a^2}{4\eta} \approx 0.5 \text{ s} \qquad (5.1)$$

for $\langle T_e \rangle$ of 0.5 keV.

The large shift of several cm can partly explain the good confinement of the relativistic electrons. In ref. [Myn-81] it is shown that due to averaging over the turbulence a reduction of transport by a factor 10^5 is possible for 25 MeV electrons. This alone, however, is not sufficient to account for the confinement time of several seconds of the runaway electrons in TEXTOR. Before reaching the energy of tens of MeV, the runaways must pass the low energy phase, where the reduction of transport by drift effects is negligible.

We have developed a simple model to estimate the fraction of runaways that survive the low energy phase. For this one has to calculate how long it takes before the orbit shift becomes comparable to the radial correlation length of the turbulence, l_{tur}. This time, τ_{tur}, in which the runaway electrons will experience no appreciable reduction of the turbulent transport is estimated from Eq. (2.12) and the condition $\delta = l_{tur}$:

$$\tau_{tur} = \frac{\left(\frac{eBl_{tur}}{q} - m_e v_{crit}\right)}{eE} \tag{5.2}$$

In our model we assume that the birth rate of runaway electrons is a Gaussian distribution with a width $\sigma(0) = 0.07$ m (see Sec. 4.2). The time behaviour of this distribution f(r,t) is governed by the acceleration in the electric field and the turbulent diffusion. The function f(r,t) is a solution of the diffusion equation:

$$\frac{\partial f(r,t)}{\partial t} = D\nabla^2 f(r,t) \tag{5.3}$$

with the boundary condition f(a,t)=0. An upper estimate of D is provided by the Rechester Rosenbluth formula [Rec-78] for transport in a fully stochastic field:

$$D = \pi q R_0 \left(\frac{B_r}{B}\right)^2 v \tag{5.4}$$

The width of the distribution at time t, $\sigma(t)$ is determined by the condition:

$$2 D t = \sigma(t)^2 - \sigma(0)^2 \tag{5.5}$$

To calculate the width of f(r,t) when the orbit shift will average out the turbulent diffusion, we take $\sigma(\tau_{tur}) = 0.25$ m, which is the radius of the observed runaway beam. Runaway survival of the low energy phase is possible for $(B_r/B)^2$ and l_{tur} obeying the condition:

$$\left(\frac{B_r}{B}\right)^2 \left(l_{tur} - \frac{q m_e v_{crit}}{eB}\right) \leq 1\times10^{-12} \tag{5.6}$$

This condition is indeed fulfilled for reasonable values of $l_{tur} = 1$ mm and $(B_r/B) = 5\times10^{-5}$. (Note that such a value for (B_r/B) is compatible with thermal confinement since this yields a contribution $D=0.25$ m^2/s whereas experimentally for the thermal transport $D=O(1$ m^2/s) is found). For τ_{tur} we calculate:

$$\tau_{tur} = 15 \text{ ms} \tag{5.7}$$

Turbulent diffusion of runaway electrons is important only in the first 15 ms after that they have passed the runaway threshold.

This model thus shows that with reasonable values of magnetic turbulence the runaway electrons can survive the low energy phase. Moreover, the model gives an upper of the diffusion since the Rechester Rosenbluth formula was used. The existence of a transport barrier as predicted by Hegna and Callen [Heg-93] will even further reduce the transport in the low energy phase. According to their calculations, this effect can be comparable to the orbit shift reduction already for small regions of good surfaces embedded in a stochastic field. Sawtoothing of the plasma will increase the transport of low energy runaway electrons. However, this effect will not deplete the total runaway population because in a time τ_{tur} there are only 2-3 sawteeth, and within one sawtooth only a small fraction of the runaway population will be lost.

In conclusion, orbit shifts of several cm have been measured for relativistic electrons of about 25 MeV, in agreement with theory. Such large shifts can explain the good confinement of these runaways if one follows the reasoning of Mynick and Strachan [Myn-81] or Myra et al. [Myr-92]. The acceleration is fast enough to let a large fraction of the newborn runaways pass the lossy low energy regime. The influence of the orbit shift limits the application of runaway electrons as a probe of magnetic turbulence. On the other hand, information about the radial correlation length of the turbulence can be gained from measurements of runaway confinement in different confinement regimes, since the reduction of runaway transport is a strong function of δ/l_{tur}. Because the relation between the runaway energy and the shift has been confirmed experimentally, the dependence of the runaway confinement time on the runaway energy provides a measure of l_{tur}.

5.3 Confinement under different plasma conditions

In this section the confinement of energetic runaway electrons in different operational regimes is investigated. In contrast to similar studies in literature, which concern the confinement in the edge, we try to measure the confinement of runaway electrons in the centre of the discharge. The basic information is contained in the time dependence of the synchrotron radiation intensity: the growth or decline of the runaway population is determined by the balance of runaway generation (primary and secondary) and loss. For an accurate interpretation the local values of $E_{//}$, T_e, n_e and Z_{eff} in the plasma centre should be known. In practice, these can only be estimated, but it will be shown that by considering limiting cases a few firm conclusions on runaway electron confinement can be drawn. As it is found that indeed runaway electron confinement degrades for increasing NBI heating power, it is possible to estimate the radial correlation length of the magnetic turbulence as a function of heating power. This will be related to thermal confinement and to results obtained in other tokamaks.

Sect. 5.3.1 deals with ohmic discharges, and considers the effect of variation of B_t and gaspuffing on runaway confinement. In Sec. 5.3.2, NBI L-mode discharges are considered,

distinguishing co- and counter-injection, at low and high power. In addition, preliminary experiments with ICRH are discussed. Finally, in Sec. 5.3.3. the effect of the sawtooth instability on runaway electron confinement is discussed.

5.3.1 Ohmic Discharges

In the literature a number of experiments to measure the runaway diffusion coefficient in ohmic discharges are reported from different tokamaks. In all these experiments the observations were restricted to runaways that were detected when they left the plasma. The main results and methods are:

i) In Ormak [Zwe-78] and TEXT [Cat-91] the runaway transport was measured by shifting the plasma column to the inside. The response of the HXR signal was interpreted as showing the runaway diffusion from the edge of the plasma to the limiter. They found D_r=0.01-1 m^2/s.

ii) In sawtoothing discharges in PLT [Bar-82] and TJ-1 [Rod-94] the HXR detector showed a delayed sawtooth behaviour. The time difference was attributed to the time the runaway electrons need to diffuse from the core of the plasma to the limiter. A runaway diffusion coefficient D_r=5-10 m^2/s was found.

iii) The magnetic field in the edge of TEXT was perturbed by externally applied helical magnetic fields [Cat-91]. The transient readjustment of the runaway flux to the limiter was used to estimate the diffusion coefficient with the result D_r=1 m^2/s in the edge and decreasing inwards.

iv) In PLT correlation between the fluctuations of the plasma (position, density, MHD) and the runaway flux to the limiter was observed [Bar-81]. These investigations yielded D_r= 0.1 m^2/s for runaway electrons of 0.5-1 MeV. The diffusion coefficient decreased with increasing B_ϕ and decreasing I_p.

v) From the steady state slope of HXR spectra in PLT, ASDEX and TJ-1 an effective confinement time of runaways was extracted [Bar-81, Kwo-88, Rod-94]. The runaway diffusion found using this method varied from D_r=0.1 m^2/s in ASDEX to D_r=5 m^2/s in TJ-1 and D_r=25 m^2/s in PLT.

vi) The decay of HXR signal in a phase in which no runaways are generated was used in ASDEX to measure of the runaway confinement time [Kwo-88]. Using this method they obtained D_r = 0.1 m^2/s with a sharp degradation of the confinement when q_a is rational.

Summarizing, from these investigations runaway diffusion coefficients in the range 0.01-25 m^2/s were found for runaway electrons in the energy range 0.5-5 MeV. For comparison the bulk particle and energy transport have transport coefficients of the order 1-10 m^2/s. This shows that the runaway transport is dominated by non-collisional transport. Low level

magnetic turbulence $(B_r/B) \approx 10^{-5}$ is sufficient to explain this but many authors note that orbit shift may reduce turbulent transport, so that the actual (B_r/B) may be higher. All these methods have in common that they are based on the measurements of the runaway flux to the limiter, and therefore characterize the edge transport of runaways and the edge turbulence rather than the core turbulence.

The synchrotron radiation diagnostic provides a method to study the runaway transport in the plasma core. Some results of such studies in ohmic TEXTOR discharges have already been reported in Chapter 4. Summarizing these findings:

- part of the runaway electrons created in the start-up phase of the discharge are lost in the first 50 ms;
- runaway electrons can acquire an energy of more than 20 MeV, which requires a confinement time $\tau_r > 1$s
- secondary generation has been demonstrated which also requires $\tau_r > t_0 \sim 1$ s, where t_0 is the avalanche time of the secondary generation process;
- orbit shifts of several cm have been observed for 25 MeV electrons;
- increasing of the density by puffing deuterium does not result in a large loss of high energy electrons;

Additional results concerning the synchrotron radiation and runaway transport studies in ohmic plasmas that have not yet been discussed include:

- The influence of the toroidal magnetic field B_t on the core runaway confinement is negligible. This is shown in Fig. 5.3 where the synchrotron intensity is shown as a function of time for $1.75\ T < B_t < 2.5\ T$. As the absolute intensity varies for the different discharges due to small changes in electric field or density, all traces have been normalized to the intensity at t=2.0 s. Until this time the plasma current is constant, and no auxiliary heating is applied. For all values of B_t curves the rise time of the signal is the same within 10 %, which implies that there is no measurable variation in runaway confinement.

  Note that while B_t=1.75 T the edge safety factor q_a is close to 3, this does not seem to degrade the runaway confinement. The HXR and Neutron signal (not shown) evolve similarly to the synchrotron intensity in the ohmic phase. The lack of a B_t or q_a dependence of the core runaway confinement for the low density TEXTOR discharges forms a contrast to the results of ASDEX [Kwo-88] and TJ-1 [Rod-94], where the confinement of runaway electrons in the edge was found to increase with increasing B_t and strongly degrades for integer q_a values. This difference may be explained by the fact that we study the core of the plasma: the runaway electron loss mechanism in the core of the plasma is apparently independent on B_t, whereas the edge transport depends on B_t or q_a.

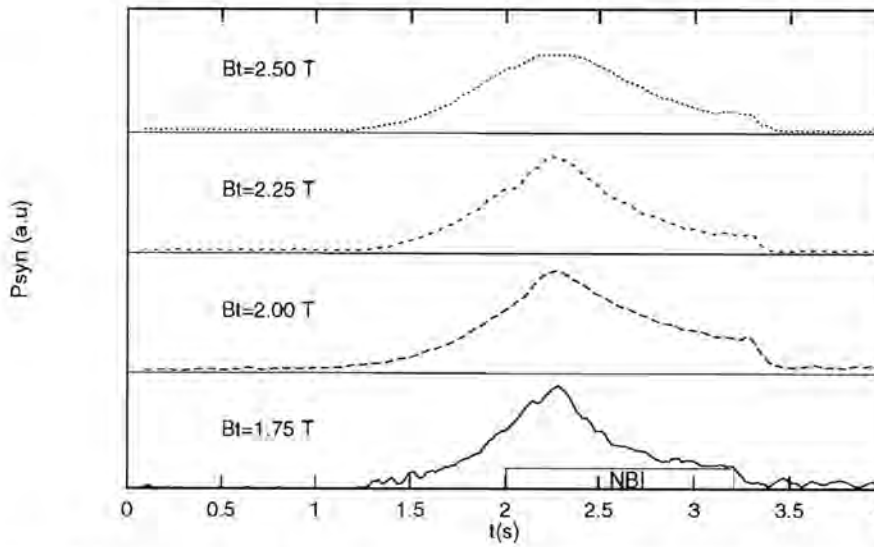

Figure 5.3: *Time traces of the synchrotron radiation for different values of B_t. Until t=2.0 s the plasma is ohmically heated. The rise of the synchrotron radiation in this phase appears not to depend on B_ϕ, indicating the same runaway confinement time. After t=2.0 s the plasma is heated by 400 kW NBI.*

- The effect of a density increase by a deuterium gaspuff has already been discussed in Sec. 4.4. If a helium puff is applied to the discharge the synchrotron emission is drastically affected. Fig. 5.4 demonstrates this. In the first case no gaspuff is applied, in the second case a deuterium puff and the third a helium puff, both at t=2.0 s. In the first two cases the IR intensity increases by about a factor of 2 between t=2.0 and 3.0 s, after which the disappearence of the radiation indicates the termination of the discharge. In both cases the rise of the signal is attributed to a growth of the runaway population, mainly due to secondary generation. Part of the increase in the case of a deuterium puff may be explained by the fact that the electric field increases as the temperature will drop as a result of the gaspuff.

  In the case of a helium puff the total synchrotron intensity increases by about a factor 5 between t=2.0 and 3.0 s. A closer look at the signal shows that the increase has two distinct phases: a fast rise during 300 ms, followed by a slower increase for the next 700 ms. The last one is attributed to the growing runaway population by the secondary generation, like in the other two cases. The first steep rise, which is not observed in the deuterium case, must be related to some transient phenomenon. The change in the electric field can account for the steep rise. From Spitzer resitivity it follows that $E \sim Z T^{-3/2}$. A sudden increase of E after the helium puff of a factor 2.5 is calculated from the observed decrease in temperature (35%) and assuming an increase of Z_{eff} from 1.5 to 2. An increase of the same amount is expected

for the synchrotron radiation on the required time scale of 300 ms. In the case of a deuterium puff the electric field does apparently not change as much, probably because the effect of the decrease in temperature is partly counteracted by a decrease of Z_{eff}. This specific experiment does not allow to obtain new information about runaway transport, although it has been observed that no dramatic loss of relativistic runaway electrons occurs if the density is increased or Z_{eff} changes.

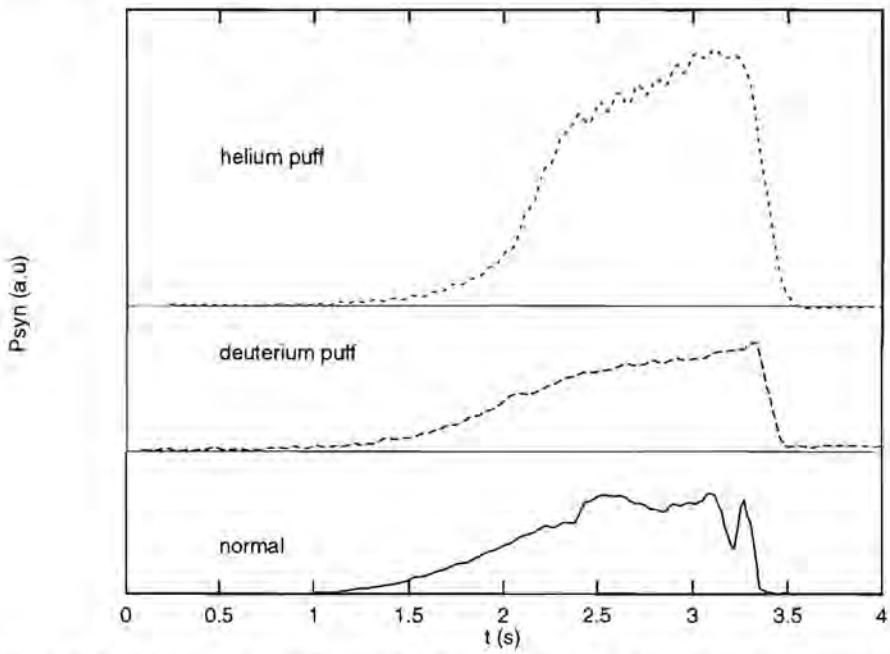

Figure 5.4: *Synchrotron radiation for 3 different cases. From top to bottom: 1. ohmic plasma where at t=2.0 s He is injected (the oscillations are due to electrical noise), 2. ohmic plasma where at t=2.0 s deuterium is injected and 3. a normal ohmic plasma where the density is kept constant until t=3 s. In the case of He injection a large rise of the signal is observed.*

5.3.2 Auxiliary heated discharges

To analyze the runaway confinement in auxiliary heated plasmas four different cases are compared below: 400 kW Neutral Beam Injection (NBI) co- and counter with respect to the plasma current, 1.3 MW NBI co-injection and 600 kW of ICRH. For each case a series of discharges was performed. Fig. 5.5 shows the typical traces of the measured synchrotron radiation intensity for the 4 conditions. The ohmic trace is included for reference. For a better comparison the signals are all normalized to the intensity at t=2.0 s.

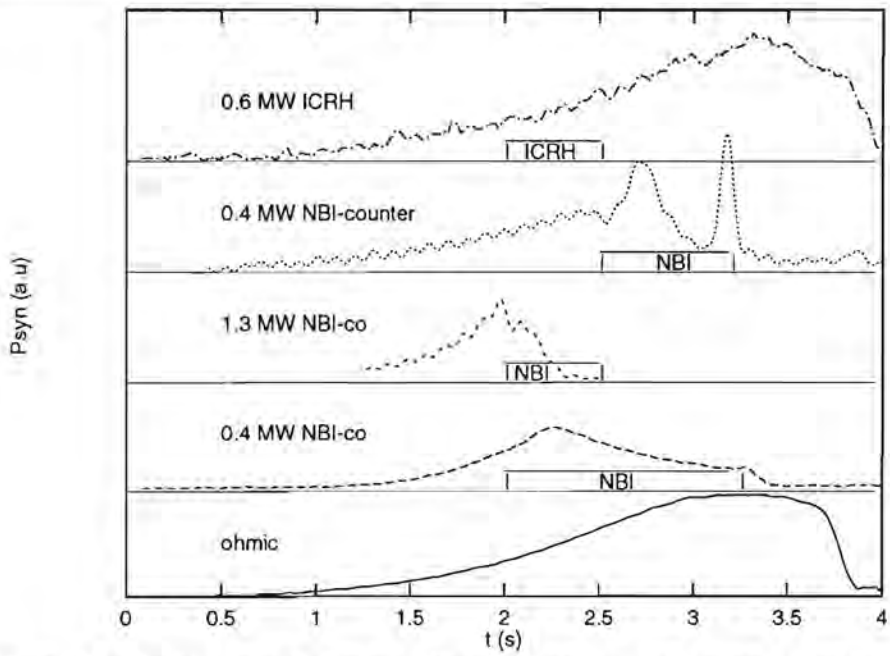

Figure 5.5: *Synchrotron radiation in auxiliary heated plasmas. From top to bottom: 1. 0.6 MW ICRH, 2. 0.4 MW NBI counter injection (the oscillations are due to electrical noise), 3. 1.3 MW NBI co-injection, 4. 0.4 MW NBI co-injection and 5. the ohmic case. Whereas ICRH does not seem to affect the plasma (probably because the poser did not couple in to the plasma) NBI does. An initial rise of 300 ms is followed by a decay of the synchrotron radiation, which is fastest for high power, and with the counter injection faster than with co-injection.*

data

We turn our attention first to the case of NBI-co-injection (i.e. counter to the electron drift velocity). NBI is switched on at t=2.0 s. For case of 400 kW, the first 300 ms the synchrotron emission continues to increase, whereafter the intensity starts to decay. The maximum in intensity is reached when the electron density (which rises in the heating phase) reaches its maximum. The e-folding time of the decay of the IR radiation amounts to $\tau_{decay} = 0.54 \pm 0.04$ s. Measurements at other values of B_t showed a similar decay. For higher power, 1.3 MW, the synchrotron radiation decays much more quickly: $\tau_{decay} \approx 0.12$ s.

For the NBI-counter case both the initial rise and the subsequent decay or the synchrotron intensity are stronger as compared to the NBI-co injection case for the same input power of 400 kW. The decay time of the intensity is found to be $\tau_{decay} = 0.19 \pm 0.04$ s. (The outward movement of the plasma causes the first drop in the intensity. The burst at t=3.2 s is not the result of increased emission but of a movement of the runaway beam, caused by the switch off of the NBI, by which a more intense part of the beam is observed). After the NBI phase the synchrotron emission does not rise further for about 1 s (after which the discharge is

terminated). It is interesting to note that on one or two frames of the IR camera small oscillations on the synchrotron radiation are observed, with a frequency of about 1 kHz. Whether these are associated with MHD activity is unclear because of a lack of complementary data from other diagnostics.

The effect of ICRH on the synchrotron radiation is almost nill. This probably related to the fact that the ICRH power did not couple in to the plasma, resulting in little heating. Therefore the same time trace of the synchrotron signal as under ohmic condition is obtained.

interpretation

For a reliable interpretation of the data the separate evolutions of n_e, T_e, Z_{eff} and $E_{//}$ have to be considered:

- The electron density n_e in all cases increased by a factor of 2 in the heating phase. For the runaway electrons the effect of this is twofold. First, the increase of the collision frequency will increase the pitch angle Θ (see Sec. 6.2) and hence the radiated power. Secondly the drag force is enhanced. Runaway electrons that were already at the radiation limit before the heating phase will loose energy and radiate less. Both effects, however, are considered negligible. The experimental justification is that a) no increase in Θ is observed and b) a similar density increase in the ohmic phase did not show a decay of the synchrotron radiation (Fig. 4, Chapter 4). Theoretically the effect of the enhanced drag is calculated to result in a drop of the synchrotron intensity of no more than 10 %. The increase in Θ as a result of collisions is expected to double the intensity on a time scale of 1 s, which is slower than the observed rise. Moreover, in Chapter 6 it is shown that the interaction with the field ripple determines the Θ distribution and this mechanism is independent of the density.
- The electron temperature T_e will rise in the heating phase. This has an indirect effect on the synchrotron radiation as it will lower the electric field E. A measurement of T_e is not available, so an accurate determination of T_e is not possible. It is interesting that the ECE signal decreases during the NBI phase. This however, cannot be interpreted as a drop of T_e, since at these low density the plasma is optically thin and the ECE signal is dominated by the emission of suprathermal electrons.
- A measurement of Z_{eff} is not present either. The dominant effect of an increase of Z_{eff} in the heating phase would be the increase of the electric field. However, since there is no measurement of Z_{eff} we will assume that it remains constant.
- The electric field affects the runaway electrons directly. Shortly after the start of the heating phase $E_{//}$ follows the changes of T_e and Z_{eff}, because the current profile can only change on a magnetic diffusion time scale (≈ 500 ms) for TEXTOR. Assuming Spitzer resistivity we have $E_{//} \sim Z_{eff} T_e^{-3/2}$. Therefore $E_{//}$ is expected to drop in the heating phase

since T_e will rise. A drop of $E_{//}$ will decelerate the runaway electrons that were at the radiation limit. A limiting case is provided by the situation were $E_{//}$ drops to zero. Then the synchrotron radiation will decay on a time scale τ_{rad}:

$$\tau_{rad}^{0} = \frac{P_{syn}}{dP_{syn}/dt} \approx \frac{W}{4}\left(\frac{dW}{dt}\right)^{-1} = \frac{W}{4ecE_{//,OH}} = 0.3 \text{ s} \qquad (5.8)$$

Here W is the runaway energy and $E_{//,OH}$ is the electric field in the ohmic phase. If $E_{//}$ does not drop to zero, one has:

$$\tau_{rad} = \frac{W}{4ec(E_{//,OH} - E_{//,aux})} \qquad (5.9)$$

Furthermore a low electric field will diminish the runaway production according to the secondary generation process, which is inversely proportional to $E_{//}$. The primary generation, described by the parameter $\varepsilon = E_{//}/E_{crit} \sim ET_e/n_e \sim 1/(ne\sqrt{T_e})$, will drop to a negligible level in the auxiliary heating phase.

For tangential injection of the neutral beam a plasma current will be driven non-inductively. For co-injection this will decrease $E_{//}$, whereas for counter injection $E_{//}$ will increase as a result of this.

With this knowledge the initial rise of the synchrotron radiation exhibited in all NBI discharges can be attributed to the acceleration of runaway electrons that were not yet at the radiation limit at the moment of beam injection. This process will continue until the runaway electrons have reached the radiation limit, in spite of the injection of neutral beams. Even if the electric field is somewhat decreased as a result of NBI, the total radiated power could increase.

The decay of the IR signal for the 400 kW NBI co-injection case can be ascribed to radiative decay with $E_{//,aux} = 0.5\ E_{//,OH}$. This would imply a rise of T_e of 60% in the NBI phase to about 2 keV. Since both $E_{//,aux}$ and T_e are not measured the validity of this interpretation cannot be proved. The possibility that part of the decay is due to the loss of runaway electrons cannot be excluded. However, the runaway confinement time must be higher than τ_{decay}: $\tau_r > 0.54$ s

For higher power NBI we find $\tau_{decay} < \tau_{rad}^{0}$. Runaway electron losses have to be invoked to account for this fast decay. The runaway confinement time τ_r is estimated from:

$$\tau_r < \left[(\tau_{decay})^{-1} - (\tau_{rad}^{0})^{-1}\right]^{-1} = 0.2 \text{ s} \qquad (5.10)$$

The confinement in this case is at least three times shorter than in the 400 kW case. Relating this loss to magnetic turbulence, the deterioration of the confinement can result from either an increase of the the turbulence level or an increase of l_{tur}. The bulk energy confinement τ_E will not differ more than a factor 1.5 in the two cases, following the empirical scaling law $\tau_E \sim n_e/\sqrt{P}$, where P is the total input power, ohmic and auxiliary. Therefore it could be hypothesized that not an increase of the turbulence level (which would affect the thermal particles as well, if they were determined by magnetic turbulence in the first place) but an increase of the correlation length is the dominant effect of additional power.

Finally, the case of NBI counter injection has to be treated. The electric field is under these conditions higher than in the NBI-co case, as the current drive is now in the counter direction. The loopvoltage increases by 30 %, which explains the initial steep rise. The faster decay of the radiation could indicate that the confinement of the runaway electrons is worse than in the NBI-co case. Since we do not expect a large radiative deceleration it is assumed that τ_{decay} in this case represents the confinement time:

$$\tau_r \approx \tau_{decay} = 0.19 \pm 0.04 \text{ s} \qquad (5.11)$$

5.3.3 Sawteeth

Sawteeth in ohmic discharges

Sawtooth behaviour has not been observed in ohmic discharges with the synchrotron radiation. For the discharges under consideration, the sawteeth observed by ECE were rather small ($\Delta T_e/T_e<10\%$) and short ($\tau_{st}\approx 5$ ms) in the ohmic phase. The fast repetition excludes detection of a modulation on the synchrotron emission, even if there were any. However, sawtoothing is detected on the HXR signal (tangential view) after coherent addition of many sawteeth. Unlike other experiments [Bar-82,Rod-94] no delay relative to the central crash of these HXR sawteeth was observed and a diffusion coefficient of runaway electrons could not been deduced this way. This implies that either a) the runaways diffuse out within one sampling time (1 ms) to the limiter, or b) plasma bremstrahlung (originating predominantly from ion-runaway collisions in the centre) rather than limiter bremstrahlung (from runaway electrons at the edge) is detected [Hoe-94]. From the first explanation $D_r > 200$ m^2/s is deduced, for the short period of the crash. If plasma bremstrahlung is detected, a pitch angle scattering mechanism of the lower energetic runaway electrons in the sawtooth crash could be responsible for the sawtoothing behaviour on the HXR signal. On the basis of these measurements, no conclusion can be drawn. The influence of sawteeth on runaways remains unclear but intriguing.

Sawteeth during NBI

The NBI-co discharges allowed to readdress the effect of sawteeth on runaway electrons. In ohmic discharges these were too small and too short to be detected with the available

equipment. Application of NBI-power to the plasma increased the amplitude as well as the repetition time of the sawteeth. However, fluctuations in the synchrotron light could not be correlated with sawteeth. Whether such a correlation is absent or present but not detectable is not clear yet. On HXR and Neutron (N) signal these could be observed more clearly now. For the 1.3 MW NBI-co discharge the HXR and N signals, both measured tangentially, and the ECE signal (thermal resonance at r=-10 cm, close to the q=1 surface) are shown in Fig. 5.6. In this figure again no time difference resulting from diffusion of runaways from the center to the edge is observed. A spike during the sawtooth crash on the N signal cannot come from either fusion neutrons, or runaway electron induced nuclear processes from the plasma (such as electro-desintegration of deuterium): the probability for these processes does not increase in a sawtooth crash because the deuterium temperature and density drop in the centre of the plasma. It is therefore concluded that both the HXR and N signal are induced by runaway electrons hitting the limiter (or some other solid material). Since no time difference between the sawtooth crash and these signals is found, this loss should occur within one sampling time (1 ms), and diffusion coefficients of the order of $D=\Delta r^2/\Delta t=0.45^2/0.001=200$ m^2/s for the short period of the crash have to be accepted. However, in each crash only a small fraction of the runaway electrons is lost and the averaged runaway confinement is larger. Moreover, the fact that on the N signal the spikes are observed shows that not only the low energetic runaway electrons but also those of several MeVs are sensitive to the sawtooth crash, because for neutron production a threshold energy of about 10 MeV is required.

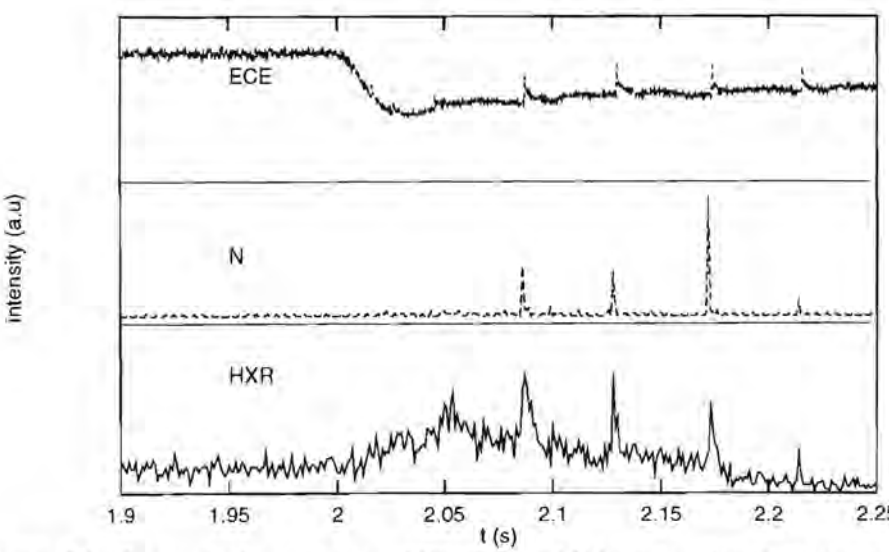

Figure 5.6: *Sawtooth observations on ECE, HXR and N for a low density discharge with 1.3 MW NBI co-injection. The spikes on the HXR and N signal coincide with the sawtooth crash, showing the rapid loss of a fraction the runaway electrons.*

5.3.4 Discussion

The runaway electrons in the core of the plasma that are diagnosed by the synchrotron radiation are very well confined in ohmic plasmas. Hardly any loss could be determined and a lower limit for the confinement time of 1 s is deduced. In NBI discharges this confinement time is lower, depending on the injected power and the direction of injection. For neutral beam injection τ_r decreases from $\tau_r > 0.5$ s for 0.4 MW to $\tau_r = 0.12$ s at 1.3 MW. For counter injection the loss seems to be enhanced over the co-injection case ($\tau_r = 0.19$ s for 0.4 MW).

An increase of l_{tur} is proposed as a plausible explanation of this increased runaway transport. Changes of l_{tur} will not affect the bulk confinement but can change the runaway confinement by several orders of magnitude. Mynick and Strachan [Myn-81] and Myra and Catto [Myr-92] calculated the enhancement of the runaway confinement time τ_r as a function of δ/l_{tur}. Myra and Catto found τ_r increases linearly with δ/l_{tur} for $\delta > l_{tur}$. Mynick and Strachan found a much stronger dependence. This difference depends on the location of the turbulence. For TEXTOR 25 MeV electrons we estimate $\delta/l_{tur}=40$ (taking $l_{tur}=1$ mm as found on ASDEX [Kwo-88], a tokamak of similar size as TEXTOR). Using the theory of [Myr-92] an increase of l_{tur} by less than a factor of 10 to $l_{tur}=1$ cm by going from ohmic phase to the 1.3 MW NBI phase is sufficient to explain the observed runaway loss at TEXTOR. Such an increase of the correlation length of density fluctuations has been observed on JET [Cri-92].

The loss of runaway electrons during a sawtooth crash can possibly be related to an increase of l_{tur} as well. Moreover, assuming the turbulence in a sawtooth crash to be of low mode number, Catto et al. [Cat-92] showed that the runaway orbits become even more stochastic than the magnetic surfaces a diffusion coefficient as high as $D=200$ m^2/s during the crash is not unreasonable.

The reduction of the runaway transport according to the theory of Hegna and Callen can provide an alternative explanation of the observed runaway behaviour. If the regions of 'good' magnetic surfaces get smaller during NBI the runaway transport would increase, and a disappearence of these good surfaces in the short period of the sawtooth crash would result in the fast runaway loss during the crash.

For all these measurements the lack of knowledge about the change in the electric field in the centre is hampering a more accurate determination and interpretation of the runaway confinement.

The determination of turbulence levels in the core of the plasma with this synchrotron technique is almost impossible. For those studies lower energetic electrons are more suitable. Large displacements of the runaway orbit from the flux surfaces reduces the transport of the relativistic electrons by magnetic turbulence to negligible levels. If the turbulence has large correlation lengths, however, runaway transport in excess of bulk transport is found as presented in the next section.

5.4 Confinement of Runaway Electrons in Stochastic Fields.

Islands of Runaway Electrons in the TEXTOR Tokamak and Relation to Transport in a Stochastic Field

R. Jaspers[1], N.J. Lopes Cardozo[1], K.H. Finken[2], B.C. Schokker[1], G. Mank[2], G. Fuchs[2] and F.C. Schüller[1]

[1]FOM-Instituut voor Plasmafysica 'Rijnhuizen', P.O. Box 1207; 3430 BE Nieuwegein
[2]Institut für Plasmaphysik, Forschungszentrum Jülich, D-52425 Jülich, Germany

Abstract
A population of 30 MeV runaway electrons in the TEXTOR tokamak is diagnosed by their synchrotron emission. During pellet injection a large fraction of the population is lost within 600 μs. This rapid loss is attributed to stochastization of the magnetic field.The remaining runaways form a narrow, helical beam at the q=1 drift surface. The radial and poloidal diffusion of this beam is extremely slow, $D < 0.02$ m^2/s. The fact that the beam survives the period of stochastic field shows that in the chaotic sea big magnetic islands must remain intact.

PACS numbers: 52.55 Fa, 52.35 Ra

The fact that the mean free path of an electron in a plasma is a strongly increasing function of its velocity gives rise to the phenomenon of electron runaway. In an electric field, electrons which exceed a critical velocity, for which the collisional drag balances the acceleration by the field, are accelerated freely and can reach very high energies. In low density tokamak discharges a considerable amount of runaway electrons with energies up to tens of MeV can thus be created. As these energetic electrons are effectively collisionless, they follow the magnetic field lines and can therefore been used to probe the magnetic turbulence in the core of the plasma [1].

In the TEXTOR tokamak a helical beam of runaway electrons is observed after injection of a deuterium pellet. This paper deals with the implications for transport and magnetic turbulence that can be deduced from the synchrotron radiation in these experiments. Before pellet injection, the runaway electrons have been confined for more than 1 s, which is evident from the high energies of several tens of MeV these electrons have acquired and also from their exponentially growing population, which results from secondary generation [2]. During the pellet injection a rapid loss of most of these runaways is observed, however, a part of them does survive the event and forms a stable and narrow beam.

In the TEXTOR tokamak (Major radius $R_0 = 1.75$ m, minor radius $a = 0.46$ m, toroidal magnetic field $B_T = 2.25$ T, plasma current $I_p = 350$ kA; circular cross-section) runaway electrons with energies up to 30 MeV have been observed directly with an infrared (IR) camera, which measures the synchrotron radiation in the wavelength range 3-14 μm [3]. The

camera is positioned to view the plasma in toroidal direction towards electron approach. This camera uses a single HgCdTe-detector and a horizontally and a vertically scanning mirror. The scanning follows the NTSC-TV standard i.e. a full 2-D picture is obtained every 1/60 s, or as an alternative by scanning only one mirror, a 1-D line is obtained every 64 μs [4]. Detectable numbers of runaways are routinely produced in low density discharges with electron density $n_e < 1.10^{19}$ m^{-3}. The runaway energy E can be deduced from the spectrum, the pitch angle Θ (ratio of the velocities perpendicular and parallel to the magnetic field) from the shape of the 2-D image, and the total number of runaways N from the absolute intensity [3]. Measurements of the extension of the runaway population were hampered by the limited field of view which covers a fraction of the plasma cross-section mainly on the high field side, where synchrotron radiation was observed up to r=-20 cm.

Further diagnostics used are magnetic loops namely Mirnov coils in particular 12 coils poloidally and 7 coils toroidally to measure the multipole momenta of the magnetic field, a 9 channel HCN interferometer to measure the density profile, one ECE channel (thermal resonance at r=-12 cm), a hard X-ray (HXR) detector viewing in toroidal direction and a VUV spectrometer to observe the ablation of the pellet by recording the Lyman β light emitted from the plasma as a function of radius.

Observations - During the steady state phase of a discharge, the IR-picture changes only slowly, corresponding to the growth of the runaway population. It has been shown [2] that the runaway electrons are born throughout the discharge duration, and that the rate of runaway production is in agreement with the theory of secondary generation, being the process in which already existing high energy runaway electrons push thermal electrons beyond the critical velocity by collisions [5]. The runaway energy saturates at the level where the radiation loss matches the acceleration in the electric field. Typical results in the steady state before pellet injection are [2,3]: E =25 MeV, Θ=0.12, $N= 1 - 30\times10^{14}$. The large spread in the number of runaways arises from the unknown energy distribution of these particles.

After the synchrotron radiation is well established, i.e. at t=2.5 s, a deuterium pellet is injected horizontally into the mid plane with v≈1200 m/s whereby one pellet contains ≈ 1-2 $\times10^{20}$ atoms. As a result, the density increases by a factor of 2-3. The injection of the pellet is followed by oscillations with frequencies in the range of 0.2-2 kHz, observed on magnetics, density, ECE and Hard X-ray signals, as shown in Fig. 1. The most dominant magnetic mode normally seen in TEXTOR is the n=1, m=1 mode if the pellet has penetrated far enough to reach the q=1 surface [6], but for the discharges reported here in more detail an n=1, m=2 mode is also evident from the Mirnov coil signals. Initially the density shows a hollow profile, which changes to a peaked one within 20 ms. As often observed in other experiments [7], the sawteeth which are present before injection, disappear after the pellet has been launched. The pellet penetrates to a minor radius of r≈10-15 cm, as measured with a Dβ diagnostic (top view of the pellet path, 1D array).

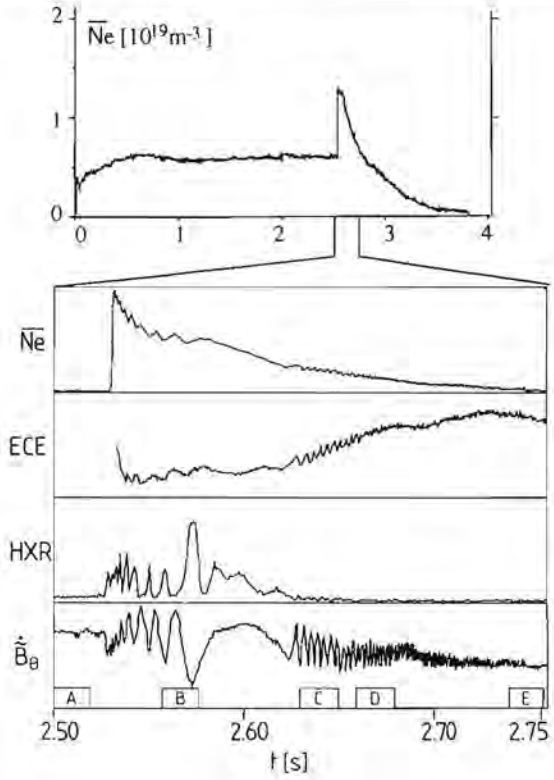

Figure 1a: *Density trace for a typical low density discharge containing a detectable amount of high energy runaways. At t=2.5 s a solid deuterium pellet is injected. This injection induces modulation of several signals. Shown are from top to bottom: line averaged electron density, ECE (thermal resonance at r=-12 cm), Hard X Ray signal and the Mirnov oscillations. The modulation sets in immediately after injection and decays within 200 ms. Indicated is also the times at which the pictures of Fig. 2 are recorded.*

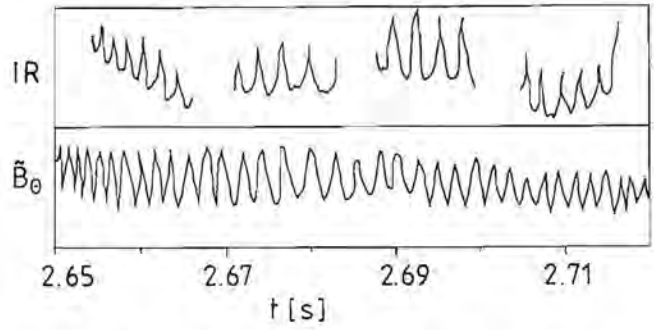

Figure 1b: *Oscillations on magnetics and on the synchrotron emission for a similar discharge as plotted in Fig 1a. The synchrotron emission is recorded in the line scan mode of the infrared camera, to obtain time information. Both signals have the same time structure.*

As a result of the pellet injection the runaways undergo three distinct phases: i) rapid loss, ii) oscillation of the runaway radiation and iii) either a final loss or the formation of a stable runaway beam. These data will be analyzed first and the beam parameters will be derived. After that the transport aspects will be discussed.

i) rapid loss - A large fraction of the runaway population is lost rapidly after injection. Using the IR camera in the line scan mode, it is observed that at the time of the pellet injection, the synchrotron radiation in the central part decreases within about 0.6 ms. The runaways spread over the entire plasma cross-section. This is deduced from the increase of the intensity at the high field side, where normally no radiation is observed. After 0.6 ms most runaways have disappeared, and only a fraction of the runaways stay confined. In four out of five discharges the remaining fraction is around 5%, whereas in one discharge it amounts to about 50 %. In the latter case the density increase was significantly less than in the other cases. Note that the remaining part is present in a plasma with high central density, of up to 5×10^{19} m^{-3}.

ii) oscillation of synchrotron radiation - After this initial loss, the synchrotron radiation, observed in the normal camera mode (2D) exposes a spectacular picture. The spot of synchrotron radiation breaks up into many smaller, elongated ones (Fig.2). This apparent filamentation of the synchrotron radiation goes on for several frames. While the size of these spots can vary in vertical extension, horizontally it is almost constant. For the interpretation it has to be considered that i) the camera picture is built up in 1/60 s and contains therefore space and time information as well and ii) the synchrotron radiation is emitted into a narrow cone in forward direction. Therefore, if a bright spot repeatedly sweeps over the detector area within the 16.7 ms exposure time, the relatively slow line to line scanning results in the multiple spot picture. These considerations are confirmed by the 1D measurements. If one mirror is stopped the vertical direction contains only time-information. The oscillations of the synchrotron radiation show the same time structure as the signals from the magnetic pick-up coils, the interferometer, ECE and several other diagnostics, see Fig. 1b.

iii) stable beam - The magnetic modes decay in about 0.2-0.3 s. At that time the synchrotron signal disappears completely in two cases, while in three other cases it forms one large spot again. This spot stays almost in the same position without change of intensity or extent over more than 0.6 s, i.e. up to the end of the discharge.

A helical m=1 beam - A number of physical parameters relevant for the runaway electrons still confined after pellet injection can directly be derived from the image. Due to the centrifugal force the relativistic electrons experience a vertical drift, meaning that their drift orbits are shifted to the low field side of the magnetic flux surfaces. This shift is given by:

$$\delta = \frac{q\, p_{//}}{e\, B_\phi} \qquad (1)$$

whereby $q=rB_\phi/RB_\theta$ is the safety factor, $p_{//}$ is the parallel momentum, e is the electron charge and B_ϕ and B_θ are the toroidal and poloidal magnetic field components.

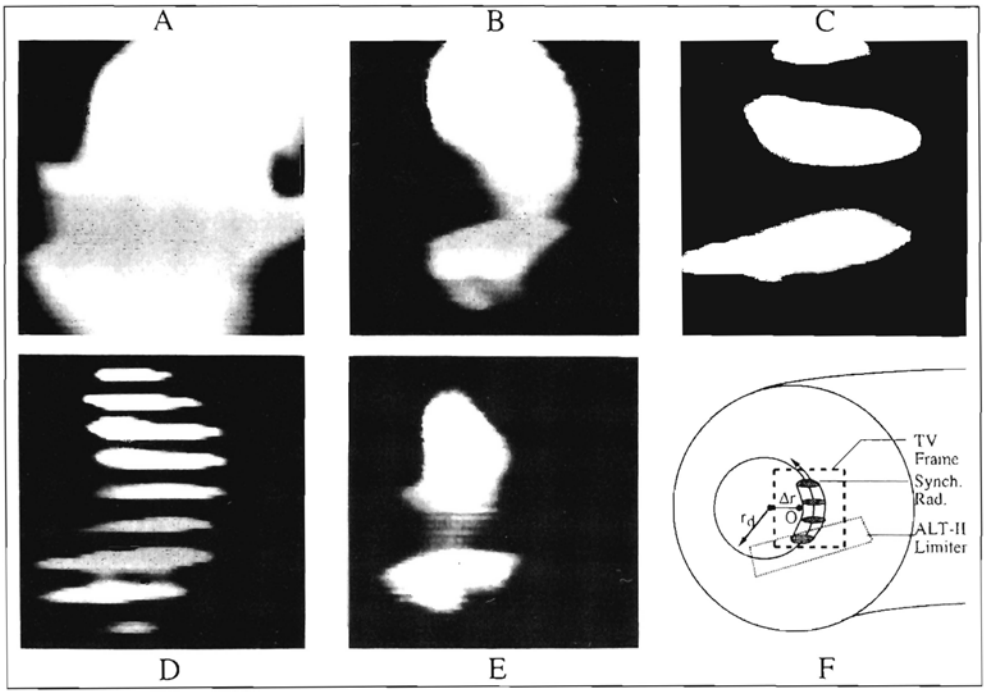

Figure 2: *Frames from the IR camera showing the synchrotron radiation at five different times, as indicated in Fig.1. Frame A is recorded just before injection, B,C and D show the oscillations of the synchrotron signal, coherent with the Mirnov oscillations. Frame E shows the situation when the magnetic modes have disappeared. In Fig. F shows a sketch of the area observed with the IR camera.*

Fig. 2 shows that the spots of synchrotron light lie on a circle. The radius (r_d) and the center (Δr) of this circle, interpreted as a drift surface, are determined from the image: $r_d = 11 \pm 2$ cm, $\Delta r = 7.5 \pm 1.0$ cm. From soft x-ray measurements before pellet injection the inversion radius of the sawteeth was inferred to be $r_{inv} = 9 \pm 1$ cm. This leads to the conclusion that the synchrotron radiation originates from a beam of runaways at the q=1 drift surface. The center of this surface is shifted to the low field side with respect to the geometrical center. Taking the Shafranov shift $s \approx 3.4$ cm into account, the displacement δ can be deduced: $\delta = \Delta r - s = 4 \pm 1$ cm. Using Eq.1, this shift corresponds to an energy $E = 28 \pm 7$ MeV. This value agrees with the independent determination of E during the steady state before pellet injection [2].

The dimensions of the runaway beam can be determined from the image. The FWHM of the spot width (sw) is determined by the actual width of the beam (w) and the pitch angle Θ (in the steady state before pellet injection determined to be Θ=0.12): $sw = R\,\Theta^2 + w$. Furthermore the poloidal length l_θ of the spot is determined as: $l_\theta \approx (2\pi\, r_d\, \Delta t_s / \Delta T) - R\,\Theta^2$, where Δt_s is the time the spot is observed, and ΔT is the time between two successive spots. For one particular case we find: w=4-5 cm, $l_\theta = 10 \pm 3$ cm. The volume of the runaway beam after injection is reduced to 2.0 ± 0.5 % of the volume before injection ($r_{beam} \approx 25$ cm, see [3]). This value agrees with the intensity ratio of the synchrotron radiation before and after pellet injection, which was deduced to be 4 ± 2 %.

Transport Results - The radial and poloidal diffusion coefficients of the runaway electrons of 28 MeV in this helical beam can be determined from the behaviour of these spots of synchrotron emission. The radial one is estimated from the small widening in time of the horizontal extent of the spots Δw: $D^{re}_r = (0.5\,\Delta w)^2 / \Delta t \approx 1\times10^{-2}$ m^2/s. The poloidal diffusion coefficient is determined from the filling up of the gaps between the different spots, interpreted as the smearing out of the runaway beam over the drift surface. This yields $D^{re}p = (0.5\,\Delta l_\theta)^2 / \Delta t \approx 1.5\times10^{-2}$ m^2/s. We recall that after the magnetic perturbations have decayed, in some of the cases the runaways are still present, but smeared out poloidally over the flux surface. This thin shell is perfectly stable and stays at nearly the same position, without change of intensity, position or extent for more than 0.6 s. This stability is an indication of the very low diffusion rate of the runaway electrons. The observation shows that an island topology is not necessary for the good confinement of the beam.

The loss of runaways within 0.6 ms requires a diffusivity of $\chi_R \approx 300$ m^2/s during that period. In the same period, the loss of diamagnetic kinetic energy is only 5%, corresponding to a temporary increase of χ_{th} to only 20 m^2/s. This difference can be understood if the rapid loss of runaways is due to strong ergodization of the field. In this case, the diffusivity is an increasing function of the particle velocity. For a fully stochastic field, the ratio $\chi_R/\chi_{th} = v_R/v_{th}$ is predicted in [8]. This agrees well with the present observations, although it is not at all clear that the conditions for the validity of this theory are fulfilled. Note that the transport of

runaways is compared to thermal transport: runaways are effectively test particles, not bound to the ion cloud by ambipolar fields.

The rapid loss of runaways is ascribed to a temporary strong ergodization of the magnetic field. Because of the large orbit shift, the runaways are only sensitive to field fluctuations with large correlation length, i.e. low mode numbers. For the rapid loss it is further required that no good magnetic surfaces remain [9]. It is therefore hypothesized that the stochastization is due to overlap of large, low m magnetic islands, e.g. an m=1 island at the q=1 surface and m=2 islands at the q=2 surface. The fact that a runaway beam persists after the phase of rapid loss shows that in the chaotic sea there are still big remnant islands, at least of the m=1 island. Thus, the overlap parameter may exceed unity, but the plasma is still far from the state of full stochasticity in which all remnants of islands are destroyed. Hence, even in the short period of high magnetic turbulence the plasma is still far from the fully stochastic regime which is prerequisite for a transport analysis such as due to Rechester and Rosenbluth [8].

Alternative explanations for the loss of synchrotron radiation that were considered were found inadequate. E.g. slowing down through direct interaction with the pellet is estimated to give less than 1 MeV energy loss, which produces a negligible effect on the measurement. Pitch angle scattering is excluded, because it would increase rather than decrease the synchrotron emission [3], and be obvious in the IR-picture.

Conclusions - In conclusion, the observations of runaway electrons during and after pellet injection give rise to the following picture. During the passage of the pellet through the plasma overlapping, low m number magnetic islands form.These are embedded in a stochastic field, from which runaway electrons are lost with an effective diffusivity of $\approx$300 m^2/s. The bulk thermal diffusivity is much smaller, in agreement with predictions for transport in a fully stochastic field. Inside the big m=1 island a beam of runaways survives the turbulent phase. This beam, a 'drift island', is shifted by 4-5 cm with respect to the magnetic island.Whether the drift island must be contained in a larger magnetic island or that it can exist outside this, as expected from guiding center calculations [10,11], is still an open question. The turbulent phase has a duration of only <1 ms, during which the magnetic mode signals have a high amplitude. The short duration is essential to explain the modest loss of thermal energy. The persistent narrow runaway beam monitors the diffusion in the quiet phase after the rapid loss. In some cases it maintains an island topology, with radial and poloidal diffusivities that are extremely low,<0.02 m^2/s. The radial diffusivity is equally small when the magnetic island decays and the runaways spread poloidally to form a thin shell.

Finally, there is a clear relation with the density 'snake' observed in JET, a m=n=1 helical tube of high density which occurs if a pellet penetrates to the q=1 surface [12]. The density snake persists for hundreds of ms and even survives sawtooth crashes. Using this analogy, the phenomenon reported here could be called a 'runaway snake'.

Acknowledgements - This work was performed under the Euratom-FOM and Euratom-KFA association agreement with financial support from NWO, KFA and EURATOM.

References

[1] J.R. Myra *et al.*, Phys. Fluids B **4**, 2092 (1992).

[2] R. Jaspers *et al.*, *Experimental Investigation of Runaway Electron Generation in TEXTOR*, accepted for publication in Nucl. Fusion.

[3] K.H. Finken *et al.*, Nucl. Fusion **30**, 859 (1990).

[4] K.H. Finken *et al.*, Nucl. Fusion **32**, 915 (1992).

[5] R. Jayakumar, H.H. Fleischmann, and S.J. Zweben, *Collisional Avalanche Exponentiation of Run-Away Electrons in Electrified Plasma*, PPPL 2849 (1992).

[6] K.N. Sato *et al.*, Proc. Int. Conf. Plasma Physics, Innsbruck, Vol. **16C**, 403 (1992).

[7] C.T. Chang, Phys. Reports **206**, 143 (1991).

[8] A.B. Rechester and M.N. Rosenbluth, Phys. Rev. Lett. **40**, 38 (1978).

[9] C.C. Hegna and J.D. Callen, Phys. Fluids B **5**,1804 (1993).

[10] G. Fussmann *et al.*, Proc.7th Int. Conf. Plasma Physics and Controlled Nuclear Fusion Research, Vol.1, IAEA, Vienna, 401 (1979).

[11] S.J. Zweben, B.V. Waddell and D.W. Swain, Nucl. Fusion **20**,477 (1980).

[12] A. Weller *et al.*, Phys. Rev. Lett. **59**, 2303 (1987).

5.5 Summary of the Runaway Transport Results

In this chapter the runaway electron confinement has been investigated under different conditions. These measurements are unique in the sense that they a) study runaway confinement in the plasma core, b) use the synchrotron radiation to obtain the transport information and c) focuss on the relativistic electrons of 20 MeV or higher. On the basis of the time behaviour of the synchrotron intensity alone, some firm conclusions can be draw:

- In ohmic discharge $\tau_r > 1$ s, which can be explained by either the large orbit shifts of the runaway electrons that averages out the magnetic turbulence or by the existence of regions of good magnetic surfaces. The acceleration is fast enough to survive the low energetic phase where the drift orbit is small.
- In NBI L-mode discharges the runaway confinement is deteriorated. For higher power shorter confinement times are found. For the case of 1.3 MW NBI co-injection $\tau_r \approx 0.2$ s. NBI counter injection gives rise to higher losses for similar heating power. It is hypothesized that the deterioration in confinement in related to an increase in l_{tur} rather than in tubulence level, since the thermal confinement is less affected than the relativistic runaway electrons.
- Sawtoothing on the synchrotron signal is not observed but cannot be excluded. Runaway electron related signals like HXR and N show spikes during the sawtooth crash. Interpreting these as resulting from runaway electrons thrown out of the plasma in a crash requires $D_r > 200$ m^2/s. Such high diffusion can indicate that l_{tur} becomes comparable to the orbit shift δ during the sawtooth crash.
- During pellet injection a large fraction of the runaway polulation is lost within 600 μs, from which a runaway diffusion coefficient is calculated of $D_r = 300$ m^2/s. This loss is attributed to stochastization of the magnetic field. The remaining runaway electrons are confined in a narrow helical beam at the q=1 surface. In this runaway snake the diffusion is extremely slow: $D_r < 0.02$ m^2/s.

CHAPTER 6

PITCH ANGLE SCATTERING OF HIGH ENERGY RUNAWAY ELECTRONS

6.1 Introduction

The synchrotron radiation diagnostic as used on TEXTOR is the only known technique in which the pitch angle (Θ) of relativistic runaway electrons is measured directly. In the standard TEXTOR runaway discharges $\Theta = 0.12$ rad was found (Sec. 3.6). This was deduced from the shape of the spot of synchrotron radiation as seen under two different angles. Up to now no satisfactory explanation for the observed value of Θ has been given. At the moment the electrons overcome the runaway threshold, the perpendicular velocity can be assumed to be distributed Maxwellian: $v_\perp \approx v_{th}$. Conservation of the perpendicular momentum during the acceleration to a relativistic energy would yield a pitch angle of:

$$\Theta = \frac{p_\perp}{p_{//}} = \frac{m_e v_{th}}{\gamma m_e c} \approx 1 \text{ mrad} \qquad (6.1)$$

The secondary generation process, in which runaways are born with rather high perpendicular momentum of order $p_\perp = m_e v_{crit}$, cannot eliminate the large discrepancy with experiment, since then:

$$\Theta = \frac{m_e v_{crit}}{\gamma m_e c} = 10 \text{ mrad} \qquad (6.2)$$

A second important observation is that Θ does not increase further once it has reached the value of Θ=0.12 rad. Diffusion in momentum space as a result of collisions with plasma ions and electrons can make Θ as large as experimentally observed, but with that mechanism it is not clear why Θ does not increase further. Another mechanism has to be invoked to explain this.

In this chapter a model is introduced which can account for the large value of Θ. This model incorporates the diffusive increase of $p_\perp$ as a result of the collisions as well as the parallel drag from the plasma. Whereas this has been treated by several authors (for instance [Fus-79]), we include the effect of radiation and of a time-dependent production rate of runaway electrons in the calculations, which will alter the results significantly. In addition, the effect of magnetic field ripple is included in the model. It turns out that inclusion of the latter effect is required to arrive at a satisfactory simulation of the experimental observations.

The pitch angle is important for at least three reasons: i) Both the spectrum and the intensity of the synchrotron radiation depend strongly on Θ as discussed in Chapter 3; ii) The maximum energy to which the runaway electrons can be accelerated decreases with increasing Θ. Enhancing Θ could therefore provide a means to reduce the possible damage runaway electrons can do to a fusion reactor; iii) Interaction of runaway electrons with plasma waves leads to an increase of Θ. The observation of such an interaction in TEXTOR will be described and analyzed in this chapter.

This chapter is structured as follows. We start with a short summary of the observations of the synchrotron radiation in a standard low density ohmic discharge. In Sec. 6.3 the basic model is presented, treating the effect of collisions, radiation and a time dependent production rate. The results of this model are compared to the experimental datain Sec. 6.4. Based on this comparison a modification of the model is proposed in Sect. 6.5 which can remove the last discrepancies between model and observations. This modification consists of the addition of the interaction between the cyclotron motion of the runaway electrons and the magnetic field ripple. A discussion of the influence of the newly obtained knowledge on previous results is given in Sec.6.6.

In the second part of this chapter we focus on an event observed in the current decay phase of several discharges in which Θ increases by a factor of 1.5 within 100 μs. A description of this fast pitch angle scattering is given in Sec. 6.7. A mechanism to explain this process is proposed in Sec. 6.8 and a final discussion on the results is given in Sec. 6.9.

6.2 Summary of the Synchrotron Radiation Observations

In this section we give a list of the observations of the synchrotron radiation that have been partially described in previous chapters and are common for all ohmic low density TEXTOR discharges:

* The pitch angle is deduced from the vertical extent of the spot of synchrotron radiation. We found $\Theta=0.12\pm0.02$ rad.
* The size of the spot appears to grow only marginally; a quantitative estimate of this increase is hampered by the simultaneous increase of the radiated power.
* The radius of the runaway beam is found to be $r_{beam}=0.20$-0.25 m.
* The intensity is distributed rather uniformly over the runaway spot.
* The energy of the runaway electrons reaches a value of $W_{max} \approx 30$ MeV. This is deduced from the filter method. Since a second detector (a CCD camera) sensitive up to wavelength of 1.2 μm did not detect any synchrotron radiation, the absolute upper bound is $W_{max} < 50$ MeV.
* The energy does hardly show any increase after t=1.5 s.
* The synchrotron radiation intensity grows exponentially in certain conditions.

The last three observations are understood if the experimental value of Θ is used. The runaway electrons are accelerated by the electric field and loose energy by radiation. At W≈30 MeV an equilibrium between the radiation loss and the acceleration is reached and the energy will not increase further. Once this equilibrium is reached, the increase of the radiation represents the increase in the runaway population. The exponential rise of the population is attributed to secondary generation of runaway electrons. The observations that are not yet explained and the open questions that will be answered in this chapter are:

-Why does Θ reach a value of 0.12 rad?
-Why does Θ not increase further?
-What is the distribution in Θ and W?
-Why is the intensity uniformly distributed over $r \leq r_{beam}$?
-In the previous chapters an assumption for the distributions of Θ and W was used. The modelling will result in theoretical distributions of Θ and W that are consistent with the measurements. Will the conclusions of the previous chapters change if these correct distributions of W and Θ are used?

6.3 Model for the Pitch Angle of Runaway Electrons

We analyze the evolution of the momentum of runaway electrons under the influence of an electric field E and a cold plasma. The individual processes that are taken into account are:

i) acceleration by the electric field: $$\frac{dp_{//}}{dt} = eE \qquad (6.3)$$

ii) parallel drag by the plasma: $$\frac{dp_{//}}{dt} = F_d \qquad (6.4)$$

iii) loss of momentum by radiation: $$\frac{dp_{//}}{dt} = -\frac{P_{syn}\cos\Theta}{c} \qquad (6.5)$$

$$\frac{dp_{\perp}}{dt} = -\frac{P_{syn}\sin\Theta}{c} \qquad (6.6)$$

iv) collisions with plasma particles: $$\frac{d\langle p_{\perp}^2\rangle}{dt} = D_{col} \qquad (6.7)$$

v) a time dependent birth rate: $$\lambda = \lambda(t) \qquad (6.8)$$

In these equations F_d is taken from eq. (A.8), P_{syn} from eq. (2.16), $\Theta=v_\perp/v_{//}=p_\perp/p_{//}$ and D_{col} represents the diffusive increase of the perpendicular momentum as a result of small angle Coulomb collisions between the runaway electrons and the plasma ions and electrons. Eq. (6.7) is valid for an ensemble average. The average change in $\langle p_\perp^2 \rangle$ is calculated for electron-ion interactions from:

$$D_{col,i} = \frac{d\langle p_\perp^2 \rangle}{dt} = \int dp \int_0^{2\pi} d\phi \int_{\theta_{min}}^{\pi} d\theta \, \sin\theta \, p_\perp^2 \, \nu_{ri}(v,\theta,\phi)) \qquad (6.9)$$

where $\nu_{ri}(v,\theta,\phi) = f_i(v)\, c\, d\sigma/d\Omega$ is the collision frequency for collisions between the runaway electron and ions of species i and

$$\frac{d\sigma}{d\Omega} = \left(\frac{Z\, e^2}{16\pi\varepsilon_0\, W_{kin}} \right)^2 \frac{1}{\sin^4\theta/2} \qquad (6.10)$$

is the differential Rutherford cross section with the assumptions $m_i >> m_e$ and $v = v_{rel} \approx c$. The integral limit θ_{min} is used to account for the Debye shielding ($1/(\sin\theta_{min}/2) = \Lambda$). Performing this integral, summing over the different ion species and using that for runaway electrons $\int f_i(v)\, v\, dv = c\, n_i$, the following result is obtained:

$$D_{col,i} = \sum_i \left(\frac{Z_i^2 e^4}{2\pi\varepsilon_0^2} \right) \frac{n_i \ln\Lambda}{c} \approx 10\, Z_{eff}\, n_e[10^{19}m^{-3}]\ m_e^2c^2/s \qquad (6.11)$$

This expression shows for relativistic electrons that the increase in perpendicular momentum due to collisions with ions has a nonzero limit. Electron-electron collisions will contribute similarly and therefore Z_{eff} should be replaced by $Z_{eff}+1$ to obtain D_{col}:

$$D_{col} \approx 10\,(Z_{eff}+1)\, n_e[10^{19}m^{-3}] = 30 \qquad m_e^2c^2/s \qquad (6.12)$$

The last equality is obtained by substituting the typical discharge parameters: $Z_{eff} = 2$ and $n_e = 1\times10^{19}m^{-3}$.

A Monte Carlo simulation is used to calculate the distribution of the runaway electrons in the (W,Θ)-plane as a function of time. The diffusion process is treated as a random walk process with stepsize $\sqrt{D_{col}dt}$.

Three different functions $\lambda(t)$ were used: 1) $\lambda(t)=C_1\delta(t)$, corresponding to the creation of runaway electrons only at t=0, 2) $\lambda(t)=C_2$, corresponding to a constant birth rate of runaway electrons, 3) $\lambda(t)=C_3\exp(t/t_0)$, corresponding to an exponentially increasing runaway production as expected from the secondary generation mechanism. The constants C_1,C_2 and C_3 are chosen arbitrarily as we are only interested in the normalized distribution in the (W,Θ)-plane.

Before turning to the results of the simulation the essential features of the processes are discussed first. Electrons that just have overcome the runaway threshold will have a large value for Θ of order v_{th}/v_{crit}. This Θ will shrink when the electrons gain parallel momentum. Subsequently, Θ will increase again under the influence of collisions. As a result of collisions the distribution in $p_\perp$ will broaden. For a higher energy and pitch angle, radiation effects become important and the parallel momentum will not increase further if the radiation limit is reached. The perpendicular momentum is in general not at equilibrium here. Due to collisions, the average $p_\perp$ ($(p_\perp)_{col} \equiv \sqrt{<p_\perp^2>}$) will increase in time, but radiative momentum loss decreases $p_\perp$. These two processes balance for an average electron (and assuming $p_{//}$=constant) if the following condition is fulfilled:

$$\left(\dot{p}_\perp\right)_{rad} + \left(\dot{p}_\perp\right)_{col} = 0 \qquad (6.13a)$$

where

$$\left(\dot{p}_\perp\right)_{rad} = -\frac{\Theta\, P_{syn}}{c} \qquad (6.13b)$$

For the average of the ensemble of runaway electrons we can take $(\dot{p}_\perp)_{col}$ to be:

$$\left(\dot{p}_\perp\right)_{col} = \frac{D_{col}}{2p_\perp} = \frac{D_{col}}{2\Theta\gamma m_e c} \qquad (6.13c)$$

This yields an equilibrium value of Θ of:

$$\Theta_{eq} = \sqrt{\frac{D_{col}}{2P_{syn}\gamma m_e}} \qquad (6.14)$$

For electrons at the radiation limit one finds:

$$\Theta_{eq} \approx \frac{0.38}{\sqrt{W(MeV)}} \qquad (6.15)$$

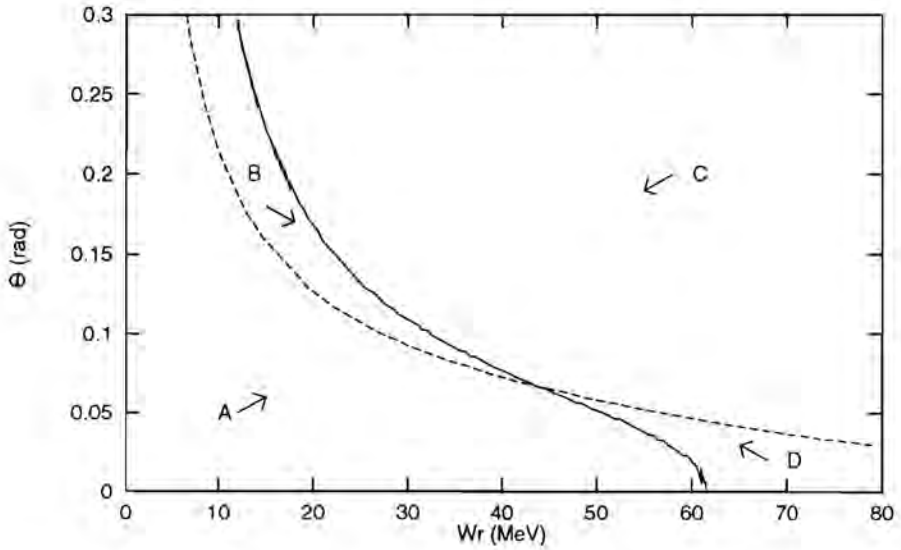

Figure 6.1: *The curves $\langle \dot{p}_\perp \rangle = 0$ (dotted) and $\dot{W} = 0$ (full line) plotted in the (W,Θ) plane. Four different regions are identified. The direction in which an averaged runaway electron will move is indicated by arrows. The runaway electrons will collect at the intersection of the two curves at (45 MeV, 0.06 rad). Here a maximum in the distribution is expected to occur. Eventually the electrons will slide down the line and move to (60 MeV, 0.0 rad).*

The curve $\langle \dot{p}_\perp \rangle = 0$ is indicated in Fig. 6.1, together with the radiation limit ($\dot{W} = 0$). Now, the (W,Θ) plane can be divided in 4 regions bounded by these curves, as indicated in Fig. 6.1. In A, the region below the curves, both W and Θ will (on the average) increase in time. In region B, still below the radiation limit, W will increase further in time, whereas Θ will decrease for an averaged electron (i.e an electron with $p_\perp = \langle p_\perp \rangle$). In region C above both curves, both W and Θ will decrease and in region D, W will decrease and Θ will increase. The distribution of electrons will initially be in region A. As time increases, both W and Θ grow, until the tail of the Θ distribution reaches the $\langle \dot{p}_\perp \rangle = 0$ curve. The growth of Θ in time will be reduced and the distribution will stay close to this curve. Since these electrons are not yet at the radiation limit, W is increased and therefore they move further to the right in the (W,Θ) - plane. Once the radiation limit is reached, W can only change by a change of Θ. A runaway distribution all over the radiation limit will build up. This distribution has a quasi stationary state at the point (W_{eq},Θ_{eq}) = (45 MeV, 0.06 rad), where both the energy and the pitch angle are in equilibrium. However, electrons at this point will have an equal probability to increase or decrease their $p_\perp$ as a result of collisions, but since the radiation always acts to reduce $p_\perp$ eventually their Θ will decrease and they will accumulate at Θ=0 rad and W ≈ 60 MeV.

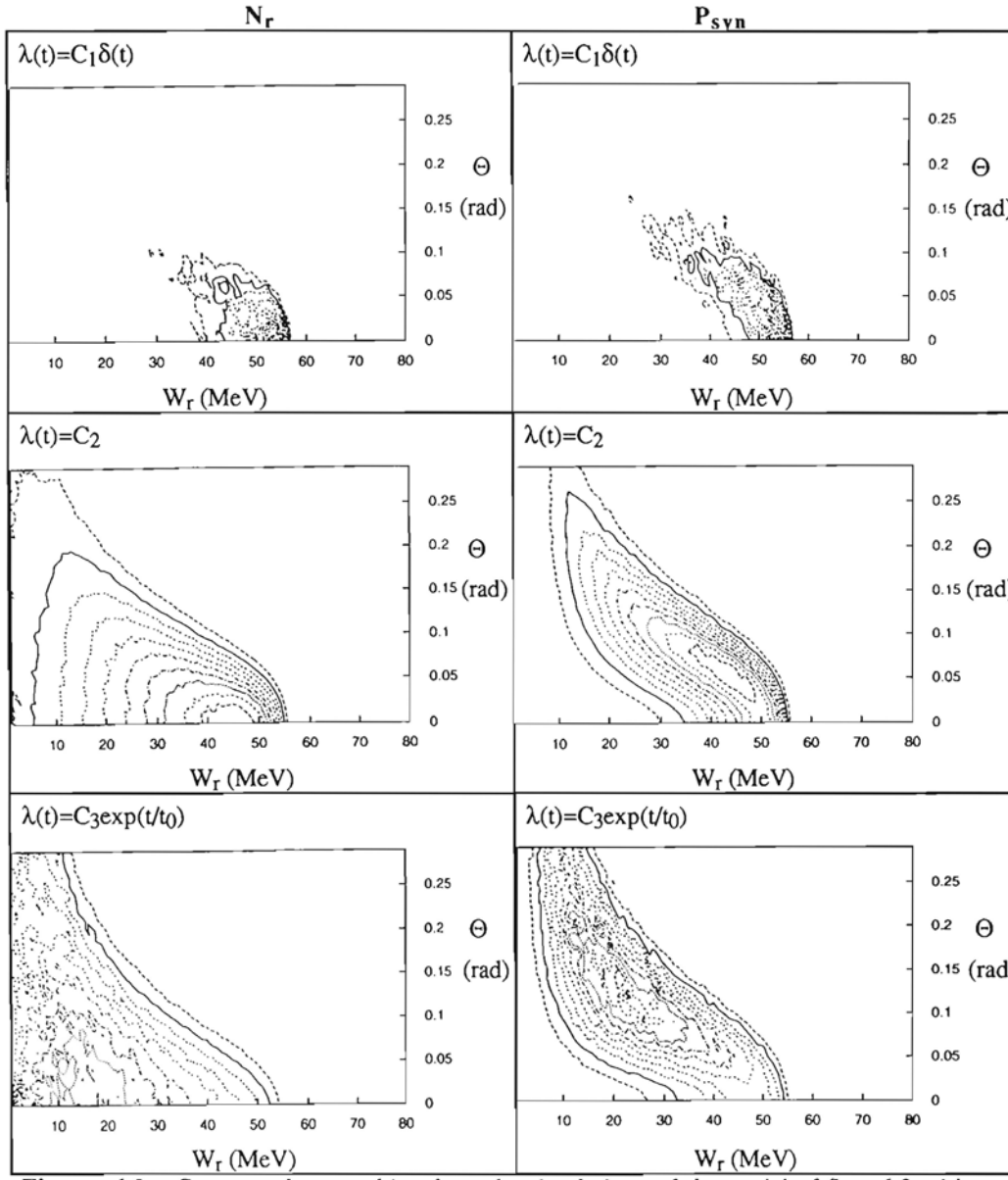

Figure 6.2: *Contour plots resulting from the simulations of the model of Sec. 6.3 with parameters: $n_e=1\times10^{19}$ m^{-3}, $E=0.09$ V/m, $Z_{eff}=2$ and $D_{col}=30$ $(m_ec)^2s^{-1}$. The left hand side shows the distribution of the number of runaway electrons, whereas on the right hand side the synchrotron intensity is plotted. All plots give the situation at $t=3$ s. Three different cases are considered. These are from top to bottom: 1) the case where the runaway electrons are only generated at $t=0s$, 2) the case where the runaway production rate is constant in time and 3) the case where the runaway generation grows exponentially in time with an avalanche time $t_0=1$ s, as expected from the secondary generation mechanism.*

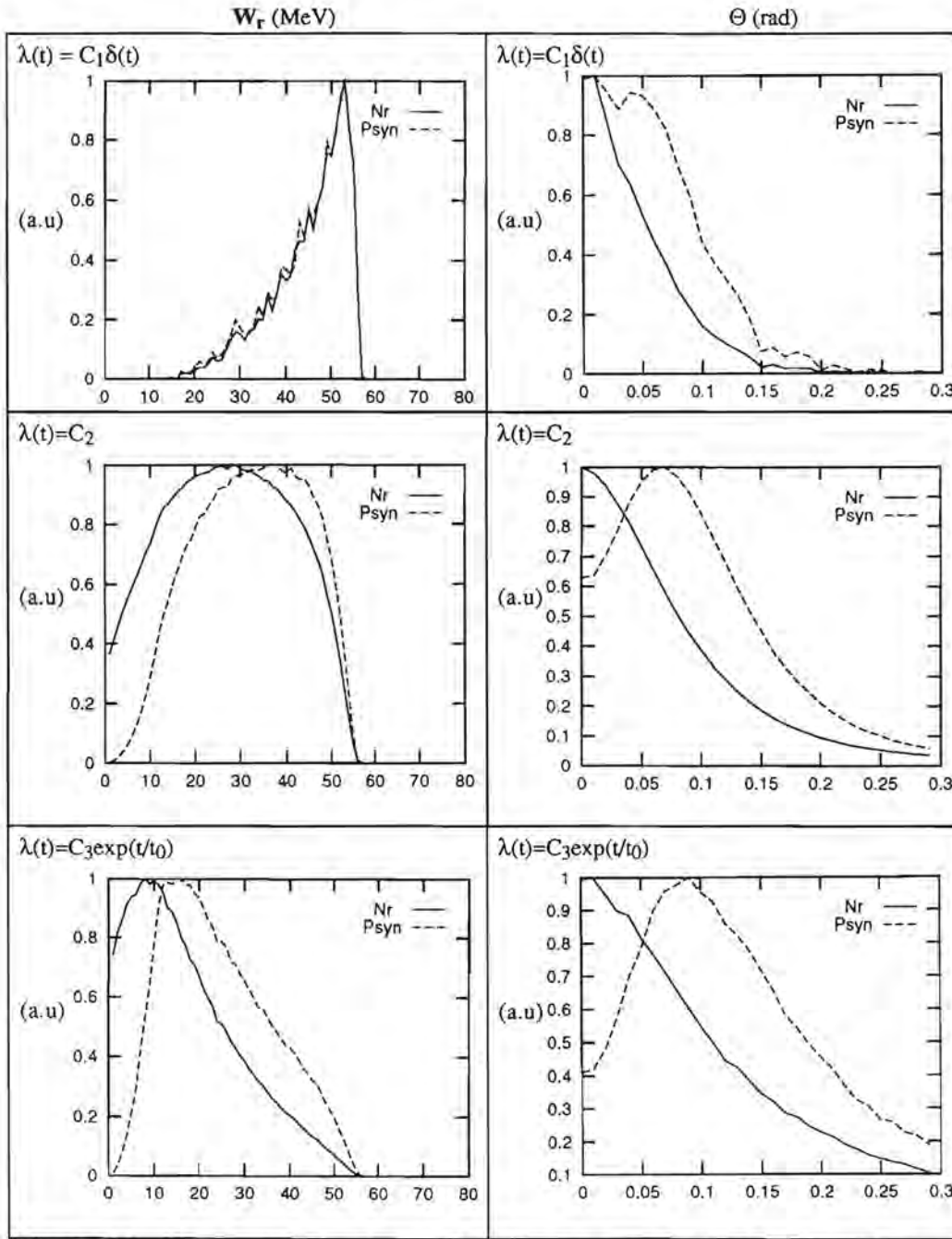

Figure 6.3: *Same simulations as in Fig. 6.3, but here the energy and pitch angle spectrum are plotted separately. The solid curves give the distributions of the number of runaway electrons and the dotted curves show the intensity distributions.*

The results of the simulations are shown in Figs. 6.2-6.4. In Fig. 6.2 the contour plots are shown at t=3 s for the three different cases. The left hand side shows the distribution of the number of runaway electrons in the (W,Θ)-plane, whereas the right hand side shows the distribution of the synchrotron radiation P_{syn}.

In the first case, in which the runaways are generated only at t=0, almost all end up in a small region around W=55 MeV and Θ=0 rad after t=3 s (Fig.6.2a). In the case of a constant birth rate the energy at which most runaways are located is lower energy (W=45 MeV) and the distribution in Θ is broader (Fig. 6.2b). In the contour plot of P_{syn} we see that the maximum intensity is radiated from the region (W,Θ)=(45 MeV,0.06 rad) which coincides with the intersection of the $\langle \dot{p}_\perp \rangle = 0$ and $\dot{W}=0$ curves. Note that the number contours are arranged around the $\langle \dot{p}_\perp \rangle = 0$ whereas the P_{syn} contours are arranged around $\dot{W}=0$. When secondary generation is taken into account the region where most radiation originates from shifts to lower energy: (W,Θ)=(20 MeV,0.10 rad). These features are more clearly observed in Fig. 6.3 where the distributions of W and Θ are plotted separately. Fig. 6.4 shows the time behaviour of W and Θ for the secondary generation. Note that the energy from which most radiation is originating hardly changes after t=1s. For longer times a shoulder in the distribution function develops at higher energies and Θ decreases to lower values, as expected from our qualitative discussion.

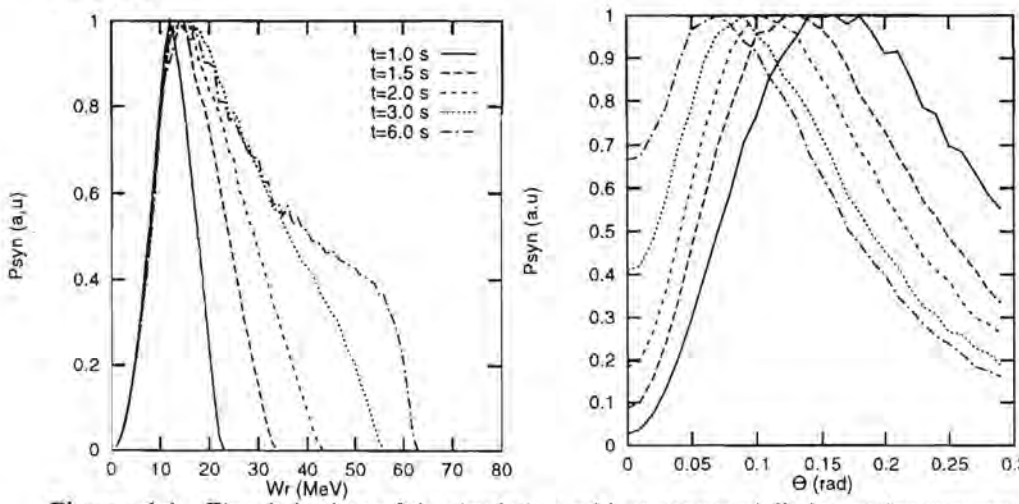

Figure 6.4: *Time behaviour of the simulations with an exponentially increasing runaway production rate with t_0=1 s. Plotted are the intensity distributions as a function of energy and pitch angle for five different times: t=1 s,t=1.5 s,t=2 s,t=3 s and t=6 s. The energy and the pitch angle from which most radiation is originating does not increase after t=1 s but stay nearly constant around W=20 MeV and Θ=0.10 rad. Note the 'shoulder' in the energy spectrum for t=6 s.*

6.4 Comparison to Experiment

Comparing the results of the simulations with the observations in TEXTOR as summarized in Sec. 6.2 a number of observations can now be understood:

- The simulations show that the pitch angle distribution after t=3.0 s is broad enough that runaway electrons with Θ=0.12 rad, the experimental value, are present.
- In this model the Θ distribution does not broaden in time after t=1.0 s. Instead, a slight narrowing of the distribution is observed.
- For the three investigated cases the energy distribution does hardly change after t=1.5 s, which is in agreement with the experimental observation.
- The W and Θ distributions do not change in time in this model after 1.5 s. This indicates that the increase in P_{syn} represents an increase in number of runaway electrons. The experimentally observed exponential increase in P_{syn} is only understood if the birth rate increases exponentially, according to the secondary generation process.

In two other respects, however, the simulations fail to describe the data:

- the maximum energy of the runaway electrons W_{max} is inconsistent with the measurements, where $W_{max} \approx 30$ MeV is found. The simulations show for the first case ($\lambda(t)=C_1\delta(t)$) that already after 1.5 s W_{max} = 55 MeV. This would be visible on the CCD camera if present but here no synchrotron radiation is detected. Also with a constant or exponential birth rate this high energy will be reached in the course of time.
- In the simulations the value of Θ from which most radiation is coming, is a factor of 1.5-2 smaller than the experimental value. However, we should remark that the experimental value is obtained by assuming no distribution in Θ. A direct comparison is therefore not possible. Nevertheless the model is not fully correct because while the simulations show that Θ is decreasing in time, this is not observed in the experiment.

The model is thus able to describe the some features of the experiments, but fails in correctly predicting the main parameters W and Θ. The interaction of runaway electrons with the ripple in the toroidal magnetic field provides a mechanism that limits the maximum attainable runaway energy. Inclusion of this mechanism in the model can thus remove the outstanding discrepancy between experiment and model. A discussion of this mechanism is presented in the next section.

6.5 Including the Runaway - Field Ripple Interaction in the Model

Laurent and Rax [Lau-90] have proposed a mechanism based on a resonant interaction between the relativistically down-shifted cyclotron frequency of the runaways and the magnetic field

ripple, resulting from the number (N) of coils to produce the toroidal magnetic field. A resonance should occur for electrons with energy:

$$W_{res}\,(MeV) = 0.511\,\frac{eBR_0}{nNcm_e} \tag{6.16}$$

For TEXTOR conditions the second and higher harmonic resonances are in the energy range of the observed electrons: $W_n = 70/n$ MeV. A simple estimate of the pitch angle scattering the runaway electrons will experience as a result of this ripple interaction will be derived here, where we follow the basic derivation of Laurent and Rax [Lau-89].

The perturbation of the magnetic field due to the ripple δB is described as $\delta B\cos(nNz/R_0)$ for slab geometry. A Lorentz transformation to the guiding center frame (gcf) yields:

$$\mathbf{E}_{gcf} = -\,v_{//}\,\gamma\,\delta B\,\cos\left(\frac{nN\gamma\,(z_{gcf}+v_{//}t_{gcf})}{R_0}\right)\mathbf{e}_x \tag{6.17a}$$

$$\mathbf{B}_{gcf} = \gamma\,\delta B\,\cos\left(\frac{n\,N\,\gamma\,(z_{gcf}+v_{//}t_{gcf})}{R_0}\right)\quad \mathbf{e}_y \tag{6.17b}$$

In the guiding centre frame the change in energy W and parallel momentum $p_{//}$ due to the interaction with the wave become:

$$\frac{dW_{gcf}}{dt_{gcf}} = e\mathbf{E}_{gcf}\cdot\mathbf{v}_{gcf} = -e\,v_{\perp,gcf}\frac{\gamma\,v_{//}\,\delta B\,\sin(\alpha)}{2} \tag{6.18a}$$

$$\frac{dp_{//gcf}}{dt_{gcf}} = e\mathbf{v}_{gcf}\times\mathbf{B}_{gcf}\,\mathbf{e}_z = e\,v_{\perp,gcf}\,\frac{\gamma\,\delta B\,\sin(\alpha)}{2} \tag{6.18b}$$

Here α is the phase angle between the cyclotron motion and the wave. Since a magnetic field cannot increase the particle energy we find by a transformation back to the laboratory frame yields $dW/dt = 0$ as expected. The parallel momentum in the laboratory frame is given by:

$$\frac{dp_{//}}{dt} = \left(\frac{dp_{//gcf}}{dt_{gcf}} + \frac{v_{//}}{c^2}\frac{dW_{gcf}}{dt_{gcf}}\right) = e\,v_{//}\,v_{\perp}\,\frac{\delta B\,\sin(\alpha)}{2c} \tag{6.19}$$

Finally the change in perpendicular momentum of the resonant electron is found by using energy conservation (p^2=constant). This results in a rate of change of Θ given by:

$$\frac{d\Theta}{dt} = -\frac{\delta B\ \omega_{ce}\ \sin(\alpha)}{2\gamma B} \tag{6.20}$$

The tokamak case differs from this slab estimate in the fact that the electron experiences the dominant effect of the ripple only on the low field side of its orbit, where the ripple is largest. The interaction time is therefore estimated by $t_{int} = \pi qR/c$ (i.e. half of the time necessary for a poloidal transit). Because of the combined effect of the rotational transform and the finite width of the ripple the phase between the ripple and cyclotron motion to be lost. The exchange between parallel and perpendicular momentum is therefore irreversible, and should be described as a diffusion process. This yields an effective pitch angle diffusion coefficient:

$$D_{\Theta\Theta} = \int_0^{t_{int}} \left(\frac{d\Theta}{dt}\right)^2 dt = \frac{\pi qc}{8R_0}\, n^2N^2 \left(\frac{\delta B}{B}\right)_n^2 \tag{6.21}$$

The process of pitch angle scattering will continue as long as the electrons are resonant with the field ripple. Either an acceleration by the ohmic electric field or the radiative deceleration caused by the increased pitch angle will stop this diffusive process. The width of the resonance $\Delta W/W$ is estimated to be:

$$\Delta W/W = \frac{1}{f_{ripple}\, t_{int}} = \frac{2}{nNq} \tag{6.22}$$

In a later paper [Lau-90] Laurent and Rax give a more sophisticated treatment using a Hamiltonian formalism. However, the main result of the basic derivation given here (eq. 6.21) agrees within a factor of 2 with the result of the Hamiltonian calculation.

In the model of Sec. 6.3 the interaction with the field ripple is included by adding to D_{col} the diffusion as a result of the ripple interaction:

$$D = D_{col} + D_{ripple} \tag{6.23}$$

where

$$D_{ripple}(W) = \frac{p_{//}^2 D_{\Theta\Theta}}{1 + (nNq)^2(1 - W/W_{res})^2} \tag{6.24}$$

The denominater determines the width of the resonance, which is assumed to be Lorentzian. For the ripple and q the values at r=10 cm were taken: q=1, $(\delta B/B)_2 = 5\times10^{-6}$, $(\delta B/B)_3 = 1\times10^{-8}$. It turns out that only the second harmonic interaction contributes significantly to the pitch angle

scattering: $D_{ripple}(W_{res})=8\times10^3\ m_e^2c^2\ s^{-1}$. Even for runaway electrons with an energy 50 % away from the resonance condition D_{ripple} is as large as D_{col}.

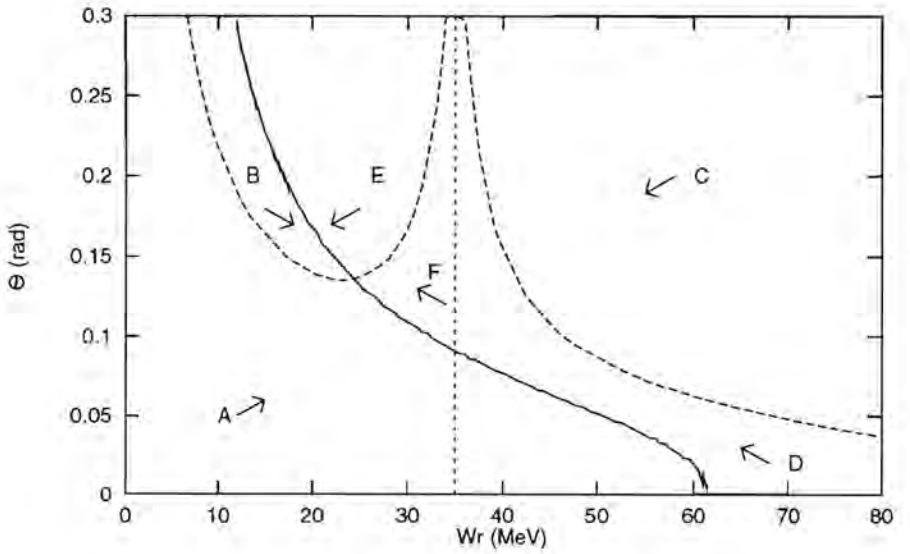

Figure 6.5: *Identical to Fig. 6.1, but now including the interaction between the runaway motion and the magnetic field ripple in the model.*

The (W,Θ) plane is shown in Fig. 6.5 with the $\dot{W}=0$ curve, the modified $\langle p_\perp\rangle=0$ curve and the energy blocking curve caused by the second harmonic resonance. Equilibrium in W and Θ is now reached at (25 MeV, 0.13 rad). Note that the experimental values are positioned at this point in the (W,Θ) plane.

The simulations performed with this model show that the runaway energy does not even reach W_{res}=35 MeV, but an effective energy blocking occurs already at W_{max}=30 MeV. This is in excellent agreement with the experimental findings. The results are plotted in Fig. 6.6 and 6.7 for the same three conditions as in Fig. 6.2 and 6.3. The time behaviour for the case $\lambda(t)=C_1\delta(t)$ is shown in Fig. 6.8. For t >2.0 s the energy distributions in the high energy region, from which the synchrotron radiation is coming, turn out to be similar for all three cases. This shows that the actual generation mechanism is not relevant for the distribution function. Concerning the Θ distribution the same conclusion can be drawn: independent of the time behaviour of the runaway production similar distributions are found. Most radiation is observed from runaway electrons with Θ=0.15-0.20 rad. The actual Θ distribution is rather broad with a width at half maximum of Θ=0.15-0.20 rad. Neither distributions change appreciable after t > 2.0 s.

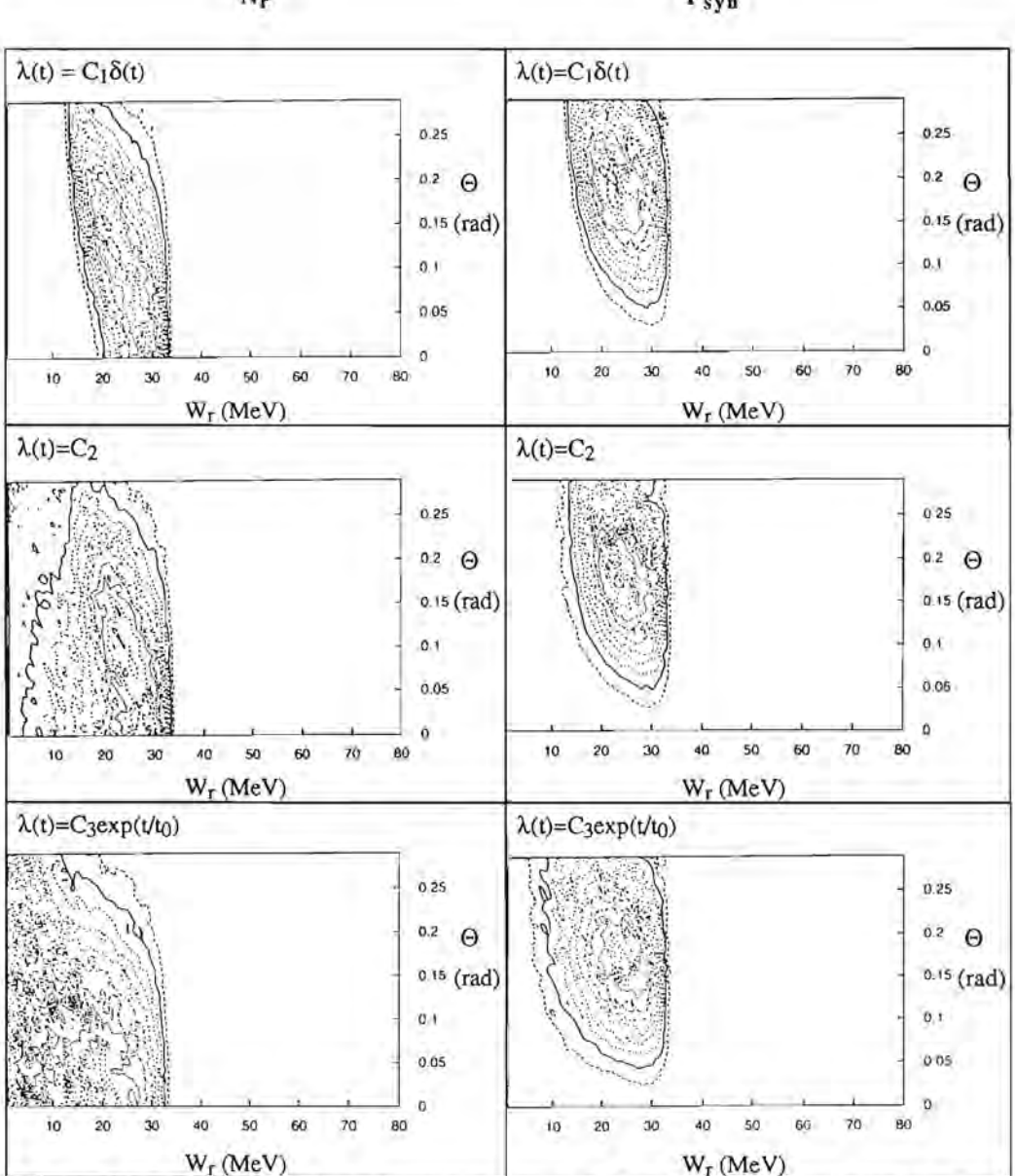

Figure 6.6: *Contour plots for the same conditions as in Fig. 6.2, with including the ripple interaction in the model.*

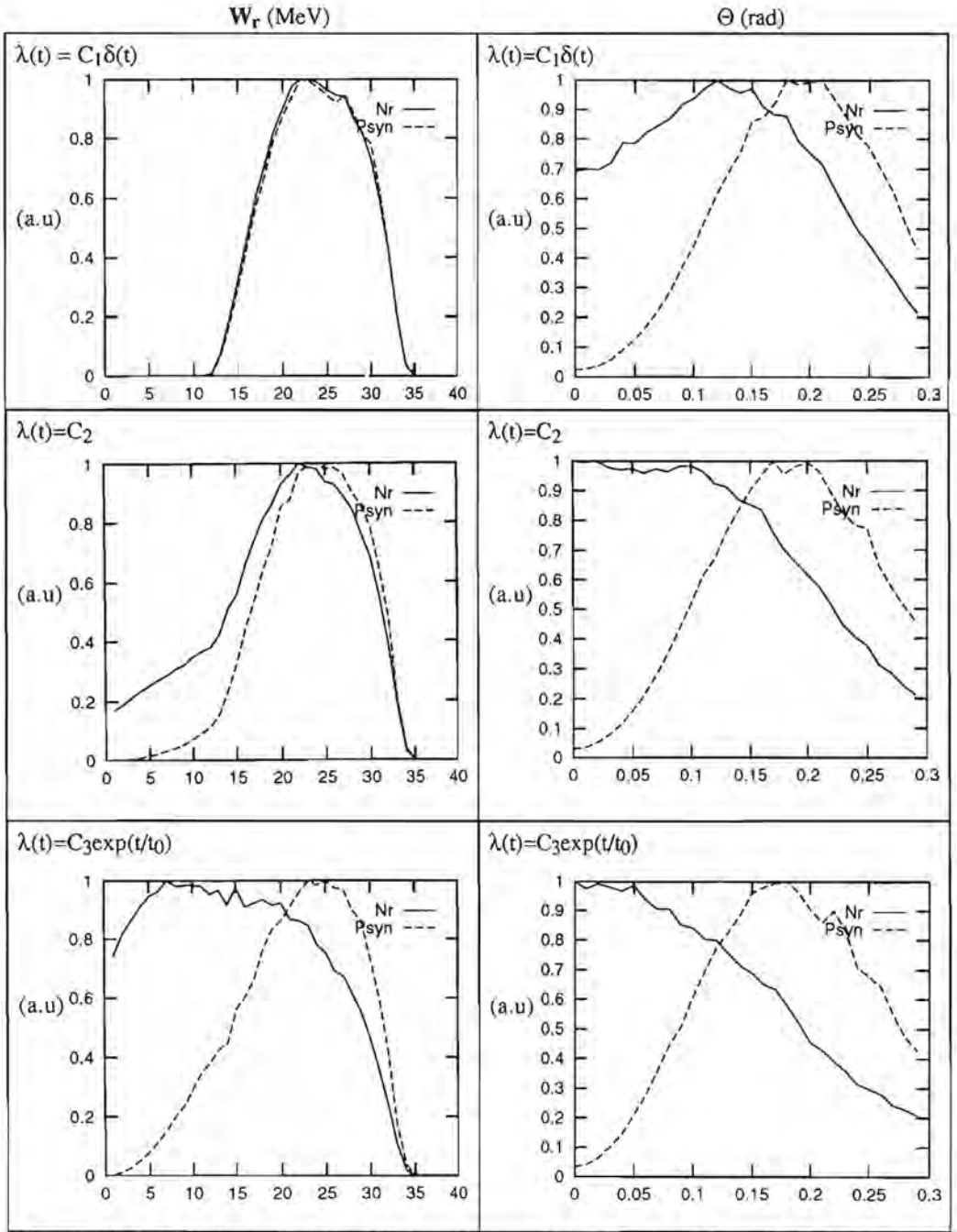

Figure 6.7: *Distributions in W and Θ plotted separately for the case with ripple interaction. It is observed that the energy reaches a maximum value of about 30 MeV, and the pitch angle distribution is now broader than without this interaction, with a maximum around Θ=0.15-0.20 rad. All three cases have similar distributions.*

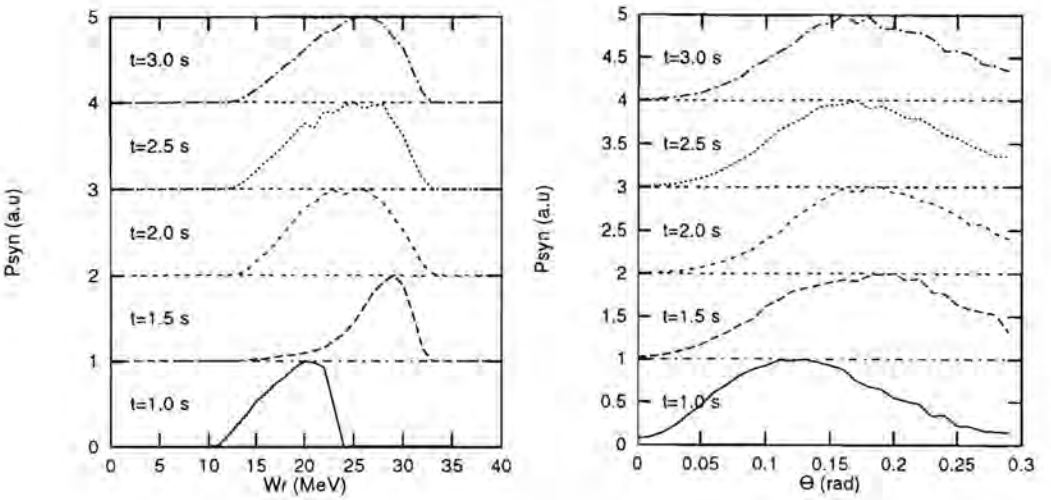

Figure 6.8: *Time behaviour of the synchrotron radiation intensity distribution as a function of energy and pitch angle. The case of a runaway generation at t=0 s is plotted, but the other two cases give similar results. It is observed that the distributions do not change after t=2 s.*

Comparing these simulations with the experiment we can conclude that in the model the energy is reproduced well. The pitch angle is calculated somewhat higher than measured. This can probably be solved by a more accurate treatment of the ripple interaction and the determination of the ripple value. The result of the model that both W and Θ do not change in time after t>2.0 s is consistent with the measurement. With these results the last unexplained features of the list of Sec. 6.2 are removed. Because of the good agreement between experiment and model one can conclude that:

- The interaction between the runaway electrons and the field ripple does indeed occur.
- The distributions of W and Θ are as follow from the simulations.

6.6 Implications for Previous Results

Without knowing the actual W and Θ distribution in the foregoing chapters, several calculations were performed in which a flat W distribution and an delta distribution for Θ was assumed. Now we have obtained these distributions from the model we can discuss which impact this new insight has on the previous results.

The flat energy distribution assumed turns out to be an acceptable guess, since for all three different generation mechanism, the energy distribution in the range 15-30 MeV is nearly flat. The departure from this for lower energies will not change the calculated number of runaway electrons in the plasma by more than a factor of 2.

A distribution in Θ was not considered, but this will not affect the results significantly, since, once Θ is larger than a few mrad P_{syn} is approximately linearly dependent on Θ^2, and instead of taking the whole distribution into account the average value for Θ^2 may be used. Since the used value of Θ=0.12 rad is close to the average value of Θ as follows from the Θ–distribution ($<\Theta^2>\approx$0.15 rad), the obtained estimate for the number of electrons is valid within a few times 10 %. The calculations do not need to be readdressed, but the errorbars in the experimental values for the bith rate λ are smaller since the distributions are known with more accuracy now. Therefore, whereas the uncertainty in λ deduced in Sec. 4.4 was estimated to be an order of magnitude, with the present knowledge we estimate $F\lambda=(1.5 \pm 0.5)\times10^{-9}$.

Finally, the constancy in these distributions and the fact that they are independent of the generation mechanism, implies that the synchrotron radiation is proportional to the number of runaway electrons in the plasma. The observed exponential increase can therefore again only be explained by secondary generation.

Not discussed yet is the fact that the synchrotron radiation is almost uniformly distributed over the observed spot, and that the spot has a rather sharp boundary of width ≈ 3 cm. Are the simulations consistent with this? The Θ-spectrum, which partly determines the boundary of the spot, does not reflect this. To explain this it is recalled that the size of the spot can be mainly determined by the extent of the runaway beam rather than the pitch angle (see Sect. 3.6). In the horizontal direction the extent L_h is given by:

$$L_h = 2r_{beam} + R\Theta^2 \qquad (6.25)$$

In the vertical direction the extent L_z is determined by the minimum of $D\sin\Theta$ or r_{beam}, where D is the distance from the emitting region to the camera:

$$L_z = \min (2r_{beam}, 2D\sin\Theta) \qquad (6.26)$$

The observations show that L_z is nearly as large as L_h: L_z-L_h = (0-5 cm). From this it follows that $\Theta > 0.1$ rad, because otherwise L_z would be much smaller than L_h. Larger values of Θ would not be noticed since then the radius of the runaway beam is the limiting factor. For r_{beam} =0.20-0.25 both L_h and L_z are mainly determined by r_{beam}. (The determination of Θ was obtained from the shape of the spot as seen under two different angles. In a single measurement Θ could not be determined accurately). The observation of a sharp boundary and

a uniform distribution of the intensity over the spot reflects the uniform distribution of the runaway electrons in a well localized area of the plasma. The region where the runaways are located is thought to be determined by three processes: i) the primary generation of the runaway electrons takes place in the central 10 cm (see Fig 4.1). Secondary generation will not alter the distribution since this process is proportional to the primary runaway density; ii) after a sawtooth crash the primary runaway electrons are uniformly distributed up to the mixing radius r_{mix}, which for TEXTOR is estimated at about $r_{mix} \approx 1.5\ r_{inv} \approx 16$ cm, r_{inv} being the sawtooth inversion radius. This process would provide a rather sharp boundary. Sawtoothing is observed on the ECE signals even for these low density discharges. Since new born runaway electrons are still at relatively low energies and hence have small orbit shifts, it is likely that they will experience the turbulence induced during the sawtooth crash; finally iii) the orbit shift of several cm of the runaway electrons once they are observed makes it plausible that the synchrotron radiation is observed up to values of r≈0.20 cm.

Summarizing we can state that with a model taking into account acceleration, radiation, collisions with the plasma electrons and ions and finally the interaction with the static perturbations of the magnetic field the synchrotron radiation observations in TEXTOR as listed in Sec. 6.2 can be understood and simulated. The results provide the first evidence for the occurrence of the interaction between runaway electrons and the magnetic field ripple. The analysis presented in previous chapters is fully compatible with the results of this study.

6.7 Observation of a Fast Pitch Angle Scattering Event

Having analyzed the behaviour of the runaway electron energy and pitch angle under normal steady state plasma conditions, we now turn our attention to transient events observed on the synchrotron radiation which give evidence of rapid changes of the pitch angle. We will make it plausible that this represents a runaway instability resulting from the interaction between the runaway electrons and plasma oscillations. We start with a description of the fast event and will then in the next section discuss a possible mechanism to explain the observations.

a. Synchrotron Radiation

In the current decay phase of these ohmic discharges the intensity of the radiation stays almost stable and the dominant feature observed is the outward movement of the spot, which is ascribed to the fact that the drift orbit displacement is inversely proportional to the current (see Fig. 5.1). In a few discharges, however, a peculiar event is observed. Within one or two line scans of the infrared camera, a change in the emission pattern occurs. This is shown in Fig. 6.9. The picture shows one frame of the IR camera recorded between t =3.000 s and t=3.015 s. The synchrotron radiation can clearly be distinguished from the thermal background

radiation. This picture differs from the previous frames by the drastic change in spot width and intensity at the point indicated by the arrow. On the subsequent frame the whole spot is symmetric again, but with an extent equal to the lower part of Fig.6.9.

The time (Δt) in which the spot increases in intensity is $\Delta t \approx 125$ μs. The synchrotron intensity can change only by a change in W, N_r or Θ. The short time scale excludes the possibility that the increase is due to an energy gain of the runaways ($\Delta W = 4$ MeV is required to account for the intensity increase, equivalent to 32 GeV/s or a loop voltage of 1kV) or an increase in the number of runaways. To ascribe the increase of the extent of the spot to a redistribution of the runaway beam over the plasma is inconsistent with the simultaneously increasing intensity of the synchrotron radiation. Fast Pitch Angle Scattering (FPAS) of the relativistic electrons is therefore the only viable explanation of this behaviour.

From the picture of Fig. 6.9 it is deduced that the pitch-angle increases in this particular example from 0.12 rad to 0.17 rad, corresponding to a change in perpendicular momentum of 2.5 $m_e c$. The intensity increases simultaneously by a factor 1.5-2. Directly after the FPAS the synchrotron signal has the same slope as just before the FPAS, continuing either to increase or decrease for the first 100 ms after the FPAS, as shown in Fig. 6.10. After these initial 100-200 ms a faster decay is seen. The e-folding time in this phase amounts to about $\tau_{dec} = 0.5$ s. The size of the spot does not increase further after the fast event.

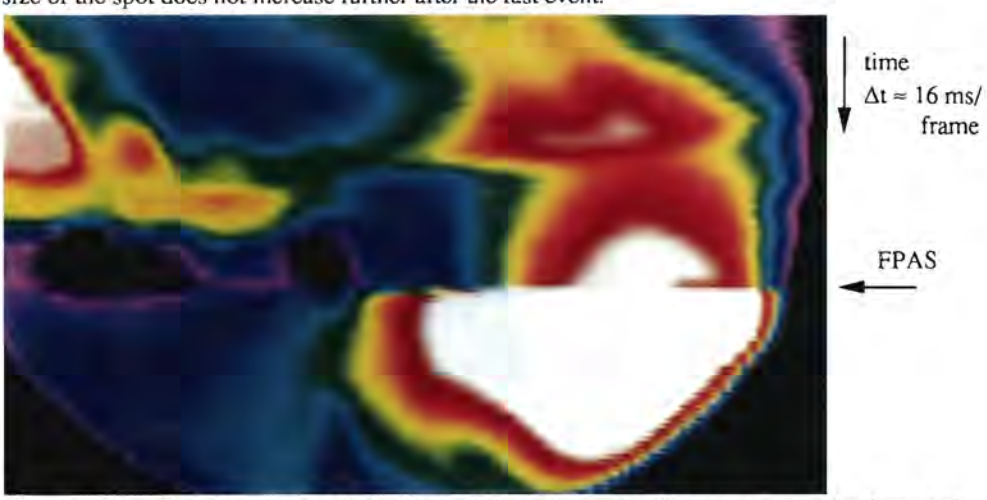

Figure 6.9: *One frame recorded with the infrared camera. The occurence of a fast pitch angle scattering process of the runaways is observed. The duration of this instability amounts to 2 line scans of the camera, corresponding to about 125 μs. After this fast event the spot of synchrotron is stable for the next few frames. The increase of the pitch angle is estimated from the horizontal increase of the spot and amounts to $\Delta\Theta$=0.05 rad. In this example the FPAS occurred in the runaway snake [Jas-94a]. For this runaway beam at q=1 the pitch angle scattering occurs as well in a similar manner.*

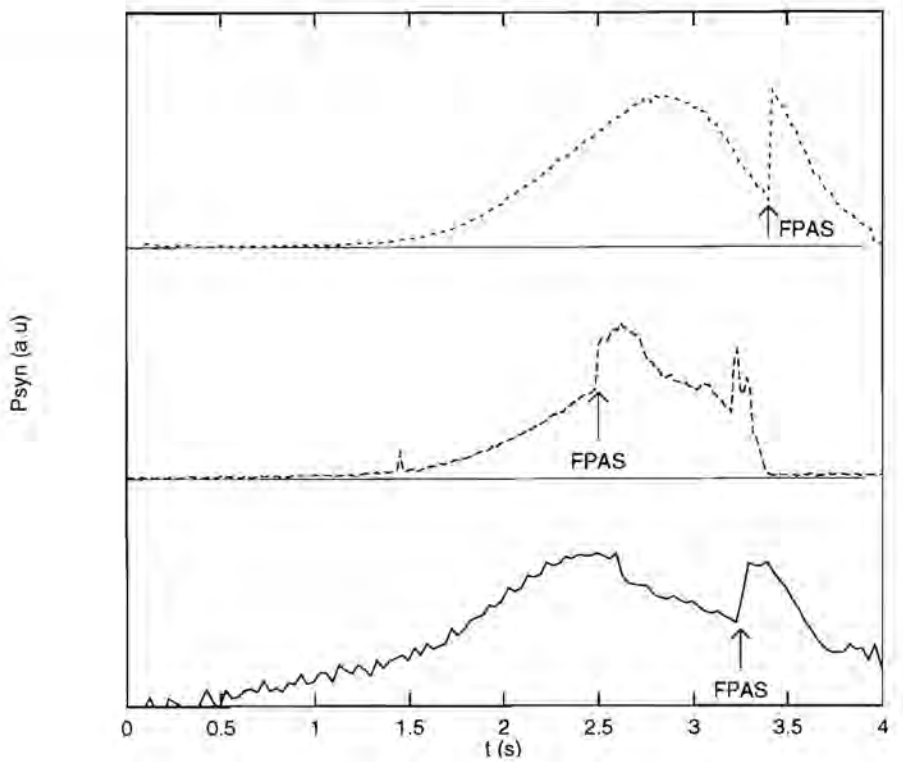

Figure 6.10: *Three time traces of the synchrotron radiation for ohmic discharges possesing a FPAS. This instant is indicated by the arrows. Note that in all three traces the slope of the signal is hardly affected for the first 100 ms after the FPAS. In the bottom trace at t=2.5 s a pellet is injected, which causes the sudden drop. From this discharge Fig. 6.9 is recorded.*

The increase in Θ is consistent with the increase in P_{syn}. For 25 MeV electrons one calculates from eq. (3.13) and (3.14):

$$\frac{P_{syn}(\Theta=0.17)}{P_{syn}(\Theta=0.12)} \approx 1.7 \qquad (6.27)$$

In fair agreement with the observed increase of a factor of 1.5-2. The decrease of the synchrotron signal is attributed to radiative deceleration. From the theoretical expression (3.13) the time constant of the change of P_{syn} due to deceleration can be calculated.

$$\tau_{rad} = \frac{P_{syn}}{dP_{syn}/dt} \approx \frac{20\times10^3}{W[MeV]^3} = 0.7 \text{ s} \qquad (6.28)$$

This compares well with the experimental value τ_{dec}=0.5 s. The initial 100-200 ms after the FPAS is not yet understood.

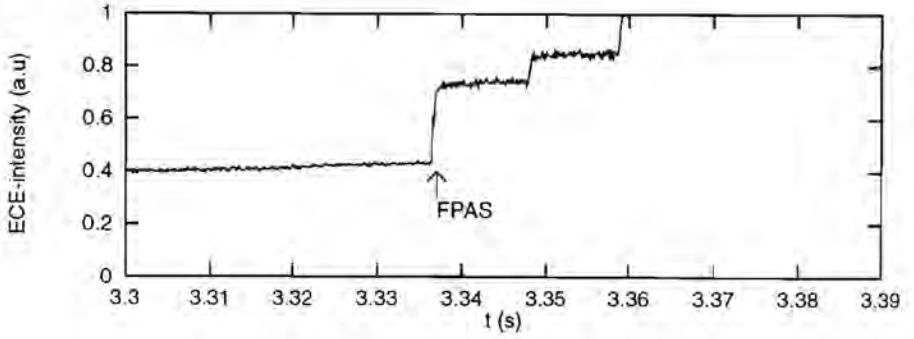

Figure 6.11: *Electron cyclotron emission for the discharge corresponding to figure 6.9. After three steps the detector went into saturation.*

b. Other Signals

Although a drastic change in the runaway emission is observed during the FPAS, this event does not seem to affect the bulk plasma. No indications of changes in density, loop voltage, confinement, impurity radiation etc. are found. Runaway related signals such as ECE, HXR- and Neutron signals do yield information about the FPAS event.

At the occurrence of the FPAS the ECE signal also shows features of a runaway instability. Only one ECE channel was available in most runaway discharges. Despite this limitation and the fact that in most cases the signal went into saturation after the FPAS two distinct observations were made. The one corresponding to Fig. 6.9 is shown in Fig. 6.11. A jump of the ECE signal coincides with the jump in synchrotron emission. Whereas the synchrotron signal decays thereafter, the ECE signal increases stepwise until it saturates. The period between the steps is 5-10 ms. In another example the FPAS coincided with a spike on the ECE signal and, even more remarkably, with the sawtooth crash. Unfortunately this is the only example in which sawteeth are observed during the FPAS process, so no definitive conclusions about the relation between FPAS and sawteeth could be drawn. Afterwards the ECE intensity shows a huge increase on a longer time scale (0.5 s) until the signal saturates.

For these low density discharges the plasma is optically thin and the ECE-signal is determined mainly by the cyclotron radiation of suprathermal electrons rather than the electron temperature of the thermal bulk. The stepwise increase of the ECE-signal at the FPAS agrees with the increase in perpendicular energy of the runaway electrons. Attention should be paid to the observation that the ECE-signal shows a multiple step process, whereas on the synchrotron signal only one such step is discovered. The huge increase in the ECE signal could indicate that the discharge went into the slide-away regime [Fus-78, Sch-94].

The Hard X-Ray (HXR) signal, measured tangentially to the plasma current, does not show the instability. Whereas in some cases no change at all is perceived in the signal, in other cases the signal decreases gradually after the FPAS, which could be attributed to a slow decrease of the energy of the runaway electrons. The fact that no burst of HXR is observed implies that no large loss of runaway electrons occurs during the FPAS event.

Neutrons are detected with two different diagnostics at TEXTOR. The liquid scintillator NE-213 [Hoe-94] detects the HXR and neutrons emitted in the tangential direction. A second neutron scintillator is positioned under the roof and detects radially emitted neutrons. Both signals show no change at all during the FPAS process. This implies that the number of high energetic runaway electrons in the plasma is unaffected, which is consistent with the HXR and synchrotron radiation signal.

The increase in perpendicular energy of the runaway beam is estimated from the number of runaways ($O(10^{14})$, [Jas-93a]) to be of the order of 10-100 J, too small to be recognized on diamagnetic measurements ($W_{dia} \approx 20$ kJ).

In summary, the ECE, HXR and N signals show that during the FPAS no loss of runaway electrons occurs. The energy of the runaway electrons after the FPAS is gradually decreasing. The steps observed in the ECE signal show that the discharge went into the slide-away regime at or after the FPAS.

c. Conditions in which FPAS occurs

To date FPAS has only been observed in the current decay phase, but it does not occur always and if it does, it is not at a unique value of I_p. As the current is decaying, the density decreases also, but no critical density value was found. It has never been tried to reach the slide-away regime in the current flat top phase. Normally the discharges were performed with a magnetic field of 2.25 T. For two discharges the magnetic field was increased to 2.5 T, and here the FPAS was also observed. If Neutral Beams were injected the FPAS was not observed. There is no evidence that the occurrence of FPAS depends on the number of runaways in the discharge as it happens at different intensities of synchrotron radiation. If the FPAS process is observed it is very reproducible for the next series of discharges, occurring at nearly the same time. However, in rather similar discharges, performed on other shot days the FPAS was not observed at all. It is hypothesized that this is related to the value of Z_{eff}, since Z_{eff} is the parameter that could differ most between otherwise very similar discharges. Finally it is noted that the FPAS has also been observed in the runaway snake, i.e. a thin, stable runaway beam at the q=1 drift surface (Sec. 5.4).

6.8 A Possible Mechanism for the Fast Pitch Angle Scattering

In this section we will try to come to a theoretical model which can describe the observations. Such a model should be able to explain the following:

- Θ increases by a factor of about 1.5;
- The time scale involved is $\Delta t \approx 100\ \mu s$;
- Occurrence in current decay phase;
- The FPAS is a single event on the synchrotron radiation;
- The ECE signal increases stepwise after the FPAS;
- The occurrence of the process is likely to depend on Z_{eff};
- The FPAS is reproducible;
- The bulk plasma is unaffected.

In this section we first test if the ripple resonance can explain the FPAS. As it will turn out that this fails to describe the data, the Parail Pogutse instability [Par-86] is discussed. Although this mechanism can account for the stepwise increase of the ECE signal, the single pitch angle scattering event of the relativistic runaway electrons cannot be understood by the Parail Pogutse instability alone. An additional process is invoked to explain the FPAS: A resonance between the cyclotron motion of the runaway electrons and the lower hybrid waves excited in the Parail Pogutse instability.

a. the ripple resonance

As discussed in Sec. 6.4 the interaction between the runaway cyclotron motion and the ripple of the magnetic field can drastically change the pitch angle of the runaway electrons. The FPAS is always observed in the current decay phase, when the runaway beam shifts to the low field side where the ripple is larger than in the centre of the plasma. It might be thought that as a consequence of this shift the ripple interaction becomes stronger and hence Θ is increased. For $r/a > 0.5$ even the third harmonic resonance is larger than D_{col}.

However, it is unlikely that the ripple resonance causes the FPAS since

a) the observed pitch angle diffusion coefficient is about one order of magnitude smaller than the estimate of eq. (6.22) (at r/a=0.5):

$$(D_{\Theta\Theta})_{exp} = \frac{(0.05)^2}{125\times10^{-6}} = 20\ \frac{rad^2}{s} \qquad (D_{\Theta\Theta})_{theor} = 200\ \frac{rad^2}{s}$$

b) no large orbit shift is observed which would account for the sudden increase of $D_{\Theta\Theta}$ and

c) the abrupt stop of the process is unexplained. To leave the resonance region for the second harmonic interaction, i.e. to radiate 2 MeV, about 35 ms are required, several orders longer than observed.

b. relation with slide-away regime and Parail-Pogutse instability

Interaction of runaway elecrons with plasma waves causes an increase in the perpendicular momentum if the runaway electrons are scattered on these waves by the anomalous Doppler interaction (see Sec. 2.6). A runaway instability in which this process occurs has been observed in many tokamaks in the slide-away regime [Ali-75, Oom-76, Fus-81, Sch-95]. This regime is characterized by an appreciable suprathermal electron population, low density, low loop voltage, improved ohmic confinement, bursts of emission around the lower hybrid frequency and the occurrence of the Parail-Pogutse instability (fan instability) [Par-86]. The slide-away state develops as follows: runaways are continuously accelerated in parallel direction resulting in a strong anisotropic velocity distribution. If the runaways reach an energy W_{beam}:

$$W_{beam} > 9\left(\frac{\omega_{ce}}{\omega_{pe}}\right)^3 W_{crit} \qquad (6.29)$$

Langmuir waves are excited. Electrons in the region W_{beam} are isotropized as a result of the anomalous Doppler resonance. Electrons at a lower energy will have a Cerenkov resonance with these waves. This creates a plateau in the distribution function, making a broad spectrum of waves unstable. This leads to an isotropization of the entire runaway region. After that, the growth of the waves ceases and they damp. In eq. (6.29) W_{crit} represents the critical energy where electrons become runaways, ω_{ce} is the electron cyclotron frequency and ω_{pe} the plasma frequency. This mechanism has a recurrent character, because after the isotropization the runaways are accelerated again until their parallel energy exceeds W_{beam} and the pitch angle scattering recurs.

The stepwise increase of ECE and the high suprathermal emission are characteristic for the slide-away regime, as also observed on other tokamaks [Cam-84, Sch-94]. This indicates the existence of a growing population of suprathermal electrons with large perpendicular energy. Moreover, since the transition into the slide-away regime depends critically on the electron density, this could be the reason why the steps in the ECE are observed in the density decay phase.

Although the ECE signal points in the direction of the Parail Pogutse instability, this process alone cannot account for the FPAS, since a) no recurrent pitch angle scattering is observed, b) the energy of the runaway electrons emitting the observed synchrotron radiation is a factor of 10 above W_{beam} and c) the Parail Pogutse theory predicts an isotropization of the

distribution function. Such a large increase in Θ for the high energy runaway electrons is not observed.

However, it should be noted that in the derivation of Parail and Pogutse no relativistic effects were included and a steady state velocity distribution was inserted. Both assumptions are questionable in the case of TEXTOR, because of the large number of relativistic electrons present in the discharge and the fact that in the current decay phase the distribution function can alter.

c. A New Mechanism: Lower Hybrid Resonance

As discussed before, the Parail and Pogutse mechanism is a two stage process. First if $W=W_{beam}$, Langmuir waves are excited. Second, a Cerenkov resonance of the electrons on these waves drives a broad spectrum of waves unstable. It has been measured in other tokamaks that this spectrum contains lower hybrid waves, peaked around the ion plasma frequency ω_{pi} [Oom-76, Sch-94]. Note that for low densities $\omega_{lh} \approx \omega_{pi}$, where ω_{lh} is the frequency of the lower hybrid waves. Anomalous Doppler resonance will pitch angle scatter the runaway electrons on the lower hybrid waves if the resonance criterion $\omega_k - n\,\omega_{ce} = k_z v_z$ is fulfilled, which for this case is conveniently rewritten as:

$$n\omega_{ce} - \omega_{lh} + \beta_{//} N_{//} \omega_{lh} = 0 \qquad (6.30)$$

Here, $N_{//}=k_{//}c$ is the parallel refractive index. If we substitute

$$\omega_{lh} \approx \omega_{pi} = \sqrt{\frac{n_i Z^2 e^2}{m_i \varepsilon_0}} = 1.3 \sqrt{\frac{Z_{eff} m_e}{A}}$$

where A is the atomic mass number, the energy of the resonant (n=-1) electrons is given by

$$W_{res}(\mathrm{MeV}) = 0.511 \frac{eB}{m_e} \frac{1}{N_{//}-1} \frac{1}{\omega_{lh}} \approx \frac{70}{(N_{//}-1)\sqrt{Z_{eff} n_e [10^{19} \mathrm{m}^{-3}]}} \qquad (6.31)$$

For typical TEXTOR parameters ($N_{//}=4$, $Z_{eff} = 2$, $n_e=0.5\times10^{19}\mathrm{m}^{-3}$) this yields $W_{res} \approx 23$ MeV, which is exactly the energy range of the observed runaway electrons.

As a possible scenario for the FPAS the following is hypothesized: in the current and density decay phase of the discharge the density becomes so low that the Parail Pogutse instability develops, which pitch angle scatters the lower energy electrons with $W=W_{beam}$. After this first stage a broadband spectrum of waves in the frequency range $[\omega_{pi},\omega_{pe}]$ are excited, peaking near ω_{pi}. Subsequently, the relativistic electrons pitch angle scatter via the

anomalous Doppler condition on the lower hybrid waves excited by the Parail Pogutse instability and this is thus a secondary effect.

This scenario is plausible concerning the time scale involved. For most tokamaks the Parail Pogutse instability is observed to be of the order of 100 μs [Par-86]. The change in perpendicular momentum of the resonant runaway electrons requires a perpendicular electric field of the wave of about

$$E_{\perp} = \frac{p_{//}}{e}\frac{d\Theta}{dt} \approx 40 \text{ V/m}. \qquad (6.32)$$

This is to be compared to the amplitude of the excited lower hybrid waves which can be calculated from the energy density of the waves $E = 0.5\,\varepsilon_0(E_{//}^2+E_{\perp}^2)$. Parail and Pogutse estimate that $(k_{//}/k)^2 \approx 1/3$, and for the energy density of the waves they found [Par-78]:

$$E \approx \frac{2}{3} n_e \sqrt{\frac{W_{beam}}{kT_e}}\, W_{beam} \left(\frac{W_{crit}}{W_{beam}}\right)^{3/2} \ln\left(\frac{W_{beam}}{W_{crit}}\right) \exp(-1/\varepsilon) \qquad (6.33)$$

where $\varepsilon = E/E_{crit}(Z_{eff}=1)$ as before. This expression depends critically on ε, so that an estimate of E is subject to a large uncertainty. Conversely, the measured pitch angle increase can be used to obtain an accurate estimate of the runaway production parameter ε. Inserting T_e=1 keV, $n_e=0.5\times10^{19}$ m^{-3} and E=0.06 V/m, we obtain ε =0.031, in agreement with eq. (2.4).

This mechanism thus comes to a consistent description of the time involved in the FPAS and the increase of the pitch angle of the runaway electrons. It is also immediately clear that the density of the high energy runaway electrons is not involved in the process, because the lower energy electrons excite the waves. The likely Z_{eff} dependence is included in this model since firstly the transition to the slide away regime occurs earlier for higher Z_{eff} and secondly W_{res} is lower at higher Z_{eff}. Not yet explained is the fact that on the synchrotron radiation only a single event is observed, whereas the ECE shows a repetitive instability. This could perhaps be related to the observation in the slide-away regime in other tokamaks that the Parail Pogutse instability is strongest at its first occurrence. For TEXTOR this is corroborated by the ECE signal of which the first step is the largest. The energy density of the excited waves in subsequent instabilities is apparently too small to increase the pitch angle noticeably. Another possibility is that the resonance conditions have changed. Since the density is decreasing W_{res} will increase. At the same time, runaway electrons are loosing energy by the enhanced radiation as a result of the FPAS.

6.9 Discussion

A temptative explanation of the FPAS process has been given. This involves a two stage process, starting with the excitation of lower hybrid waves via the Parail Pogutse instability, and the subsequent pitch angle scattering of the runaway electrons on these waves via the anomalous Doppler effect. Additional measurements are necessary to test this hypothesis. The measurements should at least involve RF-radiation measurements to look for lower hybrid waves. Variation of the parameter $\exp(-1/\varepsilon)$ is suggested to validate the relation between the increase in pitch angle and the energy density in the waves, as given in eqs. (6.32) and (6.33).

A similar resonance between the runaway motion and lower hybrid waves has been treated by Rax et al. [Rax-91]. They consider the case were the ω_{lh} waves are launched into the plasma under typical lower hybrid heating experimental conditions and therefore this mechanism does not rely on the occurrence of the Parail Pogutse instability. They found that two neighboring anomalous Doppler resonances under certain conditions will overlap, leading to a stochasticity in the runaway motion. This occurs if the Chirikov parameter S for this process is larger than one. They derive S to be:

$$S \approx \frac{4\,\gamma\, m_e \omega_{lh}\,(N_{//}-1)}{eB}\sqrt{\frac{\beta_\perp E_\perp}{2\,B\,c}} \qquad (6.34)$$

For the TEXTOR conditions in which the FPAS occurred we calculate $S=3\times10^{-4}$ and we conclude from this that overlap of the anomalous Doppler resonances does not occur.

Three more instability processes have been considered: a) the instability owing to a positive slope in the distribution function [Mik-74], b) the two stream instability [Mik-74,Tho-75,Bre-90] and c) the excitation of a parametric instability [Kaw-75, Pap-75,Che-84]. A positive slope could result from the accumulation of electrons around the radiation limit. A two stream instability is excited if one component of the plasma moves relative to the other one. Parametric instabilities were observed in heating experiments with relativistic electron beams (REB) [Bre-74,Tho-75,Sud-73]. Plasma heating is achieved by collective energy transfer from the electron beam to the plasma as a result of such parametric instability: the oscillating two stream instability. However, all three processes are considered unlikely explanations of the FPAS because they cannot account for i) the fact that the bulk plasma is unaffected, ii) the absence of the instability in more or less equal plasma conditions (only differing in Z_{eff}), iii) the fact that of the process steps before the cause of the instability has been removed, iv) the occurrence of the stepped increase of the ECE signal and the absence of an oscillating character of the synchrotron radiation and finally v) the observation that the FPAS is independent of the number of high energy electrons.

The next question to be addressed is if the FPAS is beneficial or dangerous for tokamak operation. Since the FPAS is not accompanied by HXR bursts, loss of energetic electrons from the plasma appears not to occur. Therefore damage of the vessel wall due to FPAS is not anticipated and no precautions to avoid the FPAS are required. Among the positive effects are the energy blocking: The pitch angle scattering increases the synchrotron radiation and thus lowers the radiative energy limit of the runaway electrons. If such FPAS can be triggered during a disruption the runaway damage in future devices can perhaps be restricted.

Finally it is remarked that this FPAS process could provide an explanation for the "unidentified red glows" observed in TdeV [Zuz-92]. The maximum energy that can be confined in TdeV is limited to 20 MeV due to the orbit shift. Ripple resonance will not occur below this energy. From the model of Sec. 6.2 we calculate an averaged Θ=0.1 rad for TdeV. With these values no radiation below 1 μm will be observed. Nevertheless such radiation is observed. Moreover, they measured Θ=0.5 rad. With this value synchrotron radiation below 1μm is detectable. An anomalous pitch angle of this size could be provided by the FPAS.

CHAPTER 7

RUNAWAYS AND DISRUPTIONS

7.1 Introduction

Plasma disruptions are a major concern for future tokamak operation because of their effects on wall components. A disruption is the sudden loss of the energy confinement of the plasma. This loss is thought to be the result of the turbulent destruction of the magnetic surfaces [Wes-89]. The concurrent temperature drop leads to a rapid decay of the plasma current. A short digression upon the effects will show the severe damage the disruptive instability can bring about:

i) The sudden loss of energy confinement during a disruption implies that the total plasma kinetic energy is dumped on the wall components in a short time. Heat loads as high as 10 MJ/m^2 within 0.1-1 ms are extrapolated for ITER from present day experiments [Whi-91]. Such energy fluxes will locally evaporate 1 cm of first wall material in about 100 disruptions, equivalent to several tens of kg per disruption. Moreover these power fluxes result in damage of the wall components by cracking, melting and fracture;

ii) The fast variation in plasma position induces electric fields which produce currents crossing from plasma to wall components. These lead to enormous jxB forces. For ITER-like machines forces on the vacuum vessel structure of up to 10 MN are anticipated [Mer-87]. Forces of similar strength on the vacuum vessel result from the sudden loss of the plasma pressure and the current decay, both producing a rearrangement of the toroidal magnetic field and inducing a current in the vacuum vessel [Wes-89];

iii) Finally, the increased electric field favors the production and acceleration of runaway electrons. Runaway currents as high as 10 MA and energies of 50-500 MeV are predicted for ITER. The runaway danger is twofold. Firstly, the total energy in this runaway beam may exceed 100 MJ, which can be deposited very locally as a result of the outward drift or a position instability. Secondly, as a result of the high energy, the runaways can penetrate the first wall (a rough estimate of the electron range (S) in carbon yields S=0.25 cm/MeV) and deposit their energy in the metal coolant channels of the plasma facing components. These might be damaged by melting with the possible consequence of coolant leakage into the vacuum vessel [Bol-90].

The lifetime of a fusion reactor will be limited to only a few disruptions if the above prognoses come true. Even for present day tokamaks major disruptions have led to destruction of wall

components [Tak-89, Die-88]. For this reason much effort is put in studies to understand, control and avoid disruptions.

This chapter focusses on the generation, acceleration and loss of runaway electrons during a disruption. Experimental data is scarce for present day tokamaks. The principal reason for this is the fact that runaway electrons are only indirectly observed, by HXR radiation [Gil-93], Neutron radiation [Jar-88], activation or damage of wall material [Bar-81,Jar-88] or the observation of a current plateau [Wes-89]. The interpretation of these data and extrapolations to a burning fusion reactor are in certain respects conflicting: -estimates of the runaway energy in ITER vary between 50 and 500 MeV [Rus-93,Bol-90]; -Russo and Campbell predict the runaway generation to occur predominantly at the edge of the plasma [Rus-93], whereas other studies assume central creation [Fle-93]; -a runaway current of up to 50% of the plasma current has been measured at JET [Wes-89,Gil-93], whereas at DIII-D hardly any evidence of a runaway current is found [Rus-93]; -the loss of these runaway electrons has been observed to occur suddenly or smoothly [Gil-93].

The use of the synchrotron radiation diagnostic as applied on TEXTOR can contribute substantially to the measurements and understanding of runaway electrons during disruptions as this is the only technique to observe the runaway electrons directly. As shown in previous chapters, the energy, number and position of the runaway beam can be determined accurately, allowing more reliable extrapolations towards ITER.

We start with a description of the generally accepted model for the evolution of a disruption in section 7.2. This provides the framework necessary for the understanding of the sequence of events. The runaway generation and acceleration phase is identified. An example of the observation of synchrotron radiation of 20 MeV runaway electrons which are generated during a major plasma disruption in TEXTOR is presented in section 7.3 and discussed in section 7.4. Implications for future fusion machines like ITER are addressed in Sec. 7.5.

7.2 Description of a Major Disruption

Several classes of disruptions are distinguished, such as disruptions due to high density, due to low q_a, induced by a fast current rise, due to a vertical instability etc. Whereas the features in the pre-disruptive phase depend on the kind of disruption, the major disruption itself has a similar character for all classes. Often a precursor phase of the disruption is observed with an onset of MHD activity, mainly m=2 and m=1 modes. It is assumed in most disruption models that the thermal quench starts when these modes grow and interact with each other, causing stochasticity of the magnetic field structure. In this ergodic configuration a large part of the plasma energy is lost suddenly. As this energy is dumped on the first wall, impurities are released. Due to the enhanced radiation the plasma temperature will then drop even further to values of only a few eV. During this period a redistribution of the current in the plasma takes

place, which flattens the profile and hence reduces the plasma internal inductance (l_i). The reduction of l_i is accompanied by a slight increase in I_p, since on short time scales the magnetic energy $W_{mag} = 1/2\ LI_p^2$ is constant (L being the effective plasma inductance). In most cases a negative voltage spike is observed at this time due to this expulsion of poloidal flux.

Whereas the thermal quench occurs on a time scale of 0.1-1 ms depending on the size of the machine, the subsequent current decay phase can last one or two orders of magnitude longer. The current decays because the plasma resistivity (η) is dramatically increased as a result of the temperature drop. This drop leads to an enormous increase in the parallel electric field $E_{//}$, given by $E_{//} = \eta\ j$ where j denotes the current density. As the total plasma current falls the poloidal field decays and inductively sustains a high $E_{//}$. This high $E_{//}$ leads to runaway electron production and acceleration. The runaway current generated during this time can carry an important part of the plasma current, thereby reducing the effective resistivity. The magnetic surfaces that are broken up in the thermal quench phase are expected to be restored during the current decay since the plasma still exists after the thermal quench. The loss of runaway electrons is therefore assumed negligible in the current decay phase. When the runaways cannot be confined adequately due to instabilities or loss of position control, they are dumped on the vessel wall or limiter. This is the moment when the destructive runaway damage occurs [Gil-93]. Even if they can be confined long enough to become relativistic, the runaway electrons will deposit their energy most probably on a limited region when they are eventually lost due to the increasing orbit shift, and hot spots will result. Only if the runaways are stably confined at small minor radius, a smooth and slow decay of the plasma current occurs and no serious damage to plasma facing components is expected [Gil-93]. A possible way to avoid runaway generation is according to Russo and Harris [Rus-93, Har-90] to choose a wall material with a low radiation efficiency like beryllium. The temperature of the post disruptive plasma will then drop to O(100 eV) instead of a few eV's. In that situation the resistivity and hence $E_{//}$ will not reach such high values as in the low temperature case, so that the runaway generation will be suppressed.

7.3 Measurements of Infrared Radiation during Disruptions

Under normal circumstances the IR camera views the plasma and liner tangentially. In principle data can be obtained from at least three different events accompanying a major disruption: i) the heat bursts arriving at the limiter during the thermal quench phase of the disruption, ii) loss of runaway electrons that existed already in the pre-disruptive phase, and iii) generation of runaway electrons during the disruption.

-heat bursts

During a disruption in TEXTOR a sequence of rapid increases of the surface temperature of the ALT-II limiter blades can be observed [Fin-92,Jas-94b]. In the infrared pictures this is recognized by a rise of the temperature from one scanning line to the next (Fig.7.1), i.e. within 65 μs. This behaviour is clearly different from the images observed during normal (non-disruptive) heating of the blades, where the heat pattern is smoothly distributed on the ALT-limiter and the temperature increases gradually during the discharge. The heat bursts are believed to be caused by rotating islands of low mode numbers, which touch the limiter blades. These bursts of heat deposition on the limiter blades have durations of less than 0.1 ms. Several bursts occur during the thermal quench and some are found in the current decay phase as well. Power flux densities of the order of 50 MW/m^2 have been recorded. Impurity release is observed when a heat burst hits the limiter, consistent with the picture given in the previous section. These observations allow to estimate the temperature rise of plasma facing components during the thermal quench phase of ITER, but this is outside the scope of this thesis.

-pre-disruption generated runaways

During the thermal quench it is expected that the magnetic field is subject to ergodization, caused by the overlap of several low m magnetic islands. Runaway electrons could be lost rapidly in this phase of the disruption. In fact the situation is somewhat similar to the short period of ergodization during pellet injection (Sec. 5.4), except that in the major disruption the ergodization is even more developed. As a consequence the loss rate of runaway electrons similar to or larger than with pellet injection is anticipated. Synchrotron radiation measurements with the infrared camera are a useful tool to provide information about runaway loss, and can possibly yield information about precursor events as well. In order to use the synchrotron radiation during a high density disruption the following scenario is envisaged. Initially the discharge is kept at a low density to generate a sufficient amount of runaway electron. Once the synchrotron radiation is observable, the density limit can be reached by puffing deuterium. Since runaway electrons are not lost if the density is increased (Sec. 4.4) their behaviour in the pre-disruptive phase, full of MHD activity, and in the thermal quench can be studied. Unfortunately no such experiments of runaway discharges which disrupted have been carried out at TEXTOR to date. Experiments concentrating on this possibility are foreseen for TEXTOR-94.

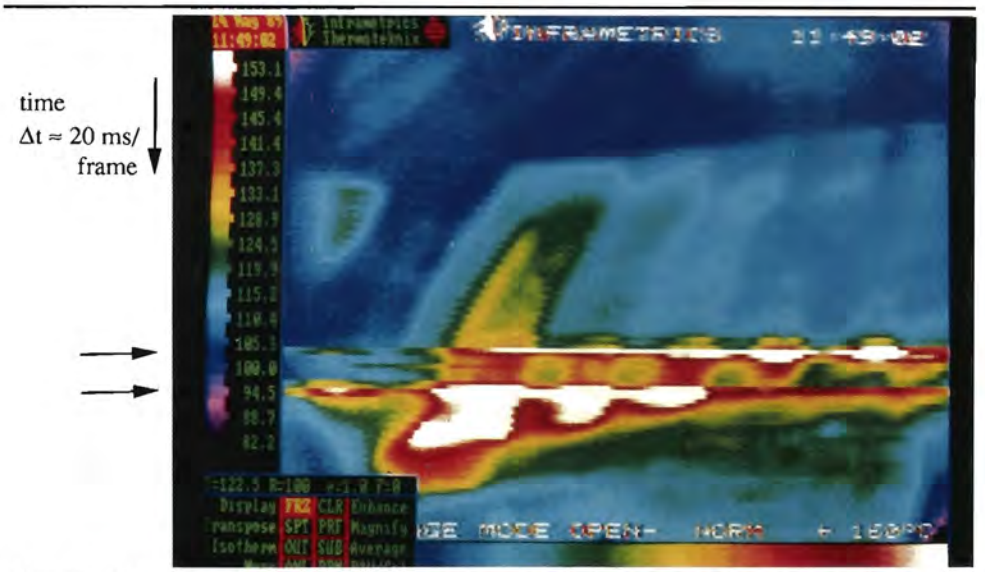

Figure 7.1: *Example of heat pulses hitting the ALT-II limiter in the thermal quench phase of the disruption. Note that time is increasing from top to bottom. A heat burst is marked by an abrupt change in the surface temperature. The arrows indicate the heat pulses. Each major thermal quench can consist of a series of bursts.*

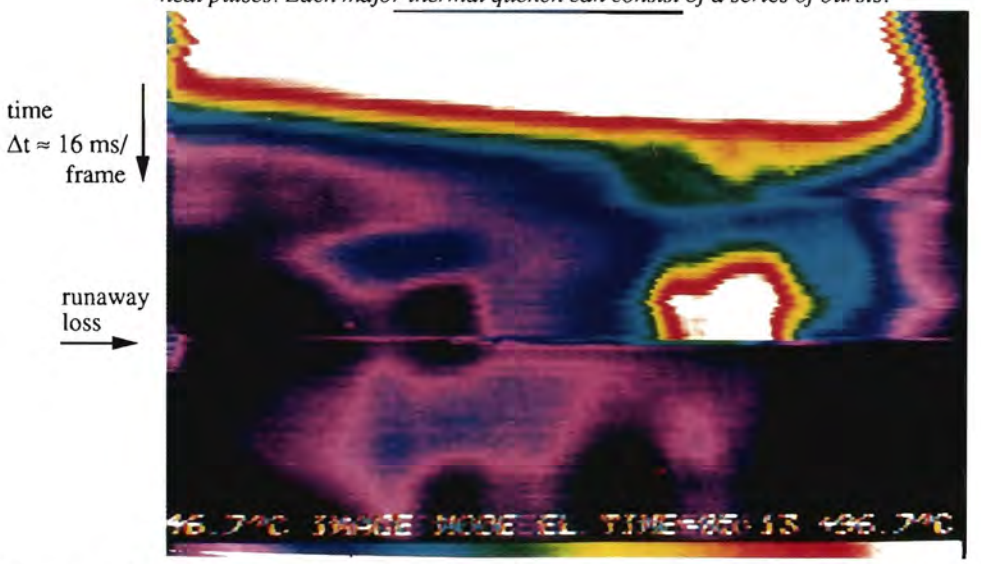

Figure 7.2: *Observation of synchrotron radiation during a disruption. The viewed area is sketched in Fig. 1.4 (small box). Due to the optical system this picture is top-bottom and left-right reversed. Time is increasing from top to bottom. At the top of the picture the ALT-II limiter blade is clearly recognized. Here the picture is overexposed, due to the high temperature of the limiter after the thermal quench of the plasma. This quench occurred about 2 ms before this frame was recorded. The bright spot in the center of the picture is the synchrotron radiation from relativistic runaway electrons. This spot is visible for about 3 ms and is then abruptly lost within 100 μs.*

-disruption generated runaway electrons

Synchrotron radiation of disruption generated runaway electrons is normally not observed in TEXTOR. Under normal operating circumstances, it cannot be detected because the infrared camera is looking in the direction of ion approach. For the few disruptions in which the camera looked in the direction of electron approach no synchrotron radiation was recorded, probably because the energy or the number of runaway electrons was too low to be observed. There is one exception, which will be discussed now.

This discharge exhibited no synchrotron radiation in the stable phase. Application of a huge gaspuff resulted in a disruption. Here, for the first time synchrotron radiation of disruption generated runaway electrons was detected. The infrared picture is shown in Fig. 7.2. In this picture the ALT-II limiter blade, a section of the ICRH antenna, some diagnostic ports and the spot of synchrotron radiation are recognized. The thermal quench starts 2 ms before this picture is recorded. Heat bursts on the limiter are observed, simultaneously with bursts of SXR, indicative of the influx of impurities (Fig. 7.3). In this picture the limiter is overexposed, probably as a result of the thermal energy deposited on it.

On the infrared picture a bright spot of synchrotron radiation becomes visible about 6 ms after the thermal quench. It remains visible for approximately 3 ms and is then lost within ≈ 100 μs. The plasma current drops from 81 kA to 63 kA in this loss phase and a burst of SXR is observed. The conclusion that the infrared spot is synchrotron radiation from relativistic runaway electrons is drawn from the following observations:

- The position of the spot coincides with the central part of the plasma.
- At this position no plasma facing component of this shape is present.
- Thermal radiation cannot decay on such short time-scale.
- After the disappearance of the spot the total current drops. This drop is attributed to the loss of the runaway current.
- The ECE-trace (Fig. 7.3) has a similar shape as the synchrotron radiation and disappears simultaneously with the loss of synchrotron radiation. Under these conditions the ECE signal is dominated by downshifted suprathermal radiation.

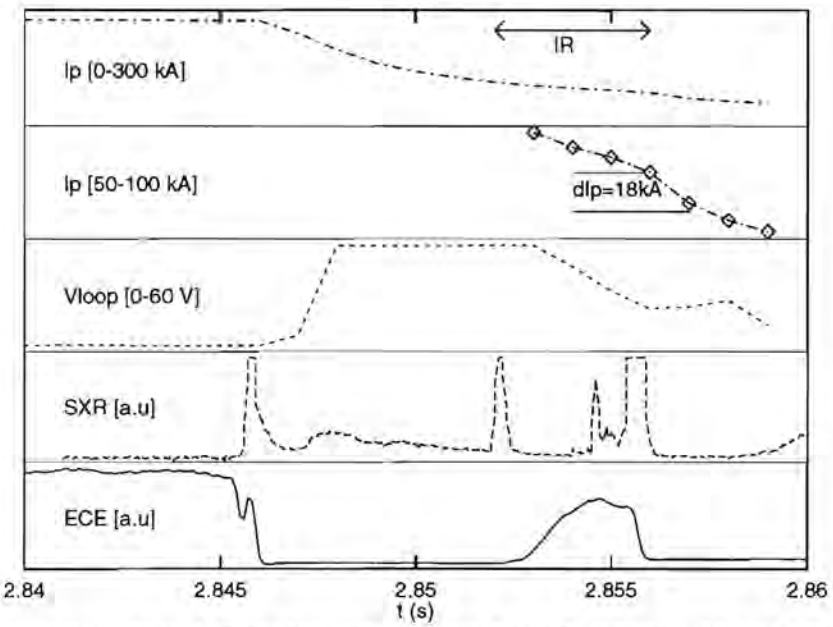

Figure 7.3: *Time evolution of several plasma parameters during the disruption belonging to Fig. 7.2. From top to bottom: The plasma current, with expanded scale in the second plot. Note the drop of about 18 kA at the time the runaways are lost. Next, the loop voltage, the soft X-ray radiation, and electron cyclotron emission (ECE). The period when synchrotron radiation is observed is indicated.*

It might be argued that the radiation originates from pre-disruptive runaway electrons. However, this is very unlikely because before the disruption no synchrotron radiation was observed. This does not exclude the possibility that there were runaway electrons present at lower energy, but there is no reason for that. Moreover, if they were present they would probably be lost in the stochastic phase of the thermal quench. We neglect the theoretical possibility that a few runaway electrons survive the stochastic phase by hiding in a big m=1 island, as was observed with pellet injection (Sec. 5.4). Thus we conclude that the spot of radiation originates from runaway electrons generated during the disruption.

7.4 Runaway Electron Parameters

Accepting the interpretation that the observed radiation originates from a runaway beam, the current, pitch angle and energy of the runaways can be estimated. The number of runaway electrons N_r can be estimated by equating the drop of I_p, ΔI_p =18 kA, to the runaway current I_r:

$$N_r = \frac{2\pi R_0 I_r}{ec} = 4 \times 10^{15} \qquad (7.1)$$

The spot size is determined by the radius of the runaway beam and the pitch angle. Since a nearly circular spot is observed, the horizontal extent allows to estimate r_{beam}, whereas from the vertical extent Θ can be determined, resulting in:

$$r_{beam} = 0.06 \pm 0.01 \text{ m} \tag{7.2}$$

and

$$\Theta = 24 \pm 4 \text{ mrad} \tag{7.3}$$

With the values of N_r, Θ and r_{beam} the energy of the runaway electrons follows from the intensity of the synchrotron power. The result depends on the energy distribution assumed, but it turns out that for a flat and mono-energetic distribution the result does not differ much: W_{max}=23 MeV and W_{max} =19 MeV, respectively. Therefore we take:

$$W_{max} \approx 20 \text{ MeV} \tag{7.4}$$

On the basis of these numbers we will now discuss the runaway production, the energy in the runaway beam, the pitch angle scattering, and the loss mechanism of the runaway electrons.

Runaway Production

To elucidate the runaway production mechanism we will calculate the production rate from N_r and compare this with several theoretical estimates. Before doing this it is first checked of N_r has a reasonable value. The maximum number ($N_{r,max}$) of runaway electrons that can be produced in the centre of the plasma after the disruption is calculated by the assumption that the plasma current density before the disruption in the centre (j_0) is replaced by the runaway current density $j_r = I_r/\pi r_{beam}^2$. To check whether N_r does not exceed $N_{r,max}$ we calculate j_0 from the profile $j(r)=j_0 (1+q_a r^2/a^2)^{-2}$ [Sch-91] and obtain for $N_{r,max}$:

$$N_{r,max} = \frac{2\pi R_0 r_{beam}^2 (q_a+1) I_p}{eca^2} = 6\times10^{15} \tag{7.5}$$

where I_p is the plasma current just before the thermal quench. Since $N_r \approx N_{r,max}$ it is likely that the runaway current has replaced most of the ohmic current in the center and that locally the electric field has become very low. This is consistent with the fact the runaway electrons are

not further accelerated as evidenced by the observation that the intensity of the synchrotron radiation spot does not increase in time.

The production rate (λ) of the runaway electrons is calculated from:

$$\begin{aligned} N_r &= 2\pi^2 R_0 r_{beam}^2 \int \lambda(t)\, n_e\, \nu_{coll}\, dt \\ &\approx 2\times10^{27}\, Z_{eff}\, n_e[10^{19}m^{-3}]^2\, T_e[eV]^{-3/2}\, \lambda\, \Delta t_{prod} \end{aligned} \qquad (7.6)$$

where ν_{coll} is the collision frequency for electrons at the thermal velocity and Δt_{prod} is the time duration of the main runaway production. An estimate of Δt_{prod} is provided by the assumption that once the runaway electrons become relativistic ($\Delta W \approx 1$MeV) they carry a nearly superconducting current, and the electric field and hence the runaway production will drop:

$$\Delta t_{prod} = \frac{\Delta W}{ecE} = \frac{\Delta W}{ecE_b}\left(\frac{T_e}{T_{eb}}\right)^{3/2}\left(\frac{Z_{eff,b}}{Z_{eff}}\right) \qquad (7.7)$$

Here the index b refers to the parameters before the disruption. Inserting this in eq. (7.6) the production rate λ follows from:

$$\lambda = 1.5\times10^{-25}\, \frac{N_r\, E_b\, T_{eb}^{3/2}}{Z_{eff,b}\, n_e^2} \approx 3\times10^{-8} \qquad (7.8)$$

with n_e in $10^{19}m^{-3}$ and T_e in eV. The density after the disruption is not known accurately, but since the disruption resulted from the influx of a large amount of gas we took $n_e=5\times10^{19}m^{-3}$. Further $Z_{eff,b} = 2$ is inserted.

We will now discuss which generation mechanism is responsible for the runaway production.

i) The Dreicer evaporation process (primary generation). Runaway generation according to this process depends exponentially on ε :

$$\varepsilon = E/E_{crit} \approx \frac{ET_e}{4.6n_e} = 4\times10^{-9}\, \frac{Z_{eff}\, j_b}{n_e\sqrt{T_e}} \qquad (7.9)$$

With n_e in 10^{19} m^{-3}, T_e in keV and j_b the current density before the disruption. Hence, the production rate is, counter intuitively, enhanced for low T_e. It is assumed that for the short times under consideration the current density will not change. Small changes in ε will change λ by orders of magnitude (see eq. 4.6), so the Dreicer process will be strongly reduced if n_e or T_e increases only slightly, or if the runaway current becomes appreciable, reducing the electric field. However, since we have already an estimate of

$\lambda=3\times10^{-8}$ an accurate determination for ε can be obtained. This yields $\varepsilon = 0.035$. So, even if the uncertainty in λ is large, the error in ε is small due to the steep dependence of λ on ε. This allows to estimate the electron temperature after the thermal quench:

$$T_e = \left(\frac{4\times10^{-9} Z_{eff}\, j_b}{n_e\, \varepsilon}\right)^2 \approx 28\ \text{eV} \tag{7.10}$$

This can be compared to an estimate of T_e based on the decay time of the current (τ_{cur}) from η:

$$\tau_{cur} \approx \frac{\mu_0 a^2}{4\eta} = 6.3\times10^{-3}\,\frac{a^2 T_e[\text{eV}]^{3/2}}{Z_{eff}\ln\Lambda} \tag{7.11}$$

This yields with τ_{cur} =4.5 ms, Z_{eff}=3 and $\ln\Lambda$=12,

$$T_e = 25\ \text{eV} \tag{7.12}$$

The consistency of these results show that an interpretation of the runaway production based on primary generation is reasonable. Nevertheless, other runaway generation mechanisms will also be considered.

ii) Collisional avalanching (secondary generation). In section 4.3 it was shown that an exponential increase of the runaway birth rate could follow from the process in which a runaway electron is generated in a close collision between an already existing runaway electron and a thermal electron. The effective time in which one new runaway is formed is approximated by:

$$t_0 = \frac{(2+Z_{eff}) m_e c \ln\Lambda}{eE} \approx 4\ \text{ms} \tag{7.13}$$

Here E=30V/m has been inserted, calculated from $E=\eta\, j_b$. This t_0 is nearly as long as the total duration of the current decay. This, together with the fact that the electric field will decay and hence t_0 will rapidly increase if runaway production occurs, leads to the conclusion that the secondary generation process will not dominate the runaway production. As an upper limit we estimated that the secondary generation does not enhance the runaway production by more than a factor of 2.

iii) Other runaway generation mechanisms exist in literature, but these are not considered, since no experimental evidence has been found to support them. For instance, the de-trapping of trapped high temperature electrons [Fle-93] is not consistent with the

observation of a central runaway beam, because most trapped electrons are located on the low field side of the plasma.

Energy of the Runaway Beam

For the maximum energy of the runaway electrons we found $W_{max} \approx 20$ MeV. The main contribution to the energy gain of the runaway electrons comes from the decaying poloidal field, via inductively generated $E_{//}$. The maximum energy therefore amounts approximately to:

$$\delta W_{ind} = ec \int E_{//} dt \approx \frac{ec}{2\pi R_0} L\, \delta I_p \qquad (7.14)$$

Here L is the total inductance and $\delta I_p = \int \dot{I}\, dt$. This L consists of three contributions:

i) the normalized *flux* inductance h_i of the plasma column. Note that h_i differs from the normalized *energy* self inductance (l_i) since:

$$h_i = \frac{2}{a^2 B_\theta(a)} \int B_\theta(r) r dr \quad \text{and} \quad l_i = \frac{2}{a^2 B_\theta^2(a)} \int B_\theta^2(r) r dr.$$

ii) the inductance of the flux between the plasma column and the vacuum vessel;

iii) the external contribution from the flux outside the vacuum vessel. On a short time scale the conducting vacuum vessel will shield the discharge and the last term will only partially contribute.

The inductance can therefore be written as:

$$L = \mu_0 R_0 \left(h_i + \ln\left(\frac{r_{ves}}{a}\right) + \exp(-\tau_w/\tau_{dis}) \left[\ln\left(\frac{8R_0}{r_{ves}}\right) - 2 \right] \right) \qquad (7.15)$$

For TEXTOR the vessel minor radius $r_{ves} = 0.55$ cm and the L/R time of the wall $\tau_w = 3$ ms [Wai-92]. For the disruption under consideration we have, at the time the runaway beam is observed: $\delta I_p = 165$ kA and $\tau_{dis} = 6$ ms. Inserting $h_i = 1.2$, which corresponds to a peaked current density profile as used in eq. (7.5), the runaway energy amounts to:

$$W_{ind} = 21 \text{ MeV} \qquad (7.16)$$

Comparing this result with eq. (7.4) we conclude that the two independent estimates of the runaway energy W_{max} are fully consistent.

The energy content W_{beam} in the runaway population is estimated from the above calculated values. The fraction of total magnetic energy that is converted into the energetic runaway electrons is:

$$\frac{W_{beam}}{W_{mag}} \approx \frac{N_r W_{max}}{1/2L(I_p^2 - (I_p - \delta I_p)^2)} = \frac{13\ kJ}{120\ kJ} = 0.11 \qquad (7.17)$$

Note that L is now calculated with h_i in eq. (7.15) replaced by $l_i/2 \approx 0.7$, since for calculating the magnetic energy the energy self inductance of the plasma should be used. The 13 kJ of runaway energy is dumped within 100 μs on plasma facing components, at which time a rise of the ALT-limiter temperature is registered.

Pitch angle

From the IR spot we found Θ =24 mrad. We try to check the consistency of the value obtained for Θ with the model developed in chapter 6. A detailed treatment would involve a time dependent electric field in the calculations. As this is not available from experimental data, a constant E-field was taken. The magnitude was chosen such as to be able to accelerate runaway electrons to 20 MeV within 6 ms, i.e. E=10 V/m (other time dependent E fields did not change the results for Θ provided that $ec\int Edt$=20 MeV). The pitch angle distribution after 6 ms had a width of $\Delta\Theta$ = 25 mrad in agreement with experimental value of Θ= 24 mrad. The consistency of the results validates the use of the model. The dominant process responsible for the pitch angle of the runaway electrons are collisions with plasma ions and electrons. Radiation losses are negligible and second or third harmonic ripple interaction does not occur at an energy of 20 MeV or lower.

Radius of runaway beam

The spot of synchrotron radiation shows that the runaway electrons are created in the plasma centre in a region with radius r_{beam}=0.06 cm. After the thermal quench the temperature and density profiles are expected to be more or less flat. The radial distribution of the runaway production is therefore related to the profile of E, which shortly after the thermal quench will be the same as the current density profile before the quench. For the peaked current density profile used ealier, we calculate the HWHM of the production region to be r=0.04 m, in fair agreement with r_{beam}.

Loss of runaway electrons

The runaway beam is suddenly lost within 100 μs. This is too fast to say anything about the change in size and position of the observed runaway beam. Three options are investigated to see whether the 20 MeV runaway electrons are lost because they cannot be confined under the present conditions:

i) loss because the orbit shift is larger than the minor radius a;

ii) loss because a separatrix in the runaway orbit will occur;

iii) loss because the vertical magnetic field is too small.

In the case of a flat current distribution, the maximum runaway energy that can be confined by the poloidal magnetic field is given by (see eq. 2.19):

$$W_{max} = \frac{ec\mu_0}{2\pi}\frac{R\ I_p}{a} = 18\ \text{MeV} \qquad (7.18)$$

Here we substituted $I_p = 81$ kA at the moment of the runaway loss. For peaked current distributions this maximum energy is higher. The fact that no large shift of the runaway electrons is observed indicates that a) the current profile must be peaked, and b) the orbit shift cannot account for the sudden loss.

In chapter 2 we found that in stationary TEXTOR discharges the occurrence of a drift separatrix in a runaway orbit is unlikely. Since the plasma parameters change drastically in a disruption, this point has to be considered under the present conditions. Fig. 7.4 shows the maximum confined runaway energy as a function of radius for a flat and for peaked current distributions, as calculated from eq. (2.15). This figure shows that in case of a peaked profile it is possible that a separatrix will occur for runaway electrons of about 20 MeV. The separatrix is expected to appear at r=0.30 cm. The observation of the runaway beam near the geometrical centre is not completely understood in this picture, but can possibly be related to the inward shift of the plasma column. The feedback circuit of the stabilizing vertical field is too slow to follow the fast current decay, which shifts the plasma to the high field side.

In the discussion of the runaway confinement we have up to now neglected the influence of the vertical magnetic field (B_z) because this is generally smaller than B_θ. In a disruption this situation can alter, since the plasma current and hence B_θ decay, whereas B_z will initially stay at its pre-disruptive value, which is given by:

$$B_z = \frac{\mu_0 I_p}{4\pi R_0}\left(\ln\frac{8R_0}{a} + \beta_p + \frac{l_i}{2} - \frac{3}{2}\right) \approx 0.04\ \text{T} \qquad (7.19)$$

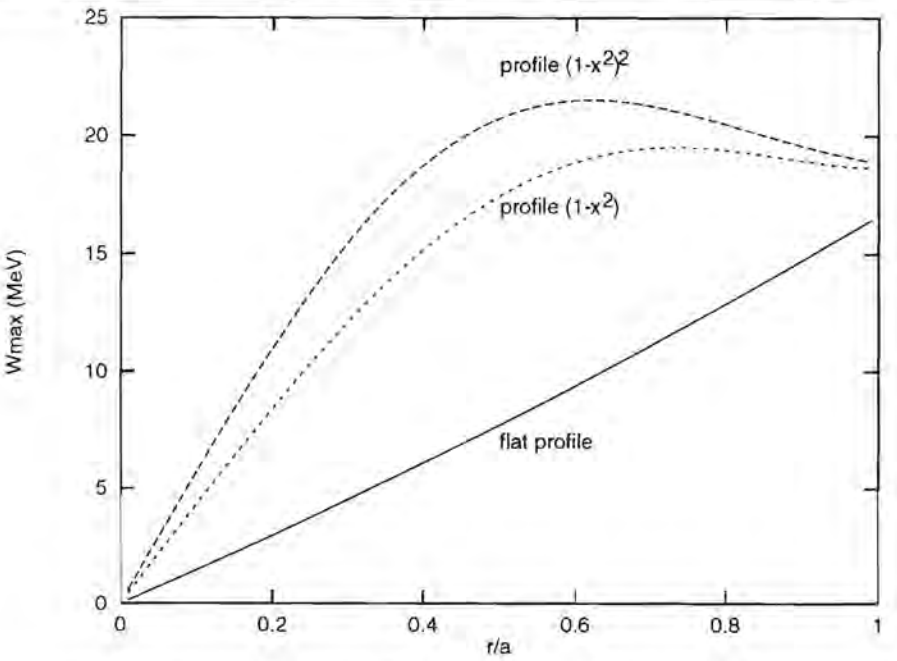

Figure 7.4: *The calculated maximum confined runaway energy in TEXTOR as a function of radius at the moment the runaway electrons are lost for different current density profiles. For a peaked profile $j(r)=j_0(1-(r/a)^2)^2$ a separatrix in the drift orbit will appear for electrons with $W_{max} > 22$ MeV at $r \approx 0.3$ m. In case of an uniform profile $W_{max} = 20$ MeV for r=a.*

The Lorentz force exerted on an electron by this field, can confine it in a circular orbit up to an energy W_{bz} of:

$$W_{bz} = ecR_0B_z = 21 \text{ MeV} \tag{7.20}$$

This shows that the vertical field plays an essential role in the runaway confinement. However, the sudden loss of runaway electrons by a decaying B_z field is questionable, since one would expect that the orbit radius of the electrons would increase for lower B_z, which is not seen.

In conclusion one has to say that up to now no satisfactory explanation for the sudden loss of runaways can be given. The occurrence of an instability causing the loss of runaway electrons is another option, not investigated yet.

Summary

The synchrotron radiation observed in a disruption at TEXTOR delivers useful information about the runaway electrons and allows to determine the parameters W, Θ, r_{beam} and N_r. An interpretation based on primary generation in which the runaway electrons take over the plasma current in the centre gives a consistent picture. Several other quantities can be deduced indirectly from the runaway parameters. In Table 7.1 these parameters are listed, the deduced values are given and a short comment on the determination and the interpretation is given. The final loss of the runaway electrons is still unexplained. The occurrence of a separatrix in the drift orbit of the runaway electrons or the decay of the vertical magnetic field are two possible causes for runaway loss, but as no shift of the runaway beam is observed they cannot account for the sudden loss.

Table 7.1 *Parameters of a TEXTOR disruption*

Runaway Parameter	Result		Determination	Interpretation
W_{max}	20	MeV	from P_{syn}	induced voltage
Θ	24	mrad	from spotsize	collisions
N_r	4×10^{15}		from ΔI_p	primary generation
r_{beam}	0.06	m	from spotsize	width generation region
Deduced Parameter			Used Parameters	
λ	3×10^{-8}		N_r, n_e*, Z_{eff}*	primary generation
h_i	1.2		W_{max}, I_p, τ_w*	peaked profile
ε	0.035		λ,n_e*	
T_e	28	eV	ε	
W_{beam}/W_{mag}	0.11		N_r, W_{max}	

* indicates assumed values: $n_e = 5\times10^{19}m^{-3}$, $Z_{eff}=3$, $\tau_w = 3$ ms;

7.5 Implications for ITER

To predict the damage of runaway electrons following a disruption for ITER an estimate of the runaway energy, current and loss mechanism is a prerequisite. Extrapolation of these parameters from the present experiment to ITER requires a reliable estimate of the runaway production rate in the thermal quench phase. This depends exponentially on ε, i.e. on T_e, n_e and $E_{//}$. Already small changes in ε will alter the results considerably. We therefore discuss in this sections the prediction of W_{max} and I_r as a function of the parameter ε. A crude estimate of ε for an ITER disruption gives:

$$\varepsilon = \frac{E\, T_e[\mathrm{keV}]}{4\, n_e[10^{19}\mathrm{m}^{-3}]} \approx \frac{200 \times 0.02}{4 \times 10} = 0.10 \qquad (7.21)$$

We apply a simple model to ITER which is able to describe the observations in TEXTOR. The model is based on the results found for TEXTOR that a) the runaway generation is predominantly governed by primary generation, b) the electric field will be reduced by the runaway current until the runaway current has replaced the ohmic plasma current and $E_{//}$=0, c) the decay of I_p is obtained from the value of the electric field and finally d) the runaway energy is calculated from the acceleration by $E_{//}$. The effect of secondary generation will also be discussed. No profile effects in the runaway generation or current distribution have been considered. It has further been assumed that the external magnetic energy is fully dissipated in the vessel wall and only the internal inductance, representing the flux within the vessel wall, will contribute to the electron acceleration. The ITER parameters that have been taken in the estimates are: $n_e=1\times10^{20}$, $Z_{eff}=3$, $I_p=20$ MA, $R_0=6$ m and $a=2.15$ m. A few notes on the runaway loss and damage will end the section.

-runaway energy and current

Before turning to the results of the model we first review some limitations to the energy the runaway electrons can attain in an ITER disruption:

- The maximum energy of the runaway electrons can never exceed the energy gained from the internal induced electric field as a result of the decay of the poloidal field. From eq. (7.14) it is found that $W_{max} \approx 1400$ MeV.
- The above value of W_{max} will never be reached in practice since the runaway electrons will loose energy by synchrotron radiation. The radiation limit depends on the value of the electric field and the pitch angle of the runaway electron. As an upper estimate for W_{max} we take Θ=0 rad and $E=E_b(T_{eb}/T_e)^{3/2}$. With T_e=20 eV, T_{eb}=10 keV, $E_b=2.7\times10^{-2}$ and eq. (2.17) the radiation limit amounts to W_{max} = 900 MeV.

- Before the synchrotron radiation limit is attained, the runaway electrons can already be lost as a result of the orbit shift, or the occurence of a separatrix in the drift orbit. This shift will increase with q and therefore depends on the current profile, the absolute value of the current and the initial orbit of the runaway electrons at low energy. An estimate can only be given for the case of a flat current profile for electrons whose initial orbit coincides with the magnetic axis. For those:

$$W_{max} = \frac{\mu_0 \, e \, c \, I_p \, R}{2\pi a} = 160 \, I_p\,(MA) \;\; MeV \tag{7.22}$$

  In this special case it would mean energy values in excess of the two limiting values mentioned above. However, for runaway electrons generated in the plasma edge, the orbit shift can be the limiting factor.
- The resonance between the runaway cyclotron motion and the magnetic field ripple can reduce the maximum energy in ITER appreciably as has been calculated by Russo [Rus-92]. He showed that the second harmonic ripple interaction (see chapter 6) in ITER is strong enough even during a disruption to prevent runaway electrons from being accelerated beyond the resonance energy. In that case the runaway energy is limited to $W_{max} = 270$ MeV.

We will now come to the model for an ITER disruption. It will be shown that under normal circumstances the maximum energy reached by the runaway electrons will be significantly lower than the above limits. This occurs because the electric field will decay when an appreciable amount of the current is carried by the runaway electrons. This has been modelled by calculating the generated runaway current as a function of the initial ϵ after the thermal quench. The above limits are not considered in the model. The electric field is calculated from the following set of equations:

$$E_{//}(t) = E_{tq}\left(1 \; - \frac{I_r(t)}{I_p(t)}\right) \tag{7.23a}$$

$$E_{//}(0) = \epsilon \, E_{crit} \tag{7.23b}$$

$$I_r(t) = \frac{ecN_r(t)}{2\pi R_0} = ec\pi n_{beam} r_r(t) \tag{7.23c}$$

$$\frac{dn_r(t)}{dt} = n_e \, \nu_{coll} \, \lambda \; + \frac{n_r(t)}{t_0(t)} \tag{7.23d}$$

$$\frac{dI_p(t)}{dt} = \frac{-2\pi R_0 E_{//}(t)}{L_{int}} \qquad (7.23e)$$

Here $E_{//}(0)$ is the electric field after the thermal quench, t_0 is the avalanching time of the secondary generation process and depends on $E_{//}$ and L_{int} is the internal inductance for which we take in the case of ITER L_{int}=10 μH.

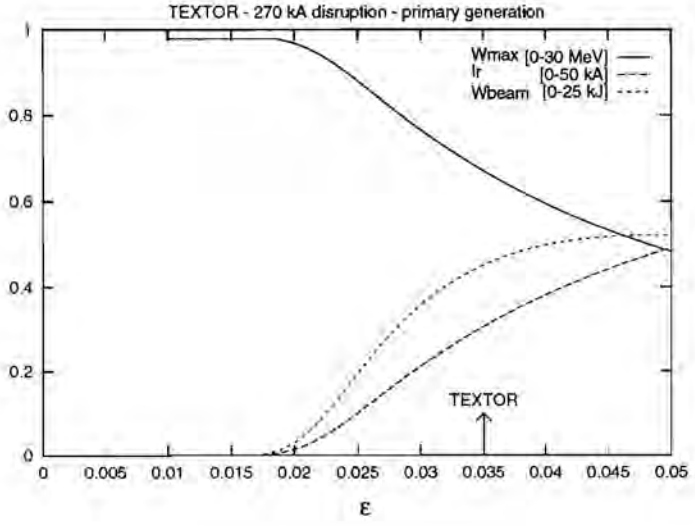

Figure 7.5a: *Result of the disruption model for TEXTOR. The runaway energy, runaway current and energy in the beam is calculated as a function of the parameter ε. The experimental result derived in Sec. 7.4 is reproduced for ε =0.035.*

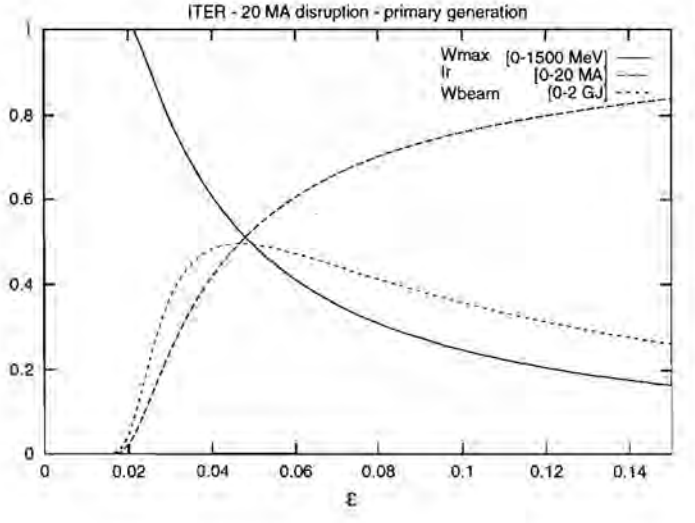

Figure 7.5b: *Prediction of the disruption model for a 20MA ITER disruption. Only primary generation is included in the model.*

The result of the simulations for the case in which the secondary generation is not included ($t_0=\infty$) is plotted as a function of initial ε is plotted in Fig.7.5 for both the TEXTOR and the ITER disruption. The maximum runaway energy W_{max}, the runaway current I_r and the total energy in the runaway beam, W_{beam} (proportional to the product $W_{max} \times I_r$) are shown. For ITER it is observed that runaway generation becomes important for $\varepsilon > 0.02$. Below this value I_r is negligible and W_{max} is just the integral of the induced electric field. Surprisingly, the runaway energy W_{max} decays if ε is increased. The current I_r rises only gradually with increasing ε, whereas one might expect a strong rise due to the exponential dependence of λ on ε. This can be understood by considering the fact that a larger production rate leads to a faster drop of $E_{//}$ and hence of λ. The time to generate and accelerate runaway electrons is therefore reduced for higher ε. The total energy in the runaway population reaches a maximum for $\varepsilon \approx 0.04$ and decreases thereafter, as a result of the limited time for runaway production and acceleration. An important conclusion of this model is that for higher values of ε the runaway electron damage is reduced in an ITER disruption!

Since we estimate for ITER $\varepsilon=0.1$, the model predicts that the runaway production is important, with the following qualitative predictions:

$$W_{max} = 350 \text{ MeV} \qquad I_r = 15 \text{ MA} \qquad W_{beam} = 700 \text{ MJ} \tag{7.24}$$

Note that in this calculation the loss of runaway electrons by orbit shift or diffusion, nor the ohmic dissipation of the induced power is considered which makes these estimates upper limits. Moreover, before the runaway energy has reached 350 MeV the interaction with the field ripple may already prevent runaway electrons from being accelerated to higher energies.

The inclusion of the secondary generation process in the model changes the previous results significantly, as is shown in Fig. 7.6. Runaway production now becomes already noticable for $\varepsilon > 0.01$. The secondary generation accelerates the runaway production and as a result the electric field will drop faster than in the previous case. This implies that W_{max} and W_{beam} are reduced with respect to the situation without secondary generation. This effect is stronger for larger values of ε. Thus one finds again that a higher ε after the thermal quench phase reduces the maximum attainable runaway energy. Moreover, for $\varepsilon > 0.03$ the result is nearly insensitive to ε. For the case $\varepsilon = 0.10$ one obtains:

$$W_{max} = 30 \text{ MeV} \qquad I_r = 18 \text{ MA} \qquad W_{beam} = 50 \text{ MJ} \tag{7.25}$$

We can conclude that the effect of the secondary generation is twofold: i) the maximum energy of a runaway electron is reduced to about $W_{max} = 50$ MeV and ii) the energy content in the runaway beam is at maximum 100 MJ for $\varepsilon > 0.03$ and is further reduced by a factor 2 for $\varepsilon > 0.1$.

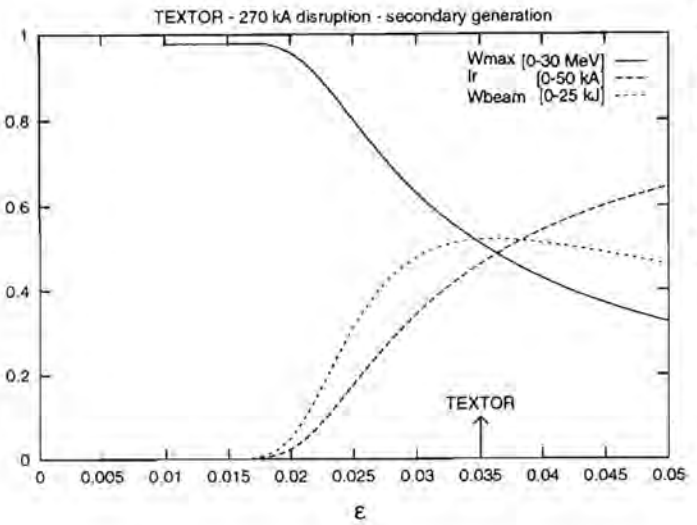

Figure 7.6a:
TEXTOR results of disruption model if secondary generation is included. Compared to Fig. 7.5a the runaway energy is decreased and the runaway current is increased by roughly 50% for the same value of ε.

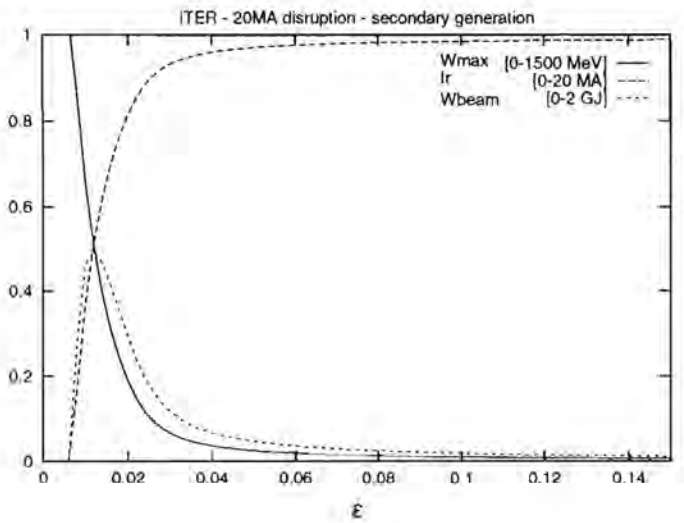

Figure 7.6b:
The results for the ITER disruption if secondary generation is included in the model. For a realistic estimate of ε the runaway energy will drastically be reduced, compared with Fig. 7.5b. The damage of the runaway electrons will be less severe if secondary generation will occur in ITER.

-loss and damage

If the energy in the runaway beam is dumped on the vessel wall large damage might occur depending on the loss mechanism. Although W_{beam} is smaller than the kinetic energy release in the thermal quench phase of the disruption by heat pulses, this does not imply that the runaway damage will be less severe. When the beam energy is deposited on a small suface, the local power loads from runaway loss may be much higher than from thermal heat pulses. Such local loss occurs when the runaway orbit strikes a limiting surface as a result of the orbit shift or when the plasma moves to the high field side when the feedback system of the stabilizing B_z field is not fast enough.

Even more serious is the penetration of the runaway electrons. On the basis of the calculations performed in this section a runaway energy of about 50 MeV is anticipated in an ITER disruption, but higher values cannot be excluded. These electrons will penetrate about 15 cm in carbon material and dump their energy in the metal coolant channels which could lead to destruction of the cooling system.

To avoid a large destruction caused by the disruption generated runaway beam the position and decay of the runaway beam has to be controlled. For this sufficiently fast vertical field coils are necessary to stabilize the position and let the runaway beam decay by radiation losses or scattering. The time scale τ_{rad} on which the runaway energy will decrease by radiation loss is found from:

$$\tau_{rad} = \frac{W}{dW/dt} = \frac{W}{P_{syn}} = 240\times10^3 \frac{R^2}{W[MeV]^3} \approx 70\ s \qquad (7.26)$$

This value can be appreciably reduced if pitch angle scattering is included which enhances the synchrotron radiation by decreasing the radius of curvature. Another option to avoid runaway damage is to induce a stochastic magnetic field to increase the radial runaway diffusion. Although the runaway electrons will be lost from the plasma and hit the plasma facing components, the effect is less harmful, since the affected area on which the runaway energy is deposited is larger.

In the present experiments other loss mechanisms of the runaways play an important role. These have not yet been attributed to any known effect. The danger or beneficial effects of such events for ITER are therefore hard to predict. For TEXTOR no consistent explanation for the runaway loss is found, and also for JET the runaway current decay is faster than synchrotron losses or small angle collisions can explain [Gil-93].

7.6 Conclusions

For the first time a disruption generated runaway beam is directly observed. Synchrotron radiation measurements revealed the generation and loss of runaway electrons in the current decay phase of a disruption in TEXTOR. These runaways can only be confined if there is at least a partial repair of the magnetic surfaces in the current decay phase. The energy and pitch angle of the runaway electrons do not reach anomalous values, indicating that turbulence or other processes do not affect them dramatically. The Dreicer process is the dominant generation mechanism but secondary generation may contribute as well. The cause of the subsequent loss of the runaway beam is not completely understood.

Extrapolations of disruption generated runaway electrons for ITER are speculative on the basis of the TEXTOR experiment. However, a simple model is deduced which can explain the TEXTOR data. Application of this model to ITER indicates that in a major disruption the maximum energy of the runaway electrons is 50 MeV and the total energy content is at maximum 100 MJ if secondary generation will contribute to the runaway production. It is predicted that a large runaway production rate is preferable for reducing the runaway energy and current, since in that case the electric field will drop faster and the time for runaway production and acceleration is reduced. A higher electric field after the thermal quench and the occurrence of secondary runaway generation is therefore favourable. Further investigations into disruption generated runaway beams is of the utmost importance before reliable operation in a fusion reactor can start. The synchrotron radiation diagnostic plays an unique role in such studies.

REFERENCES

[Ali-75] V.V. Alikaev, K.A. Razumova, Yu.A. Sokolov, *Runaway-electron Instability in the TM-3 Tokamak*, Sov.J. Plasma Phys **1** (1975) 303

[Bak-93] R.J. Bakker, *Free Electrons as a versatile source of coherent radiation*, Thesis Vrije Universiteit Amsterdam, (1993)

[Bar-81] C.W. Barnes, *Studies of Runway Electron Transport in PLT and PDX*, Thesis Princeton University (1981)

[Bar-82] C.W. Barnes and J.D. Stachan, *Sawtooth oscillations in the flux of runaway electrons to the PLT limiter*, Nucl. Fusion **22** (1982) 1090

[Bes-86] N.T. Besedin and I.M. Pankratov, *Stability of a Runaway Electron Beam*, Nucl. Fusion **26** (1986) 807

[Bol-90] H. Bolt and A. Miyahara, *Runaway - Electron - Materials Interaction Studies, Report of National Institute for Fusion Science*, Nagoya, NIFS-TECH-1 (1990)

[Bre-90] B.N. Breizman, *Collective Interaction of Relativistic Electron Beams with Plasmas*, in *Reviews of Plasma Physics*, Vol. 15, ed. by B.B. Kadomtsev (Consultants Bureau, New York, 1990)

[Bro-89] I.N. Bronstein, K.A. Semendjajew, *Taschenbuch der Mathematik*, (Verlag Harrie Deutsch, Thun und Frankfurt/Main, 1989)

[Bro-78] P. Brossier, *Runaway-driven Kinetic Instabilities in Tokamaks*, Nucl. Fusion **18** (1978) 1069

[Cam-84] D.J. Campbell, A. Eberhagen, S.E. Kissel, Analysis of Electron Cyclotron Emission from Non-Thermal Discharges in ASDEX Tokamak, Nucl. Fusion **24** (1984) 297

[Cat-90] C.R.A Catlow and G.N. Greaves, *Applications of Synchrotron Radiation*, (Blackie and Son Ltd, Glasgow,1990)

[Cat-91] P.J. Catto, J.R. Myra, P.W. Wang, A.J. Wooton and R.D. Bengtson, *Estimating the runaway diffusion coefficient in the TEXT tokamak from shift and externally applied resonant magnetic-field experiments*, Phys. Fluids B **3** (1991) 2038

[Cat-92] P.J. Catto, J.R. Myra and J.B. Taylor, *Curvature drift modifications of the magnetic field maps for runaway electrons*, Plasma Phys. and Contr. Fusion **34** (1992) 387

[Che-83] A.D. Cheetham, J.A. How, G.R. Hogg, H. Kuwahara, A.H. Morton, *Runaway electrons and rational-q surfaces in a tokamak*, Nucl. Fusion **23** (1993) 1694

[Che-84] F.F. Chen, *Introduction to Plasma Physics and Controlled Fusion*, Vol.1 (Plenum Press, New York, 1984)

[Coh-76] R.H. Cohen, *Runaway Electrons in an Impure Plasma*, Phys. Fluids **19** (1976) 239

[Con-75] J.W. Connor, R.J. Hastie, *Relativistic Limitations on Runaway Electrons*, Nucl. Fusion **15** (1975) 415

[Cop-76] B. Coppi, F. Pegoraro, R. Pozzoli, G. Rewoldt, *Slide-away Distributions and Relevant Collective Modes in High-Temperature Plasmas*, Nucl. Fusion **16** (1976) 309

[Cri-91] P. Cripwell and A.E. Costley, *Evidence for fine scale density structures on JET under additional heated conditions*, Poc. 18th EPS Conference on Controlled Fusion and Plasma Physics, Berlin (1991) I-17

[Die-88] K.J. Dietz, *Experience with Limiter- and Wall Materials in JET*, J. Nucl. Mater. **155-157** (1988) 8

[Dre-59] H. Dreicer, *Electron and Ion Runaway in a Fully Ionized Gas. I*, Phys. Rev. **115** (1959) 238

[Fin-90] K.H. Finken, J.G. Watkins, D. Rusbüldt et al., *Observation of Infrared Synchrotron Radiation from Tokamak Runaway Electrons in TEXTOR*, Nucl. Fusion **30** (1990) 859

[Fin-92] K.H. Finken, W.Y. Baek, K.H. Dippel et al., *Energy Flux to the TEXTOR Limiters during Disruptions*, Nucl. Fusion **32** (1992) 915

[Fle-93] H.H. Fleischmann and S.J. Zweben, *Evaluation of Potential Runaway Generation in Large-Tokamak Disruptions*, Report of Plasma Physics Laboratory, Princeton, PPPL-2914 (1993)

[Fus-79] G. Fussmann, *On the Motion of Runaway Electrons in Momentum Space*, Nucl. Fusion **19** (1979) 327

[Fus-81] G. Fussmann, D. Campbell, A. Eberhagen et al., *Long-Pulse Suprathermal Discharges in the ASDEX Tokamak*, Phys. Rev. Lett. **47** (1981) 1004

[Fus-82] G. Fussmann, G. Becker, K. Behringer et al., Investigations of Suprathermal Discharges in the ASDEX Tokamak, Proc. 9th IAEA conference, Baltimore (1982) III-295

[Gil-93] R.D. Gill, *Generation and Loss of Runaway Electrons following Disruptions in JET*, Nucl. Fusion **33** (1993) 1613

[Gio-49] R.G. Giovanelli, *Electron Energies Resulting from an Electric Field in a Highly Ionized Gas*, Phil. Mag. **40** (1949) 206

[Gra-91] E. Graffmann, Z.S. Fang, H. Soltwisch K. Wang, *The scaling of sawtooth parameter and the occurence of single sawteeth in the start-up phase of TEXTOR*, Proc. 18th EPS Conference on Controlled Fusion and Plasma Physics, Berlin (1991) II-13

[Gur-61] A.V. Gurevich, *On the Theory of Runaway Electrons*, Sov. Phys.-JETP **21** (1961) 931

[Har-60] E.R. Harrison, *Runaway and Suprathermal Particles*, Plasma Phys. **1** (1960) 105

[Heg-93] C.C. Hegna and J.D. Callen, *Plasma transport in mixed magnetic topologies*, Phys. Fluids B5 (1993) 1804

[Hoe-94] F. Hoenen, E. Graffmann, K.H. Finken, H.J. Barrenscheen, H. Klein, R. Jaspers, *Liquid Scintillation Detectors for Gamma and Neutron Diagnostic at TEXTOR and Results of Runaway and Sawtooth Oscillations*, Rev. Sci. Instrum. **65** (1994) 2594

[Jan-91] R.K. Janev and A. Miyahara, *Plasma-Material Interaction Issues in Fusion Reactor Design and Status of the Database*, Suppl. to Nucl. Fusion **1** (1991) 123

[Jar-88] O.N. Jarvis, G. Sadler, J.L. Thompson, *Photoneutron Production Accompanying Plasma Disruptions in JET*, Nucl. Fusion **28** (1988) 1981

[Jas-93] R. Jaspers, K.H. Finken, G. Mank et al., *Experimental Investigation of Runaway Electron Generation in TEXTOR*, Nucl. Fusion **33** (1993) 1775

[Jas-94a] R. Jaspers, N.J. Lopes Cardozo, K.H. Finken et al., *Islands of Runaway Electrons in the TEXTOR Tokamak and Relation to Transport in a Stochastic Field*, Phys. Rev. Lett. **72** (1994) 4093

[Jas-94b] R. Jaspers, T. Grewe, K.H. Finken et al., *Observations of Infrared Radiation during Disruptions in TEXTOR: Heat Pulses and Runaway Electrons*, J. Nucl. Mater. (1994)

[Jay-92] R. Jayakumar, H.H. Fleischmann, S.J. Zweben, *Collisional Avalanche Exponentiation of Run-Away Electrons in Electrified Plasmas*, PPPL-2849 (1992)

[Kaw-75] P.K.Kaw, W.L.Kruer, C.S. Liu, K. Nishikawa, *Parametric Instabilities in Plasma*, in *Advances in Plasma Physics*, Vol. 6, ed. by A. Simon, W.B. Thompson (Wiley, New York, 1975)

[Kno-79] H. Knoepfel and D.A. Spong, *Runaway Electrons in Toroidal Discharges*, Nucl. Fusion **19** (1979) 785

[Kru-64] M. Kruskal, I.B. Bernstein, *Runaway Electrons in an Ideal Lorentz Plasma*, Phys. Fluids **7** (1964) 407

[Kul-73] R.M. Kulsrud, Y.C. Sun, N.K. Winsor, H.A. Fallon, *Runaway Electrons in a Plasma*, Phys. Rev. Lett. **31** (1973) 690

[Kwo-88] O.J. Kwon, P.H. Diamond, F. Wagner, G. Fussmann, ASDEX and NI Teams, *A Study of Runaway Electron Confinement in the ASDEX Tokamak*, Nucl. Fusion **28** (1988) 1931

[Lau-89] L. Laurent and J.M. Rax, *Runaway-ripple interaction in tokamaks*, EUR-CEA-FC-1374 (1989)

[Lau-90] L.Laurent and J.M. Rax, *Stochastic Instability of Runaway Electrons in Tokamaks*, Europhys. Lett. **11** (1990) 219

[Lop-93] N.J. Lopes Cardozo, *Anomalous Transport Due to Magnetic Turbulence*, Trans. of Fus. Techn. **25** (1994) 146

[Mer-87] B.J. Merrill and S.C. Jardin, *Consequences of Resistive Disruptions on Vacuum Vessel Components*, J. Nucl. Mater. **145-147** (1987) 881

[Mik-74] A.B. Mikhailovskii, *Theory of Plasma Instabilities*, Vol. 1 (Consultants Bureau, New York, 1974)

[Myn-81] H.E. Mynick and J.D. Strachan, *Influence of Stochastic Magnetic Fields on the Confinement of Runaway Electrons and Thermal Electron Energy in Tokamaks*, Phys. Fluids **24** (1981) 695

[Myr-92] J.R. Myra, P.J. Catto, A.J. Wootton, R.D. Bengtson, P.W. Wang, *Runaway Electrons as a Diagnostic of Magnetic Fluctuations in the Edge Plasma of the Texas Experimental Tokamak*, Phys. Fluids B4 (1992) 2092

[Oha-88] H.C. Ohanian, *Classical Electrodynamics*, (Allyn and Bacon, Inc, Boston, 1988)

[Oom-76] A.A.M. Oomens, L.Th.M. Ornstein, R.R. Parker, F.C. Schüller and R.J. Taylor, *Observation of High-Frequency Radiation an Anomalous Ion Heating on Low-Densitiy Discharges in Alcator*, Phys. Rev. Lett. **36** (1976) 255

[Pap-75] K. Papadopoulos, *Nonlinear Stabilization of Beam Plasma Interactions by Parametric Effects*, Phys. Fluids **18** (1975) 1769

[Pap-77] K. Papadopoulos, B.Hui, N. Winsor, *Formation of Positive Slope on Electron Runaway Distribution in Tokamaks*, Nucl. Fusion **17** (1977) 1087

[Par-78] V.V. Parail and O.P. Pogutse, *The Kinetic Theory of Runaway Electron Beam Instability in a Tokamak*, Nucl. Fusion **18** (1978) 303

[Par-86] V.V. Parail and O.P. Pogutse, *Runaway Electrons in a Tokamak*, in *Reviews of Plasma Physics*, Vol. 11, ed. by M.A. Leontovich (Consultans Bureau, New York, 1986)

[Rax-91] J.M. Rax, L.Laurent, D. Moreau, *Stochastic Instability of Relativistic Runaway Electrons due to Lower Hybrid Waves*, Europhys. Lett. **15** (1991) 497

[Rec-78] A.B. Rechester and M.N. Rosenbluth, *Electron Heat Transport in a Tokamak with Destroyed Magnetic Surfaces*, Phy. Rev. Lett. **40** (1978) 38

[Rob-93] D.C. Robinson, M.R. O'Brien, C.A. Gardner and M. Valovic, *Transport of Non-thermal Electrons in Tokamaks*, Proc. 20th Eur. Conf. on Controlled Fusion and Plasma Physics, Lisbon (1993) III-1041

[Rod-94] L. Rodríguez-Rodrigo, A.Rodrígues-Yunta, F. Castejón et al., *Runaway transport studies in the TJ-I tokamak*, Nucl. Fusion **34** (1994) 649

[Rus-74] D. Rusbüldt and K. Thimm, *The synchrotron as a radiation standard for the vacuum ultraviolet*, Nucl. Instr. and Meth. **116** (1974) 125

[Rus-91] A.J. Russo, *Effect of Ripple on Runaway Electrons in Tokamaks*, Nucl. Fusion **31** (1991) 117

[Rus-93] A.J. Russo and R.B. Campbell, *A Model for Disruption Generated Runaway Electrons*, Nucl. Fusion **33** (1993) 1305

[Sch-49] J. Schwinger, *On the Classical Radiation of Accelerated Electrons*, Phys. Rev. **75** (1949) 1912

[Sch-91] F.C. Schüller, D.C. Schram, J. Konings et al., *Profile Consistency as a Result of Coupling between the Radial Profile Functions of Pressure and Current Density*, Proc. 18th Eur. Conf. on Controlled Fusion and Plasma Physics, Berlin, Vol. 15C-IV (1991) 185

[Sch-94] B.C. Schokker, P.C. de Vries, A.A.M. Oomens, F.C. Schüller, N.J. Lopes Cardozo, and RTP-Team, *Characterization of the RTP Slideaway Regime and its Fast Electron Population*, Proc. 21th Eur. Conf. on Controlled Fusion and Plasma Physics, Montpellier (1994) I-286

[Sch-95] B.C. Schokker, Ph. D. Thesis, Technical University Eindhoven, The Netherlands 1995.

[Sok-68] A.A. Sokolov, I.M. Ternov, *Synchrotron Radiation*, (Akademie Verlag, Berlin, 1968)

[Spi-57] L. Spitzer, *Physics of fully ionized gases*, (Intersience Publishers, New York, 1957)

[Sud-73] R.N. Sudan, *Applications of Intense Relativistic Electron Beams to Controlled Thermonuclear Fusion*, Proc. of the 6th Eur. Conf. on Controlled Fusion and Plasma Physics, Moscow, Vol. II (1973) 184

[Tak-89] H. Takatsu, T. Ando, M. Yamamoto et al., *Operation Experiences of the JT-60 First Walls during High-Power Additional Heating Experiments*, Fusion Eng. and Design **9** (1989) 3

[TFR-76] Equipe TFR, *Electrons decouples et diffusion anomale des electrons pieges dans les miroirs locaux du tokamak TFR*, Nucl. Fusion **16** (1976) 473

[Tho-75] L.E. Thode and R.N. Sudan, *Plasma Heating by Relativistic Electron Beams. I. Two Stream Instability*, Phys. Fluids 18 (1975) 1552

[Urb-93] W.H. Urbanus, R.W.B Best, W.A. Bongers et al., *Design of the 1 MW, 200 GHz, FOM- Fusion- FEM*, Nucl. Instr. and Meth. A331 (1993) 235

[Wat-66] G.N. Watson, *A treatise on the theory of Bessel functions*, (Cambridge University Press, Cambridge, 1966)

[Wes-87] J.Wesson, *Tokamaks*, (Oxford University Press, Oxford,1987)

[Wes-89] J.A. Wesson, R.D. Gill, M. Hugon et al., *Disruptions in JET*, Nucl. Fusion 29 (1989) 641

[Whi-91] J.B. Whitley, W.B. Gauster, R.D. Watson, J.A. Koski, A.J. Russo, *Pulse Heating and Effects of Disruptions and Runaway Electrons on First Walls and Divertors*, Suppl. to Nucl. Fusion **1** (1991) 109

[Yag-91] Y.Yagi, Y.Hirano, T.Shimada, K. Hattori et al., *Plasma Current and Energetic Electrons in the Core Plasma of a Reversed Field Pinch*, Plasma Phys. and Contr. Fusion **33** (1991) 1391

[Zeh-81] H.P. Zehrfeld, G. Fussmann, B.J. Green, *Electric Field Effects on Relativistic Charged Particle Motion in Tokamaks*, Plasma Physics **23** (1981) 473

[Zuz-92] W.W. Zuzak, B.L. Stansfield, C.Janicki et al.,*URG Emision from the Tokamak de Varennes*, Internal Report CCFM-RI 375e (1992)

[Zwe-78] S.J. Zweben, D.W. Swain, and H.H. Fleischmann, *Radial transport of high energy runaway electrons in ORMAK*, Nucl. Fusion **18** (1978) 1679

SUMMARY

Although over 99 % of the matter in the universe is in the plasma state, on earth plasmas are rare, where the most common natural example is lightning. In the laboratory plasmas can be created by heating a gas until it ionizes. One of the most challenging applications of the plasma is found in the thermonuclear research, where one tries to obtain energy from nuclear fusion reactions by imitating the conditions of the sun (which is a gigantic plasma). The most successful experiments in this area are done in so-called tokamaks, in which a deuterium (a hydrogen isotope) plasma of several tens of million degrees is confined by magnetic fields in a toroidal system.

The work described in this thesis focusses on the behaviour of relativistic runaway electrons in such a tokamak plasma. If an electric field is applied to the plasma a class of electrons will be continuously accelerated since the drag force experienced from collisions with the plasma particles, falls off strongly with the energy of the electrons. These electrons are called runaway electrons.

Runaway electrons are inherently present in a tokamak, in which an electric field is applied to drive a toroidal current. The experimental work of this thesis is performed in the tokamak TEXTOR. Here runaway electrons can acquire energies of up to 30 MeV.

The runaway electrons are studied in TEXTOR by measuring their synchrotron radiation, which is emitted in the infrared wavelength range. The studies presented are unique in the sense that they are the first ones in tokamak research to employ this radiation. Hitherto, studies of runaway electrons revealed information about their loss in the edge of the discharge. The behaviour of confined runaways was still a terra incognita. The measurement of the synchrotron radiation allows a direct observation of the behaviour of runaway electrons in the hot core of the plasma. Information on the energy, the number and the momentum distribution of the runaway electrons is obtained. The production rate of the runaway electrons, their transport and the runaway interaction with plasma waves are studied. New fundamental information about these processes is gained. Moreover, it turns out that these investigations can have consequences for thermonuclear research and future fusion reactors.

The production rate of the runaway electrons was hitherto described by the Dreicer process, i.e the evaporation in phase space of electrons from the thermal distribution into the runaway region under influence of the electric field. In TEXTOR an additional generation process was experimentally identified. This secondary generation process, in which already existing high energy electrons kick thermal electrons in the runaway region, had already been predicted by theoreticians. In

TEXTOR it is under certain conditions the dominant production mechanism resulting in an exponential growth of the runaway population in time.

Runaway electrons are found to be extremely well confined in the plasma core. This is ascribed to the fact that with increasing energy the runaway orbits are shifted from the magnetic flux surfaces, which make them increasingly insensitive to magnetic turbulence. This orbit shift has been measured directly and it can explain the good confinement. Auxiliary heating is found to have a detrimental effect on the confinement of the runaway electrons. This is attributed to an increase of the correlation length of the magnetic fluctuations. A fast loss of runaway electrons in a sawtooth instability is probably also related to large scale turbulence. Runaway electron confinement studies can thus provide information about magnetic turbulence in the plasma core.

The transport of runaway electrons in a stochastic magnetic field is investigated by injecting a pellet into the discharge. A fast loss of runaway electrons is observed following the pellet injection. This is explained by a short period of ergodization of the magnetic field. A part of the runaway electron population however, stays confined in a narrow helical tube with a winding ratio of 1, i.e it makes one poloidal turn in one toroidal transit. This shows that in the stochastic field at least one large magnetic island remains intact. The diffusion of the runaway electrons in this newly discovered 'runaway snake' is extremely slow.

The transport of the runaway electrons in phase space is next investigated. Here, diffusion (pitch angle scattering) and convection (acceleration and radiation) effects play a role. The distribution of the perpendicular momentum of the runaway electrons is initially determined by the collisions with the plasma ions and electrons. For runaway electrons with an energy in excess of 20 MeV the cyclotron motion can be in resonance with the spatial periodicity of the magnetic field, resulting from the finite number of toroidal field coils in a tokamak. This interaction will scatter the runaway electrons in pitch angle, i.e convert longitudinal momentum into perpendicular momentum. As a consequence of this process, the radiation limit (at which the electrons radiate as much power as they gain from the electric field) of the runaway electrons is decreased and they can acquire no more than 30 MeV of energy in TEXTOR. Another fast pitch angle scattering process has been observed in the current decay phase of the discharge. This has been explained by an interaction of the runaway electrons with lower hybrid waves. These waves are excited by lower energy runaway electrons in the socalled Parail Pogutse instability. As a possible application this instability can be used to lower the maximum runaway energy. This is useful in a reactor as is discussed next.

For future fusion reactors runaway electrons will cause severe damage to the machine if they have high energies and the runaway population is large. This situation is predicted to occur in a plasma disruption, which is the event in which the

confinement of the plasma is suddenly lost and large electric fields are induced. A runaway beam generated in a disruption has been observed for the first time by the synchroton radiation. The measured runaway parameters like energy number and pitch angle, the data can be described by a simple model. This model is applied to a fusion reactor presently being designed, named ITER. According to the model the maximum energy of the runaway electrons will not exceed 60 MeV, which is tolerable for ITER. For comparison, other studies predict energies of several hundreds of MeV. Moreover, from the model larger runaway production rates are predicted to cause less damage.

SAMENVATTING

Ondanks het feit dat 99% van de materie in het universum in de plasma toestand verkeert, zijn plasma's op aarde zeldzaam, waar het bekendste natuurlijk voorbeeld van een plasma de bliksem is. In een laboratorium kan een plasma gemaakt worden door een gas te verhitten totdat het ioniseert. Een van de meest uitdagende toepassingen van plasma's wordt gevormd door het thermonucleair onderzoek. Daar probeert men energie te verkrijgen uit kernfusie reacties door de omstandigheden van de zon (die zelf een reusachtig plasma is) na te bootsen. De succesvolste experimenten op dit gebied worden gedaan in zogenaamde tokamaks. Hierin wordt een deuterium (een waterstof isotoop) plasma van enkele tientallen miljoen graden opgesloten in een toroïdaal systeem door magnetische velden.

Het werk dat in dit proefschrift beschreven wordt is gericht op het gedrag van relativistische runaway electronen in zo'n tokamak. Wanneer men aan een plasma een electrisch veld aanbrengt zal een bepaalde groep electronen continu versneld worden, omdat de afremmende kracht, die de electronen ondervinden door botsingen met andere plasma deeltjes, sterk afneemt met de energie van de electronen. Dit zijn de electronen die runaway electronen genoemd worden.

Runaway electronen zijn inherent aan iedere tokamak, omdat in een tokamak een electrisch veld wordt aangelegd om een toroidale stroom te voeren. Het experimenteel werk van dit proefschrift is uitgevoerd in de tokamak TEXTOR, waar runaway electronen een energie van 30 MeV kunnen bereiken.

De runaway electronen in TEXTOR worden bestudeerd door hun synchrotron straling te meten. Deze straling wordt uitgezonden in het infrarood. De hier beschreven studie is uniek in die zin dat het de eerste keer in het thermonucleair onderzoek is dat er gebruik wordt gemaakt van deze straling. Tot nog toe gaven studies van runaway electronen alleen informatie over hun verlies in de rand van de ontlading. Het gedrag van runaway electronen die in het centrum van het plasma waren opgesloten was nog een terra incognita. Door de synchrotron straling te meten wordt de mogelijkheid geboden direct het gedrag van de runaway electronen in de hete kern van het plasma te bestuderen. Informatie over de energie, het aantal en de impulsverdeling van de runaway electronen kan hieruit worden verkregen. De productie van runaway electronen, hun transport en de interactie met plasma golven werden bestudeerd. Nieuwe fundamentele gegevens over deze processen werden gewonnen. Verder bleek dat deze onderzoekingen consequenties kunnen hebben voor het thermonucleaire onderzoek en toekomstige fusie reactoren.

De productie van runaway electronen werd tot nog toe beschreven met het Dreicer proces. Dit is de diffusie in de fase ruimte van de electronen van de thermische

verdeling naar het runaway gebied, onder invloed van het electrische veld. In TEXTOR werd experimenteel nog een ander generatie proces geïdentificeerd. Dit secundair generatie proces, waarbij een reeds bestaand hoog energetisch electron thermische electronen in het runaway gebied stoot door middel van botsingen, was reeds door theorieën voorspeld. In TEXTOR is dit mechanisme onder bepaalde condities het dominante productie mechanisme, hetgeen resulteert in een exponentiële groei van de runaway populatie in de tijd.

Experimenteel blijkt dat runaway electronen buitengewoon goed zijn opgesloten in het plasma centrum. Dit wordt toegeschreven aan het feit dat als de energie van de runaways toeneemt hun banen steeds meer verschoven zijn ten opzichte van de magnetische oppervlakken. Dit maakt hen in toenemende mate ongevoelig voor de magnetische turbulentie. Deze drift verplaatsing kon direct worden gemeten en kan de goede opsluiting verklaren. De opsluiting van de electronen wordt verslechterd door additionele verhitting van het plasma. Dit kan worden toegeschreven aan een toename van de correlatie lengte van de magnetische fluctuaties. Een snel verlies van een deel van de runaway electronen tijdens de zaagtand instabiliteit kan ook aan een toename van de correlatie lengte gewijd worden. Uit deze metingen blijkt dat de runaway electronen informatie kunnen verschaffen over de magnetische turbulentie in de plasma kern.

Het transport van de runaway electronen in een stochastisch veld werd onderzocht door een ijskogeltje het plasma in te schieten. Na injectie werd een snel verlies van een gedeelte van de runaway electronen gemeten. Dit kan worden verklaard door aan te nemen dat er gedurende een kort periode een ergodisering van het magneet veld optrad. Een ander gedeelte van de runaway populatie bleef opgesloten zitten in een smalle helische buis die een windingsverhouding van 1 had, d.w.z door een keer toroïdaal rond te gaan werd ook een keer poloïdaal rond gegaan. Dit betekent dat in het stochastische veld minstens een groot magnetische eiland blijft bestaan. De diffusie van de runaway electronen in deze nieuw ontdekte 'runaway slang' is uitermate gering.

Het transport van runaway electronen in de fase ruimte werd vervolgens onderzocht. In deze ruimte speelt diffusie (pitch angle verstrooiing) en convectie (versnelling and straling) een rol. De verdeling van de loodrechte impuls van de runaway electronen wordt aanvankelijk bepaald door botsingen met plasma ionen en electronen. Voor runaway electronen met energieën hoger dan 20 MeV kan hun cylcotron beweging in resonantie geraken met de ruimtelijke periodiciteit van het magneetveld, als gevolg van een eindig aantal toroïdale veld spoelen in een tokamak. Deze interactie verstrooit runaway electronen in pitch angle, d.w.z. dat parallelle impuls wordt omgezet in loodrechte impuls. Dit heeft als consequentie dat de stralingslimit (waar de electronen evenveel vermogen uitstralen dan ze uit het electrisch veld winnen)

van de runaway electronen verlaagd wordt, zodat ze in het geval van TEXTOR geen energie hoger dan 30 MeV kunnen bereiken. Een ander fenomeen dat voor een snelle toename van de pitch angle zorgde werd waargenomen tijdens de stroomafval-fase van de ontlading. Dit wordt verklaard door een interactie tussen de runaway electronen en lower hybrid golven. Deze golven worden aangeslagen door de lager energetische runaway electronen in de zogenaamde Parail Pogutse instabiliteit. Dit zou gebruikt kunnen worden om de maximale energie die de runaway electronen kunnen bereiken te verlagen.

In toekomstige fusie reactoren kunnen de runaway electronen ernstige schade veroorzaken aan de machine als zij een hoge energie hebben en de runaway populatie groot is. Het kan worden verwacht dat zo'n situatie zal ontstaan tijdens een plasma disruptie. Een disruptie is een gebeurtenis waarin de opsluiting van het plasma plotseling verloren gaat en grote electrische velden geïnduceerd worden. Voor de eerste keer is er nu een runaway bundel waargenomen door middel van de synchrotron straling die tijdens zo'n disruptie was ontstaan. De gemeten runaway parameters zoals energie, aantal en pitch angle, konden met een eenvoudig model verklaard worden. Dit model werd toegepast op een toekomstige fusie reactor, ITER. Volgens deze berekeningen zal de maximale energie van de runaway electronen de 60 MeV niet overtreffen. Dit kan voor ITER nog getolereerd worden. Ter vergelijk, uit ander studies wordt een energie van enkele honderden MeV's voorspeld. Verder blijkt uit dit model dat hoe groter de productie van de runaway electronen is, hoe kleiner de schade is die aangericht wordt.

DANKWOORD

Vier jaar lang ben ik full-time bezig geweest met een klein onderwerp van een groot project. Wat begon met een reactie of een kleine personeelsadvertentie, groeide uit tot een grote uitdaging. De eerste paar maanden in dit voor mijn nieuwe vakgebied, voelde ik me nog een kleintje in deze wereld. Op deze plaats, aan het eind van het proefschrift aangekomen, had ik even het euforistische gevoel een grote te zijn op dit specifieke gebied. Gelukkig realiseer ik me nu toch dat ik nog steeds dat kleintje uit het begin zou zijn als ik niet geprofiteerd had van alle hulp, groot en klein, die ik in deze periode van vele kanten heb gekregen.

Op wetenschappelijk gebied heb ik het geluk gehad begeleid te worden door een grote kei in de plasmafysica, Niek. Voor zijn duidelijke uitleg, zijn groot inzicht in de materie, zijn motiverende hulp en nimmer aflatend enthousiasme voor de runaway resultaten wil ik hem allerhartelijkst bedanken. Verder heb ik veel over de plasmafysica geleerd van de discussies met Boudewijn en Chris. Vervolgens volgt nog een heel rijtje van mensen die ervoor gezorgd hebben dat ik de werksfeer zowel op Rijnhuizen als in Jülich als zeer plezierig heb ervaren: Rik, Peter, Theo, Arjen, Robert, Joop, Dick, de voetballers (FC ALT-II, Dynamo TEXTOR en De Rijnhuizen boys) en eigenlijk iedereen op Rijnhuizen.

Die Idee für ein Clustering der drei Institute für Plasma Physik aus Belgien, Nordrhein-Westfalen und den Niederlanden hat eine groβe Zukunft, wenn meine persönliche Erfahrung hier maβgeblich ist. Als erster 'Holländer' (eigentlich Niederländer) kam ich in die Gruppe von Dr. Finken. Er hat die ersten Messungen und Veröffentlichungen über Synchrotron Strahlung in Tokamaks gemacht und ist der Initiator dieser Doktorarbeit. Ich bedanke mich bei ihm herzlich für seine Hilfe und Ideen bei der Interpretation der Messungen. Neben ihm sorgten mehrere Leute für ein gutes Arbeitsklima. Dafür möchte ich mich bei der ganzen ALT-Gruppe und insbesondere bei Günter, Thomas, Bert und Mario bedanken.

Ut letste dankwoad is veur degene die mich ut meeste gestimuleerd had. Alhoewels dich mer u kleineke woars wat betreft de hulp mit der inhoud van ut proefschrif woars dich zeker de groetste ondersteuning bie ut schrieve. Lea, ich wil dich veur alles bedanke en dorum hub ich dit buukske och aan dich opgedrage.

CURRICULUM VITEA

Ik ben geboren op 20 april 1968 te Mechelen-Wittem. Op het "Sophianum" te Gulpen volgde ik mijn VWO-opleiding. Hier behaalde ik op 29 mei 1986 mijn diploma. Het volgende traject in mijn studie loopbaan ging naar Utrecht. Aan de rijksuniversiteit studeerde ik van 1 september 1986 tot 30 november 1990 Experimentele Natuurkunde. Mijn afstudeeronderzoek deed ik in de vakgroep kernfysica onder leiding van Prof. René Kamermans. Ook hier zat ik in het fusie onderzoek, al was hier niet de doelstelling energie uit het fusie-proces te winnen. De reactie tussen Calcium- en Titaan- kernen werd bestudeerd om te kijken by welke energieën van de oorspronkelijke kernen er nog een fusiekern kon ontstaan. Het experimentele werk daartoe verrichtte ik op de versnellersfaciliteit SARA te Grenoble in Frankrijk. Meteen aansluitend aan het behalen van mijn doctoraal bul begon ik in dienst van het FOM te werken op 'Rijnhuizen'. Na een leuke en leerzame periode, waarin ik me de grondbeginselen van de plasmafysica en het fusie onderzoek probeerde eigen te maken, vertrok ik een jaar later naar Jülich. Het werk dat ik daar gedaan heb aan het bestuderen van het gedrag van runaway electronen met behulp van synchrotron straling is beschreven in dit proefschrift. Het feit dat ik nog een hele poos op het 'Institut für Plasmaphysik' in Jülich blijf werken getuigt ervan dat zowel ik als mijn Duitse collega's die periode als prettig hebben ervaren.

Roger.

STELLINGEN

Behorend bij het proefschrift

Relativistic Runaway Electrons in Tokamak Plasmas

Roger Jaspers

Eindhoven, 3 Februari 1995

I

Hoewel de naam anders doet vermoeden, zijn relativistische runaway electronen die deeltjes die het beste opgesloten blijven in een tokamak, zowel in de reële als in de fase ruimte.

Dit proefschrift, Hoofdstuk 5 en 6.

II

De schade die door runaway electronen, ontstaan tijdens een plasma disruptie, aan een fusie reactor wordt aangericht, is kleiner naarmate er meer runaway electronen ontstaan.

Dit proefschrift, Hoofdstuk 7.

III

Het transport van hoog-energetische runaway electronen in het centrum van een tokamak plasma geeft, in tegenstelling tot dat van laag energetische electronen, voornamelijk informatie over de correlatie-lengte van de magnetische fluctuaties en niet over de amplitude hiervan.

Dit proefschrift, Hoofdstuk 5.

IV

De 'Unidentified Red Glow' zoals waargenomen in TdeV, is synchrotron straling van runaway electronen met een relatief hoge impuls loodrecht op het magneetveld.

W.W. Zuzak, B.L. Stansfield, C. Janicki et al., URG Emission from the Tokamak de Varennes, Internal Report CCFM-RI 375e (1992).

V

Drift-eilanden in de baan van runaway electronen kunnen ook bestaan buiten magnetische eilanden.

VI

De maximale excitatie-energie van een kern ontstaan in de fusiereactie tussen zware ionen is niet gelimiteerd tot een waarde beneden de bindingsenergie van de nucleonen.

T.M.V. Bootsma, The Evaporation Process of a Highly Excited Nucleus, Proefschrift Universiteit Utrecht (1993).

VII

Omdat de meeste neutronendetectoren, zoals gebruikt in het thermonucleair onderzoek voor metingen van bijvoorbeeld temperatuur of runaway electronen, ook gevoelig zijn voor hoog energetische fotonen zijn betrouwbare metingen van neutronen alleen mogelijk als beide contributies gesepareerd kunnen worden.

F. Hoenen et al., Liquid scintillation detectors for gamma and neutron diagnostic at TEXTOR, Rev. Sci. Instrum. 65 (1994) 2594

VIII

Ook de vierde aggregatietoestand van materie, het plasma, moet, in tegenstelling tot wat nu het geval is, in het natuurkunde programma van het VWO opgenomen worden.

IX

Zolang men het in de Europese Unie niet eens kan worden over de ambtelijke voertaal is er geen sprake van Europese eenwording.

X

Naast de verruiming van de openingstijden van winkels zouden ook de openingstijden van de overheidsinstellingen uitgebreid kunnen worden.

XI

In analogie met de sport, waar de prestaties verhoogd worden door competitie, zou het goed zijn om in de wetenschap naast een promotie- ook een degradatieregeling in te voeren.